Engineering Hierarchical Vasculature for Regenerative Medicine

by

Emily A. Margolis

A dissertation submitted in partial fulfillment
of the requirements for the degree of
Doctor of Philosophy
(Biomedical Engineering)
in the University of Michigan
2023

Doctoral Committee:

       Professor Andrew J. Putnam, Chair
       Professor Lonnie D. Shea
       Associate Professor Ming-Sing Si, University of California, Los Angeles
       Professor Jan P. Stegemann

Emily A. Margolis

emargol@umich.edu

ORCID iD: 0000-0002-1181-0581

Dedication

To my family, for always encouraging me to pursue my dreams, what I love, and any and every opportunity that comes my way. Thank you for the years of unwavering love and support. I wouldn't be where I am today without your constant encouragement.

To Brian, my soon to be chosen family, for your limitless encouragement, support of my dreams, and love. You have cheered me on throughout this entire process, picking me up in the low times and celebrating all the wins no matter how big or small. I can't wait to start forever with you. I love you.

Acknowledgements

There are so many people I would like to thank for helping me along the way. First and foremost, I would like to thank my thesis advisor, Dr. Andrew Putnam. I would not be the scientist I am today without your continuous support, guidance, and mentorship over the last five years. You have helped me to push boundaries, think critically, develop thoughtful experiments, and continue learning every day. Thank you for fostering my enthusiasm for science and encouraging me to never lost it.

I would also like to thank the members of my committee, Dr. Lonnie Shea, Dr. Ming-Sing Si, and Dr. Jan Stegemann for asking insightful questions that opened new avenues for my thesis work. Your knowledge and thought-provoking conversations have brought in new perspectives to my work and challenged me to think critically to advance the science. I appreciate all of the support and collaboration along the way.

I would like to thank all the current and former members of the Putnam Lab for providing insights on my research, making lab a fun environment to work, and the exciting science discussions. I am especially grateful to Nicole Friend, who has been there for every step of my Ph.D. Thank you for your friendship, for picking me up when I was down, for celebrating all the big wins, and countless times you have provided insights towards my research. You are an extraordinary scientist, and I can't wait to watch your academic career grow and the start of your own research group! I would also like to thank Lucia Choi, an extraordinary undergraduate student whom I had the pleasure of working with and mentoring. I can't wait to see your career flourish.

I would like to thank members of my lab as well as collaborators for instrumental help in conducting the research within this dissertation by co-authoring publications with me throughout my doctoral degree. Nicole Friend, Marsha Rolle, Eben Alsberg, and Andrew Putnam are co-authors on the review manuscript that is currently under review at Trends in Biotechnology and makes up a substantial portion of Chapter 2. David Cleveland, Yen Kong, Jeffrey Beamish, William Wang, Brendon Baker, and Andrew Putnam are co-authors on the work published in Lab on a Chip in 2021 that makes up a substantial portion of Chapter 3. Lucia Choi, Nicole Friend, and Andrew Putnam are co-authors on the work contained within Chapter 4 that is currently in preparation for submission to a peer reviewed journal. Finally, Andrew Putnam is a co-author on the work contained within Chapter 5 which is in preparation for submission as a peer reviewed journal article.

I would also like to acknowledge my previous research mentors. I would like to thank Dr. Joe Tien for giving me my first research opportunity, helping to mature and fine tune my research

skills as an undergraduate researcher, and the continued support since then. I would additionally like to thank Dr. Muhammad Zaman for his support as an undergraduate research mentor and throughout my research career. I am thankful to my industry mentors, Dr. Rebecca Duffy and Dr. Barbara Nsiah, for giving me the opportunity to conduct cutting edge research towards my career goal on engineering functional organs and continued support as I finished my doctoral degree.

To my friends, near and far, thank you for keeping me sane during this entire process. Thank you for encouraging me to get out of the lab every once in a while. Whether it was happy hours, dinners, hockey and football games, exploring Detroit, or anything in between, these moments helped provide relief from the stress of graduate school.

I would like to thank my family for continued support. To my parents, thank you for your support and guidance, pushing me to follow my dreams, and being the best role models. You have pushed me to put my best foot forward in every endeavor and always knew I could achieve anything I set my mind to. I would not be the person, or scientist, I am today without your boundless love and encouragement. To my grandparents, thank you for never doubting me, your excitement over every accomplishment and news of the day announcement, and love and encouragement throughout the journey. You pushed me to reach for the moon and knew I could achieve extraordinary things. I cherish our memories together and I am grateful for all of the love and support you have provided. I love you all more than I can put into words.

Lastly, to my fiancé, Brian, thank you for your constant love and support. You have been there at every turning point during this process, to pick me up during the lowest lows, celebrate the highest highs, and every milestone in between. You have been an endless source of inspiration, encouraged me to purse every opportunity, challenged me to think about things from a new

perspective, and most importantly believed in me at every step along the way. I could not have

done this without you. I love you and living life with you more than anything else!

Table of Contents

List of Tables

List of Figures

Figure 2.2: Fabrication strategies for each length scale of the vascular tree. Schematic examples of distinct strategies for forming vasculature ranging from arteries to capillaries. (A-C) Fabrication of artery-scale grafts has been achieved using an annular molding technique with (A) liquid prepolymer solutions containing cells, (B) cell suspensions alone, or (C) sheets of decellularized ECM. (D-F) Methods to fabricate mesoscale vasculature employ (D) 3D printing of sacrificial glass (Abbreviations: Panel (D) Par VP = parallel vascular patch, Grid VP = grid vascular patch, Sm_D VP = Small diameter vascular patch, EP = endothelial patch, AP = acellular patch) or (E, F) removable solid templates – spring (E) or needle (F). (G-I) Capillary-scale structures have been fabricated via (G) monocultures of cells with angiogenic factors to elicit vasculogenesis-like self-assembly, (H) co-culture of cells which undergo vasculogenesis-like self-assembly, or (I) angiogenic sprouting from existing blood vessels. Panels (A), (B), (C), (D), (E), (F), and (G) reproduced with permission from [26] (from Springer Nature – Copyright 2021, Biomedical Engineering Society), [28] (from Mary Ann Liebert – Copyright 2018, Mary Ann Liebert, Inc.), [30] (from John Wiley and Sons – Copyright FASEB), [41] (from Springer Nature – Copyright 2017, Macmillan Publishers Limited), [47] (used under Creative Commons license CC BY-NC), [45] (from PNAS, available through open access), and [50] (from Elsevier – Copyright 2020 Elsevier Inc.), respectively. Panels (H) and (I) created using BioRender.com. . 29

Figure 2.3: Engineered vasculature connects to the host yielding perfused vasculature in vivo. (A) Engineered large caliber decellularized vascular grafts have been shown to support cellular infiltration and remodeling upon transplantation. Panel A shows a macroscopic image of the vascular graft pre-implantation (left) and fluorescent images taken upon explantation of the graft (right). A neoadvential layer with a vasa vasorum is observed at 16 weeks (A, top right) while an endothelialized lumen is observed at 44 weeks (A, bottom right). (B) Parallel patterned mesovessels restored blood flow to ischemic tissues. The Par VP (schematic shown in Fig. 2D) inosculates with the host yielding perfusion of ischemic limbs by day 5 as shown by Laser Doppler Perfusion Imaging. (C, D) Microvascular and (E) hierarchical micro-mesovascular constructs connected to host tissues yielded host blood-perfused vessels within engineered tissues. Panel C shows perfused vessels integrated with the host circulation. Implanted human self-assembled vessels (red) and hydrogel-infiltrating mouse vessels (green) were perfused with a lectin to stain species-specific EC via tail vein injection to identify only perfused vessels. There is evidence of chimeric vasculature in both red stained vessels. Panel D shows engineered vessels (green) perfused with dextran (red) via a tail vein injection. The lack of red stain throughout the rest of the image indicates functional, non-leaky vasculature. Panel E shows the perfusion of engineered vessels within the implanted multiscale vascular tissue via the host circulation – engineered vessels (green), host vessels (blue), dextran (red). Panels (A), (B), (C), (D), and (E) reproduced and adapted with permission from [35] (from Science Translational medicine – Copyright 2019, Kirkton, RD. et al.), [41] (from Springer Nature – Copyright 2017, Macmillan Publishers Limited), [58] (from Springer Nature used under Creative Commons CC BY license – Copyright 2017, Kang, K.-T., et al.), [40] (from Mary Ann Liebert – Copyright 2013, Mary Ann Liebert, Inc.), and [63] (from Elsevier used under Creative Commons CC BY license – Copyright 2021, Debbi, L., et al.), respectively. 33

Figure 2.4: Surgically anastomosed grafts with structurally complex hierarchical architecture perfuse and integrate with host tissues. (A) A two-scale artery-capillary hierarchy surgically connected to host arteries showed evidence of blood perfusion in capillaries formed within a cell-laden bioprinted hydrogel. The top panel shows macroscopic perfusion of the

implanted construct after clamp removal. The middle and bottom images show matured vessels within the construct as evidenced by sheaths of BM (laminin) and perivascular stromal cell association (αSMA). (B) Engineered devices containing meso-microvascular hierarchies surgically anastomosed with host arteries also yielded functional perfusion. (C) Surgically anastomosed three-scale vascular hierarchies have been shown to yield significantly greater functional perfusion than hierarchies that were not surgically anastomosed, or microvascular only cell sheets. The panel shows bioluminescent perfusion with significant signal shown in the anastomosed group and limited signal in the other two groups. Panels (A), (B), and (C) reproduced and adapted with permission from [67] (from John Wiley and Sons – Copyright 2021, Szklanny, A.A., et al.), [65] (from Springer Nature – Copyright 2016, Macmillan Publishers Limited), and [68] (from Springer Nature used under a Creative Commons license CC BY-NC-SA – Copyright 2013, Sekine, H., et al.), respectively. 42

in culture over a 7-day culture period showing limited axial compaction and some radial compaction of wall thickness. (B) Fluorescent image of a tissue ring showing small vessel segments and a distinct fibroblast sheath around the outside of the graft. (C-D) Fluorescent images of grafts embedded in acellular fibrin imaged longitudinally showing (C) capillaries aligned in the direction of the lumen and (D) sprouting into the surrounding hydrogel (white arrows). White dashed line denotes the boundary between the graft (upper left) and the hydrogel (lower right). White arrows indicate sprouted vessels. (E) fluorescent images showing that fibroblasts in the graft take on a pericyte like phenotype as shown by expression of αSMA (top), NG2 (middle) and PDGFRβ (bottom). Red – EC, Green – actin (B) or pericyte markers (E), Blue – nuclei. 140

List of Appendices

List of Abbreviations

(Symbols, Numerical Order, Alphabetical Order)

°C	Degrees Celsius
3D	Three-dimensional
α-SMA	Alpha-smooth muscle actin
Ang-1	Angiopoietin 1
ANOVA	Analysis of variance
Anti-Anti	Antibiotic antimycotic
AV	Artery-vein
bFGF	Basic fibroblast growth factor
BSA	Bovine serum albumin
BM	Basement membrane
BMEC	Brain microvascular endothelial cells
CABG	Coronary artery bypass grafting
CLI	Critical limb ischemia
CVD	Cardiovascular disease
D10	DMEM + 10% FBS
DAPI	4',6- diamidino-2-phenylindole
DF	Normal human dermal fibroblast

DMEM	Dulbecco's modified eagle medium
DMSO	Dimethyl sulfoxide
DSU	Disc spinning unit
EC	Endothelial cells
ECFC	Endothelial colony forming cells
ECM	Extracellular matrix
EGM-2	Endothelial growth medium – 2
ePTFE	Expanded polytetrafluoroethylene
FBS	Fetal bovine serum
FDA	Food and Drug Administration
FGF-2	Fibroblast growth factor-2
FRESH	Freeform reversible embedding of suspended hydrogels
FSS	Fluid shear stress
G'	Shear modulus
GelMA	Gelatin methacrylol
GF	Growth factor
HAV	Human acellular vessel
HUVEC	Human umbilical vein endothelial cells
IF	Immunofluorescent
IPA	Isopropyl alcohol
IPN	Interpenetrating network
iPSC	Induced pluripotent stem cells
IVC	Inferior vena cava

LF	Normal human lung fibroblast
MMP	Matrix metalloproteinase
MSC	Mesenchymal stem cell
NG2	Neuron-glial antigen 2
NIH	National Institutes of Health
PA	Polyacrylamide
PAD	Peripheral artery disease
PBS	Phosphate buffered saline
PDGF-B	Platelet derived growth factor B
PDGFRβ	Platlet derived growth factor receptor beta
PDMS	Polydimethylsiloxane
PEG	Poly (ethylene glycol)
PLLA	Poly-L-lactic acid
RGD	Arginine-Glycine-Aspartic Acid peptide sequence
RM	Regenerative medicine
RPM	Revolutions per minute
RT	Room temperature
S1P	Sphingosine 1 phosphate
SC	Stromal cells
SF-EGM2	Serum free EGM-2
SIS	Small intestinal submucosa
SLATE	Stereolithographic apparatus for tissue engineering
SMC	Human aortic smooth muscle cells or smooth muscle cells generally

SWIFT	Sacrificial writing into functional tissue
TBS	Tris buffered saline
TCP	Tissue culture plastic
TE	Tissue engineering
TEVG	Tissue engineered vascular graft
TFM	Traction force microscopy
TGFβ	Transforming growth factor beta
TNL	Total network length
UEA	Ulex europaeus agglutinin I
uPa	Urokinase-type plasminogen activator
uPAR	Urokinase-type plasminogen activator receptor
VE-cadherin	Vascular endothelial cadherin
VEGF	Vascular endothelial growth factor
Z-fix	Zinc-buffered formalin fixative

Abstract

In the human body, blood flows from the heart to organs and tissues through a hierarchical vascular tree, consisting of large arteries that branch into arterioles and further into capillaries where gas and nutrient exchange occur. Engineering a complete, integrated vascular hierarchy possessing vessels large enough to suture, strong enough to withstand hemodynamic forces, and a branching structure to permit immediate perfusion of a fluidic circuit across length scales would be transformative for the field of regenerative medicine, enabling the translation of engineered tissues of clinically-relevant size, and perhaps whole organs. Within the field of tissue engineering, there has been extensive research towards engineering vessels at each caliber individually, while hierarchical vasculature has been comparatively understudied. This dissertation investigated the engineering of various two-scale hierarchical vascular tissues (HVT) which were integrated to form a complete, three-scale HVT composed of capillaries, mesovessels, and a macrovessel suitable for surgical anastomosis.

Aim 1 investigated the fabrication of meso-microvascular hierarchies and explored how stromal cell (SC) identity influenced endothelial cell (EC) morphogenesis and the formation of perfusable HVT. A microfluidic lab-on-a-chip system was adopted and modified to enable the formation of both microvascular capillary beds and mesovessels, and then used to evaluate inosculation between the two scales to support functional perfusion. The presence of supportive SC that can adopt perivascular phenotypes was essential, and lung fibroblasts (LF), dermal fibroblasts, and mesenchymal stem cells were compared and contrasted for their abilities to support EC morphogenesis and subsequent perfusion of the HVT. LF supported microvascular network

morphologies with the highest vessel density, diameter, and interconnectivity, and were the only SC type to support functional perfusion of the hierarchy. By comparing three SC types and their abilities to support the formation of multiscale HVT, this study provided insights regarding the choice of cells for vascular cell-based therapies and highlighted the importance of SC identity in the regulation of tissue-specific vasculature.

Aim 2 focused on incorporating a functional macrovessel to suture the HVT into circulation. We compared and contrasted vessels of venous, arterial, thoracic, and femoral origins for their ability to sprout EC capable of inosculating with surrounding microvasculature. We identified the thoracic aorta as the vessel yielding the greatest degree of sprouting and interconnection to surrounding capillaries and the only vessel capable of cannulation. The presence of cells undergoing vascular morphogenesis in the surrounding hydrogel attenuated EC sprouting from the macrovessel, but ultimately sprouted EC interacted with capillaries in the bulk supporting an interconnected HVT. This study yielded HVT suitable for surgical anastomosis and a platform to study vascular inosculation to provide insights for cell-based therapies.

Aim 3 focused on the biomanufacturing of fibrin-based tissue engineered vascular grafts for scale-up of HVT towards translational applications avoiding the need for autologous vessel harvest. Three-layered grafts mimicking the native tunica intima, media, and adventitia composed of smooth muscle cells (media layer), LF and EC (adventitial layer), and EC only (intima layer) were successfully engineered and evaluated. Cells in the adventitial layer formed a vasa vasorum that sprouted into surrounding hydrogels that also contained microvasculature and mesovessels to support the formation of integrated HVT. Extended adventitia culture was critical for integration across length scales. Overall, this dissertation integrated top-down and bottom-up fabrication

approaches towards the engineering of a complete HVT suitable for surgical anastomosis for translational regenerative medicine applications.

Chapter 1 – Introduction

1.1 The Need for Vascularization in Tissue Engineering

The field of tissue engineering (TE) operates at the intersection of biology and engineering to fabricate functional bioartificial constructs to replace damaged tissues or whole organs [1, 2]. The goal of the field is for these engineered tissue constructs to fulfil part or all of the functionality of the replaced tissue or organ. The need for transplantable organs significantly exceeds the availability of donor organs. Despite 2021 reaching the milestone of the most organ transplants in a single year, over 100,000 people are still awaiting a life-saving transplant and over 6,000 people per year still die awaiting an organ transplant [3] because the number of people on the waiting list far outweighs the number of donors available and the number of transplants performed (Fig. 1.1). The field of tissue engineering aims, in part, to solve this organ shortage through the development of tissues to maintain, restore, and improve biological tissue and organ function.
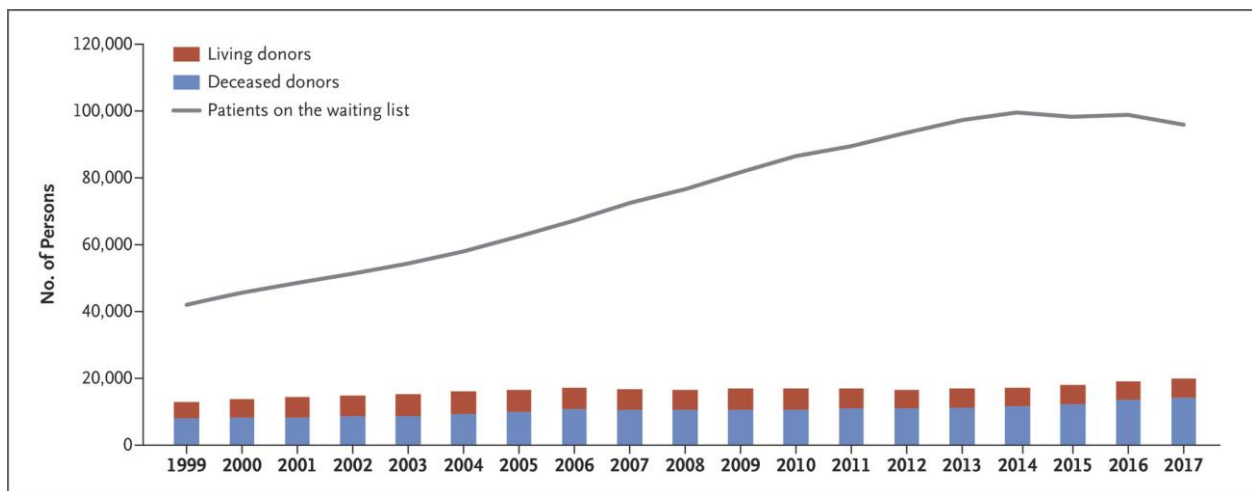
Figure 1.1: Organ waiting list and donor statistics. Number of patients waiting for a kidney transplant in comparison to the number of kidneys available from deceased and living donors in the United States. Image reproduced with permission from [4], Copyright 2018, Massachusetts Medical Society.

1

The fabrication of tissue engineered constructs traditionally requires three components: scaffolds, cells, and bioactive signaling molecules, together called the tissue engineering triad (Fig. 1.2). These three factors are critical to recapitulating properties of native tissues [5-7]. Each tissue within the body has its own set of material properties, cell identities, and growth factors (GF) that are essential for the proper function of that tissue and its replication in the lab. For vasculature, common scaffolding materials include fibrin, collagen, gelatin methacryloyl (GelMA), Matrigel, poly (ethylene glycol) (PEG), and poly-L-lactic acid (PLLA), and common cells include endothelial cells (EC), fibroblasts, and mesenchymal stem cells (MSC). These and other examples of vascular specific components of the TE triad are indicated in italics in Figure 1.2.
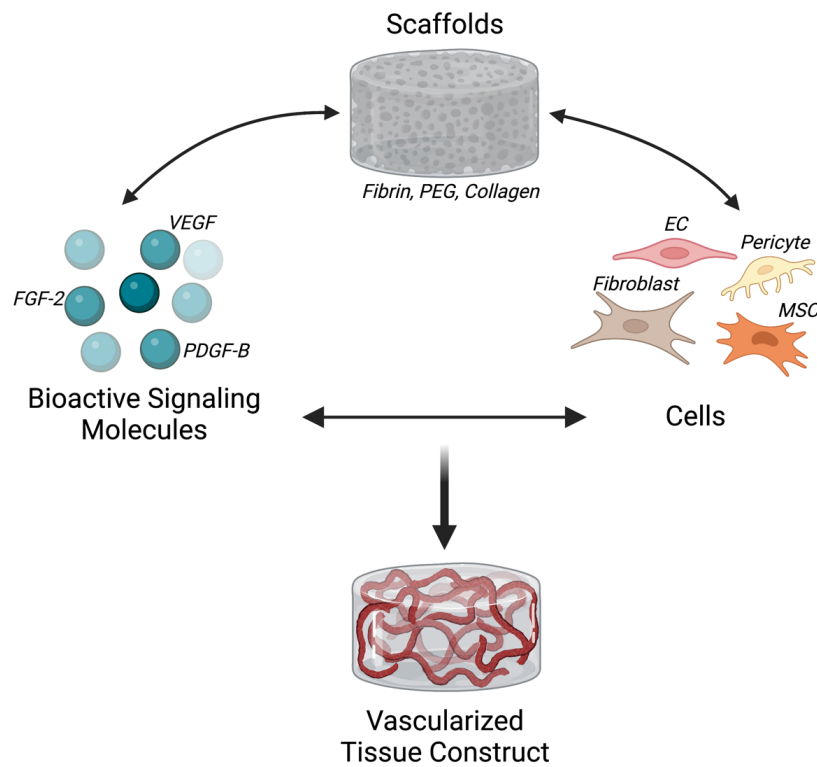
Figure 1.2: The tissue engineering triad. *Examples of vascular specific components are indicated in italics. Figure created with Biorender.com.*

Engineered vascular tissues are typically fabricated using all components of the TE triad. Biomaterial scaffolding is critical to mimic the native *in vivo* tissue environment, EC and stromal

cells (SC) are critical to the formation of functional vessels, and growth factors are critical to support EC morphogenesis into fully developed vasculature. The successful engineering of nearly all functional tissues requires a hierarchical vascular blood supply. With the exception of cartilage, cornea, and epithelial tissue, all native tissues are vascularized. Implantable tissues greater than 200 μm in thickness, the diffusion limit of nutrients and gasses in most solid tissues, may not remain viable upon implantation *in vivo* due to limited and untimely ingrowth of host vasculature [8]. This ingrowth rate is typically on the order of microns per day [9]. Therefore, implantable tissues must contain a preformed vascular network that can inosculate with the host upon implantation. A substantial number of studies have investigated engineered meso- and microvasculature *in vitro* [10-17] and *in vivo* [18-24]. However, engineered tissue constructs containing only meso- and microvasculature still do not inosculate with host vasculature immediately, and have been shown to take up to five days to connect with the host [25]. On the other hand, significant advancements have been made in engineered macrovessels suitable for surgical anastomosis [26-29], though these grafts do not solve the problem of capillary perfusion to parenchymal cells and surrounding tissues. Thus, it is critical that engineered tissues and organs contain a preformed hierarchical vasculature across length scales that can be sutured to the host blood supply via microsurgical anastomosis yielding immediate perfusion of the implanted engineered tissue or organ [30].

1.2 Fibrin as a Material for Tissue Engineering

Fibrin is a natural fibrous biomaterial found within the body. It is the primary component of provisional blood clots and is critical for wound healing and tissue regeneration [31]. Fibroblasts and other cells present at the wound site readily remodel the fibrin matrix and (among other things)

induce angiogenic sprouting to revascularize healing wounds. Therefore, fibrin has been a repeatedly used material in the field of TE for vascular applications.

The fibrin matrix is a conglomerate of fibrils that are crosslinked when fibrinogen, specifically fibrinopeptides A and B are cleaved by thrombin, a clotting enzyme (Fig. 1.3) [31]. Fibrinogen is a soluble protein dissolved in the blood until thrombin transforms it into the insoluble fibrin matrix [31]. In turn, fibrin clots are degraded primarily through the action of plasmin, a fibrinolytic protease. Plasminogen, a plasma protein also found in blood serum, is converted to the active form, plasmin, by urokinase-type plasminogen activator (uPa)-induced cleavage [32]. Plasmin is one of the key mediators, among others, of fibrin proteolysis allowing cells to degrade and move through the fibrin clot to form blood vessels to vascularize the wound site and begin the healing process.

Fibrin is well-suited as a biomaterial for tissue engineering applications as it is a natural, self-assembling, biocompatible material that cells can directly bind to, degrade, and remodel. EC and SC interact directly with the fibrin matrix through integrin binding to peptide sequences, including Arginine-Glycine-Aspartic Acid (RGD) [33, 34]. EC can additionally bind to fibrin via vascular endothelial cadherin (VE-cadherin) receptors, which normally mediate cell-cell interactions but also may be critical for vessel formation in 3D fibrin gels [35]. EC and SC can also interact indirectly with the fibrin matrix through basement membrane (BM) proteins, which are capable of binding to the fibrin matrix. In particular, fibronectin found in blood serum and/or secreted by EC is an important component of the vascular BM. Additionally, GF such as fibroblast growth factor-2 (FGF-2) and vascular endothelial growth factor (VEGF), which aid in the vascularization of provisional fibrin matrices at wound sites, are capable of binding to fibrin.

In tissue engineered fibrin matrices, it has been shown that uPa and its receptor, uPAR, are required for EC migration and the formation of capillary-like structures [36, 37]. Yet, there are also other mechanisms of fibrin degradation induced by cell secreted molecules. EC and SC must degrade the fibrin matrix to migrate and form vessels within the material. Another family of matrix-degrading enzymes, termed matrix metalloproteinases (MMP), also play important roles in this process in addition to plasmin-mediated degradation. Our lab has shown that EC employ different mechanisms of fibrin degradation (e.g., plasmin- or MMP-mediated) and utilize different types of MMPs in manner that depends on the identity of the SC in both vasculogenic and angiogenic co-culture models [10, 38]. These studies showed that in addition to cell-ECM interactions, cell-cell interactions and paracrine signaling are critically important factors in vascularizing engineered fibrin matrices.
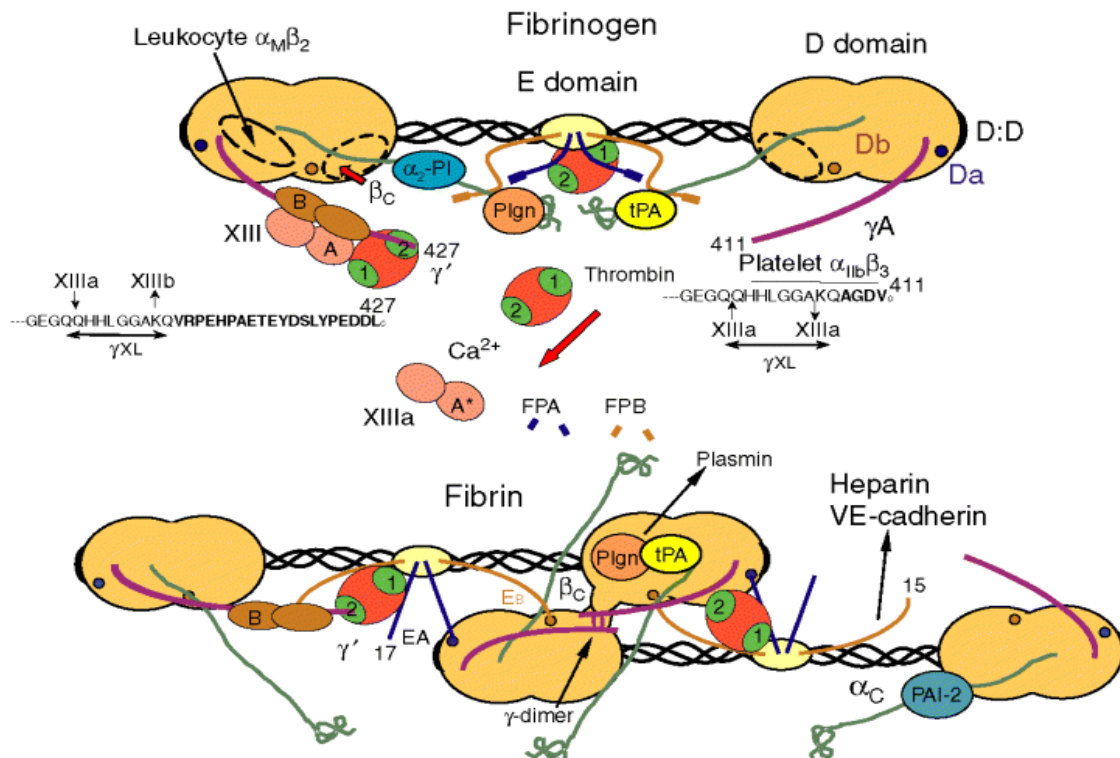
Figure 1.3: Fibrin Assembly. *Schematic diagram of fibrinogen structure, its conversion to fibrin, and the thrombin-mediated conversion of native factor XIII to XIIIa. Binding sites for proteins, enzymes, receptors, and other molecules that participate in fibrin(ogen) functions are illustrated. Reproduced with permission from Elsevier from reference [39]. Copyright 2005, International Society on Thrombosis and Haemostasias.*

1.3 The Role and Importance of Stromal Cells at All Vascular Length Scales

SC provide critical support for blood vessels at all length scales during morphogenesis, and for maturation and proper functioning [40]. SC are found in abundance throughout the body, making up the connective tissue of nearly all organs. At the vascular level, SC can differentiate into constituents of the tunica media and tunica adventitia layers of blood vessels. In the context of this dissertation, SC is used as a somewhat general term that encompasses pericytes, mesenchymal stem/stromal cells (MSC), smooth muscle cells (SMC), and fibroblasts. Pericytes are a type of mesenchymal cell that reside within vessel wall of capillaries [41]. They have many functions including in vessel maturation, contractility, and regulation of vascular permeability.

During development, the vasculature is formed by a process called vasculogenesis, the *de novo* formation of a primitive vascular network, in which angioblasts cluster into cord-like vessel structures and subsequently lumenize (Fig. 1.4) [42, 43]. Through angiogenesis, the sprouting of new vessels from existing blood vessels, the primitive vascular plexus remodels into an arteriovenous vascular network making up the human circulatory system (Fig. 1.4). After primitive vessels and vessel networks are formed, SC play a crucial role in vessel remodeling, maturation, and stabilization through both direct and indirect EC-SC interactions [44, 45]. At the capillary scale, EC secrete platelet-derived growth factor B (PDGFB) to recruit PDGFR-β expressing SC to the vessel wall (Fig. 1.5) [46-49]. The secretion of this GF results in SC migration towards developing blood vessels, leading to perivascular association of SC and consequently maturation of the blood vessel. There are many additional GF critical to the maturation of blood vessels, including the angiopoietin family of GF, sphingosine-1 phosphate (S1P), and transforming growth factor-beta (TGF-β), among many others [50, 51]. An important aspect of blood vessel maturation is the development of tight barrier function enacted by EC, which form the barrier between blood

and all surrounding tissues, only permitting the passage of fluids, nutrients, waste products, and some cells. Once SC are recruited to the vessel wall, EC and SC maintain close association through cell-cell and cell-ECM junctions to maintain proper barrier function. To promote EC quiescence and vessel maturation, SC secrete BM proteins and angiopoietin 1 (Ang-1). EC bind to Ang-1 secreting SC via Tie-2 receptors (Fig. 1.5) [52, 53]. These signals further induce capillary maturation by inducing the formation of EC-EC junctions through VE-cadherin. These VE-cadherin junctions ensure vessels maintain a tight, non-leaky barrier by preventing VEGF induced sprouting.

Capillaries consist of a small number of SC (pericytes specifically) in relation to the number of EC. The ratio of EC to pericytes and percentage of vessels covered with pericytes varies widely between tissues depending on the capillary function within the tissue. The ratio of EC to pericytes can vary from 1:1 to 10:1 while the pericyte coverage can range from 10 to 70% [54]. These capillary-associated SC are typically localized to EC cell-cell junctions. In contrast, larger arterioles and arteries are wrapped in sheaths of SC, primarily SMC, concentrically wrapped around the endothelial intima. Concurrent with development of larger vessels from the vascular plexus, pericytes differentiate into SMC (Fig. 1.4) [55, 56]. Arterioles, the next scale up from capillaries, have one to five rings of SMC, while large muscular arteries are composed of a much thicker SMC layer. In larger vessels with a greater distance between the vessel lumen and surrounding tissues, SC are responsible for different functions. In the arterioles, the SMC are responsible for regulating vascular tone [57, 58]. EC secrete vasoactive signals causing the SMC to constrict or dilate the vessel accordingly. In large arteries, SMC help maintain the high blood pressure within the vessel needed to transport blood throughout the entire vascular system [59]. Additionally, SC in the adventitia layers of large vessels support the development of a network of

capillaries called the vasa vasorum, which supplies blood to the large quantity of cells within the thick vessel wall. Overall, SC play a critical role at all levels of the vascular system and help maintain the proper functioning of the vascular system.
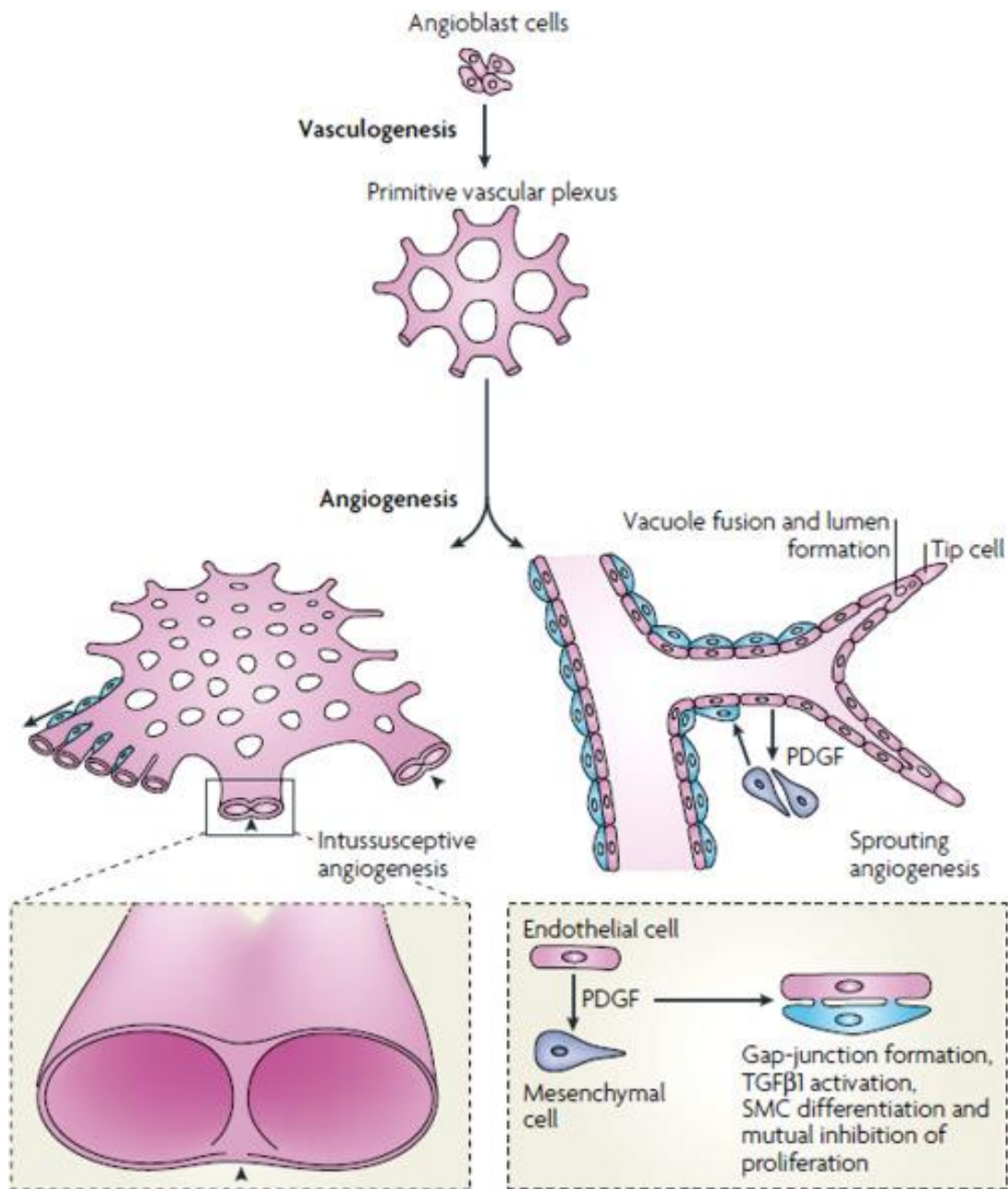
Figure 1.4: Vasculogenesis and Angiogenesis. *The differentiation of angioblasts, or endothelial precursor cells, from mesoderm and the formation of primitive vascular plexus from angioblasts are the two distinct steps during the onset of vascularization that together constitute vasculogenesis. Angiogenesis refers to the growth of new capillaries from preexisting blood vessels either via sprouting or intussusception. Reproduced with permission from Elsevier from reference [42]. Copyright 2016, Elsevier Inc.*
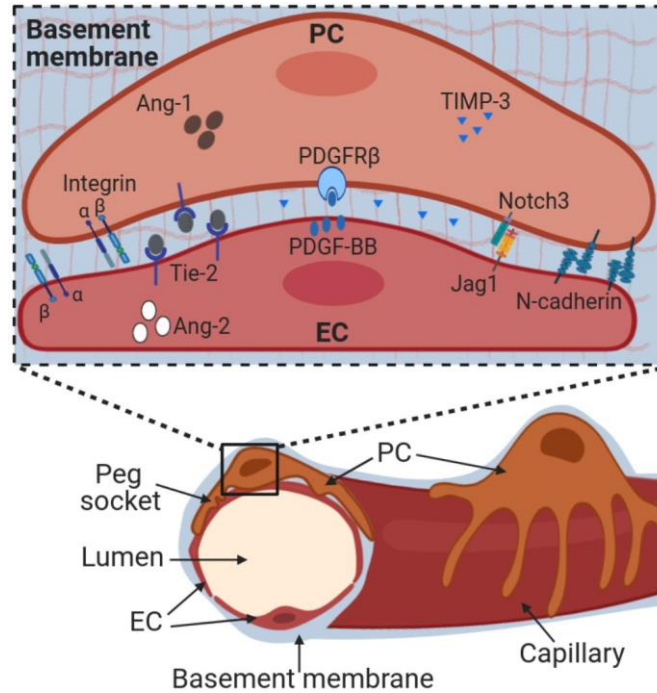
Figure 1.5: Pericyte-endothelial interactions. *Pericytes are embedded into a basement membrane that is shared with endothelial cells and composed primarily by collagen IV and laminins. Adherence to the basement membrane occurs via integrins. Pericyte adherence to endothelial cells at 'peg and socket' connections is mediated by N-cadherins and other junctional proteins. Pericyte-endothelial cell cross-talk occurs through multiple molecular pathways, including PDGF-BB/PDGFRβ, Notch receptors and ligands, Angiopoietin-Tie2 and TIMPs. Alteration of these interactions directly impacts pericyte-endothelial interactions and ultimately vessel stability. Ang-1, angiopoietin-1; Ang-2, angiopoietin-2; EC, endothelial cells; Jag1, Jagged1; PC, pericytes; PDGF-BB, platelet derived growth factor; PDGFRβ, PDGF receptor β; TIMP-3, tissue inhibitor of matrix metalloproteinases-3. Reproduced from reference [49], used under Creative Commons CC BY license. Copyright 2020, Nwadozi, E., et al.*

1.4 Specific Aims

The following specific aims were proposed to achieve the overarching goal of this dissertation to bring tissue engineered hierarchical vascular tissue constructs suitable for surgical anastomosis closer to realization.

Aim 1: Investigate the influence of stromal cell identity on the formation of perfusable two-scale hierarchical vascular networks. This aim focused on integrating engineered capillary networks and mesovessels to fabricate a two-scale hierarchical vascular tissue construct. Meso-

vessels formed by sacrificial templating and subsequent seeding of ~300 µm diameter channels were integrated with capillary networks formed by co-cultures of EC with three different SC types embedded within fibrin hydrogels in order to directly compare the effects of SC identity. Physical (capillary diameter, density, and interconnectedness) and functional (mesovessel patency and perfusion, meso-microvessel integration, and capillary perfusion) metrics were quantified at multiple timepoints.

Aim 2: Integrate functional macro-scale vessels and engineered capillaries to yield a hierarchical tissue construct suitable for surgical anastomosis. This aim assessed the integration of functional macrovessels and engineered capillaries. Hierarchical vascular networks were fabricated by embedding *ex vivo* murine vessels within cellularized fibrin hydrogels, enabling self-assembly of microvasculature capable of inosculating with the larger vessel. Macrovessels of different origins were explored (arterial and venous, thoracic and femoral). Endothelial cell sprouting was quantified using two metrics, percentage of explant perimeter that sprouted and sprout distance into the hydrogel from the explant edge, at multiple timepoints. The morphology of sprouted endothelial cells and inosculation with capillaries in the bulk hydrogel were analyzed. The impact of sprouting on hydrogel mechanical properties was analyzed as well as the correlation between endothelial sprouting and hydrogel stiffening.

Aim 3: Create tissue engineered vascular grafts (TEVG) to adapt and scale-up hierarchical vascular tissue constructs towards translational applications. In this aim, the scale-up of hierarchical vascular tissue constructs towards clinical utility was assessed by fabricating TEVG to use in place of the explanted murine macrovessels in Aim 2. A three-layer TEVG was fabricated, mimicking the native three-layer morphology of native arteries (i.e., tunica intima, tunica media, and tunica adventitia). The adventitia layer was analyzed for the formation

of a vasa vasorum, the media layer was analyzed for proper smooth muscle cell alignment, and the fabrication of a complete endothelial cell monolayer was analyzed within the intima layer. Further, this aim sought to integrate the meso- and microvascular hierarchy developed in Aim 1 to engineer a complete vascular hierarchy containing all three vascular length scales suitable for surgical anastomosis. The overall construct size was scaled by ~20-fold from Aim 1 yielding a more clinically translatable tissue. Integration and inosculation between macro- and microvasculature and meso- and microvasculature were analyzed via confocal microscopy and via dextran perfusion.

1.5 Translational Potential

Clinical translation of engineered tissues and organs requires approval by the Food and Drug Administration (FDA). There are currently no FDA approved and successfully commercialized cellular solid tissues and organs. The regulatory hurdle for new biomaterials is significant as biocompatibility with the human body must be determined; however, for materials that are deemed substantially equivalent to existing approved devices, the path to market is much clearer through the 510(k) pathway [60]. Fibrin is FDA cleared as a sealant and a sealant patch [61] and therefore an engineered vascular tissue construct fabricated from this material may have an easier route to clinical translation.

Despite the use of an approved biomaterial within this dissertation, there is still the regulatory hurdle associated with the use of human-derived cells. There are currently no approved therapies that are categorized as tissue and tissue products and fewer than 30 therapies categorized as cellular and gene therapy products have been approved by the FDA [62]. Beyond biocompatibility and safety, efficacy is a critical hurdle for cellular therapies, particularly autologous cell therapies where variability between cells from different patients exists.

Additionally, the approval of combination products composed of a drug, device, or biological products presents additional hurdles for clinical translation [63]. Therefore, while the long-range goals of the strategies described in this dissertation include eventual clinical translation, the final hierarchical tissue construct presented in Aim 3 represents a proof-of-concept for such a construct that, with more research and development, could be applied towards clinical applications for patients.

The models presented herein may provide insights to better engineer vascular tissue constructs for implantation and study drug development. The model developed in Aim 1 could be further developed towards emulating tissue specific vasculature and subsequently used to study drug interactions with the vascular system within specific parenchymal tissues. The model developed in Aim 2 could be used to better study host-implant vascular inosculation without long-term, costly animal studies. Despite numerous studies investigating vascular development *in vitro* and the ability of engineered vasculature to function *in vivo*, to my knowledge only one study has investigated mechanisms of host-implant vascular inosculation [64]. However, this study required the use of specialized knockout mouse models and complex intravital imaging technologies. The model developed in Aim 2 of this thesis can be used with standard mouse strains, is performed in simple three-dimensional (3D) hydrogels, and only requires more standard confocal microcopy techniques, thereby providing an easier methodology to investigate how engineered vasculature interacts and inosculates with host vasculature, which could greatly improve engineered vascular constructs and aid more rapid clinical translation. Finally, the TEVG and hierarchical vascular tissue construct developed in Aim 3 could be used to better understand arteriogenesis and how implanted vascular grafts integrate with the surrounding tissue. If implanted *in vivo*, many questions could be answered including but not limited to how quickly arteriogenesis is initiated

and how it progresses, how the composition of the vessel wall impacts integration of blood vessels across length scales, and how sprouting from a macrovessel could support the proper functioning of implanted parenchymal cells (e.g., transplanted islets or muscle cells).

1.6 Overview of Dissertation

The overarching goal of this dissertation was to engineer a complete hierarchical vascular tissue construct suitable for surgical anastomosis. To accomplish this, three distinct methodologies were used to fabricate vessels of each caliber. Macro-scale vessels were created using a two-step annular molding process, meso-scale vessels were fabricated using sacrificial needle templating and subsequent cell seeding, and microvessels were fabricated by vascular self-assembly in a manner akin to developmental vasculogenesis. Chapter 1 highlighted the motivation for the dissertation, the specific aims to address the overarching goal, and the translational potential of the work.

Chapter 2, currently under review at *Trends in Biotechnology*, provides background information on the native vascular hierarchy, previous work in engineering vessels of each caliber, and recent advances in engineering hierarchical vasculature. Chapter 2 includes an assessment of the current state of the art in vascularization and how best to proceed towards meeting the grand challenge of the TE field, manufacturing a hierarchical vascular tissue construct for transplanting functional engineered tissues. The remaining chapters present my own original experimental work towards engineering hierarchical vascular tissue constructs.

To address Aim 1 of this thesis, the studies described in Chapter 3 utilized a microfluidic chip platform to engineer perfusable two-scale hierarchical tissue constructs composed of mesovessels and capillaries. This work revealed that EC co-cultured with lung fibroblasts (LF)

resulted in a dense, interconnected capillary network that inosculated with patent and perfusable mesovessels, yielding an interconnected two-scale hierarchy. Dermal fibroblast (DF)- and mesenchymal stem cell (MSC)-supported capillary networks failed to yield perfusable hierarchies. Parts of Chapter 3 were published in *Lab on a Chip* in 2021 following peer review.

In Chapter 4, explanted mouse vessels were integrated *ex vivo* with human engineered capillary networks. This work showed that macrovessels can sprout from the longitudinal edge of the vessel into surrounding acellular and cellular fibrin matrices, despite the dogmatic view that presumably quiescent vessels only sprout from cut or damaged ends. Sprouting was diminished in the presence of human cells, yet sprouted endothelial cells did interact with self-assembled capillaries in the surrounding cellular fibrin gel yielding chimeric, hierarchical vascular structures. This chapter is in preparation for submission as a peer-reviewed journal article.

In Chapter 5, this work was scaled-up towards translational applications by exchanging the explanted mouse vessel for a newly developed TEVG. The mesovessel length was increased 3.67-fold from Chapter 3 and the overall tissue volume was scaled ~20-fold from Chapter 3 and 1.5-fold from Chapter 4. Further, all three length scales were integrated into one single tissue construct to create a complete vascular hierarchy suitable for surgical anastomosis. TEVG were composed of a tunica media (SMC in fibrin) and tunica adventitia (LF and EC in fibrin) fabricated via sequential annular molding and a tunica intima (EC monolayer) fabricated by seeding the inner lumen of the graft with EC. This work ultimately yielded a complete proof-of-concept three-scale hierarchical vascular tissue construct that was perfusable across two length scales. This chapter is in preparation for submission as a peer-reviewed journal article.

Finally, a summary of key findings is presented in Chapter 6. Additionally, future directions for each aim are presented. The model systems developed in Aims 1 and 2 could be

applied to study a number of mechanistic questions about vascular morphogenesis and integration of engineered tissue constructs with host tissues. The tissue construct engineered in Aim 3 represents a proof-of-concept for the idea of a complete vascular hierarchy that could be further developed and implemented clinically to treat a myriad of diseases, or towards developing organ-specific vasculature and tissue implants.

1.7 References

[1]   Petit-Zeman, S. (2001) Regenerative medicine. *Nat Biotechnol* 19, 201-206

[2]   Langer, R. and Vacanti, J.P. (1993) Tissue engineering. *Science* 260, 920-926

[3]   Organ, Eye and Tissue Donation Statistics. https://www.donatelife.net/statistics/

[4]   Tullius, S.G. and Rabb, H. (2018) Improving the Supply and Quality of Deceased-Donor Organs for Transplantation. *New England Journal of Medicine* 378, 1920-1929

[5]   O'Brien, F.J. (2011) Biomaterials & scaffolds for tissue engineering. *Materials Today* 14, 88-95

[6]   Murphy, W.L., McDevitt, T.C., and Engler, A.J. (2014) Materials as stem cell regulators. *Nat Mater* 13, 547-557

[7]   Nurzynska, D., Iruegas, M.-E.P., Castaldo, C., Müller-Best, P., and Di Meglio, F. (2013) Application of Biotechnology in Myocardial Regeneration-Tissue Engineering Triad: Cells, Scaffolds, and Signaling Molecules. *BioMed Research International* 2013, 236893

[8]   Rouwkema, J., Rivron, N.C., and van Blitterswijk, C.A. (2008) Vascularization in tissue engineering. *Trends Biotechnol* 26, 434-441

[9]   Laschke, M.W., Vollmar, B., and Menger, M.D. (2009) Inosculation: connecting the life-sustaining pipelines. *Tissue Eng Part B Rev* 15, 455-465

[10]   Ghajar, C.M., Kachgal, S., Kniazeva, E., Mori, H., Costes, S.V., George, S.C., and Putnam, A.J. (2010) Mesenchymal cells stimulate capillary morphogenesis via distinct proteolytic mechanisms. *Exp Cell Res* 316, 813-825

[11]   Ghajar, C.M., Blevins, K.S., Hughes, C.C., George, S.C., and Putnam, A.J. (2006) Mesenchymal stem cells enhance angiogenesis in mechanically viable prevascularized tissues via early matrix metalloproteinase upregulation. *Tissue Eng* 12, 2875-2888

[12] Crosby, C.O., Hillsley, A., Kumar, S., Stern, B., Parekh, S.H., Rosales, A., and Zoldan, J. (2021) Phototunable interpenetrating polymer network hydrogels to stimulate the vasculogenesis of stem cell-derived endothelial progenitors. *Acta Biomater* 122, 133-144

[13] Morin, K.T., Dries-Devlin, J.L., and Tranquillo, R.T. (2014) Engineered microvessels with strong alignment and high lumen density via cell-induced fibrin gel compaction and interstitial flow. *Tissue Eng Part A* 20, 553-565

[14] Mandrycky, C., Hadland, B., and Zheng, Y. (2020) 3D curvature-instructed endothelial flow response and tissue vascularization. *Sci Adv* 6

[15] Price, G.M., Wong, K.H., Truslow, J.G., Leung, A.D., Acharya, C., and Tien, J. (2010) Effect of mechanical factors on the function of engineered human blood microvessels in microfluidic collagen gels. *Biomaterials* 31, 6182-6189

[16] Linville, R.M., Boland, N.F., Covarrubias, G., Price, G.M., and Tien, J. (2016) Physical and Chemical Signals That Promote Vascularization of Capillary-Scale Channels. *Cell Mol Bioeng* 9, 73-84

[17] Andree, B., Ichanti, H., Kalies, S., Heisterkamp, A., Strauss, S., Vogt, P.M., Haverich, A., and Hilfiker, A. (2019) Formation of three-dimensional tubular endothelial cell networks under defined serum-free cell culture conditions in human collagen hydrogels. *Sci Rep* 9, 5437

[18] Chen, Y.C., Lin, R.Z., Qi, H., Yang, Y., Bae, H., Melero-Martin, J.M., and Khademhosseini, A. (2012) Functional Human Vascular Network Generated in Photocrosslinkable Gelatin Methacrylate Hydrogels. *Adv Funct Mater* 22, 2027-2039

[19] Friend, N.E., Rioja, A.Y., Kong, Y.P., Beamish, J.A., Hong, X., Habif, J.C., Bezenah, J.R., Deng, C.X., Stegemann, J.P., and Putnam, A.J. (2020) Injectable pre-cultured tissue modules catalyze the formation of extensive functional microvasculature in vivo. *Sci Rep* 10, 15562

[20] Li, S., Nih, L.R., Bachman, H., Fei, P., Li, Y., Nam, E., Dimatteo, R., Carmichael, S.T., Barker, T.H., and Segura, T. (2017) Hydrogels with precisely controlled integrin activation dictate vascular patterning and permeability. *Nat Mater* 16, 953-961

[21] Kang, K.T., Lin, R.Z., Kuppermann, D., Melero-Martin, J.M., and Bischoff, J. (2017) Endothelial colony forming cells and mesenchymal progenitor cells form blood vessels and increase blood flow in ischemic muscle. *Sci Rep* 7, 770

[22] Zhang, B., Montgomery, M., Chamberlain, M.D., Ogawa, S., Korolj, A., Pahnke, A., Wells, L.A., Masse, S., Kim, J., Reis, L., Momen, A., Nunes, S.S., Wheeler, A.R., Nanthakumar, K., Keller, G., Sefton, M.V., and Radisic, M. (2016) Biodegradable scaffold with built-in vasculature for organ-on-a-chip engineering and direct surgical anastomosis. *Nat Mater* 15, 669-678

[23] Redd, M.A., Zeinstra, N., Qin, W., Wei, W., Martinson, A., Wang, Y., Wang, R.K., Murry, C.E., and Zheng, Y. (2019) Patterned human microvascular grafts enable rapid vascularization and increase perfusion in infarcted rat hearts. *Nat Commun* 10, 584

[24] Mirabella, T., MacArthur, J.W., Cheng, D., Ozaki, C.K., Woo, Y.J., Yang, M., and Chen, C.S. (2017) 3D-printed vascular networks direct therapeutic angiogenesis in ischaemia. *Nat Biomed Eng* 1

[25] Chen, X., Aledia, A.S., Ghajar, C.M., Griffith, C.K., Putnam, A.J., Hughes, C.C., and George, S.C. (2009) Prevascularization of a fibrin-based tissue construct accelerates the formation of functional anastomosis with host vasculature. *Tissue Eng Part A* 15, 1363-1371

[26] Kirkton, R.D., Santiago-Maysonet, M., Lawson, J.H., Tente, W.E., Dahl, S.L.M., Niklason, L.E., and Prichard, H.L. (2019) Bioengineered human acellular vessels recellularize and evolve into living blood vessels after human implantation. *Sci Transl Med* 11

[27] Luo, J., Qin, L., Zhao, L., Gui, L., Ellis, M.W., Huang, Y., Kural, M.H., Clark, J.A., Ono, S., Wang, J., Yuan, Y., Zhang, S.M., Cong, X., Li, G., Riaz, M., Lopez, C., Hotta, A., Campbell, S., Tellides, G., Dardik, A., Niklason, L.E., and Qyang, Y. (2020) Tissue-Engineered Vascular Grafts with Advanced Mechanical Strength from Human iPSCs. *Cell Stem Cell* 26, 251-261 e258

[28] Syedain, Z.H., Graham, M.L., Dunn, T.B., O'Brien, T., Johnson, S.L., Schumacher, R.J., and Tranquillo, R.T. (2017) A completely biological "off-the-shelf" arteriovenous graft that recellularizes in baboons. *Sci Transl Med* 9

[29] Li, X., Xu, J., Bartolak-Suki, E., Jiang, J., and Tien, J. (2020) Evaluation of 1-mm-diameter endothelialized dense collagen tubes in vascular microsurgery. *J Biomed Mater Res B Appl Biomater* 108, 2441-2449

[30] Sekine, H., Shimizu, T., Sakaguchi, K., Dobashi, I., Wada, M., Yamato, M., Kobayashi, E., Umezu, M., and Okano, T. (2013) In vitro fabrication of functional three-dimensional tissues with perfusable blood vessels. *Nat Commun* 4, 1399

[31] Ceccarelli, J. and Putnam, A.J. (2014) Sculpting the blank slate: how fibrin's support of vascularization can inspire biomaterial design. *Acta Biomater* 10, 1515-1523

[32] Kroon, M.E., Koolwijk, P., van Goor, H., Weidle, U.H., Collen, A., van der Pluijm, G., and van Hinsbergh, V.W. (1999) Role and localization of urokinase receptor in the formation of new microvascular structures in fibrin matrices. *Am J Pathol* 154, 1731-1742

[33] Gailit, J., Clarke, C., Newman, D., Tonnesen, M.G., Mosesson, M.W., and Clark, R.A. (1997) Human fibroblasts bind directly to fibrinogen at RGD sites through integrin alpha(v)beta3. *Exp Cell Res* 232, 118-126

[34] Pierschbacher, M.D. and Ruoslahti, E. (1984) Cell attachment activity of fibronectin can be duplicated by small synthetic fragments of the molecule. *Nature* 309, 30-33

[35] Bach, T.L., Barsigian, C., Yaen, C.H., and Martinez, J. (1998) Endothelial cell VE-cadherin functions as a receptor for the beta15-42 sequence of fibrin. *J Biol Chem* 273, 30719-30728

[36] Koolwijk, P., van Erck, M.G., de Vree, W.J., Vermeer, M.A., Weich, H.A., Hanemaaijer, R., and van Hinsbergh, V.W. (1996) Cooperative effect of TNFalpha, bFGF, and VEGF on the formation of tubular structures of human microvascular endothelial cells in a fibrin matrix. Role of urokinase activity. *J Cell Biol* 132, 1177-1188

[37] Pepper, M.S., Sappino, A.P., Stocklin, R., Montesano, R., Orci, L., and Vassalli, J.D. (1993) Upregulation of urokinase receptor expression on migrating endothelial cells. *J Cell Biol* 122, 673-684

[38] Beamish, J.A., Juliar, B.A., Cleveland, D.S., Busch, M.E., Nimmagadda, L., and Putnam, A.J. (2019) Deciphering the relative roles of matrix metalloproteinase- and plasmin-mediated matrix degradation during capillary morphogenesis using engineered hydrogels. *J Biomed Mater Res B Appl Biomater* 107, 2507-2516

[39] Mosesson, M.W. (2005) Fibrinogen and fibrin structure and functions. *J Thromb Haemost* 3, 1894-1904

[40] Bergers, G. and Song, S. (2005) The role of pericytes in blood-vessel formation and maintenance. *Neuro Oncol* 7, 452-464

[41] Attwell, D., Mishra, A., Hall, C.N., O'Farrell, F.M., and Dalkara, T. (2016) What is a pericyte? *J Cereb Blood Flow Metab* 36, 451-455

[42] Kolte, D., McClung, J.A., and Aronow, W.S. (2016) Chapter 6 Vasculogenesis and Angiogenesis. In *Translational Research in Coronary Artery Disease*, pp. 49-65

[43] Davis, G.E., Stratman, A.N., Sacharidou, A., and Koh, W. (2011) Molecular basis for endothelial lumen formation and tubulogenesis during vasculogenesis and angiogenic sprouting. *Int Rev Cell Mol Biol* 288, 101-165

[44] Hughes, C.C. (2008) Endothelial-stromal interactions in angiogenesis. *Curr Opin Hematol* 15, 204-209

[45] Stratman, A.N., Malotte, K.M., Mahan, R.D., Davis, M.J., and Davis, G.E. (2009) Pericyte recruitment during vasculogenic tube assembly stimulates endothelial basement membrane matrix formation. *Blood* 114, 5091-5101

[46] Hellstrom, M., Kalen, M., Lindahl, P., Abramsson, A., and Betsholtz, C. (1999) Role of PDGF-B and PDGFR-beta in recruitment of vascular smooth muscle cells and pericytes during embryonic blood vessel formation in the mouse. *Development* 126, 3047-3055

[47] Lindahl, P., Johansson, B.R., Leveen, P., and Betsholtz, C. (1997) Pericyte loss and microaneurysm formation in PDGF-B-deficient mice. *Science* 277, 242-245

[48] Benjamin, L.E., Hemo, I., and Keshet, E. (1998) A plasticity window for blood vessel remodelling is defined by pericyte coverage of the preformed endothelial network and is regulated by PDGF-B and VEGF. *Development* 125, 1591-1598

[49] Nwadozi, E., Rudnicki, M., and Haas, T.L. (2020) Metabolic Coordination of Pericyte Phenotypes: Therapeutic Implications. *Front Cell Dev Biol* 8, 77

[50] Iivanainen, E., Nelimarkka, L., Elenius, V., Heikkinen, S.M., Junttila, T.T., Sihombing, L., Sundvall, M., Maatta, J.A., Laine, V.J., Yla-Herttuala, S., Higashiyama, S., Alitalo, K., and Elenius, K. (2003) Angiopoietin-regulated recruitment of vascular smooth muscle cells by endothelial-derived heparin binding EGF-like growth factor. *FASEB J* 17, 1609-1621

[51] Gaengel, K., Genove, G., Armulik, A., and Betsholtz, C. (2009) Endothelial-mural cell signaling in vascular development and angiogenesis. *Arterioscler Thromb Vasc Biol* 29, 630-638

[52] Davis, S., Aldrich, T.H., Jones, P.F., Acheson, A., Compton, D.L., Jain, V., Ryan, T.E., Bruno, J., Radziejewski, C., Maisonpierre, P.C., and Yancopoulos, G.D. (1996) Isolation of angiopoietin-1, a ligand for the TIE2 receptor, by secretion-trap expression cloning. *Cell* 87, 1161-1169

[53] Wakui, S., Yokoo, K., Muto, T., Suzuki, Y., Takahashi, H., Furusato, M., Hano, H., Endou, H., and Kanai, Y. (2006) Localization of Ang-1, -2, Tie-2, and VEGF expression at endothelial-pericyte interdigitation in rat angiogenesis. *Lab Invest* 86, 1172-1184

[54] Geevarghese, A. and Herman, I.M. (2014) Pericyte-endothelial crosstalk: implications and opportunities for advanced cellular therapies. *Transl Res* 163, 296-306

[55] Nehls, V. and Drenckhahn, D. (1991) Heterogeneity of microvascular pericytes for smooth muscle type alpha-actin. *J Cell Biol* 113, 147-154

[56] Hirschi, K.K. and D'Amore, P.A. (1996) Pericytes in the microvasculature. *Cardiovasc Res* 32, 687-698

[57] Dora, K.A. (2016) Endothelial-smooth muscle cell interactions in the regulation of vascular tone in skeletal muscle. *Microcirculation* 23, 626-630

[58] Tykocki, N.R., Boerman, E.M., and Jackson, W.F. (2017) Smooth Muscle Ion Channels and Regulation of Vascular Tone in Resistance Arteries and Arterioles. *Compr Physiol* 7, 485-581

[59] Wall, V.Z. and Bornfeldt, K.E. (2014) Arterial smooth muscle. *Arterioscler Thromb Vasc Biol* 34, 2175-2179

[60]   Prestwich, G.D., Bhatia, S., Breuer, C.K., Dahl, S.L., Mason, C., McFarland, R., McQuillan, D.J., Sackner-Bernstein, J., Schox, J., Tente, W.E., and Trounson, A. (2012) What is the greatest regulatory challenge in the translation of biomaterials to the clinic? *Sci Transl Med* 4, 160cm114

[61]   Fibrin. https://www.fda.gov/vaccines-blood-biologics/approved-blood-products/fibrin

[62]   Vaccines, Blood & Biologics. https://www.fda.gov/vaccines-blood-biologics

[63]   Tian, J., Song, X., Wang, Y., Cheng, M., Lu, S., Xu, W., Gao, G., Sun, L., Tang, Z., Wang, M., and Zhang, X. (2022) Regulatory perspectives of combination products. *Bioact Mater* 10, 492-503

[64]   Cheng, G., Liao, S., Kit Wong, H., Lacorre, D.A., di Tomaso, E., Au, P., Fukumura, D., Jain, R.K., and Munn, L.L. (2011) Engineered blood vessel networks connect to host vasculature via wrapping-and-tapping anastomosis. *Blood* 118, 4740-4749

Chapter 2 – Manufacturing the Multiscale Vascular Hierarchy: Progress Towards Solving Tissue Engineering's Grand Challenge

*This chapter is currently in review at *Trends in Biotechnology* following the approval of a pre-submission inquiry.

2.1 The Native Vascular Hierarchy

The field of regenerative medicine (RM) has captivated the attention of physicians, scientists, and patients alike, with the hope that engineered tissues and organs may become reality for individuals afflicted with traumatic injuries, birth defects, or awaiting an organ transplant. In the US alone there are more than 100,000 people on the organ transplant list, with a new person added every 9 minutes [1]. Groundbreaking developments, including the generation of induced pluripotent stem cells (iPSC), decellularized organs, 3D bioprinting, the FDA approval of engineered skin and cartilage products, and clinical trials for hollow organs and vessels, have furthered the field towards the brink of new therapies for the heart, kidney, lungs, and nearly every solid tissue and organ in the body. Despite numerous advancements, off-the-shelf organs to end the organ shortage and transplant waiting lists remain more promise than reality. The grand challenge of the field arguably remains the engineering of a fully interconnected, perfusable, hierarchical vascular tree. Solving this challenge is essential to enable the promise of engineered whole organs to be fulfilled.

The native vascular hierarchy within the human body consists of arteries, arterioles, capillaries, venules, and veins. Blood flows from the heart through the large caliber arteries to branching smaller arterioles and finally through the capillary beds [2, 3]. Nutrient and gas exchange occurs primarily in the capillary beds, along with the collection of waste products that are transported back through the venous system to the heart. Each of these vessels has unique anatomy to support the physiological function of the cardiovascular system (Fig. 2.1).

Vessels of all calibers have a tunica intima comprised of a single endothelial monolayer and a basement membrane (BM). The smallest vessels in the body, the capillaries, facilitate transport of oxygen, nutrients, and other small molecules and typically only have a single discontinuous layer of supportive pericytes beyond the tunica intima. These pericytes are critical for blood vessel formation, maintenance, and barrier function [4]. Pericytes are also characterized by alpha-smooth muscle actin (a-SMA) expression, which plays a role in maintaining the contractile tone of these blood vessels. There are three main categories of capillaries - continuous, fenestrated, and sinusoid - characterized by their different functions and their different endothelial and pericyte phenotypes. Continuous capillaries are characterized by tight cell-cell junctions permissive only to the transport of water, gases, and some small molecules. The endothelial cell (EC) monolayer and BM are completely intact. Fenestrated capillaries maintain tight cell-cell junctions, but also contain small pores between some cells and within the BM to allow the transport of larger molecules through the vessel wall. These capillaries are prevalent in tissues that require significant exchange between the blood and the tissues, such as the kidney and small intestine, responsible for filtration of waste products and absorption of nutrients from food, respectively. Finally, sinusoid capillaries are the leakiest. These capillaries lack tight cell-cell junctions leading to gaps in the endothelial monolayer permissive to the transport of very large molecules and some
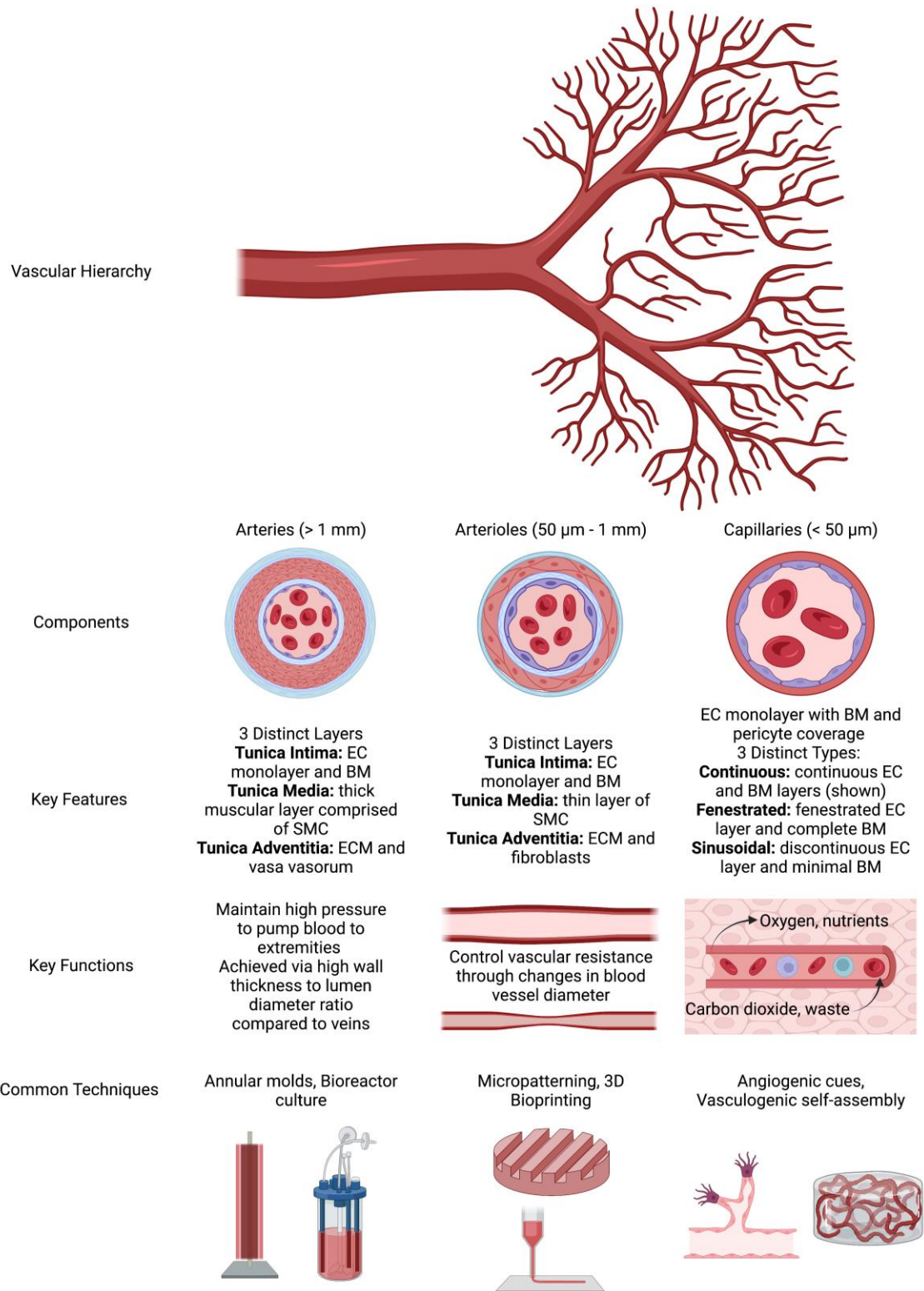
Figure 2.1: The native vascular hierarchy and methods for engineering the individual components. *The human vascular system is a complex hierarchical network with three main vessel types: arteries, arterioles, and capillaries. Arteries branch into smaller arterioles which branch further into a complex network of*

cells such as new blood cells and immune cells. In addition to gaps in the endothelial monolayer, these vessels have gaps in the BM layer and decreased pericyte coverage compared to that of continuous and fenestrated capillaries. Sinusoid capillaries are prevalent in the liver and bone marrow.

Arterioles, the next caliber of vessels, have a thicker vessel wall composed of 1-5 layers of smooth muscle cells (SMC), extracellular matrix (ECM), and adventitia [5]. The smooth muscle layers of these vessels are responsible for changes in diameter, and therefore blood flow, in response to tissues' needs for nutrients and oxygen. While the SMC enact changes in arteriole diameter, EC in the intimal layer sense and respond to shear stresses and inflammatory cues by secreting vasoactive compounds to signal the SMC to contract or relax, thereby regulating arteriole diameter. A critical result of this ability to change vessel diameter is dilation in response to both tissue hypoxia and high metabolic activity in downstream parenchymal tissues, both of which necessitate increased blood flow to the tissues.

Arteries, the largest caliber vessels, have a much thicker tunica media and tunica adventitia to support large volumes of blood flow and maintain blood pressure. Muscular arteries (e.g., femoral artery, brachial artery) have a thick tunica media composed of many layers of SMC and a thinner tunica adventitia compared to elastic arteries (e.g., aorta, pulmonary artery), which have a few layers of SMC and many layers of elastin, which allows for a constant maintenance of vessel pressure. The adventitial layer of these vessels is composed of supportive connective tissue and contains small capillaries, called the vasa vasorum, to supply nutrients to cells within thick vessel walls.

Despite the hierarchical nature of the cardiovascular system (Fig. 2.1), and the multi-length scale damage caused by cardiovascular diseases (CVD), many clinical interventions typically focus on a single length scale. For example, synthetic vascular grafts (e.g., Dacron) used to treat peripheral artery disease (PAD) bypass around a blockage in an artery to restore blood flow. With the advent of tissue engineering (TE), new biological grafts are being explored. Other clinical interventions involve an atherectomy to break up the blockage and the use of stents to hold the vessel open. These strategies show clinical benefit and have been successful, but they only focus on the blocked artery and do not address downstream damage to the tissues and/or occlusive disease in smaller caliber vessels. Newer regenerative medicine strategies have focused on injection of pro-angiogenic factors or cells to the downstream ischemic site to generate new blood vessels and reestablish capillary blood flow. These therapeutic angiogenesis strategies focus on revascularizing the necrotic tissues, but alone do not address the blocked artery which created the initial ischemia. To fully mitigate disease symptoms and progression, there is a significant, unmet need to restore perfusion across length scales from capillaries to arteries.

Hierarchical vasculature can potentially meet this need, and is similarly needed to engineer functional organs for transplant. Clinical successes in TE have been achieved in thin (e.g., skin) [6], tubular (e.g., urethra) [7], or hollow (e.g., bladder) [8] tissues and organs. These tissues and organs are typically characterized by their thin nature and lower complexity. By contrast, solid organ engineering has not yet reached clinical success due to the need for extensive vascularization throughout the entire thickness beyond diffusion limitations of ~200 μm [9] to support the large numbers of unique cell types needed to carry out each function within the organ. The development of more complex tissues or solid organs with unique vascular architectures has been stymied by the difficulty of engineering multiscale vasculature.

To engineer, and eventually transplant, a solid organ for clinical applications, a hierarchical vascular blood supply is needed. In this review, we highlight select recent advances in engineering vasculature at individual length scales, studies that have integrated two or more length scales into a primitive hierarchy, key anatomical features required for hierarchical and organ-specific vasculature, and key barriers to the translation of hierarchical vasculature. We conclude with our vision for furthering the engineering of hierarchical vascular constructs for clinical utility.

2.2 Engineering the Vascular Tree

Over the past few decades, significant research efforts have focused on engineering various components of the native vascular hierarchy, but the integration of these components across length scales in the context of TE is a more recent endeavor. For this review, capillaries are considered <50 μm in diameter, mesoscale vessels are considered 50-1000 μm, and vascular grafts are considered >1 mm.

2.2.1 Tissue engineered vascular grafts

Since the 1950s, synthetic materials, such as Dacron, expanded polytetrafluoroethylene (ePTFE), and polyurethane [10], have been used as vascular grafts for repair of large diameter vessels. These medical devices have high patency rates (>90%) for large diameter vessel applications (e.g., in the treatment of aortic aneurysms), but are not well-suited for small diameter (< 6 mm) applications due in part to compliance mismatch with native vessels that can give rise to disturbed blood flow, which in turn contributes to the formation of acute thrombi and chronic stenosis [11]. Instead of synthetic grafts, such smaller diameter applications, including coronary

artery bypass grafting (CABG), typically use autologous vessels such as the saphenous vein or mammary artery. However, these autologous vessels vary in quality from patient to patient due to age, cardiovascular health, and other comorbidities. Saphenous vein grafts also present potential compliance mismatch complications when used in arterial applications. To overcome these limitations, tissue engineered vascular grafts (TEVG) have been a major focus of the TE/RM community for nearly 30 years.

TEVG fabrication typically combines vascular cells with tubular scaffolds composed of natural and/or synthetic hydrogels, degradable polymers, or decellularized human and animal tissues. Natural hydrogels and decellularized tissues are generally biocompatible and biodegradable, but often lack the mechanical integrity required to withstand burst pressures in the arterial system. While the mechanical properties of natural materials have been improved via chemical crosslinking, synthetic materials, including both macroporous polymeric scaffolds and hydrogels, have also been extensively explored and offer the potential advantages of better mechanical tunability and control of cell adhesion and degradation. TEVG fabricated from either natural or synthetic scaffolds have also been matured via mechanotransduction strategies, typically involving mechanical loading in perfusion bioreactor systems. Physiologic loading regimens have been shown to significantly improve the mechanical properties of TEVG by inducing new matrix deposition [12-14].

Recent progress within the TEVG field has been more extensively summarized in other reviews [15-17]. Several TEVG fabrication techniques are progressing towards clinical implementation, and are relevant for fabricating hierarchical vasculature. These include tubular/annular molding, cell sheets [18], electrospinning [19, 20], decellularization [21], and 3D bioprinting [22]. Annular molding involves injection of a liquid hydrogel precursor into an annular

mold; following crosslinking of the hydrogel, the inner mandrel is removed leaving an open lumen. Cell sheets and electrospinning typically use a mandrel, with sheets of cells and ECM wrapped around a mandrel or electrospun polymer collected around a mandrel, yielding a lumen upon removal from the mandrel. Decellularization techniques often employ detergents to remove cellular material from human or animal arteries, leaving behind the hollow lumens and some native matrix proteins present within the vessel. These decellularized vessels can be further modified with other proteins and growth factors and/or seeded with EC to create an antithrombogenic lining. 3D bioprinting is the newest methodology employed to fabricate vascular grafts [23, 24] and mesovasculature. One promising technique to print soft materials within a supportive slurry bath allows for the printing of vascular constructs and even larger organ structures [22, 25].

Other novel techniques for engineering vascular grafts have emerged in recent years. One study described a new stepwise molding technique to fabricate TEVG with three distinct layers mimicking the three layers of a native artery (Fig. 2.2A) [26]. The authors first fabricated the tunica media comprised of dense fibrin and SMC within an annular mold. The tunica adventitia was fabricated next with lower density fibrin, EC, and stem cells cast around the media layer. Finally, the inner lumen was seeded with EC to create the tunica intima, and then the graft was cultured under pulsatile flow. The complete TEVG displayed similar properties to a native carotid artery. A similar three-layer vascular graft was fabricated by a unique drop-on-demand 3D printing technique where each layer was comprised of merged microdroplets [27]. The tunica intima was fabricated by printing droplets of dissolvable gelatin containing a high density of EC. The tunica media layer was fabricated by printing droplets of an SMC containing fibrinogen ink and a thrombin-based ink integrated to create a thin layer of SMC containing fibrin around the inner gelatin layer. Then a hybrid fibrin-collagen hydrogel containing fibroblasts was cast around the

3D printed object to fabricate the adventitia layer. Finally, the sacrificial gelatin was dissolved leaving behind the ECs lining the inside of the media layer as the tunica intima. The authors showed that both printed and cast cells remained in the distinct layers. Of note, they were able to successfully print fibrin hydrogels, a typically challenging material to print, with this novel printing technique.

Figure 2.2: Fabrication strategies for each length scale of the vascular tree. *Schematic examples of distinct strategies for forming vasculature ranging from arteries to capillaries. (A-C) Fabrication of artery-scale grafts has been achieved using an annular molding technique with (A) liquid prepolymer solutions containing cells, (B) cell suspensions alone, or (C) sheets of decellularized ECM. (D-F) Methods to fabricate mesoscale vasculature employ (D) 3D printing of sacrificial glass (Abbreviations: Panel (D) Par VP = parallel vascular patch, Grid VP = grid vascular patch, Sm_D VP = Small diameter vascular patch, EP = endothelial patch, AP = acellular patch) or (E, F) removable solid templates – spring (E) or needle*

29

(F). (G-I) Capillary-scale structures have been fabricated via (G) monocultures of cells with angiogenic factors to elicit vasculogenesis-like self-assembly, (H) co-culture of cells which undergo vasculogenesis-like self-assembly, or (I) angiogenic sprouting from existing blood vessels. Panels (A), (B), (C), (D), (E), (F), and (G) reproduced with permission from [26] (from Springer Nature – Copyright 2021, Biomedical Engineering Society), [28] (from Mary Ann Liebert – Copyright 2018, Mary Ann Liebert, Inc.), [30] (from John Wiley and Sons – Copyright FASEB), [41] (from Springer Nature – Copyright 2017, Macmillan Publishers Limited), [47] (used under Creative Commons license CC BY-NC), [45] (from PNAS, available through open access), and [50] (from Elsevier – Copyright 2020 Elsevier Inc.), respectively. Panels (H) and (I) created using BioRender.com.

Not all TEVG approaches fully replicate the typical three distinct layers of native arteries; simpler constructs containing only single layer organization have also advanced to preclinical and clinical trials. One approach from two of the co-authors fabricated tissue rings from various types of stromal cells (SC), including SMC, mesenchymal stem cells (MSC), and iPSC-SMC, using an annular agarose mold around a central mandrel [28, 29]. Multiple rings were then merged to form a full graft (Fig. 2.2B). Polymer cuffs were incorporated at the ends of the vessel to facilitate anastomosis. Other studies implanted acellular grafts into rodent models, showing successful perfusion and the maintenance of patency achieved by recruiting host cells to populate the grafts. One such study used an annular mold and naturally derived small intestinal submucosa (SIS) commercially available from Cook Biotech [30]. The SIS material was rolled around a mandrel and subsequently functionalized with heparin and vascular endothelial growth factor (VEGF) (Fig. 2.2C). These acellular TEVG were implanted as arterial interpositional grafts in the descending aorta of adult mice. Addition of VEGF to the graft prior to implantation significantly increased cellularization of the graft but did not improve patency over heparin-only grafts (60% perfused in both groups at the conclusion of a one-month study). Further, the cellularization of VEGF grafts correlated well with native arterial anatomy with CD144 EC marker expression on the lumenal side and a-SMA SC marker expression in the wall of the graft, whereas expression was mixed in the heparin only group. Increased cellularization correlated with increased remodeling, where a

greater percentage of the implanted SIS had degraded in the VEGF group compared to the heparin only group. Another study used a similar methodology of rolling a decellularized tissue around a mandrel [31]. In this work, decellularized bovine pericardial ECM integrated with poly(propylene fumarate) was used to create a biohybrid vascular graft with circumferential stresses and suture retention strengths comparable to those of native porcine arteries. Two grafts implanted as interpositional grafts in the rat abdominal aorta remained patent throughout the two-week study with evidence of host cell recruitment.

Cell-seeded TEVG have also been fabricated with both natural and synthetic biodegradable matrices. One study seeded aortic EC into the lumens of collagen grafts and implanted them interpositionally in the femoral artery of inbred Lewis rats [32]. A one-week implantation study revealed that 40% of the grafts remained patent and expressed endothelial markers on the lumenal surface and the outside of the graft. In this study, an endothelial lining was required to prevent thrombosis, as none of the grafts seeded with EC that subsequently detached from the surface after surgical handling remained thrombus free. However, this may be animal model or material specific as other studies, as noted in the preceding paragraph, have shown somewhat surprising success without lumenal seeding when host cells populate and endothelialize the graft. Another study implanted iPSC-SMC seeded vascular grafts fabricated from biodegradable synthetic materials into the abdominal aorta of nude rats [33]. When grafts were cultured for 8 weeks under pulsatile radial stress, they exhibited burst pressures and suture retention strengths comparable to human saphenous veins (commonly used for bypass surgeries). The high mechanical strength of these grafts prevented rupture and deformation during a one-month *in vivo* study. The implanted grafts remained cellularized throughout the study and showed evidence of collagen deposition and host cell recruitment.

Excitingly, a few studies have now shown long-term patency of TEVG in large animal and human studies, leading to commercialization efforts. Building on the success of their TEVG in baboons, sheep, and pigs, one such effort to commercialize allografts for human clinical applications has led to the formation of a start-up called Vascudyne. Their approach involves first seeding fibrin-based TEVG with human dermal fibroblasts, followed by culture in a pulsed flow/mechanical stretch bioreactor to attain suitable tissue mechanical properties and then decellularization prior to implantation [34]. The burst pressures and suture retention strengths were comparable to those of the internal mammary artery, commonly used for CABG. When implanted in baboons, patency rates were 83% at 3 months and 60% at 6 months. Grafts at both timepoints exhibited significant mesenchymal cell recruitment within all regions of the graft. Host EC infiltrated the graft at 3 months with a complete lumenal endothelium present at 6 months. The grafts exhibited extensive remodeling, no signs of calcification or aneurysm, and only minimal inflammatory responses, all positive indications for future clinical testing.

A similar strategy involving decellularization of TEVG is being commercialized by Humacyte, a North Carolina-based start-up that has significantly advanced their technology, human acellular vessels (HAV), through multiple clinical trials. Initially focused on creating grafts as vascular access for kidney dialysis patients, HAV are fabricated by seeding human vascular cells onto degradable polyglycolic acid tubular scaffolds, subjected to radial strain via a pulsatile flow bioreactor during a maturation period of 8 weeks, and then subsequently decellularized and implanted as an HAV [35]. In a pivotal study, suture strengths and burst pressures of the HAV were comparable to, or exceeded, that of the human internal mammary artery. Grafts underwent significant remodeling and host cellular infiltration, eventually developing into a native vessel mimetic with three distinct layers. Originally a single layer graft, a neoadventitial layer formed

around the graft after implantation, along with lumenal endothelialization representative of an intima (Fig. 3.3A). As early as 16 weeks, capillaries mimicking the vasa vasorum were observed within the adventitial layer, and complete endothelialization of the lumen was observed at 44 weeks. Humacyte has also reported positive progress in the development of their grafts for CABG and the treatment of traumatic injuries [36-39].

Figure 2.3: Engineered vasculature connects to the host yielding perfused vasculature in vivo. *(A) Engineered large caliber decellularized vascular grafts have been shown to support cellular infiltration and remodeling upon transplantation. Panel A shows a macroscopic image of the vascular graft pre-implantation (left) and fluorescent images taken upon explantation of the graft (right). A neoadvential layer with a vasa vasorum is observed at 16 weeks (A, top right) while an endothelialized lumen is observed at 44 weeks (A, bottom right). (B) Parallel patterned mesovessels restored blood flow to ischemic tissues. The Par VP (schematic shown in Fig. 2D) inosculates with the host yielding perfusion of ischemic limbs by day 5 as shown by Laser Doppler Perfusion Imaging. (C, D) Microvascular and (E) hierarchical micro-mesovascular constructs connected to host tissues yielded host blood-perfused vessels within engineered tissues. Panel C shows perfused vessels integrated with the host circulation. Implanted human self-assembled vessels (red) and hydrogel-infiltrating mouse vessels (green) were perfused with a lectin to stain species-specific EC via tail vein injection to identify only perfused vessels. There is evidence of chimeric vasculature in both red stained vessels. Panel D shows engineered vessels (green) perfused with dextran (red) via a tail vein injection. The lack of red stain throughout the rest of the image indicates functional, non-leaky vasculature. Panel E shows the perfusion of engineered vessels within the implanted multiscale vascular tissue via the host circulation – engineered vessels (green), host vessels (blue), dextran (red). Panels (A), (B), (C), (D), and (E) reproduced and adapted with permission from [35] (from Science Translational medicine – Copyright 2019, Kirkton, RD. et al.), [41] (from Springer Nature – Copyright 2017, Macmillan Publishers Limited), [58] (from Springer Nature used under Creative Commons CC BY license – Copyright 2017, Kang, K.-T., et al.), [40] (from Mary Ann Liebert – Copyright 2013, Mary Ann Liebert, Inc.), and [63] (from Elsevier used under Creative Commons CC BY license – Copyright 2021, Debbi, L., et al.), respectively.*

While initial efforts in the creation of TEVG focused on biological mimicry of the native vascular anatomy, recent progress with acellular grafts suggests two questions. How critical is it that an engineered graft be comprised of three distinct layers representing the tunica intima, tunica media, and tunica adventitia prior to implantation? Can function be satisfied without complete structural mimicry? Many of the studies described above showed successful patency, perfusion, and remodeling by the host without mimicking the exact native architecture of arteries when initially implanted *in vivo*. Single layer grafts and grafts lacking an antithrombogenic EC lining showed substantial success. Therefore, at this length scale, function may be achieved with a more simplistic structure that matures into a more native-like structure over time post-implantation, potentially providing an easier route to clinical translation. Relying on host remodeling upon implantation, rather than trying to fully prescribe the anatomical architecture, may also be applicable for creating a more complete hierarchical vasculature.

2.2.2 Mesovascular tissue engineering

Vascular engineering at the mesoscale has similarly focused on both acellular and cellular tissues and constructs. One simple approach has been to incorporate acellular mesoscale channels within engineered tissue constructs to increase the surface area for diffusion of nutrients from media (or blood when implanted *in vivo*) [41]; in some studies, these channels have been seeded with endothelial cells to fabricate mesoscale vessels comparable to the size of arterioles found *in vivo* (Fig. 2D, AP vs. Par VP) [42]. Similar to studies fabricating single-layer TEVG, strategies to fabricate these cellular mesovessels have not necessarily incorporated the characteristic smooth muscle layers found in arterioles *in vivo*, but rather have been fabricated with a single EC layer mimicking the arteriole intima layer.

Acellular channels have also been used to better integrate biomaterial implants with host vasculature. Host cells and vessels that infiltrate an engineered tissue construct must traverse solid tissue to reach the center; by contrast, in constructs containing channels, host cells can migrate through empty channels and populate the interior more easily. However, this technique has had varying success in different *in vivo* models. One study examining silk implants with or without channels in a subcutaneous model observed increased tissue ingrowth and vessel perfusion in channeled implants compared to unchanneled bulk implants [43]. In another study, acellular channels alone failed to restore limb perfusion in a model of hindlimb ischemia [42]. However, mesovessels seeded with EC were spatially patterned into parallel and grid-like orientations (Fig. 2.2D), with the former arrangement able to effectively restore limb perfusion (Fig. 2.3B); acellular channels or disorganized cells alone did not rescue perfusion.

Efforts to engineer the mesovasculature have examined a range of vascular morphologies (Fig. 2.2D-F), including single linear channels, uniquely shaped and branched channels, and multilayered gridded structures. Studies have investigated both blood and lymphatic vasculature at this scale. Two studies investigated single linear lymphatic vessels and their barrier function within collagen microfluidic hydrogels [44, 45]. Another study fabricated single blood vessels within collagen hydrogels with varying ratios of supportive MSC to EC, where the MSC are intended to function as pericytes or SMC *in vivo* [46] (Fig. 2.2F). Vessels surrounded by a greater number of MSC exhibited greater barrier function characterized by lower permeability to both 10 kDa and 70 kDa fluorescent tracers. These types of models have been used to study changes resulting from flow or pressure, cell-cell interactions, response to inflammatory cues, and other pathophysiological conditions.

New 3D bioprinting technologies have also enabled the fabrication of linear channels and more complex curved, zigzagging, winding, and branched channels, and many other complex geometries. For example, coaxial printing methods were used to fabricate three differently shaped channels from a decellularized ECM bioink and examine EC morphology, permeability, anti-adhesion to platelets, and inflammatory response [47]. These vessels additionally supported pump-driven perfusion throughout the duration of culture, a distinction over traditional polydimethylsiloxane (PDMS)-based microfluidic devices which often rely on gravity-driven flow. Another unique technique enabled the fabrication of a 3D spiral shaped vessel using a spring to template the vessel (Fig. 2.2E), rather than a needle traditionally used for single linear vessels (Fig. 2.2F) [48]. The authors used this model to assess endothelial flow responses in a curved geometry more replicative of *in vivo* anatomy, observing an increased cell proliferation rate in spiral channels compared to straight channels despite similar morphologic response to various flow rates. This approach enabled patterning a solid cylinder of cells inside of the spiral shape and cells dispersed throughout the gel outside of the spiral shape. The authors used this model to engineer a tumor with the surrounding spiral vasculature, and a cardiac model with dispersed cardiomyocytes.

Compared to the large numbers of studies and impressive translational progress on macrovasculature, very few studies have focused on mesovascular engineering, with even fewer advancing to preclinical studies. Most focus on using these vessels as models of vascular pathophysiology and/or for drug testing applications. Furthermore, only one of the above studies incorporated SC to support the EC. SMC in the tunica media of native arterioles play critical roles in the physiologic functions of arterioles, in part by regulating vascular resistance and vessel diameter as blood flows from larger arteries into smaller capillaries (Fig. 2.1). The replication of both the tunica intima and the tunica media will likely be critical to the proper functioning of

mesovasculature, but it is not yet clear if such complexity needs to be fully prescribed a priori. Much like studies with TEVG have shown for macroscale vessels, morphogenetic adaptation may take over to remodel crude mesoscale conduits into bona fide arterioles, especially when subjected to blood flow and host cells upon transplantation. There is also a need to better understand the integration of engineered vasculature across length scales. In the body, the vascular hierarchy is a continuum, with a gradual tapering of vessel sizes as they branch, dictated in part by flow-mediated mechanotransduction. Reproducing this hierarchical and biomechanical continuum represents a significant challenge and opportunity.

2.2.3 Engineering capillary networks

The primary methodologies for engineering capillaries seek to replicate vasculogenesis, the *de novo* formation of new vasculature from individual cells (Fig. 2.2G, H), and/or angiogenesis (Fig. 2.2I), the formation of new blood vessels from existing blood vessels. Both processes rely on supportive SC, which regulate the development of vessel networks through the secretion of growth factors and take on a perivascular phenotype to promote maturation and proper function of the microvasculature [49]. Matrix composition, stiffness, and degradability also significantly impact these processes.

Despite the critical support SC provide for developing microvasculature, cell-based vascularization strategies involving multiple cell types may complicate regulatory approval and clinical translation, which has prompted focus on acellular approaches or those using EC or EC progenitors alone. One such study fabricated a hydrogel composed of a collagen and norbornene-modified hyaluronic acid interpenetrating network (IPN) [50]. The authors observed the degree of vascular formation, the number of branch points in the resulting network, and vessel lumenization

were dependent on the IPN stiffness, which was modified by increasing the crosslinking. Another recent study reported that hydrogels containing dynamic crosslinks supported self-assembly of EC into vessel-like networks [51]. Vascular assembly depended on cellular contractility to promote integrin recruitment and focal adhesion development. Another paper investigated neutral-swelling synthetic PEG hydrogels [52]. These gels were fabricated by incorporating a helical PEG macromer into the hydrogel and yielded enhanced capillary morphogenesis compared to controls, though they observed minimal lumen formation.

While the aforementioned studies successfully engineered microvasculature without SC, their presence and tissue-specific origins have also been shown to influence microvascular network formation and function in both natural and synthetic hydrogels. For example, recent work from one of our groups revealed that fibroblasts from either lung or skin supported a greater degree of vessel formation than bone marrow SC in co-culture models of vasculogenic self-assembly [53]. This mirrors a prior study in a fibrin-based sprouting angiogenesis model system, which demonstrated that SC identity affects the mechanism of fibrinolysis during vascular morphogenesis [54]. Another recent study involving SC focused on endothelial network formation in animal-component-free constructs under serum-free conditions, potentially providing a more reproducible route for clinical translation and regulatory approval [55]. The authors combined human umbilical vein EC (HUVEC) and human adipose derived SC in a human collagen and decellularized porcine SIS and cultured these constructs under serum-free conditions, yielding similar network parameters to cells cultured in Matrigel and rat tail collagen controls in the presences of serum.

While *in vitro* studies are useful to investigate the mechanisms underlying the formation of microvascular networks, *in vivo* investigations are critical for vascularization strategies to

progress to clinical translation. They shed light on inosculation between host and engineered vasculature and the ability to restore physiologic vascular function in regenerative and disease models. In a recent study, a subset of our team investigated modular microbead constructs and showed that prevascularization catalyzed the formation of new microvasculature at the implant site [56]. A key element of microvascular engraftment and inosculation is the host inflammatory response. Utilizing a subcutaneous mouse model, another group found that prevascularized networks failed to inosculate with host vessels upon transplantation when neutrophils were first depleted in the host [57]. Vascularization was recovered when neutrophils were transferred to mice. Such insights suggest vascularized constructs may perform differently in immune-deficient patient populations. Other studies have shown that cells suspended in hydrogels capable of assembly into microvascular networks salvaged limbs, prevented necrosis, and restored blood perfusion compared to single cell type or hydrogel only controls [58, 59], with one observing similar effects using prevascularized tissue constructs. These hindlimb ischemia models bear some resemblance to human PAD and serve as a key step towards progressing cell-based therapies to the clinic. In an ischemic stroke model, a study of integrin binding in engineered hydrogels showed that scaffolds capable of supporting $\alpha3/\alpha5\beta1$ integrin binding led to increased angiogenesis at the stroke site, yielding non-tortuous, non-leaky vasculature by day 10 post stroke (Fig. 3.3C) [60].

Though several studies have advanced to animal models focused on ischemic injuries, cell-based approaches to restore perfusion have not yet been successfully translated into human patients, despite a large number of clinical trials using cells like MSC or EC by themselves. There are many possible reasons, including poor cell survival upon delivery into an ischemic tissue as well as issues of cell sourcing and the underlying health status of the patient. Approaches containing both EC and SC in hydrogel delivery vehicles have not progressed into clinical trials,

to the best of our knowledge. However, in our view, cell-based microvasculature is unlikely to be effective as a treatment alone for a disease that begins with an arterial blockage (e.g., PAD, stroke), unless the blockage is also cleared and/or the occluded vessel is stented open. Similarly, stenting or vascular grafting alone, without microvasculature, may not fully restore perfusion to the tissue if the function of the existing capillary beds has been compromised by underlying disease. Given these challenges, vascular integration across length scales may be also required in the treatment of ischemic conditions, as we expect it will be for engineering whole, functional, solid organs.

2.2.4 Engineering multiscale hierarchical vasculature

While many studies have engineered vasculature at single scales, progress towards engineered hierarchical vasculature has been much more limited. As described above, each vascular length scale often involves different fabrication techniques, which presents a challenge to engineering a complete vascular tree. Initial efforts focused on integrating capillary-artery, capillary-arteriole, or arteriole-artery vascular networks, with more recent efforts to create three-scale hierarchies spanning capillary-arteriole-artery.

Several groups, including ours, have engineered capillary-mesoscale hierarchical vasculature, mostly within microfluidic chips. A common approach involves templating larger mesoscale channels with acupuncture needles [61, 62] or with a sacrificial ink via 3D bioprinting [63], followed by seeding the lumens with EC. Capillaries are then formed via vasculogenic assembly of co-cultured SC and EC between the two channels. An important distinction between these studies is the presence of flow within the system and how the fluidic circuit is established. Samples were either cultured statically [61], under oscillatory flow applied via a rocker plate [62], or under unidirectional flow via a syringe pump [63]. Such microphysiological systems identify

40

key parameters for engineering functional hierarchies, enable fundamental studies to assess vascular morphogenesis, perfusion, and permeability, and have been touted as innovative platforms to evaluate and screen drugs and/or biologics. However, their small size and encasing within glass/PDMS chambers limits their potential as transplantable tissue constructs. Two studies engineering capillary-arteriole hierarchies created larger tissue implants and evaluated their hierarchical structure versus capillary-only implants in a subcutaneous mouse model [64] and rat infarct model [65]. In the subcutaneous model, host vessel infiltration into hierarchical implants and blood perfusion were increased compared to capillary only implants (Fig. 2.3E). Similarly, in the ischemia model, increased numbers of perfused vessels and increased density of transplanted human cardiac cells were observed in hierarchical implants. One of the more advanced of these capillary-mesoscale vascular systems is a particularly innovative microtechnology called the AngioChip [66]. This multiscale vascular construct featured capillaries that sprouted from 100-500 μm mesovessels, supported parenchymal cell function, and was successfully integrated with host vasculature via both an artery-to-artery and an artery-to-vein surgical anastomosis aided by surgical cuffs and tissue glue (Fig. 2.4B).

Though less physiologic initially, capillary-artery hierarchical vasculature has also been investigated in a few studies. These approaches have the advantage of direct surgical anastomosis of the artery *in vivo* to provide immediate perfusion to interconnected capillaries within the engineered hierarchy. One study investigated sprouting between two segments of isolated artery *ex vivo*, tested with both rodent and human vessels [67]. Artery segments were connected by sprouted capillaries within 21 days and successfully perfused. The survival and functionality of co-cultured cardiomyocytes were also assessed by culturing on top of the vascular bed. In the presence of hierarchical vasculature, cardiomyocytes exhibited a lower excitation threshold and

more organized sarcomeres compared to controls. A promising recent study described the fabrication of similar capillary-artery hierarchical vasculature by integrating vasculogenic self-assembly and 3D printing [68]. The artery-like conduit was fabricated from a synthetic polymer containing small pores along its length while the capillary-like network was fabricated via vasculogenic self-assembly of a co-culture of EC and SC bioprinted within methacrylated collagen. The polymeric artery-like structure was seeded with EC which sprouted through the pores to integrate with capillaries in the surrounding hydrogel. The hierarchy was assessed *in vivo* in a rat femoral artery ligation model. Host vasculature infiltrated the hierarchical construct, with many vessels invested with mural cells expressing a-SMA (Fig. 2.4A). The vasculature within the entirety of the construct was also perfused via the host blood circulation.

Figure 2.4: Surgically anastomosed grafts with structurally complex hierarchical architecture perfuse and integrate with host tissues. *(A) A two-scale artery-capillary hierarchy surgically connected to host arteries showed evidence of blood perfusion in capillaries formed within a cell-laden bioprinted hydrogel. The top panel shows macroscopic perfusion of the implanted construct after clamp removal. The middle and bottom images show matured vessels within the construct as evidenced by sheaths of BM (laminin) and perivascular stromal cell association (αSMA). (B) Engineered devices containing meso-microvascular hierarchies surgically anastomosed with host arteries also yielded functional perfusion. (C) Surgically*

Only a few studies have attempted to engineer a complete vascular hierarchy containing capillaries, arterioles, and arteries. Similar to capillary-artery hierarchies, there are two distinct strategies: explanted functional vasculature integrated with tissue engineered microvasculature or creation of a fully tissue-engineered structure. As an example of the former, one group explanted rat femoral tissue containing an artery-vein bundle and the surrounding branching arterioles, and then cultured this vasculature with EC-containing cardiac cell sheets [69]. The artery and vein pair were connected to a syringe pump *in vitro* and could be sutured into existing circulation upon transplantation into a second animal. In the presence of growth factors, EC in the cell sheets assembled into vessels and inosculated with the explanted vascular bed, creating an integrated vascular hierarchy capable of supporting a parenchymal cell population. When implanted *in vivo* in the neck of a nude rat, the surgically anastomosed hierarchical vasculature integrated with the rat's blood circulation to a significantly greater degree than capillaries within cell sheets alone or non-surgically anastomosed hierarchies (Fig. 2.4C). As an example of the latter approach, a recent study tissue engineered a complete hierarchy by employing vasculogenic self-assembly, needle templating, and annular molding to fabricate the three different vascular length scales [70]. Fibrin-based artery-scale vessels were fabricated using annular molds and fixed into a bioreactor. Subsequently, ~1 mm diameter needles were inserted perpendicular to the artery-scale vessels, around which a bulk fibrin matrix containing EC and SC was molded. Upon removal of sacrificial needles and seeding of the meso-scale channels, the final construct contained two artery-scale

vessels, 4 arteriole-scale vessels, and cells to undergo vasculogenic self-assembly to form capillaries. Although this hierarchical construct was not evaluated *in vivo* in this study, the hydrogel and cell components used were all human-derived, suggesting a clearer path towards clinical translation of this promising approach.

3D bioprinting, as briefly mentioned above, is quickly emerging as a new technology to engineer hierarchical vasculature, organ models, and full-scale organs. One group described a projection stereolithography-based printing approach, named SLATE (Stereolithographic Apparatus for Tissue Engineering), to generate multiscale vascular tissue constructs resembling alveolar morphology and a grid-like structure capable of supporting co-transplanted parenchymal liver cells *in vivo* [71]. Another group employed a microbead slurry support bath to bioprint multiscale vasculature from MRI and models of the human heart [22]. This technique, named FRESH (Freeform Reversible Embedding of Suspended Hydrogels), allows for the high-resolution printing of soft hydrogel-based materials with micron-scale precision. In a similar approach, another group developed a microbead support bath composed of high density cell aggregates (organoids) capable of forming functional microtissues around the printed vasculature [25]. Their approach, termed SWIFT (Sacrificial Writing into Functional Tissue), enabled the successful printing of multiscale vascular tissue capable of supporting the perfusion and function of an engineered cardiac muscle tissue. Another unique printing technique developed by one of our groups is the use of cell-only bioinks without the support of hydrogel materials [72], which could be applied as a means to facilitate the interconnection of vasculature across different length scales. While these studies have collectively made promising strides, bioprinted constructs containing hierarchical vasculature, with macroscale vessels large enough for surgical anastomosis integrated

with meso- and microscale vessels capable of supporting the immediate perfusion of embedded parenchymal cells, have not yet been realized, to the best of our knowledge.

2.3 Replication of Anatomical Vasculature and Key Barriers to Translation

As engineered tissues progress towards the clinic, replication of physiologic vascular function is critical. But is complete replication of vascular anatomy a priori also required? At the arterial scale, function has been largely achieved with TEVG meeting the thresholds for suture strength and burst pressure to remain functional upon implantation, despite not fully replicating all anatomical features (i.e., three distinct layers representing the tunica intima, media, and adventitia). Compliance is a parameter of critical importance in small diameter (<6 mm) vascular grafts, as compliance mismatch leads to reduced long-term patency rates due to intimal hyperplasia. One group studying this problem elucidated the effects of compliance specifically on intimal hyperplasia and developed a system to screen vascular grafts for cellular markers of this pathophysiology [73]. At the arteriole scale, a critical function that has not yet been replicated in engineered mesovessels is the ability to regulate vessel diameter. In the human body, this function is achieved through SMC in the tunica media, an anatomical feature often lacking in engineered mesovascular models. Replicating contractile smooth muscle will be important to ensure that mesovessels within an implanted construct can regulate blood flow from arteries into surrounding capillary beds immediately upon implantation.

At the microvascular scale, tissue-specific capillary density and permeability are critical to the normal function of native tissues. With respect to the former, skeletal muscle has a density of ~500-1500 capillaries/mm^2 [74], while cardiac muscle has a density of ~2000-4000 capillaries/mm^2 [75]. Approaches are therefore needed to engineer constructs with tissue-specific

vascular densities. However, current approaches have largely ignored these tissue-specific differences, and often do not even meet the lower threshold of the capillary density in the skeletal muscle. For example, several studies, including our own, report ~100-200 vessels/mm^2 in varying *in vivo* models [56, 76]. Though these engineered tissues may function *in vitro* and provide therapeutic benefit in small animal models, strategies to achieve an appropriate capillary density will likely be necessary for the proper functionality of human-scale engineered tissues and organs. With respect to the latter, physiologic control of permeability is a key tissue-specific function of the vasculature [77, 78]. For example, brain microvasculature (continuous) is highly impermeable to constitute the blood-brain barrier [79], while kidney microvasculature (fenestrated) is leakier to facilitate nutrient exchange and glomerular filtration. Vascular permeability is also tightly correlated with endothelial phenotype. Whether the use of specialized EC will be required to create vasculature with tissue-specific permeability requirements remains unclear. It's also possible that EC may have some degree of phenotypic plasticity [80, 81], enabling them to adapt to distinct tissue-specific microenvironments.

Related to the issue of tissue specificity, the question of cell source remains a significant challenge for vascularizing engineered tissues. HUVEC have been widely used as a model EC type for proof-of-concept studies throughout the literature. They readily and reproducibly form robust microvasculature both *in vitro* and *in vivo*, but their applicability for clinical applications is often questioned, in part due to their venous origins. Significant progress has been achieved with other cell sources, including endothelial colony forming cells (ECFC) [82-84] and EC derived from induced pluripotent stem cells (iPSC-EC) [85].

An important consideration when evaluating iPSC-EC and other alternative, potentially more translatable, EC types, is the suitability of the assay in which they are studied. In general,

there is a lack of standardization with respect to assays used to evaluate EC phenotypes and functions. For example, the Matrigel cord assay, though widely-used, involves EC cultured in 2D on top of Matrigel; the cord-like structures that form in this environment typically lack hollow lumens, and form via a process that does not require proteolytic remodeling of the ECM. Recent studies directly comparing the potential of iPSC-EC and HUVEC have yielded different results, depending on the functional outcome measured in a specific assay [85-87]. For example, our lab published a head-to-head comparison of HUVEC and iPSC-EC in a sprouting angiogenesis assay in which EC coated on microcarrier beads were evaluated for their ability to undergo vascular morphogenesis in the presence of supportive SC [87]. While HUVEC reliably sprouted and formed vessels, iPSC-EC sprouted to significantly lesser degrees and in some cases did not sprout at all. Despite diminished sprouting, the iPSC-EC derived capillary structures displayed characteristics of BM proteins and other characteristics of mature capillaries. In a follow-up study, we showed that iPSC-EC fared better at forming capillaries *in vivo*, albeit still to a lesser degree than HUVEC [88]. These results further highlight the need for pre-clinical characterization of engineered cell- and tissue-based therapeutics.

Another group conducted a head-to-head comparison of HUVEC and iPSC-derived human brain microvascular endothelial cells (BMEC) in a model consisting of a single EC-lined tube within a hydrogel [86]. In this study, the authors examined and compared the ability of the EC to form a monolayer on the channel wall and assessed vascular permeability and the expression of junctional and cytoskeletal markers. In this model, EC proliferate and migrate to form a confluent monolayer and develop tight cell-cell junctions to maintain good barrier function, a critical feature of the blood brain barrier. These functions are distinct from those required for a sprouting angiogenesis assay. Their study revealed that BMEC had ~100-fold lower permeability to 3 kDa

dextran than HUVEC on day 1 and ~10-fold lower on days 7 and 14. Perfusion of the engineered vasculature led to sustained 100-fold differences in barrier function over time, a finding which was reproducible across different iPSC lines. Consistent with low permeability, the iPSC-derived BMEC expressed and properly localized occludin and claudin-5 at the cell-cell junctions, as well as VE-cadherin both in static and perfused conditions. Together, the results of these studies suggest the need to standardize assays evaluating EC for multiple functions before adopting a specific population for clinical translation.

Despite iPSC-derived cells being hailed as a potentially autologous cell source for clinical translation, a recent study found that 72% of skin cell derived iPSC and 18% of blood-derived iPSC at one cell bank may harbor genetic mutations [89]. Some of these mutations were detected in genes implicated in multiple types of cancer. These mutations were not previously identified because the required testing for banking cells is much lower than the clinical standard of practice. Therefore, despite the increased interest in using pluripotent stem cells to generate cells for therapies and engineered tissues, many significant challenges must be overcome before these cells represent a clinically viable source for creating vascularized tissue constructs.

Another important consideration with all EC sources is the age of the donor. The vast majority of cells purchased or isolated by labs are from young, healthy adults and/or children. The results from studies using these cells may not readily translate to autologous cell therapies for older adults with cardiovascular disease or other comorbidities. In addition, both the sex and ancestral background of the cell source may also influence how cells respond to different stimuli used in creating engineered tissue constructs [90, 91]. Understanding the influence of patient-specific differences may therefore be an additional consideration when fabricating engineered tissues and organs that represent equitable clinical solutions.

Finally, another key barrier to clinical translation is the source of natural materials. Many current therapies that have advanced to the clinic use human-derived materials or synthetic materials. However, much of the academic community uses animal-derived natural materials such as rat tail collagen, bovine fibrinogen, and porcine gelatin. Further, nearly all cells are grown in medium containing fetal bovine serum. Though many companies are progressing animal-based decellularized tissues and organs towards the clinic, ensuring robustness of responses across different material sources represents a significant challenge.

2.4 Concluding Remarks and Future Perspectives

The field of tissue engineering has progressed considerably towards transplantable tissues and whole organs over the last three decades; however, the number of tissue-engineered products progressing towards FDA approval remains somewhat underwhelming. This review highlights the need for hierarchical vasculature as a critical limiting factor, if not THE limiting factor, in realizing the potential of this field. Many examples cited herein provide proof of principle techniques to engineer vasculature at individual length scales. However, integrating these techniques (or creating new ones) to engineer hierarchical vasculature will be essential to manufacture functional implantable tissues and organs.

While this so-called "vascularization challenge" has long been recognized, it has yet to be solved. The advent of new biofabrication techniques over the last 15-20 years, along with dedicated funding streams, led to a pivot towards using microfluidic lab- and organ-on-chip systems for drug development and as model systems for development and disease. The recent passage of the FDA Modernization Act to utilize such systems in lieu of small animal models is especially exciting, and will undoubtedly lead to more widespread adoption [92, 93]. Emulate, a

company focused on these devices, has already endorsed the act publicly [94]. These systems are useful for mechanistic investigations of vessel development in healthy and diseased states as well, but their small sizes mean that cells within can often be sustained by diffusive transport of oxygen and nutrients alone.

To solve this grand challenge of the field of tissue engineering, perhaps it is time for a vascularization "moon shot." The technical breadth required to solve a problem of this scope is immense, and will necessitate collaboration between scientists, engineers, and clinicians with complementary skill sets. Both knowledge and technical gaps exist, including the need to better understand vascular biology at each length scale, the requirements for tissue- and organ-specific vascular form and function, and the technologies to fabricate large constructs, perfuse them, and maintain their viability and sterility over prolonged periods of time. Solving a problem of this magnitude will require collaborative and cooperative teams incentivized to solve this grand challenge.

Excitingly, the maturation of existing methodologies and the emergence of new technologies has the community poised to achieve this long-standing goal. Recent advancements in 3D bioprinting have yielded remarkable progress, and bioprinting strategies to fabricate vasculature of multiple length scales within a single construct are beginning to emerge. However, like most emergent technologies, the promotion has so far outpaced the reality. More progress has been made in the development of instrumentation and bioinks than large living tissue constructs. Cell viability and function in bioprinted constructs, following either extrusion and/or photocrosslinking, and the stability of printed architectures also remain concerns [95]. In addition to scientific concerns, there are moral and ethical concerns raised by some members of society over the widespread use of these technologies [96]. While these (and many other) critical hurdles

need to be overcome, and many questions remain unanswered, we are optimistic the vascularization challenge will not be cited as the biggest hurdle to the clinical translation of engineered solid tissues and organs in 20 years, as it has been for the last 20 years!

2.5 References

[1]   Organ, Eye and Tissue Donation Statistics. https://www.donatelife.net/statistics/

[2]   Semenza, G.L. (2007) Vasculogenesis, angiogenesis, and arteriogenesis: mechanisms of blood vessel formation and remodeling. *J Cell Biochem* 102, 840-847

[3]   Ouarne, M., Pena, A., and Franco, C.A. (2021) From remodeling to quiescence: The transformation of the vascular network. *Cells Dev* 168, 203735

[4]   Grant, M.A., Karsan, A. (2018) The Blood Vessel Wall. In *Hematology* (Seventh edn), pp. 1843-1856, Elsevier

[5]   Martinez-Lemus, L.A. (2012) The dynamic structure of arterioles. *Basic Clin Pharmacol Toxicol* 110, 5-11

[6]   Sierra-Sanchez, A., Kim, K.H., Blasco-Morente, G., and Arias-Santiago, S. (2021) Cellular human tissue-engineered skin substitutes investigated for deep and difficult to heal injuries. *NPJ Regen Med* 6, 35

[7]   Rashidbenam, Z., Jasman, M.H., Hafez, P., Tan, G.H., Goh, E.H., Fam, X.I., Ho, C.C.K., Zainuddin, Z.M., Rajan, R., Nor, F.M., Shuhaili, M.A., Kosai, N.R., Imran, F.H., and Ng, M.H. (2019) Overview of Urethral Reconstruction by Tissue Engineering: Current Strategies, Clinical Status and Future Direction. *Tissue Eng Regen Med* 16, 365-384

[8]   Horst, M., Eberli, D., Gobet, R., and Salemi, S. (2019) Tissue Engineering in Pediatric Bladder Reconstruction-The Road to Success. *Front Pediatr* 7, 91

[9]   Jain, R.K., Au, P., Tam, J., Duda, D.G., and Fukumura, D. (2005) Engineering vascularized tissue. *Nat Biotechnol* 23, 821-823

[10]   Brewster, L., Brey, E.M., Greisler, H.P. (2007) Blood Vessels. In *Principles of Tissue Engineering* (Third edn), pp. 569-584, Academic Press

[11]   Stewart, S.F. and Lyman, D.J. (1992) Effects of a vascular graft/natural artery compliance mismatch on pulsatile flow. *J Biomech* 25, 297-310

[12]   Udelsman, B.V., Khosravi, R., Miller, K.S., Dean, E.W., Bersi, M.R., Rocco, K., Yi, T., Humphrey, J.D., and Breuer, C.K. (2014) Characterization of evolving biomechanical

properties of tissue engineered vascular grafts in the arterial circulation. *J Biomech* 47, 2070-2079

[13] Schmidt, J.B. and Tranquillo, R.T. (2016) Cyclic Stretch and Perfusion Bioreactor for Conditioning Large Diameter Engineered Tissue Tubes. *Ann Biomed Eng* 44, 1785-1797

[14] Hahn, M.S., McHale, M.K., Wang, E., Schmedlen, R.H., and West, J.L. (2007) Physiologic pulsatile flow bioreactor conditioning of poly(ethylene glycol)-based tissue engineered vascular grafts. *Ann Biomed Eng* 35, 190-200

[15] Shi, X., He, L., Zhang, S.M., and Luo, J. (2021) Human iPS Cell-derived Tissue Engineered Vascular Graft: Recent Advances and Future Directions. *Stem Cell Rev Rep* 17, 862-877

[16] Ong, C.S., Zhou, X., Huang, C.Y., Fukunishi, T., Zhang, H., and Hibino, N. (2017) Tissue engineered vascular grafts: current state of the field. *Expert Rev Med Devices* 14, 383-392

[17] Fleischer, S., Tavakol, D.N., and Vunjak-Novakovic, G. (2020) From arteries to capillaries: approaches to engineering human vasculature. *Adv Funct Mater* 30

[18] Xing, Q., Qian, Z., Tahtinen, M., Yap, A.H., Yates, K., and Zhao, F. (2017) Aligned Nanofibrous Cell-Derived Extracellular Matrix for Anisotropic Vascular Graft Construction. *Adv Healthc Mater* 6

[19] Elliott, M.B., Ginn, B., Fukunishi, T., Bedja, D., Suresh, A., Chen, T., Inoue, T., Dietz, H.C., Santhanam, L., Mao, H.Q., Hibino, N., and Gerecht, S. (2019) Regenerative and durable small-diameter graft as an arterial conduit. *Proc Natl Acad Sci U S A* 116, 12710-12719

[20] Radakovic, D., Reboredo, J., Helm, M., Weigel, T., Schurlein, S., Kupczyk, E., Leyh, R.G., Walles, H., and Hansmann, J. (2017) A multilayered electrospun graft as vascular access for hemodialysis. *PLoS One* 12, e0185916

[21] Gui, L., Muto, A., Chan, S.A., Breuer, C.K., and Niklason, L.E. (2009) Development of decellularized human umbilical arteries as small-diameter vascular grafts. *Tissue Eng Part A* 15, 2665-2676

[22] Lee, A., Hudson, A.R., Shiwarski, D.J., Tashman, J.W., Hinton, T.J., Yerneni, S., Bliley, J.M., Campbell, P.G., and Feinberg, A.W. (2019) 3D bioprinting of collagen to rebuild components of the human heart. *Science* 365, 482-487

[23] Wang, D., Maharjan, S., Kuang, X., Wang, Z., Mille, L.S., Tao, M., Yu, P., Cao, X., Lian, L., Lv, L., He, J.J., Tang, G., Yuk, H., Ozaki, C.K., Zhao, X., and Zhang, Y.S. (2022) Microfluidic bioprinting of tough hydrogel-based vascular conduits for functional blood vessels. *Sci Adv* 8, eabq6900

[24] Dolati, F., Yu, Y., Zhang, Y., De Jesus, A.M., Sander, E.A., and Ozbolat, I.T. (2014) In vitro evaluation of carbon-nanotube-reinforced bioprintable vascular conduits. *Nanotechnology* 25, 145101

[25] Skylar-Scott, M.A., Uzel, S.G.M., Nam, L.L., Ahrens, J.H., Truby, R.L., Damaraju, S., and Lewis, J.A. (2019) Biomanufacturing of organ-specific tissues with high cellular density and embedded vascular channels. *Sci Adv* 5, eaaw2459

[26] Helms, F., Lau, S., Aper, T., Zippusch, S., Klingenberg, M., Haverich, A., Wilhelmi, M., and Boer, U. (2021) A 3-Layered Bioartificial Blood Vessel with Physiological Wall Architecture Generated by Mechanical Stimulation. *Ann Biomed Eng* 49, 2066-2079

[27] Schoneberg, J., De Lorenzi, F., Theek, B., Blaeser, A., Rommel, D., Kuehne, A.J.C., Kiessling, F., and Fischer, H. (2018) Engineering biofunctional in vitro vessel models using a multilayer bioprinting technique. *Sci Rep* 8, 10430

[28] Strobel, H.A., Hookway, T.A., Piola, M., Fiore, G.B., Soncini, M., Alsberg, E., and Rolle, M.W. (2018) Assembly of Tissue-Engineered Blood Vessels with Spatially Controlled Heterogeneities. *Tissue Eng Part A* 24, 1492-1503

[29] Strobel, H.A., Calamari, E.L., Alphonse, B., Hookway, T.A., and Rolle, M.W. (2018) Fabrication of Custom Agarose Wells for Cell Seeding and Tissue Ring Self-assembly Using 3D-Printed Molds. *J Vis Exp*

[30] Smith, R.J., Jr., Yi, T., Nasiri, B., Breuer, C.K., and Andreadis, S.T. (2019) Implantation of VEGF-functionalized cell-free vascular grafts: regenerative and immunological response. *FASEB J* 33, 5089-5100

[31] Kimicata, M., Allbritton-King, J.D., Navarro, J., Santoro, M., Inoue, T., Hibino, N., and Fisher, J.P. (2020) Assessment of decellularized pericardial extracellular matrix and poly(propylene fumarate) biohybrid for small-diameter vascular graft applications. *Acta Biomater* 110, 68-81

[32] Li, X., Xu, J., Bartolak-Suki, E., Jiang, J., and Tien, J. (2020) Evaluation of 1-mm-diameter endothelialized dense collagen tubes in vascular microsurgery. *J Biomed Mater Res B Appl Biomater* 108, 2441-2449

[33] Luo, J., Qin, L., Zhao, L., Gui, L., Ellis, M.W., Huang, Y., Kural, M.H., Clark, J.A., Ono, S., Wang, J., Yuan, Y., Zhang, S.M., Cong, X., Li, G., Riaz, M., Lopez, C., Hotta, A., Campbell, S., Tellides, G., Dardik, A., Niklason, L.E., and Qyang, Y. (2020) Tissue-Engineered Vascular Grafts with Advanced Mechanical Strength from Human iPSCs. *Cell Stem Cell* 26, 251-261 e258

[34] Syedain, Z.H., Graham, M.L., Dunn, T.B., O'Brien, T., Johnson, S.L., Schumacher, R.J., and Tranquillo, R.T. (2017) A completely biological "off-the-shelf" arteriovenous graft that recellularizes in baboons. *Sci Transl Med* 9

[35]   Kirkton, R.D., Santiago-Maysonet, M., Lawson, J.H., Tente, W.E., Dahl, S.L.M., Niklason, L.E., and Prichard, H.L. (2019) Bioengineered human acellular vessels recellularize and evolve into living blood vessels after human implantation. *Sci Transl Med* 11

[36]   Gutowski, P., Gage, S.M., Guziewicz, M., Ilzecki, M., Kazimierczak, A., Kirkton, R.D., Niklason, L.E., Pilgrim, A., Prichard, H.L., Przywara, S., Samad, R., Tente, B., Turek, J., Witkiewicz, W., Zapotoczny, N., Zubilewicz, T., and Lawson, J.H. (2020) Arterial reconstruction with human bioengineered acellular blood vessels in patients with peripheral arterial disease. *J Vasc Surg* 72, 1247-1258

[37]   (2022) Humacyte Human Acellular Vessel (HAV) in Patients With Vascular Trauma. https://clinicaltrials.gov/ct2/show/NCT03005418?term=human+acellular+vessel&draw=2&rank=1

[38]   (2022) Humacyte Presents Six-Month Human Acellular Vessel™ (HAV™) Coronary Artery Bypass Graft (CABG) Data at the American Heart Association Scientific Sessions 2022 Meeting. https://humacyte.gcs-web.com/news-releases/news-release-details/humacyte-presents-six-month-human-acellular-vesseltm-havtm

[39]   (2021)
Humacyte's   HAV   for   Femoro-Popliteal   Bypass   in   Patients   With   PAD. https://clinicaltrials.gov/ct2/show/NCT02887859?term=human+acellular+vessel&draw=2&rank=4

[40]   Grainger, S.J., Carrion, B., Ceccarelli, J., and Putnam, A.J. (2013) Stromal cell identity influences the in vivo functionality of engineered capillary networks formed by co-delivery of endothelial cells and stromal cells. *Tissue Eng Part A* 19, 1209-1222

[41]   Lim, K.S., Baptista, M., Moon, S., Woodfield, T.B.F., and Rnjak-Kovacina, J. (2019) Microchannels in Development, Survival, and Vascularisation of Tissue Analogues for Regenerative Medicine. *Trends Biotechnol* 37, 1189-1201

[42]   Mirabella, T., MacArthur, J.W., Cheng, D., Ozaki, C.K., Woo, Y.J., Yang, M., and Chen, C.S. (2017) 3D-printed vascular networks direct therapeutic angiogenesis in ischaemia. *Nat Biomed Eng* 1

[43]   Tang, F., Manz, X.D., Bongers, A., Odell, R.A., Joukhdar, H., Whitelock, J.M., Lord, M.S., and Rnjak-Kovacina, J. (2020) Microchannels Are an Architectural Cue That Promotes Integration and Vascularization of Silk Biomaterials in Vivo. *ACS Biomater Sci Eng* 6, 1476-1486

[44]   Gong, M.M., Lugo-Cintron, K.M., White, B.R., Kerr, S.C., Harari, P.M., and Beebe, D.J. (2019) Human organotypic lymphatic vessel model elucidates microenvironment-dependent signaling and barrier function. *Biomaterials* 214, 119225

[45] Thompson, R.L., Margolis, E.A., Ryan, T.J., Coisman, B.J., Price, G.M., Wong, K.H.K., and Tien, J. (2018) Design principles for lymphatic drainage of fluid and solutes from collagen scaffolds. *J Biomed Mater Res A* 106, 106-114

[46] Alimperti, S., Mirabella, T., Bajaj, V., Polacheck, W., Pirone, D.M., Duffield, J., Eyckmans, J., Assoian, R.K., and Chen, C.S. (2017) Three-dimensional biomimetic vascular model reveals a RhoA, Rac1, and N-cadherin balance in mural cell-endothelial cell-regulated barrier function. *Proc Natl Acad Sci U S A* 114, 8758-8763

[47] Gao, G., Park, J.Y., Kim, B.S., Jang, J., and Cho, D.W. (2018) Coaxial Cell Printing of Freestanding, Perfusable, and Functional In Vitro Vascular Models for Recapitulation of Native Vascular Endothelium Pathophysiology. *Adv Healthc Mater* 7, e1801102

[48] Mandrycky, C., Hadland, B., and Zheng, Y. (2020) 3D curvature-instructed endothelial flow response and tissue vascularization. *Sci Adv* 6

[49] Kim, S., Lee, H., Chung, M., and Jeon, N.L. (2013) Engineering of functional, perfusable 3D microvascular networks on a chip. *Lab Chip* 13, 1489-1500

[50] Crosby, C.O., Hillsley, A., Kumar, S., Stern, B., Parekh, S.H., Rosales, A., and Zoldan, J. (2021) Phototunable interpenetrating polymer network hydrogels to stimulate the vasculogenesis of stem cell-derived endothelial progenitors. *Acta Biomater* 122, 133-144

[51] Wei, Z., Schnellmann, R., Pruitt, H.C., and Gerecht, S. (2020) Hydrogel Network Dynamics Regulate Vascular Morphogenesis. *Cell Stem Cell* 27, 798-812 e796

[52] Brown, A., He, H., Trumper, E., Valdez, J., Hammond, P., and Griffith, L.G. (2020) Engineering PEG-based hydrogels to foster efficient endothelial network formation in free-swelling and confined microenvironments. *Biomaterials* 243, 119921

[53] Beamish, J.A., Juliar, B.A., Cleveland, D.S., Busch, M.E., Nimmagadda, L., and Putnam, A.J. (2019) Deciphering the relative roles of matrix metalloproteinase- and plasmin-mediated matrix degradation during capillary morphogenesis using engineered hydrogels. *J Biomed Mater Res B Appl Biomater* 107, 2507-2516

[54] Ghajar, C.M., Kachgal, S., Kniazeva, E., Mori, H., Costes, S.V., George, S.C., and Putnam, A.J. (2010) Mesenchymal cells stimulate capillary morphogenesis via distinct proteolytic mechanisms. *Exp Cell Res* 316, 813-825

[55] Andree, B., Ichanti, H., Kalies, S., Heisterkamp, A., Strauss, S., Vogt, P.M., Haverich, A., and Hilfiker, A. (2019) Formation of three-dimensional tubular endothelial cell networks under defined serum-free cell culture conditions in human collagen hydrogels. *Sci Rep* 9, 5437

[56] Friend, N.E., Rioja, A.Y., Kong, Y.P., Beamish, J.A., Hong, X., Habif, J.C., Bezenah, J.R., Deng, C.X., Stegemann, J.P., and Putnam, A.J. (2020) Injectable pre-cultured tissue modules catalyze the formation of extensive functional microvasculature in vivo. *Sci Rep* 10, 15562

[57] Lin, R.Z., Lee, C.N., Moreno-Luna, R., Neumeyer, J., Piekarski, B., Zhou, P., Moses, M.A., Sachdev, M., Pu, W.T., Emani, S., and Melero-Martin, J.M. (2017) Host non-inflammatory neutrophils mediate the engraftment of bioengineered vascular networks. *Nat Biomed Eng* 1

[58] Bang, S., Tahk, D., Choi, Y.H., Lee, S., Lim, J., Lee, S.-R., Kim, B.-S., Kim, H.N., Hwang, N.S., & Jeon, N.L. (2021) 3D Microphysiological System-Inspired Scalable Vascularized Tissue Constructs for Regenerative Medicine. *Advanced Functional Materials* 32

[59] Kang, K.T., Lin, R.Z., Kuppermann, D., Melero-Martin, J.M., and Bischoff, J. (2017) Endothelial colony forming cells and mesenchymal progenitor cells form blood vessels and increase blood flow in ischemic muscle. *Sci Rep* 7, 770

[60] Li, S., Nih, L.R., Bachman, H., Fei, P., Li, Y., Nam, E., Dimatteo, R., Carmichael, S.T., Barker, T.H., and Segura, T. (2017) Hydrogels with precisely controlled integrin activation dictate vascular patterning and permeability. *Nat Mater* 16, 953-961

[61] Margolis, E.A., Cleveland, D.S., Kong, Y.P., Beamish, J.A., Wang, W.Y., Baker, B.M., and Putnam, A.J. (2021) Stromal cell identity modulates vascular morphogenesis in a microvasculature-on-a-chip platform. *Lab Chip* 21, 1150-1163

[62] Song, H.G., Lammers, A., Sundaram, S., Rubio, L., Chen, A.X., Li, L., Eyckmans, J., Bhatia, S.N., and Chen, C.S. (2020) Transient Support from Fibroblasts is Sufficient to Drive Functional Vascularization in Engineered Tissues. *Adv Funct Mater* 30

[63] Lee, V.K., Lanzi, A.M., Haygan, N., Yoo, S.S., Vincent, P.A., and Dai, G. (2014) Generation of Multi-Scale Vascular Network System within 3D Hydrogel using 3D Bio-Printing Technology. *Cell Mol Bioeng* 7, 460-472

[64] Debbi, L., Zohar, B., Shuhmaher, M., Shandalov, Y., Goldfracht, I., and Levenberg, S. (2022) Integrating engineered macro vessels with self-assembled capillaries in 3D implantable tissue for promoting vascular integration in-vivo. *Biomaterials* 280, 121286

[65] Redd, M.A., Zeinstra, N., Qin, W., Wei, W., Martinson, A., Wang, Y., Wang, R.K., Murry, C.E., and Zheng, Y. (2019) Patterned human microvascular grafts enable rapid vascularization and increase perfusion in infarcted rat hearts. *Nat Commun* 10, 584

[66] Zhang, B., Montgomery, M., Chamberlain, M.D., Ogawa, S., Korolj, A., Pahnke, A., Wells, L.A., Masse, S., Kim, J., Reis, L., Momen, A., Nunes, S.S., Wheeler, A.R., Nanthakumar, K., Keller, G., Sefton, M.V., and Radisic, M. (2016) Biodegradable scaffold with built-in vasculature for organ-on-a-chip engineering and direct surgical anastomosis. *Nat Mater* 15, 669-678

[67] Chiu, L.L., Montgomery, M., Liang, Y., Liu, H., and Radisic, M. (2012) Perfusable branching microvessel bed for vascularization of engineered tissues. *Proc Natl Acad Sci U S A* 109, E3414-3423

[68]   Szklanny, A.A., Machour, M., Redenski, I., Chochola, V., Goldfracht, I., Kaplan, B., Epshtein, M., Simaan Yameen, H., Merdler, U., Feinberg, A., Seliktar, D., Korin, N., Jaros, J., and Levenberg, S. (2021) 3D Bioprinting of Engineered Tissue Flaps with Hierarchical Vessel Networks (VesselNet) for Direct Host-To-Implant Perfusion. *Adv Mater* 33, e2102661

[69]   Sekine, H., Shimizu, T., Sakaguchi, K., Dobashi, I., Wada, M., Yamato, M., Kobayashi, E., Umezu, M., and Okano, T. (2013) In vitro fabrication of functional three-dimensional tissues with perfusable blood vessels. *Nat Commun* 4, 1399

[70]   Helms, F., Zippusch, S., Theilen, J., Haverich, A., Wilhelmi, M., and Boer, U. (2022) An encapsulated fibrin-based bioartificial tissue construct with integrated macrovessels, microchannels, and capillary tubes. *Biotechnol Bioeng* 119, 2239-2249

[71]   Grigoryan, B., Paulsen, S.J., Corbett, D.C., Sazer, D.W., Fortin, C.L., Zaita, A.J., Greenfield, P.T., Calafat, N.J., Gounley, J.P., Ta, A.H., Johansson, F., Randles, A., Rosenkrantz, J.E., Louis-Rosenberg, J.D., Galie, P.A., Stevens, K.R., and Miller, J.S. (2019) Multivascular networks and functional intravascular topologies within biocompatible hydrogels. *Science* 364, 458-464

[72]   Jeon, O., Lee, Y.B., Jeong, H., Lee, S.J., Wells, D., and Alsberg, E. (2019) Individual cell-only bioink and photocurable supporting medium for 3D printing and generation of engineered tissues with complex geometries. *Mater Horiz* 6, 1625-1631

[73]   Post, A., Diaz-Rodriguez, P., Balouch, B., Paulsen, S., Wu, S., Miller, J., Hahn, M., and Cosgriff-Hernandez, E. (2019) Elucidating the role of graft compliance mismatch on intimal hyperplasia using an ex vivo organ culture model. *Acta Biomater* 89, 84-94

[74]   McGuire, B.J. and Secomb, T.W. (2003) Estimation of capillary density in human skeletal muscle based on maximal oxygen consumption rates. *Am J Physiol Heart Circ Physiol* 285, H2382-2391

[75]   Rakusan, K., Flanagan, M.F., Geva, T., Southern, J., and Van Praagh, R. (1992) Morphometry of human coronary capillaries during normal growth and the effect of age in left ventricular pressure-overload hypertrophy. *Circulation* 86, 38-46

[76]   Chuang, C.H., Lin, R.Z., Melero-Martin, J.M., and Chen, Y.C. (2018) Comparison of covalently and physically cross-linked collagen hydrogels on mediating vascular network formation for engineering adipose tissue. *Artif Cells Nanomed Biotechnol* 46, S434-S447

[77]   Bang, S., Lee, S.R., Ko, J., Son, K., Tahk, D., Ahn, J., Im, C., and Jeon, N.L. (2017) A Low Permeability Microfluidic Blood-Brain Barrier Platform with Direct Contact between Perfusable Vascular Network and Astrocytes. *Sci Rep* 7, 8083

[78]   Wang, X., Phan, D.T., Sobrino, A., George, S.C., Hughes, C.C., and Lee, A.P. (2016) Engineering anastomosis between living capillary networks and endothelial cell-lined microfluidic channels. *Lab Chip* 16, 282-290

[79] Linville, R.M., DeStefano, J.G., Sklar, M.B., Xu, Z., Farrell, A.M., Bogorad, M.I., Chu, C., Walczak, P., Cheng, L., Mahairaki, V., Whartenby, K.A., Calabresi, P.A., and Searson, P.C. (2019) Human iPSC-derived blood-brain barrier microvessels: validation of barrier function and endothelial cell behavior. *Biomaterials* 190-191, 24-37

[80] Pasut, A., Becker, L.M., Cuypers, A., and Carmeliet, P. (2021) Endothelial cell plasticity at the single-cell level. *Angiogenesis* 24, 311-326

[81] Zhao, G., Lu, H., Liu, Y., Zhao, Y., Zhu, T., Garcia-Barrio, M.T., Chen, Y.E., and Zhang, J. (2021) Single-Cell Transcriptomics Reveals Endothelial Plasticity During Diabetic Atherogenesis. *Front Cell Dev Biol* 9, 689469

[82] Peters, E.B. (2018) Endothelial Progenitor Cells for the Vascularization of Engineered Tissues. *Tissue Eng Part B Rev* 24, 1-24

[83] Melero-Martin, J.M. (2022) Human Endothelial Colony-Forming Cells. *Cold Spring Harb Perspect Med* 12

[84] Chen, Y.C., Lin, R.Z., Qi, H., Yang, Y., Bae, H., Melero-Martin, J.M., and Khademhosseini, A. (2012) Functional Human Vascular Network Generated in Photocrosslinkable Gelatin Methacrylate Hydrogels. *Adv Funct Mater* 22, 2027-2039

[85] Macklin, B.L., Lin, Y.Y., Emmerich, K., Wisniewski, E., Polster, B.M., Konstantopoulos, K., Mumm, J.S., and Gerecht, S. (2022) Intrinsic epigenetic control of angiogenesis in induced pluripotent stem cell-derived endothelium regulates vascular regeneration. *NPJ Regen Med* 7, 28

[86] Faley, S.L., Neal, E.H., Wang, J.X., Bosworth, A.M., Weber, C.M., Balotin, K.M., Lippmann, E.S., and Bellan, L.M. (2019) iPSC-Derived Brain Endothelium Exhibits Stable, Long-Term Barrier Function in Perfused Hydrogel Scaffolds. *Stem Cell Reports* 12, 474-487

[87] Bezenah, J.R., Kong, Y.P., and Putnam, A.J. (2018) Evaluating the potential of endothelial cells derived from human induced pluripotent stem cells to form microvascular networks in 3D cultures. *Sci Rep* 8, 2671

[88] Bezenah, J.R., Rioja, A.Y., Juliar, B., Friend, N., and Putnam, A.J. (2019) Assessing the ability of human endothelial cells derived from induced-pluripotent stem cells to form functional microvasculature in vivo. *Biotechnol Bioeng* 116, 415-426

[89] Rouhani, F.J., Zou, X., Danecek, P., Badja, C., Amarante, T.D., Koh, G., Wu, Q., Memari, Y., Durbin, R., Martincorena, I., Bassett, A.R., Gaffney, D., and Nik-Zainal, S. (2022) Substantial somatic genomic variation and selection for BCOR mutations in human induced pluripotent stem cells. *Nat Genet* 54, 1406-1416

[90] James, B.D. and Allen, J.B. (2021) Sex-Specific Response to Combinations of Shear Stress and Substrate Stiffness by Endothelial Cells In Vitro. *Adv Healthc Mater* 10, e2100735

[91]   Ryan, H., Bister, D., Holliday, S.A., Boehlein, J., Lewis, A., Silberman, J., Allen, J.B., and Moore, E. (2022) Ancestral Background Is Underreported in Regenerative Engineering. *Regen Eng Transl Med* 8, 499-503

[92]   Ingber, D.E. (2022) Human organs-on-chips for disease modelling, drug development and personalized medicine. *Nat Rev Genet* 23, 467-491

[93]   Nahle, Z. (2022) A proof-of-concept study poised to remodel the drug development process: Liver-Chip solutions for lead optimization and predictive toxicology. *Front Med Technol* 4, 1053588

[94]   Emulate (2021) Emulate Endorses the FDA Modernization Act of 2021. https://emulatebio.com/fda-modernization-act/

[95]   Jayasinghe, S.N. (2017) Thoughts on Scaffolds. *Adv Biosyst* 1, e1700067

[96]   Pavlovich, S. (2016) Should Society Encourage The Development Of 3D Printing, Particularly 3D Bioprinting Of Tissues And Organs? *International Journal of Scientific & Technology Research* 5, 41-46

Chapter 3 – Stromal Cell Identity Modulates Vascular Morphogenesis in a Microvasculature-on-a-Chip Platform

3.1 Introduction

Capillaries are necessary to transport blood, oxygen, and other nutrients throughout the body. Vascularization of engineered tissues is required to avoid tissue death and allow convective transport of nutrients in metabolically active tissues that are too thick to be sustained via diffusion alone [1]. An important objective in biomedical engineering is to create functional (perfusable) capillary networks that can rapidly inosculate with host blood vessels upon transplantation to regenerate large tissue volumes. The ability to create functional and stable blood vessels remains a significant hurdle in the clinical implantation of nearly all engineered tissues [2]; without microvasculature, many tissues greater than 200 μm in thickness may not remain viable [3]. Existing methods to form functional vasculature include creating prepatterned vessel structures seeded with endothelial cells [4, 5] or harnessing existing vasculature's ability to undergo angiogenesis to create new vessels [6]. While these methods can create vasculature in as short as 3 days, the vessels often lack supportive mural cells required to maintain long-term function and stability *in vivo* [7, 8].

Another approach to achieving neovascularization involves vascular self-assembly, which occurs when endothelial cells (EC) and stromal cells (SC) are co-cultured in three-dimensional hydrogels and undergo a process akin to developmental vasculogenesis. Our group has developed several assays to investigate neovascularization in the presence of multiple SC types including sprouting vascular bead assays [9-11], vasculogenesis in bulk hydrogels [12-14], and vasculogenesis in modular microtissues [15]. However, these methods lack the ability to study perfusion of microvessels in a physiologic manner *in vitro*. In this study, we examined the ability of various SC to aid the formation of functional microvasculature when co-cultured with EC in a perfusable microfluidic system. While the creation of microvasculature using co-culture systems within microfluidic platforms has been previously explored [16-18], comparisons across systems have been limited by differences in microfluidic geometries, endothelial cell lineages, types of anastomoses (i.e., to openings in PDMS channels or to endothelialized vessels), and culture duration. In this study, we directly compared the abilities of different SC to modulate network formation and function within a single physiologically-relevant model system, and the abilities of microvascular networks to inosculate with mesovessels within the chip to form perfusbale, hierarchical vascualture. Notable key features in our comparison were the use of a consistent EC source to isolate the effect of SC identity and the use of endothelialized channels within the hydrogel to simulate biologically relevant inosculation of microvessels to arteriole-scale vessel structures rather than PDMS channels (endothelial cell lined or not) in a chip. In the present study, we successfully developed a widespread capillary bed within a microfluidic hydrogel and deciphered the roles of each SC type in modulating vessel formation, inosculation, and perfusion over time. The three SC types chosen for this study (lung fibroblasts (LF), dermal fibroblasts (DF), and mesenchymal stem cells (MSC)) are known to support vessel formation in a range of 3D

culture systems. LF have been shown to robustly support vascular morphogenesis of various EC types [9]. DF and MSC potentially represent more clinically-relevant cell sources capable of supporting vascular morphogenesis [12, 19], accessible via skin biopsy and bone marrow isolation, respectively. MSC in particular secrete pro-angiogenic factors [20-22] and are capable of taking on a pericyte phenotype [16, 23] important for vessel maturation and stability over extended culture periods. We measured multiple properties of the resultant microvascular networks pertaining to both formation and function to capture differences in the support provided by each SC type, finding that the degree of vascular formation and function were dependent on the SC type used to support microvascular networks. Further, we identified SC identity as a critical parameter in regulating inosculation between meso- and microvasculatue to yield perfuable hierarchical vasculature. This study highlights the need for more comparative studies elucidating key differences in commonly used cell types and possible mechanisms underlying vascular formation and function.

3.2 Materials and Methods

3.2.1 Cell culture

Human umbilical vein endothelial cells (EC) were isolated from fresh umbilical cords (obtained via an IRB-exempt protocol from the University of Michigan Mott's Children's Hospital), cultured in fully supplemented endothelial growth medium-2 (EGM-2; Lonza, Walkersville, MD), and used until passage 7. Bone marrow derived mesenchymal stem cells (MSC; RoosterBio, Frederick, MD) were cultured in Rooster Nourish (RoosterBio) and used until passage 7. Normal human dermal fibroblasts (DF; Lonza) and normal human lung fibroblasts (LF; Lonza) were cultured in high glucose Dulbecco's modified eagle medium (DMEM; Gibco,

Waltham, MA) supplemented with 10% fetal bovine serum (FBS; Gibco) and used until passage 15. All cells were cultured at 37 °C and 5% CO_2 with medium exchanges every other day.

3.2.2 Vasculogenesis assay within microfluidic chip platform

A vasculogenesis assay widely used in our lab [12, 13] was modified for use within a microfluidic chip system (Fig. 3.1) [24]. SC and EC suspended in serum free EGM-2 were combined at 2:1 (2M/mL SC with 1M/mL EC or 1M/mL SC with 500K/mL EC) or 1:1 (1M/mL of each cell type or 500K/mL of each cell type) ratios (Table 3.1) [17, 18, 22, 25], encapsulated in fibrin precursor solutions, and injected into insertion ports within the chip to polymerize around two 290 μm diameter needles (Fig. 3.1A, B). Precursor solutions contained 2.5 mg/mL (clottable protein) filtered bovine fibrinogen (Sigma, St. Louis, MO), 1 U/mL bovine thrombin (Sigma), and 10% FBS. Following gelation and swelling, needles were removed, needle tracks were sealed with vacuum grease (Dow Corning, Midland, MI), and empty channels were seeded with additional ECs suspended at 2.5 M/mL. Chips were statically cultured in fully supplemented EGM-2 exchanged daily (50 μL reservoir, 200 μL per sample) and cultured for one or two weeks. To confirm vascular formation using the specific combination of EC and SC within each device, cell-containing bulk fibrin hydrogels were created as described above, in 48-well culture plates, and cultured in EGM-2 for 7 days, with medium exchanges on days 1, 3, and 5. Chips were discarded if vascular formation was not observed in control gels.

CONDITION	SC-EC RATIO	SC DENSITY	EC DENSITY
1	2:1	2 M/mL	1 M/mL
2	1:1	1 M/mL	1 M/mL
3	2:1	1 M/mL	500 K/mL
4	1:1	500 K/mL	500 K/mL

Table 3.1: *Cellular ratio and density conditions used to fabricate samples throughout the study.*
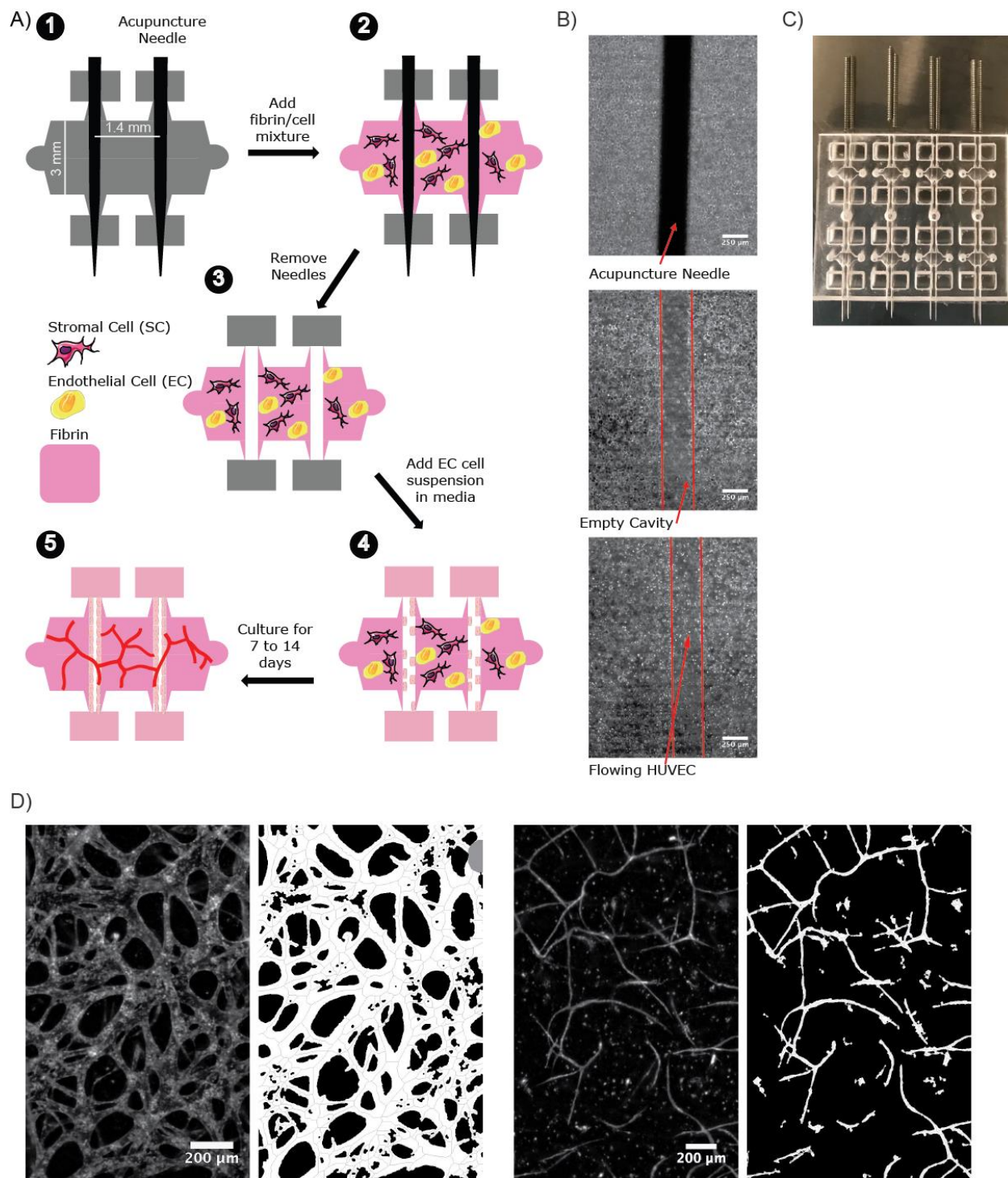
Figure 3.1: Methods for the formation and analysis of microvascular networks. *(A) Schematic diagram and (B) corresponding phase-contrast images of gelation, seeding, and culture procedures (steps 2-4). (C) Color image of the PDMS mold bonded to a glass slide with acupuncture needles inserted. (D) Maximum intensity projection of a confocal z-stack and binarization for network analysis for LF-EC networks (left) and MSC-EC networks (right).*

3.2.3 Microcarrier bead assembly

Cytodex microcarrier beads (Sigma) were suspended in phosphate buffered saline (PBS; Gibco) and autoclaved for sterilization. The concentration of beads in suspension was determined by counting the beads from a small sample and extrapolating to the entire volume. Beads were stored for up to 6 months at 4 °C.

To prepare EC coated beads, approximately 10,000 beads were taken from the stock vial and washed thrice in EGM2. EC were trypsinized and suspended at 1 M/mL. The beads and 4 M EC were combined in an upright T-25 flask (5 mL total volume). The flask was shaken for 1 minute and placed in the incubator in the upright position. The flask was shaken again after 5 minutes, 20 minutes, and every 30 minutes thereafter for a total time of 4 hours. After shaking the beads, the suspension was transferred to a new T-25 flask and 5 mL fresh EGM2 was added (total volume 10 mL). The beads were incubated overnight in standard cell culture position (flat, not upright). EC coated beads were incorporated in fibrin gels at a density of approximately 50 beads/gel. Fibrin gels also contained 25 K/mL LF, 1 U/mL thrombin, 10% FBS, and 2.5 mg/mL fibrinogen.

3.2.4 Channel patency and network perfusion

On the final day of culture, fluorescein dextran (10 kDa, 25 µg/mL) was inserted into media reservoirs at a hydrostatic pressure difference of ~0.1 cmH$_2$O and imaged in real time. If dextran flowed through the channels, the channels were considered patent and if dextran flowed through vessel network, the network was considered perfused.

3.2.5 Immunofluorescence staining and imaging

Chips were fixed on the last day of culture on a rocker plate for 1 hour in 4% paraformaldehyde (Sigma) and washed with phosphate buffered saline (PBS; Gibco) for at least 12 hours. Bulk gels were fixed on day 7 for 15 minutes in aqueous buffered zinc formalin fixative (Z-fix; Anatech, Battle Creek, MI). Following fixation and washing, control gels and chips were permeabilized for 1 hour in 0.1% Triton X-100 (Fisher Scientific, Waltham, MA) in PBS and blocked for 4 hours in blocking solution (2% bovine serum albumin (BSA; Sigma) dissolved in tris buffered saline-Tween20 (TBS-T; Fisher Scientific). Samples were stained overnight with rhodamine-conjugated Ulex europaeus Agglutinin I (UEA; Vector Laboratories, Burlingame, CA) at 1:200 dilution and 4', 6-diamidino-2-phenylindol (DAPI; 1μg/mL, Sigma) to label ECs and all cell nuclei, respectively. Staining dilutions were made in blocking solution. Following staining, samples were washed with TBS-T for at least 12 hours before imaging. TBS-T was exchanged after washing and before imaging. For all staining processes, chips were maintained on a rocker plate and control gels were maintained in static conditions.

Selected samples were further stained for alpha smooth muscle actin (αSMA), neuron-glial antigen 2 (NG2), and platelet derived growth factor receptor beta (PDGFRβ) to identify SC within the gels. Samples were incubated overnight at 4ºC with a primary antibody for αSMA (Sigma, A2547, mouse IgG$_{2a}$ isotype, 1:200 dilution), NG2 (abcam, ab255811, rabbit IgG isotype,1:200 dilution), or PDGFRβ (Sigma, HPA028499, 1:100 dilution) and washed with TBS-T overnight at 4ºC. Samples were then incubated overnight at 4ºC with the appropriate Alexa Fluor 488 conjugated secondary antibody (Invitrogen, A11001, goat-*anti*-mouse IgG$_{H+L}$, 1:200 dilution or Invitrogen, A11008, goat-*anti*-rabbit IgG$_{H+L}$, 1:500 dilution) and washed with TBS-T overnight at 4ºC. Antibody dilutions were made in blocking solution.

Images were acquired with an Olympus IX81 inverted fluorescent microscope equipped with a confocal Disc Spinning Unit (DSU; Olympus America, Center Valley, PA) and Metamorph Software (Molecular Devices, Sunnyvale, CA). Control gels were imaged to confirm the presence of vasculature, but not further quantified. Confocal z-stacks (4 slices/stack) of chips were obtained and compressed into maximum intensity projections preceding analysis. Quantification of total network length and network interconnectedness were performed on 225 μm stacks (75 μm/slice) obtained at 4x magnification. Quantification of vessel diameter and qualitative analysis of αSMA, NG2, and PDGFRβ expression were performed on 30 μm stacks (10 μm/slice) obtained at 10x magnification. Images acquired at 4x spanned the region between the two parent channels and images acquired at 10x were in close proximity to the parent channels not the boundaries of the chip. Total network length per volume, number of connected vessel sets per volume, and vessel diameter were quantified using the Angiogenesis Tube Formation module in Metamorph (Fig. 3.1D). This program creates a binary mask of the fluorescent images based on user inputted values for threshold above background and minimum/maximum vessel size. Any region of the white mask that is within the user inputted size range is considered a vessel and is added to the total network length value; regions of the mask above the size range are considered nodes and not counted towards the network length value. Network interconnectedness is measured via the number of connected vessel sets, in which the program counts the number of separate, non-connected masked regions and determines the network length of each independent set. Vessel diameter is an average value for the image calculated by dividing total network area by total network length. Multiple images per sample were quantified and averaged to obtain a single value per sample for each metric. Cell counts were performed on 4x DAPI images. Images were

binarized and nuclei were counted using a custom ImageJ script. The change in cell number was calculated as a percentage of the theoretical initial cell density.

3.2.6 Traction force microscopy

Traction force microscopy was performed on all three SC types, using previously described methods [26-28], to gain an understanding of differences in the magnitude of tractional vectors produced by each SC type. Square cover glass (22 mm; VWR, Radnor, PA) was etched with piranha solution (1-part H_2O_2 (Fisher Scientific) with 3-parts sulfuric acid (Fisher Scientific)) and functionalized with 1% glutaraldehyde (Sigma). Two kPa polyacrylamide (PA) gels with 0.2 μm fluorescent beads (Invitrogen, Carlsbad, CA) were formed on top of the glass slides, followed by conjugation of 50 μg/mL type-I collagen (Advanced Biomatrix, San Diego, CA) via sulfo-sanpah (Proteochem, Hurricane, UT). Fluorescent beads in the PA gel served as displacement markers during imaging. Cells were seeded onto the gels at 1000 cells/mm^2. Individual cells and bead planes were imaged one day post-seeding both before and after cell lysis to measure bead displacements. Displacement vectors and traction were computed via the particle image velocimetry (PIV) and fourier transform traction cytometry (FTTC) plugins in ImageJ, respectively. Traction data were analyzed via a custom MATLAB (Mathworks, Natick, MA) script. Experimental number included 12-16 cells per slide and two slides per cell type, which were pooled together for statistical analysis.

3.2.7 Statistics

Prism 8 (GraphPad, San Diego, CA) was used to analyze data for statistical significance. All data are represented as mean ± standard deviation. Microfluidic chip data were analyzed with statistical tests performed on n = 3 independent replicates. For the independent replicates in each condition, data from 3-4 technical replicates were averaged together resulting in a single data point per independent replicate. Data were analyzed using a one-way ANOVA with Sidak's multiple comparisons post-hoc test for pre-specified comparisons. For TFM data, each cell was considered an independent sample (n = 28-30 cells per condition across 2 different substrates) and the data were analyzed with a Kruskal-Wallis test with Dunn's multiple comparisons post-hoc test. $p < 0.05$ was considered statistically significant.

3.3 Results

3.3.1 EC fail to form microvessels in the absence of stromal cells

We examined capillary formation in three distinct assays: angiogenic sprouting from EC coated Cytodex beads, angiogenic sprouting from arteriole-scale endothelialized channels, and a hybrid angiogenic/vasculogenic model of sprouting from arteriole-scale endothelialized channels and self-assembly similar to developmental vasculogenesis within the surrounding hydrogel. In all three assays, EC failed to form vessels in the absence of SC.

In the Cytodex bead assay, EC coated beads were co-cultured with LF in bulk fibrin hydrogels. In the absence of LF, EC sprouted as single cells and failed to form microvasculature. In the presence of LF, EC sprouted as multicellular vessel-like structures. Further the sprouted capillaries branched into bifurcated vessels in some regions (Fig. 3.2A). In the mesovessel angiogenic sprouting assay, a mesovessel was fabricated within a microfluidic chip and the

69

surrounding hydrogel was acellular or contained embedded LF. Without LF in the bulk, the mesovessel failed to sprout microvasculature into the surrounding hydrogel. When LF were incorporated into the bulk, EC sprouted from the vessel forming capillaries in the surrounding hydrogel (Fig. 3.2B).
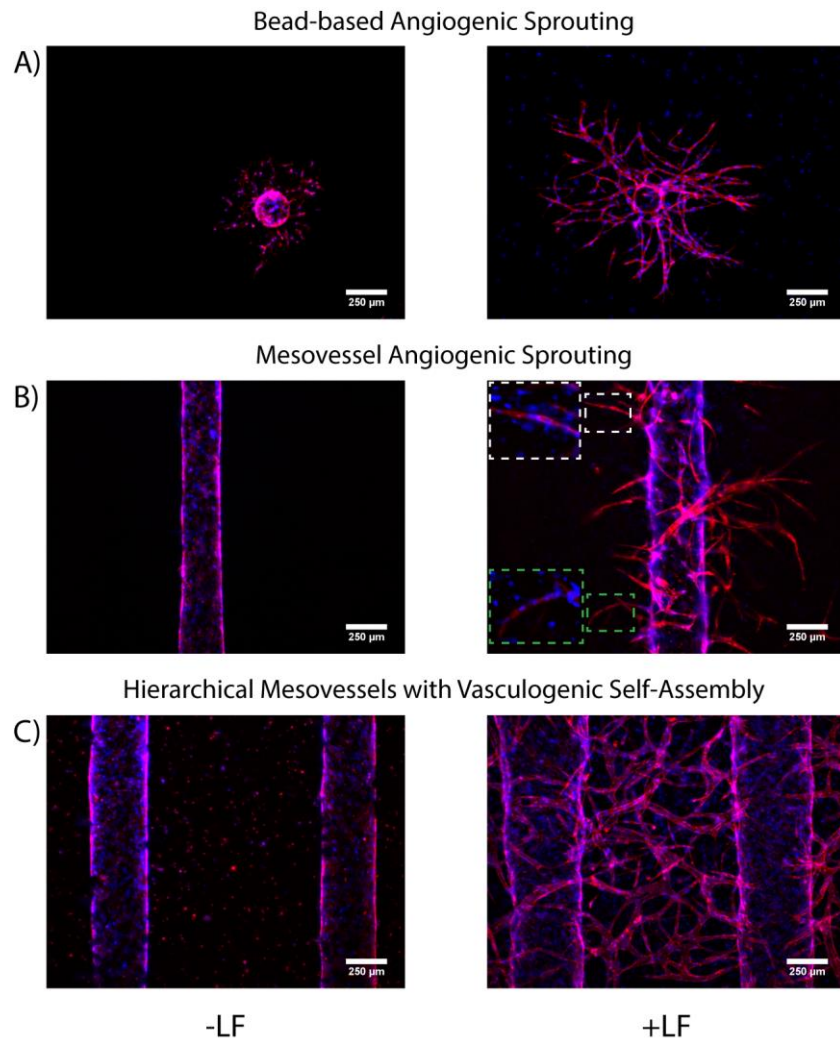
Figure 3.2: Stromal cells are critical for vascular morphogenesis. Representative UEA (red) and DAPI (blue) stained images of vasculature formed without (left) or with (right) LF from a (A) bead based angiogenic sprouting model, (B) mesovessel angiogenic sprouting model (insets show magnified, higher contrast image to see multicellular structures), and (C) hierarchical model composed of mesovessels with capillary vasculogenic self-assembly.

Finally, in the multiscale hierarchical model used throughout the rest of this chapter, EC in the bulk remained single cells when cultured without LF and the mesovessels failed to sprout.

When co-cultured with LF, EC in the bulk self-assembled into capillary networks and the mesovessel sprouted to interconnect to surrounding capillaries (Fig. 3.2C).

3.3.2 All three stromal cell types facilitate the formation of microvascular networks

We examined capillary network formation via a self-assembly process similar to developmental vasculogenesis within a microfluidic chip platform to enable studies of perfusion. We examined four different co-culture conditions (Table 3.1) that varied in cell density and SC-EC ratio in order to determine if these parameters, in addition to SC identity, influenced vascular morphogenesis. Past studies have examined differing densities and ratios further complicating cross-comparison between distinct studies. Therefore, we sought to enable these comparisons within a single multiplexed microfluidic chip system which facilitated the assessment of a broad range of conditions. LF, DF, and MSC supported the formation of microvascular networks by day 7 (Fig. 3.3A, top & Fig. 3.3B, left) which persisted up to day 14 (Fig. 3.3A, bottom & Fig. 3.3B, right) across all conditions.

To quantify the amount of vasculature formed we assessed the total length of microvascular networks in each condition. On day 7, networks formed with support from LF and DF exhibited significantly longer total network length (TNL) than networks formed with support from MSC in all four conditions (Fig. 3.3B, left). LF-supported networks were significantly longer than DF-supported networks only at the highest (condition 1) and lowest (condition 4) initial cell densities tested (Fig. 3.3B, left). At intermediate cell densities (conditions 2 and 3), DF were capable of supporting network formation to the same extent as LF. By day 14, LF-supported networks exhibited greater TNL compared to DF-supported networks across conditions 1-3, while DF-supported networks exhibited greater TNL compared to MSC-supported networks across

conditions 2-4 (Fig. 3.3B, right). At the highest initial cell densities examined (condition 1), MSC were capable of supporting network formation to the same extent as DF; at the lowest initial cell densities tested (condition 4), LF and DF supported vascular morphogenesis to similar extents, with both significantly greater than MSC. LF consistently supported greater TNL than MSC, regardless of condition. These studies indicate that fibroblasts aid more extensive vascular formation than MSC.

After examining changes in TNL between the three SC types we aimed to determine if TNL increased over time for each SC type. Examining each SC type separately we compared each condition across time points (i.e., LF condition 1 day 7 vs. LF condition 1 day 14). MSC- and DF-supported networks did not display significant differences in TNL between day 7 and day 14 for networks of the same condition (Fig. 3.3C, middle and right). Conversely, LF-supported networks displayed differences in one condition only, condition 3, which showed a significant increase in TNL by day 14 compared to day 7 (Fig. 3.3C left). We also sought to determine if TNL was maintained regardless of initial cell density, therefore, we examined differences on a single day for a single SC type across conditions (i.e., DF condition 1 day 7 vs. DF condition 3 day 7). LF-supported networks showed significant differences on day 14 between conditions 1 and 4 and between conditions 3 and 4, while DF- and MSC- supported networks displayed no significant differences between conditions at either timepoint. While not statistically significant, MSC-supported networks displayed a downward trend in network length as the initial cell density decreased. Taken together, these data suggest that all three SC types supported the formation of vasculature that was maintained over extended periods of culture without significant loss of network length due to vessel pruning or other network modifications, though LF yielded the most dense and interconnected microvascular networks.
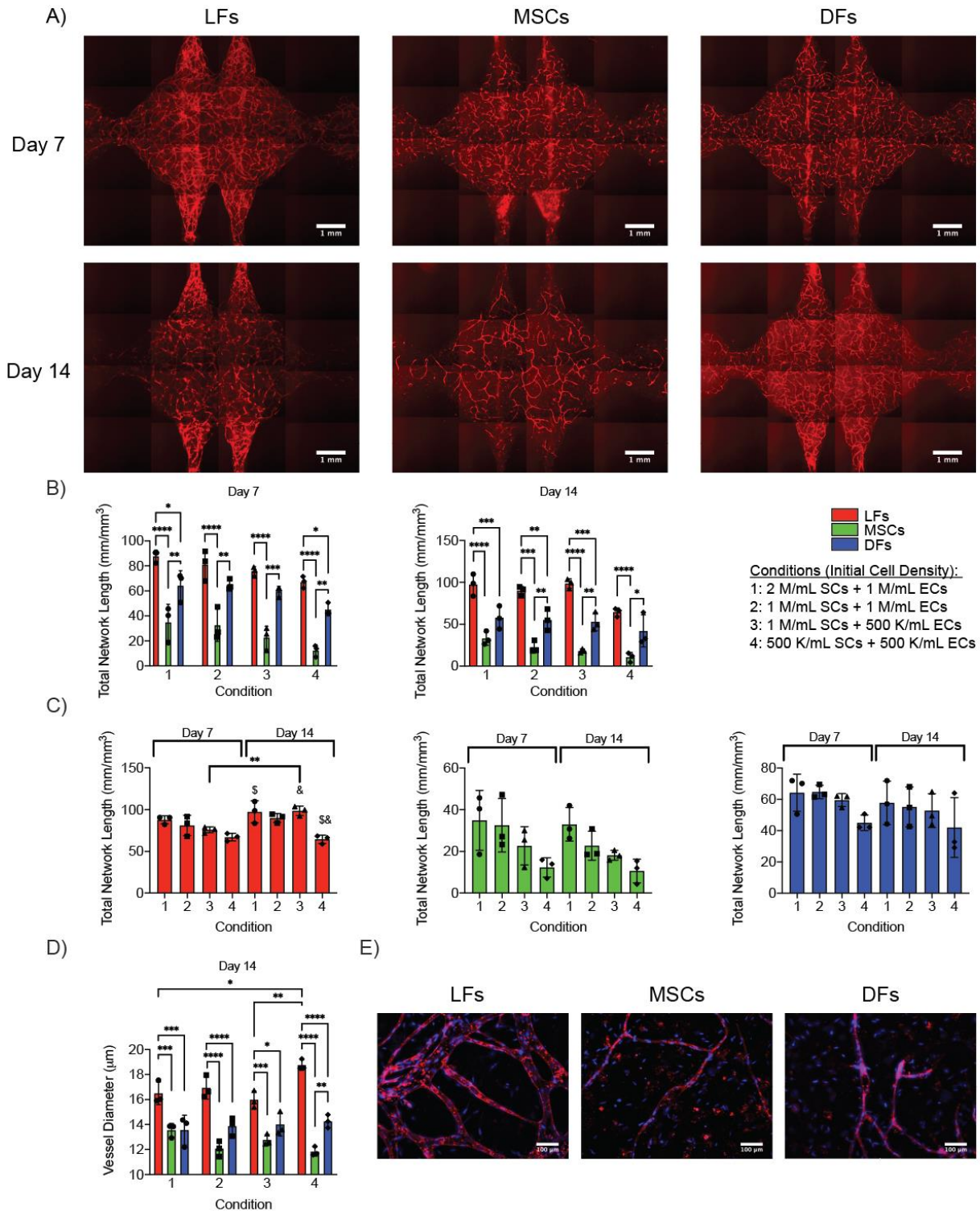
***Figure 3.3: Microvascular morphogenesis is impacted by stromal cell identity.** (A) Representative UEA stained images of microvascular networks formed from LF-EC (left), MSC-EC (middle), and DF-EC (right) co-cultures on day 7 (top) and day 14 (bottom). (B) Quantification of total network length on day 7 (left) and day 14 (right). (C) Data in (B) repopulated into separate graphs to make comparisons within a single cell type. (D) Quantification of vessel diameter on day 14. (E) Representative UEA (red) and DAPI (blue)*

stained images of microvascular networks formed from LF-EC (left), MSC-EC (middle), and DF-EC (right) condition 4 co-cultures on D14 depicting differences in vessel diameter. α < 0.05 was considered significant. * p < 0.05, ** p < 0.01, *** p < 0.001, **** p < 0.0001, $ p < 0.05, & p < 0.01. Matched symbols and brackets with symbols indicate significance. Two (TNL) or three (diameter) ROIs were assessed per technical replicate, with a minimum of 3 technical replicates per condition, per time point, per cell type and N = 3 independent replicates per condition, per time point, per cell type analyzed. Data points correspond to independent replicates.

We also quantified the effects of SC identity on the diameter of the microvessels at day 14. LF facilitated the formation of vessels with larger diameters compared to those formed in the presence of both DF and MSC (Fig. 3.3D, E). DF- and MSC-supported vessels exhibited similar diameters that were not significantly different from each other in three of the four conditions (Fig. 3.3D). While LF-supported vessels were consistently larger than DF- and MSC-supported vessels, there were also differences in diameter between LF-supported vessels of different conditions (conditions 1 vs. 4 and conditions 3 vs. 4). The differences in diameter were between the same conditions that displayed differences in TNL. These data show that engineered capillaries formed with each of the three SC types had diameters on the order of capillary vessels *in vivo*, typically less than 50 μm [29]. The larger diameter of LF-supported vasculature appeared to yield lumenized capillaries as opposed to cord-like structures that developed with support from DF and MSC (Fig. 3.3E LFs vs. DFs and MSCs).

3.3.3 Stem cells are capable of supporting changes in network interconnectedness over time

With the exception of one condition (LF, condition 3), networks formed by the same SC type did not exhibit significant differences in TNL between day 7 and day 14 (Fig. 3.3B, C); therefore, network interconnectedness was examined. TNL provided insight into the total vessel density supported by each SC type. Further examination into the number of connected vessel sets

per volume elucidated the level of network interconnectedness each SC type facilitated. Fewer connected sets per volume indicated that the network was more interconnected rather than separate, dispersed vessel segments. LF and DF did not elicit significant differences in network interconnectedness over the second week in culture (Fig. 3.4A, C, respectively); however, MSC-supported microvascular networks did show significant differences in the degree of network interconnectedness for two of the four conditions (Fig. 3.4B). Vessel networks formed with support from MSC with higher initial cell densities (conditions 1 and 2) exhibited a decrease in the number of connected sets over the second week in culture (day 7 vs. day 14). However, LFs supported the formation of significantly more interconnected networks overall (~20 connected sets/mm^3 compared to ~50-100 connected sets/mm^3 for DF- and MSC-supported networks) (Fig. 3.4D, E).

Though LF consistently aided in the formation of interconnected networks, DF- and MSC-supported networks did trend towards a decrease in connected sets over time (Fig. 3.4D, E). On day 7, LF-supported networks had significantly fewer connected sets than both DF- and MSC-supported networks in all four conditions (Fig. 3.4D). By day 14, differences were only observed in 1:1 SC:EC ratios (Fig. 3.4E). These data indicate a trend towards decreasing connected sets in DF- and MSC-supported networks despite the lack of significance when compared with conditions of the same cell type across time periods.

3.3.4 Stromal cell type determines network perfusability

In addition to morphological assessments of the microvascular networks, we also assessed critical functional aspects such as vessel perfusion. We hypothesized that a more interconnected network would facilitate better perfusion of the region between the two parent channels. To perfuse
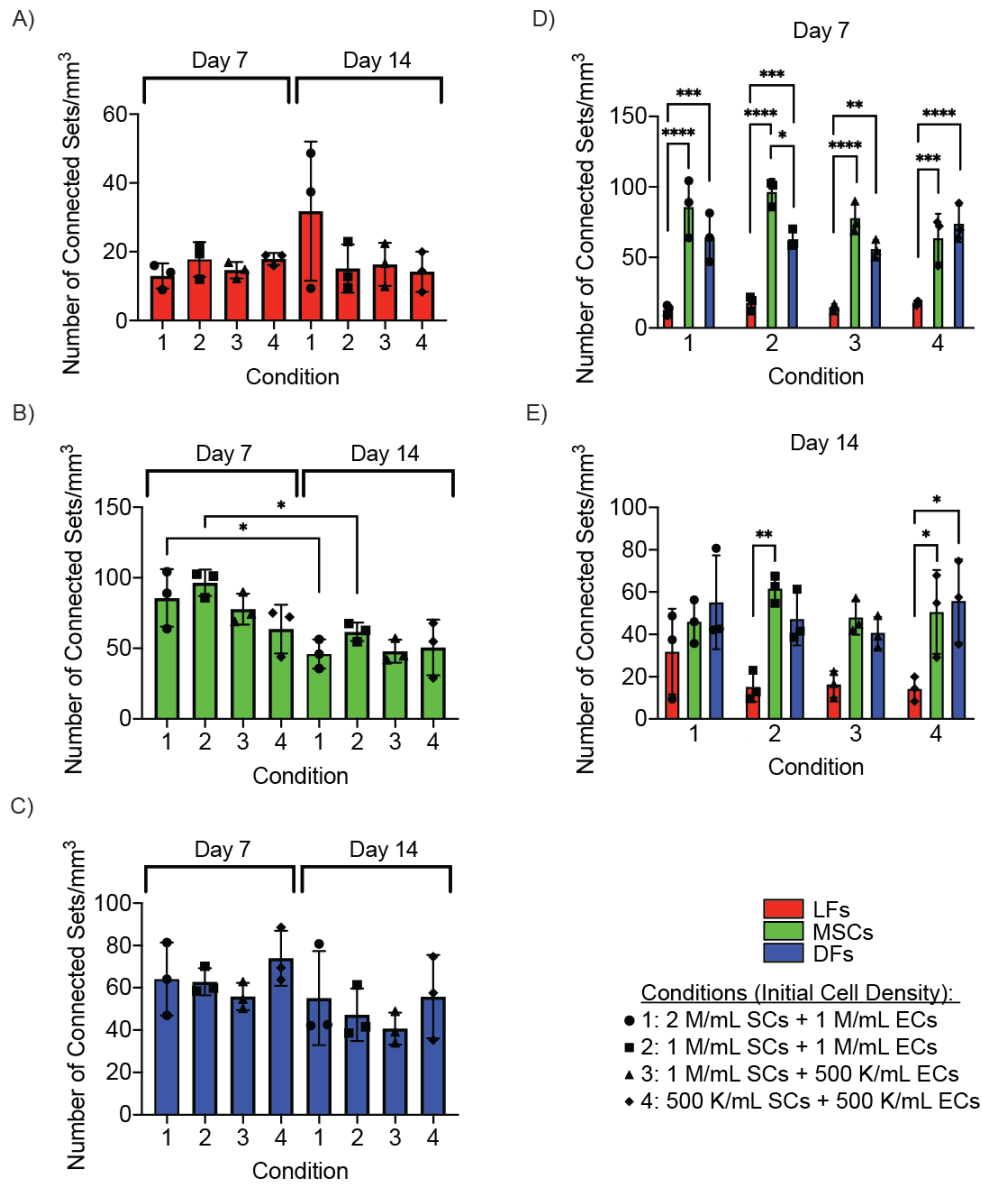
Figure 3.4: Bone marrow-derived mesenchymal stem cells induce changes in network interconnectedness over time. *Quantification of network interconnectedness over time for (A) LF-EC, (B) MSC-EC, and (C) DF-EC co-cultures. (D, E) Data repopulated from (A)-(C) to make comparisons of network interconnectedness between each stromal cell type on (D) day 7 and (E) day 14. $\alpha < 0.05$ was considered significant. * $p < 0.05$, ** $p < 0.01$, *** $p < 0.001$, **** $p < 0.0001$. Two ROIs per technical replicate, a minimum of 3 technical replicates per condition, per time point, per cell type and N = 3 independent replicates per condition, per time point, per cell type were analyzed. Data points correspond to independent replicates.*

the microvascular network, three criteria were needed: 1) patent parent channels, 2) inosculation of microvessels to the parent channels, and 3) patent microvessels. Here we showed that stromal cell identity influenced these criteria, which were assessed via the infusion of 10 kDa fluorescent dextran into the parent channels [30-32]. LF-containing devices had patent parent channels in 100% of samples (Fig. 3.5B, Fig. S3.1A) and perfused microvascular networks in greater than 50% of samples on day 7 and day 14 (Fig. 3.5A, C, Fig. S3.1B). Conversely, MSC- and DF-containing devices yielded microvascular networks that did not perfuse (Fig. 3.5C, Fig. S3.1B), despite some percentage of parent channel patency (Fig. 3.5B, Fig. S3.1A). Samples with two patent parent channels were considered completely open. DF-containing samples had at least one patent parent channel 56% of the time (27% completely open) on day 7, but this percentage dropped considerably by day 14 to only 6% with a single patent channel (0% completely open). MSC-containing samples had 100% patency in at least one parent channel on day 7 (83% completely open) which decreased slightly by day 14 to 88% with at least one patent channel (69% completely open).

In this system, the second and third criteria could only be assessed in tandem, i.e., dextran only flowed through the network if microvessels were both patent and inosculated to the parent channel. It is possible that in DF- and MSC-supported networks, there were patent microvessels that were not inosculated, inosculated microvessels that were not patent, or microvessels that were neither patent nor inosculated. However, in this system, these separate scenarios could not be distinguished.
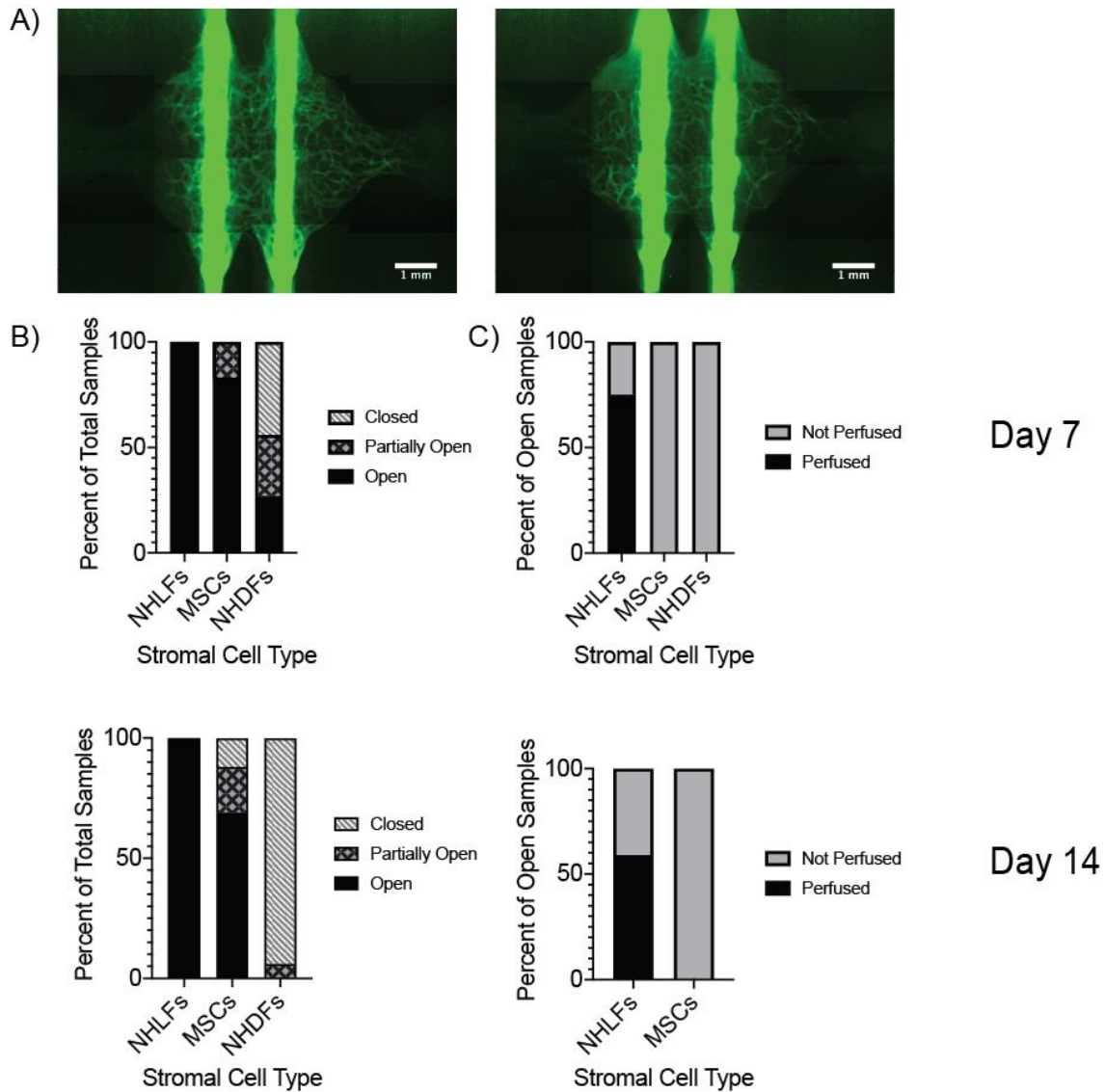
Figure 3.5: Stromal cell type determines vessel patency and microvascular network perfusion. *(A) LF-EC networks perfused with 10 kDa dextran on day 14 in condition 3 (left) and condition 4 (right). Images show complete perfusion. (B) Channel patency and (C) network perfusion for each cell type on day 7 (top) and day 14 (bottom). (B, C) Data from all four conditions pooled by cell type. A minimum of 3 technical replicates per condition, per time point, per cell type and N = 3 independent replicates included per condition, per time point, per cell type were analyzed.*

3.3.5 Total cell number impacted the ability of stromal cells to aid in network formation

To further characterize differences in microvascular networks formed in the presence of each SC type, we examined total cell number and change in cell number at the final time point of

culture. In samples formed with each of the three SC types, changes in cell number over the culture duration led to an equilibration of cell density within the devices by the final day in culture (either day 7 or day 14) (Fig. 3.6A). MSC-supported networks exhibited the lowest final cell density. In LF-containing and DF-containing samples, the final cell density for each condition was roughly equal to the mean (or slightly below) of the four cell densities used at the start of the experiment, while for MSC-containing samples the final cell density for each condition was around the lowest initial cell density (or slightly below) used at the start of the experiment. LF- and DF- supported networks exhibited both increases and decreases in cell number over time, indicating an optimal total initial cell density between 1.5-2M total cells/mL that would result in no change in cell number. In these constructs, total initial cell densities less than 2M cells/mL led to an increase in cell number, while total initial cell densities above 2M cells/mL led to a decrease in cell number (Fig. 3.6B, left and right). Conversely, MSC-supported networks exhibited decreases in cell number across all conditions (Fig. 3.6B, middle).

3.3.6 Stromal cell traction forces may influence microvascular network formation

Previous studies from our group and others have implicated EC-mediated contractile forces in angiogenic sprouting and the formation of microvascular networks in natural matrices [10, 33, 34]. The impact of stromal cell contractile forces on vascular morphogenesis is comparatively understudied, despite relevance for vascular development, engineered tissues, and tumor angiogenesis. Therefore, we aimed to determine if SC-generated traction forces may account for the observed differences in network formation, channel patency, and network perfusion in various SC-supported networks. Differences in LF-, DF-, and MSC-generated traction forces were quantified by culturing cells on collagen-functionalized polyacrylamide gels containing 0.2 µm

beads as fiduciary markers and performing 2D traction force microscopy (TFM). LF and DF produced significantly greater levels of median traction compared to MSC (Fig. 3.6C, D).
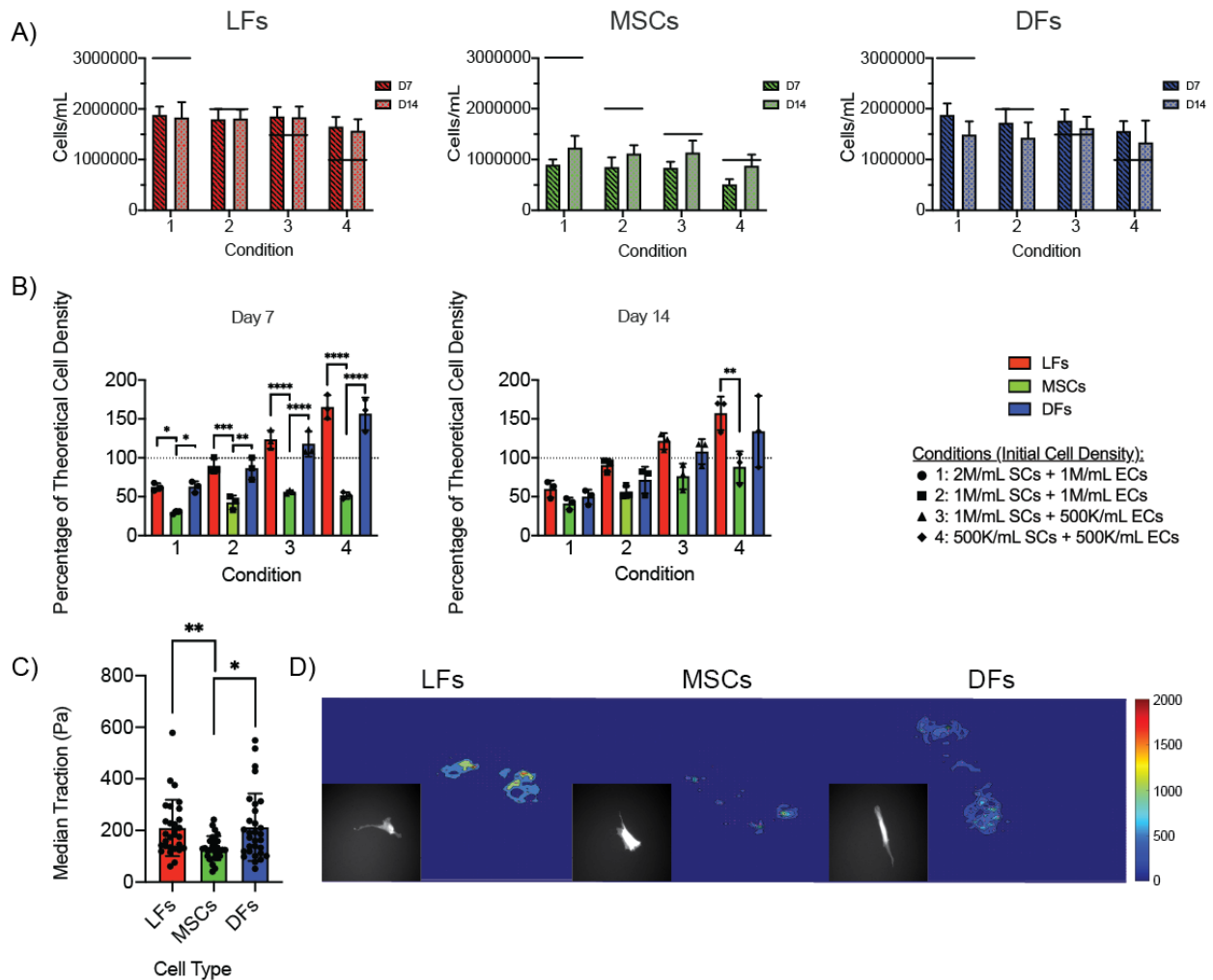
Figure 3.6: Network morphogenesis is influenced by cell number and cell-imparted traction. *(A) Total cell number at the endpoint of culture for all three stromal cell types. (B) Change in cell number for all three network formations. (C) Cell imparted traction on collagen-coated polyacrylamide matrices. (D) Representative images of cell traction for each SC type. α < 0.05 was considered significant. * p < 0.05, ** p < 0.01. N = 28-30 cells per cell type analyzed; data points represent individual cells.*

3.3.7 Stromal cells express αSMA and reside in perivascular locations in this on-chip platform

Prior studies have shown SC from a range of tissue origins are capable of adopting a perivascular morphology and expressing a subset of pericyte markers, when co-cultured in

hydrogels [34-36]. Therefore, we sought to qualitatively assess αSMA expression and SC localization in relation to the vessel networks that formed within the microfluidic devices, focusing on a subset of samples fabricated using the cell density and ratio of condition 2. All three SC types displayed αSMA protein expression at day 7 in culture (Fig. 3.7A). LF, DF, and MSC displayed a spread and elongated morphology within the gels, with the DF appearing to spread most extensively and uniformly throughout the gels in the representative images shown. By day 14, LF expression of αSMA appeared qualitatively diminished with less perivascular association (Fig. 3.7B). In contrast, DF and MSC remained closely associated with the microvasculature (Fig. 3.7B), adopting a sheath-like morphology marked by αSMA expression around vessels (Fig. 3.7B, white arrowheads). In the case of cultures containing MSC, αSMA expression appeared to be restricted to cells in perivascular locations, especially at day 14; in contrast, cultures containing DF showed αSMA expression in cells found throughout the gel.

3.3.8 Lung fibroblasts express additional pericyte markers, NG2 and PDGFRβ, specifically in perivascular locations in this on-chip platform

Given that LF supported the highest mircovessel density and interconnectedness and were the only SC type to support functional perfusion, we sought to examine other markers of a pericyte phenotype in these cells. We qualitatively examined NG2 (Fig. 3.8A, C) and PDGFRβ (Fig. 3.8B, D) expression and localization of these pericyte-like cells to vessel networks that developed within the microfluidic devices. LF displayed expression for both markers at day 7 (Fig. 3.8A, B) and day 14 (Fig. 3.8C, D) in culture. NG2+ LF displayed a spread morphology at day 7 (Fig. 3.8A) with some elongation alongside microvessels. By day 14, NG2+ LF morphology was more elongated
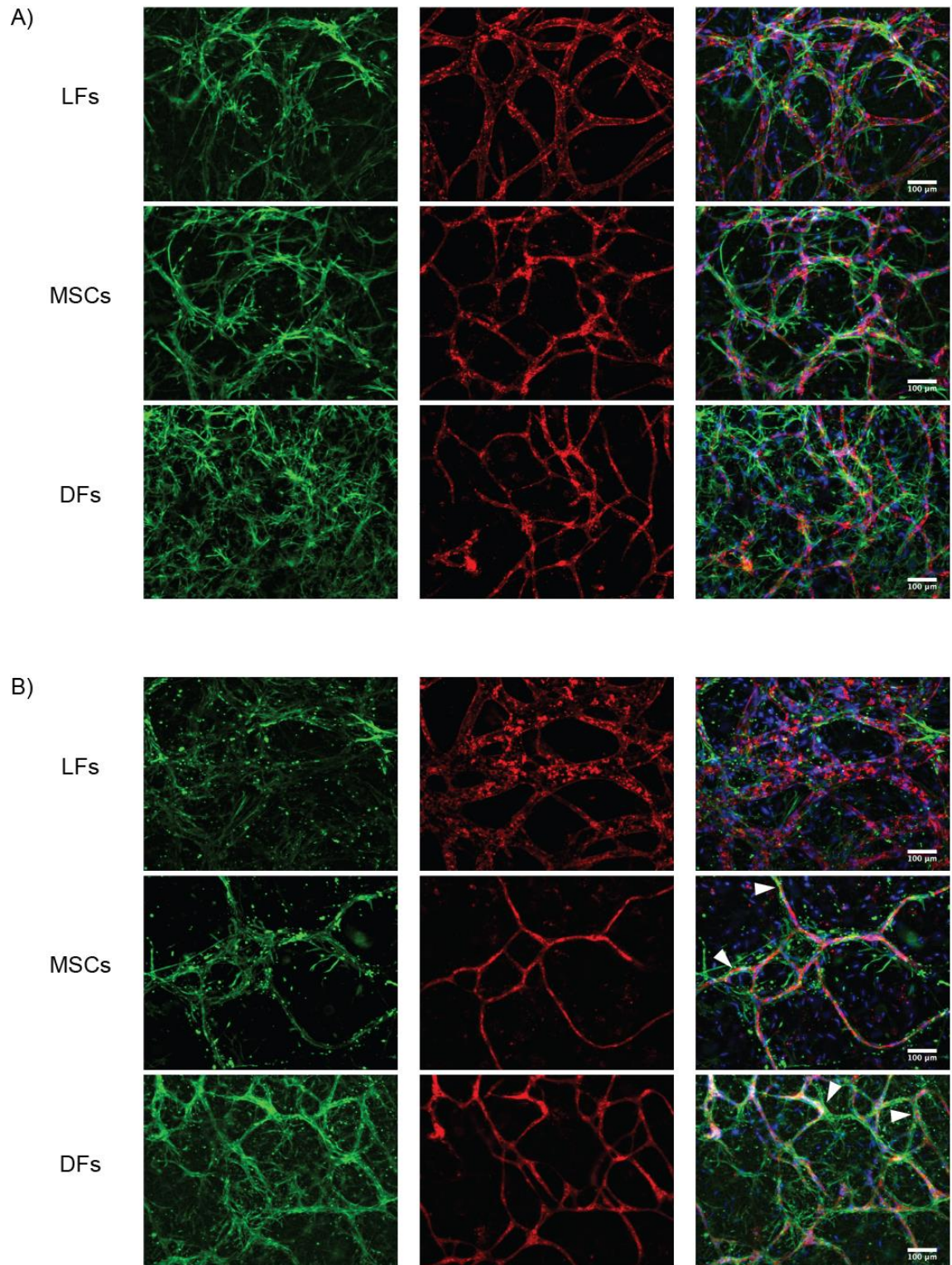
Figure 3.7: DFs and MSCs exhibit closer perivascular association than do LFs in SC-EC co-cultures.
Alpha smooth muscle actin (αSMA) expression on (A) day 7 and (B) day 14. Representative immunofluorescence staining for αSMA (green) counterstained with UEA (red) and DAPI (blue) to show the position of SCs relative to vessels. All samples are from condition 2. White arrowheads depict the sheath-like association of αSMA+ SCs to UEA+ microvessels.

along microvessels and these cells were exclusively located in perivascular locations (Fig. 3.8C). PDGFRβ+ LF adopted a sheath-like morphology around vessels at both time points (Fig. 3.8B, D). In contrast to the αSMA expression which diminished over time, NG2 expression increased over time and PDGFRβ expression remained constant over time.

3.4 Discussion

Stromal cells play a critical role in tissue vascularization in development and wound healing, and a clear understanding of their roles in capillary formation is critical to developing more complex engineered tissues with tissue-specific, specialized functions and a more complete vascular hierarchy. We demonstrated that SC play a critical role in vascular morphogenesis in three different assays of angiogenesis, vasculogenesis, and a hierarchical vascular model of mixed angiogenesis and vasculogenesis. In each model, EC alone failed to form vasculature. While vessel formation in EC-SC co-cultures within microfluidic chips has been previously studied [37-39], direct comparisons between SC types across distinct studies are difficult to make due to differences in microfluidic geometries, EC source, SC source, medium formulations, fluid flow, culture duration, and the type of anastomosis. In this study, we used an on-chip platform for static co-culture of EC and SC using a consistent medium source, EC source, and microfluidic geometry in order to make head-to-head comparisons in the abilities of three different SC types to direct vascular assembly. Parent channels approximating arteriole diameters were fully encapsulated within a fibrin matrix within this device, thereby supporting physiologically-relevant anastomoses between *de novo* formed microvascular network structures within the matrix and these mesovessels. Consistent with other reports investigating co-culture models of vascular

83
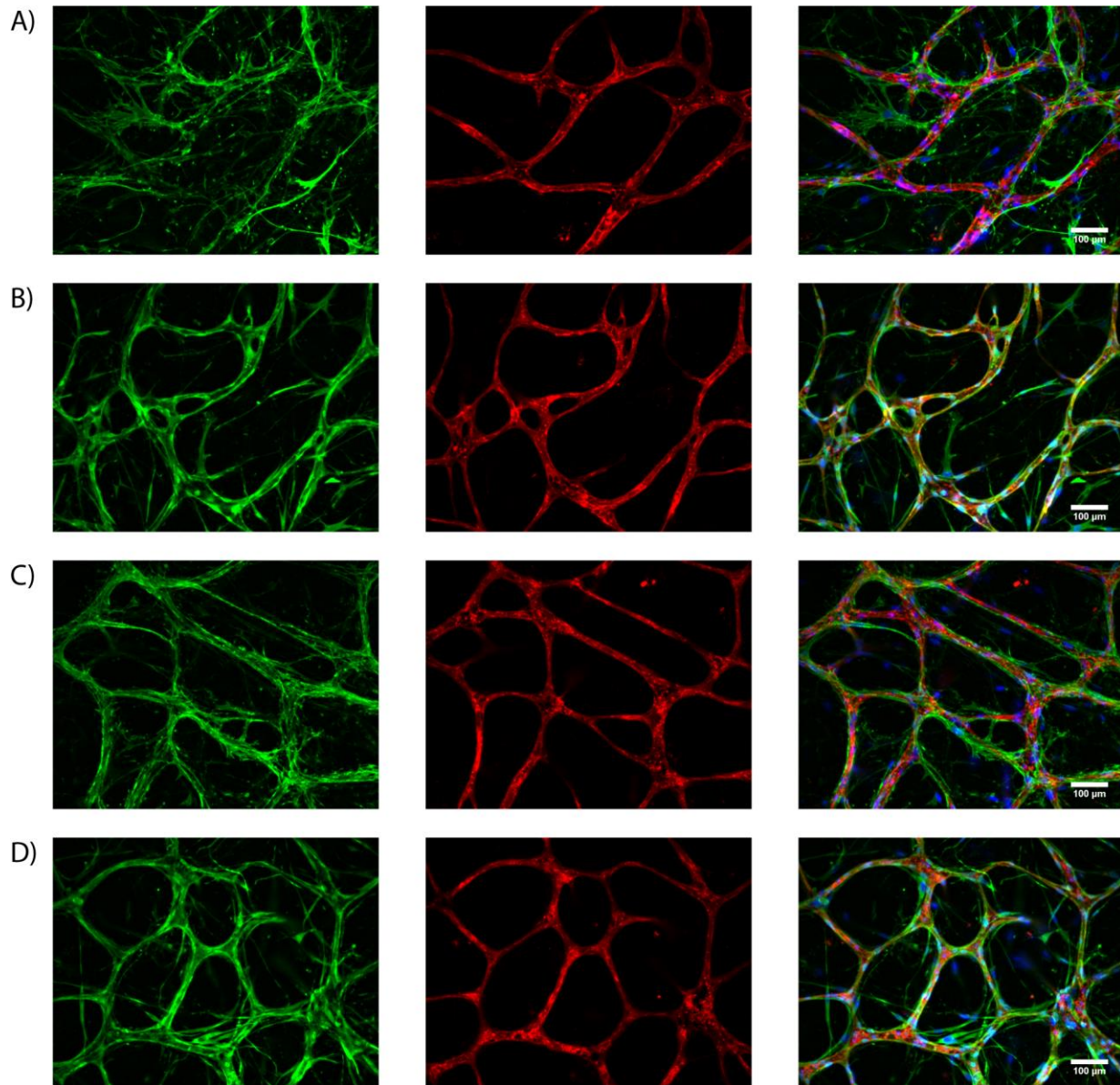
Figure 3.8: LF display close perivascular association of NG2 and PDGFRβ. *(A, C) NG2 expression and (B, D) PDGFRβ expression on (A, B) day 7 and (C, D) day 14. Representative immunofluorescent staining for NG2 (green, A, C) and PDGFRβ (green, B, D) counter stained with UEA (red) and DAPI (blue) to show the position of LF relative to vessels. All samples are from condition 3.*

morphogenesis in natural matrices in on-chip systems [16-18], EC formed microvascular networks

within this on-chip platform using LF, DF, and MSC as the supportive cells. LF and DF supported

more expansive network formation compared to MSC-supported samples. Over time in culture,

MSC supported changes to microvascular network organization, including a greater degree of

network interconnectedness, while fibroblast-supported networks remained more constant over a longer duration for the parameters measured.

In an effort to better understand how SC of different tissue origins give rise to endothelial networks that are quantitatively and qualitatively distinct, we investigated two candidate possibilities by focusing on cell densities and traction forces. Our analysis of cell density identified differences between samples containing fibroblasts and MSC. Co-cultures containing fibroblasts showed an increase in cell number when the initial seeding density was low, but a reduction in cell number when the initial seeding density was high. Co-cultures containing MSC decreased in cell number regardless of the initial seeding density. These changes in cell density correlate with the degree of vascularization as quantified by measuring TNL (note the similar shapes to the graphs in Figure 3.3B vs. Figure 3.6B), and therefore may partially explain the significantly lower TNL in MSC-supported samples compared to fibroblast-supported samples, as well as inconsistencies in vascular morphogenesis and function. More broadly, these observations suggest two possibilities: SC density is tightly regulated to support vascular morphogenesis, lumenogenesis, and patency, or SC regulate EC density to control the same parameters. However, our data do not address if the EC or SC are preferentially dying or proliferating in our microfluidic devices.

One study of neovascularization in modular fibrin microtissues containing EC-fibroblast co-cultures of 1:1 and 1:3 ratios, similar to the ratios used here, showed preferential proliferation of the fibroblasts [25]. Another study showed that fibroblasts regulate vascular morphogenesis and lumenogensis in part by secreting paracrine angiogenic factors to enable sprouting and ECM proteins that stiffen the matrix to enable lumenogensis [40]. In our results, elevated paracrine secretions of pro-angiogenic factors and ECM could potentially be due to elevated numbers over time of SC in our LF-EC and DF-EC co-cultures relative to the MSC-EC co-cultures. On the other

hand, a particularly innovative recent study used an inducible caspase-9 kill-switch gene to preferentially induce apoptosis in fibroblasts, and revealed that transient support of fibroblasts (as little as 3 days) is sufficient to drive the formation of functional microvasculature [41]. That study used cell densities that were 3-9x higher than those we used here, and thus it seems likely the time required for the presence of the fibroblasts depends on the number present. A potentially important complicating factor in dissecting the mechanisms by which SC modulate vascular morphogenesis in co-culture systems is the choice of culture medium. We used EGM-2 for consistency across conditions, but the different SC may alter their secretome and/or their ability to synthesize and remodel the ECM in this medium relative to their basal culture medium.

Differences in SC-generated traction forces may also play a role in the observed differences in vascular morphogenesis and perfusion. It has been well-established that EC-generated traction forces play important roles in vascular morphogenesis [42-45], in part by reorganizing ECM fibers to enhance EC migration and invasion [46]. However, the roles of SC-generated forces in vascular assembly are comparatively understudied. Quantification of traction stresses using 2D traction force microscopy suggested a correlation between SC-generated forces and TNL, as both LF and DF generate larger traction stress and support vascular assembly to a greater extent than MSC. Since fibroblasts support more extensive endothelial network formation than do MSC, higher levels of tension in the ECM imparted by higher levels of traction force exerted by SC may play a role. LF and DF produced similar levels of traction, despite yielding microvascular networks with clear differences in channel patency and network perfusion. This suggests that the magnitude of SC-mediated traction forces cannot fully explain the observed differences in microvascular function in our system. DF, LF, and MSC reside in different tissue microenvironments and serve different functions *in vivo,* and our use of 2D TFM as a surrogate for traction forces in 3D

86

multicellular microenvironments at a single time point may not capture nuanced differences between SC types in terms of the timing and duration of traction forces. The use of 3D TFM approaches [47] and/or microrheology [10] in future work may shed some additional light on differences in SC forces during vascular morphogenesis, but are beyond the scope of this particular study.

The qualitative differences in αSMA expression observed in our study may also implicate differences in SC-generated traction forces. αSMA expression has been linked to increased traction forces and a myofibroblast phenotype in fibroblasts [48, 49]. One study showed increased expression of αSMA enhanced the contractile activity of cultured fibroblasts [50]. Qualitatively, DF showed the greatest degree of αSMA expression on both days 7 and 14, and a more uniform distribution of αSMA+ cells throughout the entire gel compared to both LF and MSC. DF-generated traction forces distributed over a larger gel volume, while perhaps initially beneficial to accelerate vascular assembly by stiffening the fibrous ECM and enhancing long-range communication, may accelerate fibrin compaction and/or remodeling when sustained over prolonged periods in a manner akin to fibrosis that adversely affect parent channel patency. In contrast, αSMA expression in LFs appeared to decrease over time, coinciding with sustained parent channel patency. The αSMA expression levels and localization patterns we observed are also consistent with the observed differences in microvessel diameter. Capillary pericytes have been shown to control blood flow by modulating capillary diameter [51]. In our co-cultures, MSC and DF exhibited a greater degree of perivascular association and sustained this association for a longer duration compared to LF, perhaps leading to the smaller vessel diameters observed in MSC-EC and DF-EC co-cultures compared to LF-EC co-cultures.

The additional pericyte markers examined in LF samples may coincide with quantitative microvascular network results. NG2 has been implicated in pericyte proliferation and as an activator of integrin signaling leading to enhanced vessel maturation [52]. LF supported the most interconnected vessel networks and therefore the increase in perivascular NG2 expression may be critical for maintenance of this mature vessel quality in this on-chip platform. PDGFRβ is required for pericyte migration to and migration along the microvessel wall [53, 54], which is critical for maturation of nascent capillaries. Perivascular mural cells stabilize vessels by preventing endothelial proliferation and the inducing the production of basement membrane proteins [55]. The sheath of PDGFRβ+ and NG2+ LF around vessels at day 14 may play a role in the reduction in cell number observed in this system to maintain a mature vascular phenotype.

Perfusion of endothelial microvessels is critical for long-term tissue function *in vitro* and *in vivo*. In this study, samples were cultured statically for 7 or 14 days followed by a brief addition of flow to assess dextran infusion into parent channels and microvascular networks. Here we show that LF were the only SC type tested that could facilitate perfusion of endothelial microvessels in the absence of flow preconditioning. However, our previous *in vivo work* [7] has shown successful lumenization and perfusion of EC-MSC vessels, suggesting that the absence of continuous flow in our system may explain the lack of perfusion in MSC- and DF-supported vessels. A recent study which showed perfusion of DF-supported vessels used a much higher cell density and incorporated flow into the system [41], while a study that showed perfusion of MSC-supported vessels also examined vessels under static culture but used a microfluidic device where anastomosis occurred to openings in a PDMS channel [16] rather than physiologic anastomosis to an endothelialized, matrix-encapsulated channel. Our results, coupled with the results from others cited above, further

highlight the need for consistency in study parameters to specifically parse out the role of SC in vascular morphogenesis and vessel perfusion.

To summarize, we report the use of a microfluidic chip platform to evaluate if differences in SC identity induce changes in vascular morphogenesis and function in 3D natural hydrogel matrices. We used this system to characterize vasculature formed by co-culturing EC with tissue-specific SC [56]. We demonstrated that co-cultures of EC and fibroblasts generated more expansive vascular networks compared to co-cultures of EC and MSC. We further showed that vascular morphogenesis induced by LF and DF yielded capillary networks that may correlate with the distinct functions of their organ-specific origins. LF-supported microvasculature displayed wider diameters, which may be important to facilitate gas exchange in the alveoli [57]; by contrast, DF-supported microvasculature coincided with closure of the arteriole-scale parent channels, potentially due to DF-mediated contraction of the fibrin matrix consistent with the role of DF in remodeling provisional clots during wound healing and DF undergoing a transition to a myofibroblast phenotype [58]. Future studies could also incorporate tissue-specific EC [56], such as normal human lung microvascular EC co-cultured with LF rather than the more widely used HUVEC. Overall, the reproducibility, simplicity, and flexibility (cell type, matrix composition, matrix density, etc.) of this microfluidic microvascular system provides a platform to probe fundamental vascular biology questions during neovascularization, to gain an understanding of tissue-specific vasculature, and to guide strategies to vascularize engineered tissues and organs.

3.5 Supplementary Figure
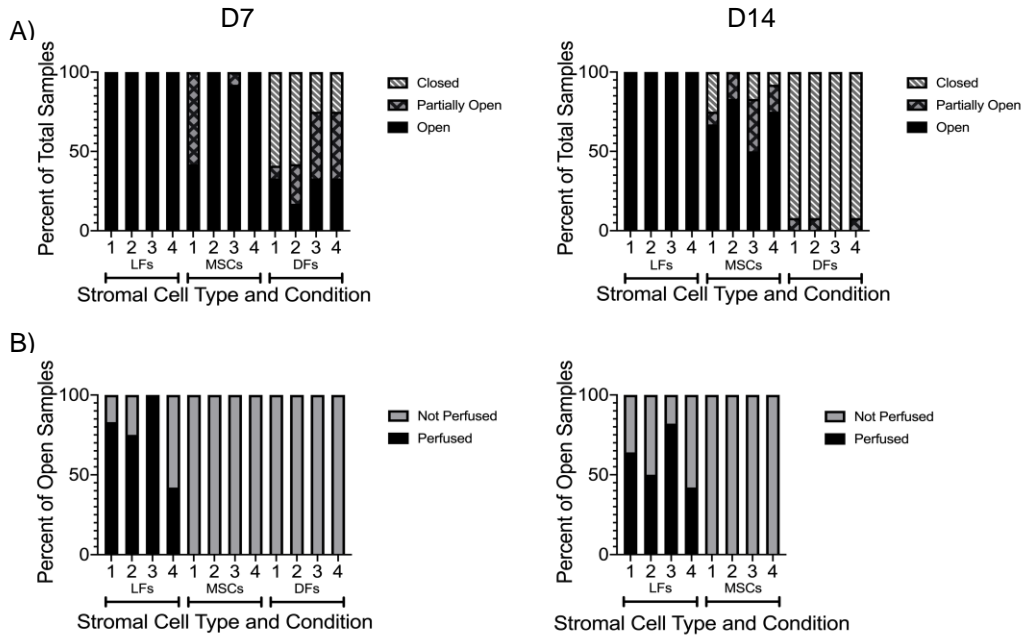
Supplementary Figure 3.1: Stromal cell type determines vessel patency and microvascular network perfusion. *(A) Channel patency and (B) network perfusion for each cell type on day 7 (left) and day 14 (right). A total of n = 3-4 per condition, per time point, per cell type and N = 3 independent replicates included per condition, per time point, per cell type were analyzed.*

3.6 References

[1]   Auger, F.A., Gibot, L., and Lacroix, D. (2013) The pivotal role of vascularization in tissue engineering. *Annu Rev Biomed Eng* 15, 177-200

[2]   Rouwkema, J., Rivron, N.C., and van Blitterswijk, C.A. (2008) Vascularization in tissue engineering. *Trends Biotechnol* 26, 434-441

[3]   Jain, R.K., Au, P., Tam, J., Duda, D.G., and Fukumura, D. (2005) Engineering vascularized tissue. *Nat Biotechnol* 23, 821-823

[4]   Chan, K.L.S., Khankhel, A.H., Thompson, R.L., Coisman, B.J., Wong, K.H.K., Truslow, J.G., and Tien, J. (2014) Crosslinking of collagen scaffolds promotes blood and lymphatic vascular stability. *J Biomed Mater Res A* 102, 3186-3195

[5]   Linville, R.M., Boland, N.F., Covarrubias, G., Price, G.M., and Tien, J. (2016) Physical and Chemical Signals That Promote Vascularization of Capillary-Scale Channels. *Cell Mol Bioeng* 9, 73-84

[6]   Nguyen, D.H., Stapleton, S.C., Yang, M.T., Cha, S.S., Choi, C.K., Galie, P.A., and Chen, C.S. (2013) Biomimetic model to reconstitute angiogenic sprouting morphogenesis in vitro. *Proc Natl Acad Sci U S A* 110, 6712-6717

[7]   Grainger, S.J., Carrion, B., Ceccarelli, J., and Putnam, A.J. (2013) Stromal cell identity influences the in vivo functionality of engineered capillary networks formed by co-delivery of endothelial cells and stromal cells. *Tissue Eng Part A* 19, 1209-1222

[8]   Alimperti, S., Mirabella, T., Bajaj, V., Polacheck, W., Pirone, D.M., Duffield, J., Eyckmans, J., Assoian, R.K., and Chen, C.S. (2017) Three-dimensional biomimetic vascular model reveals a RhoA, Rac1, and N-cadherin balance in mural cell-endothelial cell-regulated barrier function. *Proc Natl Acad Sci U S A* 114, 8758-8763

[9]   Bezenah, J.R., Kong, Y.P., and Putnam, A.J. (2018) Evaluating the potential of endothelial cells derived from human induced pluripotent stem cells to form microvascular networks in 3D cultures. *Sci Rep* 8, 2671

[10]   Juliar, B.A., Keating, M.T., Kong, Y.P., Botvinick, E.L., and Putnam, A.J. (2018) Sprouting angiogenesis induces significant mechanical heterogeneities and ECM stiffening across length scales in fibrin hydrogels. *Biomaterials* 162, 99-108

[11]   Grainger, S.J. and Putnam, A.J. (2011) Assessing the permeability of engineered capillary networks in a 3D culture. *PLoS One* 6, e22086

[12]   Beamish, J.A., Juliar, B.A., Cleveland, D.S., Busch, M.E., Nimmagadda, L., and Putnam, A.J. (2019) Deciphering the relative roles of matrix metalloproteinase- and plasmin-mediated matrix degradation during capillary morphogenesis using engineered hydrogels. *J Biomed Mater Res B Appl Biomater* 107, 2507-2516

[13]   Juliar, B.A., Beamish, J.A., Busch, M.E., Cleveland, D.S., Nimmagadda, L., and Putnam, A.J. (2020) Cell-mediated matrix stiffening accompanies capillary morphogenesis in ultra-soft amorphous hydrogels. *Biomaterials* 230, 119634

[14]   Vigen, M., Ceccarelli, J., and Putnam, A.J. (2014) Protease-sensitive PEG hydrogels regulate vascularization in vitro and in vivo. *Macromol Biosci* 14, 1368-1379

[15]   Rioja, A.Y., Tiruvannamalai Annamalai, R., Paris, S., Putnam, A.J., and Stegemann, J.P. (2016) Endothelial sprouting and network formation in collagen- and fibrin-based modular microbeads. *Acta Biomater* 29, 33-41

[16]   Jeon, J.S., Bersini, S., Whisler, J.A., Chen, M.B., Dubini, G., Charest, J.L., Moretti, M., and Kamm, R.D. (2014) Generation of 3D functional microvascular networks with human mesenchymal stem cells in microfluidic systems. *Integr Biol (Camb)* 6, 555-563

[17]   Wang, X., Phan, D.T., Sobrino, A., George, S.C., Hughes, C.C., and Lee, A.P. (2016) Engineering anastomosis between living capillary networks and endothelial cell-lined microfluidic channels. *Lab Chip* 16, 282-290

[18] Kim, S., Lee, H., Chung, M., and Jeon, N.L. (2013) Engineering of functional, perfusable 3D microvascular networks on a chip. *Lab Chip* 13, 1489-1500

[19] Ghajar, C.M., Blevins, K.S., Hughes, C.C., George, S.C., and Putnam, A.J. (2006) Mesenchymal stem cells enhance angiogenesis in mechanically viable prevascularized tissues via early matrix metalloproteinase upregulation. *Tissue Eng* 12, 2875-2888

[20] Chen, Q.H., Liu, A.R., Qiu, H.B., and Yang, Y. (2015) Interaction between mesenchymal stem cells and endothelial cells restores endothelial permeability via paracrine hepatocyte growth factor in vitro. *Stem Cell Res Ther* 6, 44

[21] Maacha, S., Sidahmed, H., Jacob, S., Gentilcore, G., Calzone, R., Grivel, J.C., and Cugno, C. (2020) Paracrine Mechanisms of Mesenchymal Stromal Cells in Angiogenesis. *Stem Cells Int* 2020, 4356359

[22] Rao, R.R., Peterson, A.W., Ceccarelli, J., Putnam, A.J., and Stegemann, J.P. (2012) Matrix composition regulates three-dimensional network formation by endothelial cells and mesenchymal stem cells in collagen/fibrin materials. *Angiogenesis* 15, 253-264

[23] Loibl, M., Binder, A., Herrmann, M., Duttenhoefer, F., Richards, R.G., Nerlich, M., Alini, M., and Verrier, S. (2014) Direct cell-cell contact between mesenchymal stem cells and endothelial progenitor cells induces a pericyte-like phenotype in vitro. *Biomed Res Int* 2014, 395781

[24] Wang, W.Y., Lin, D., Jarman, E.H., Polacheck, W.J., and Baker, B.M. (2020) Functional angiogenesis requires microenvironmental cues balancing endothelial cell migration and proliferation. *Lab Chip* 20, 1153-1166

[25] Tiruvannamalai Annamalai, R., Rioja, A.Y., Putnam, A.J., and Stegemann, J.P. (2016) Vascular Network Formation by Human Microvascular Endothelial Cells in Modular Fibrin Microtissues. *ACS Biomater Sci Eng* 2, 1914-1925

[26] Aratyn-Schaus, Y., Oakes, P.W., Stricker, J., Winter, S.P., and Gardel, M.L. (2010) Preparation of complaint matrices for quantifying cellular contraction. *J Vis Exp*

[27] Tseng, Q., Duchemin-Pelletier, E., Deshiere, A., Balland, M., Guillou, H., Filhol, O., and Thery, M. (2012) Spatial organization of the extracellular matrix regulates cell-cell junction positioning. *Proc Natl Acad Sci U S A* 109, 1506-1511

[28] Kong, Y.P., Rioja, A.Y., Xue, X., Sun, Y., Fu, J., and Putnam, A.J. (2018) A systems mechanobiology model to predict cardiac reprogramming outcomes on different biomaterials. *Biomaterials* 181, 280-292

[29] Traore, M.A. and George, S.C. (2017) Tissue Engineering the Vascular Tree. *Tissue Eng Part B Rev* 23, 505-514

[30] Pearce, S.C., Al-Jawadi, A., Kishida, K., Yu, S., Hu, M., Fritzky, L.F., Edelblum, K.L., Gao, N., and Ferraris, R.P. (2018) Marked differences in tight junction composition and macromolecular permeability among different intestinal cell types. *BMC Biol* 16, 19

[31] Brown, T.D., Nowak, M., Bayles, A.V., Prabhakarpandian, B., Karande, P., Lahann, J., Helgeson, M.E., and Mitragotri, S. (2019) A microfluidic model of human brain (muHuB) for assessment of blood brain barrier. *Bioeng Transl Med* 4, e10126

[32] Price, G.M., Wong, K.H., Truslow, J.G., Leung, A.D., Acharya, C., and Tien, J. (2010) Effect of mechanical factors on the function of engineered human blood microvessels in microfluidic collagen gels. *Biomaterials* 31, 6182-6189

[33] Davis, G.E. and Camarillo, C.W. (1995) Regulation of endothelial cell morphogenesis by integrins, mechanical forces, and matrix guidance pathways. *Exp Cell Res* 216, 113-123

[34] Ghajar, C.M., Kachgal, S., Kniazeva, E., Mori, H., Costes, S.V., George, S.C., and Putnam, A.J. (2010) Mesenchymal cells stimulate capillary morphogenesis via distinct proteolytic mechanisms. *Exp Cell Res* 316, 813-825

[35] Kosyakova, N., Kao, D.D., Figetakis, M., Lopez-Giraldez, F., Spindler, S., Graham, M., James, K.J., Won Shin, J., Liu, X., Tietjen, G.T., Pober, J.S., and Chang, W.G. (2020) Differential functional roles of fibroblasts and pericytes in the formation of tissue-engineered microvascular networks in vitro. *NPJ Regen Med* 5, 1

[36] Pill, K., Melke, J., Muhleder, S., Pultar, M., Rohringer, S., Priglinger, E., Redl, H.R., Hofmann, S., and Holnthoner, W. (2018) Microvascular Networks From Endothelial Cells and Mesenchymal Stromal Cells From Adipose Tissue and Bone Marrow: A Comparison. *Front Bioeng Biotechnol* 6, 156

[37] Lee, S., Ko, J., Park, D., Lee, S.R., Chung, M., Lee, Y., and Jeon, N.L. (2018) Microfluidic-based vascularized microphysiological systems. *Lab Chip* 18, 2686-2709

[38] Haase, K. and Kamm, R.D. (2017) Advances in on-chip vascularization. *Regen Med* 12, 285-302

[39] Bersini, S. and Moretti, M. (2015) 3D functional and perfusable microvascular networks for organotypic microfluidic models. *J Mater Sci Mater Med* 26, 180

[40] Newman, A.C., Nakatsu, M.N., Chou, W., Gershon, P.D., and Hughes, C.C. (2011) The requirement for fibroblasts in angiogenesis: fibroblast-derived matrix proteins are essential for endothelial cell lumen formation. *Mol Biol Cell* 22, 3791-3800

[41] Song, H.G., Lammers, A., Sundaram, S., Rubio, L., Chen, A.X., Li, L., Eyckmans, J., Bhatia, S.N., and Chen, C.S. (2020) Transient Support from Fibroblasts is Sufficient to Drive Functional Vascularization in Engineered Tissues. *Adv Funct Mater* 30

[42]   Yoon, C., Choi, C., Stapleton, S., Mirabella, T., Howes, C., Dong, L., King, J., Yang, J., Oberai, A., Eyckmans, J., and Chen, C.S. (2019) Myosin IIA-mediated forces regulate multicellular integrity during vascular sprouting. *Mol Biol Cell* 30, 1974-1984

[43]   Sieminski, A.L., Hebbel, R.P., and Gooch, K.J. (2004) The relative magnitudes of endothelial force generation and matrix stiffness modulate capillary morphogenesis in vitro. *Exp Cell Res* 297, 574-584

[44]   Kniazeva, E. and Putnam, A.J. (2009) Endothelial cell traction and ECM density influence both capillary morphogenesis and maintenance in 3-D. *Am J Physiol Cell Physiol* 297, C179-187

[45]   Vaeyens, M.M., Jorge-Penas, A., Barrasa-Fano, J., Steuwe, C., Heck, T., Carmeliet, P., Roeffaers, M., and Van Oosterwyck, H. (2020) Matrix deformations around angiogenic sprouts correlate to sprout dynamics and suggest pulling activity. *Angiogenesis* 23, 315-324

[46]   Davidson, C.D., Wang, W.Y., Zaimi, I., Jayco, D.K.P., and Baker, B.M. (2019) Cell force-mediated matrix reorganization underlies multicellular network assembly. *Sci Rep* 9, 12

[47]   Legant, W.R., Miller, J.S., Blakely, B.L., Cohen, D.M., Genin, G.M., and Chen, C.S. (2010) Measurement of mechanical tractions exerted by cells in three-dimensional matrices. *Nat Methods* 7, 969-971

[48]   Wang, J., Zohar, R., and McCulloch, C.A. (2006) Multiple roles of alpha-smooth muscle actin in mechanotransduction. *Exp Cell Res* 312, 205-214

[49]   Davidson, C.D., Jayco, D.K.P., Matera, D.L., DePalma, S.J., Hiraki, H.L., Wang, W.Y., and Baker, B.M. (2020) Myofibroblast activation in synthetic fibrous matrices composed of dextran vinyl sulfone. *Acta Biomater* 105, 78-86

[50]   Hinz, B., Celetta, G., Tomasek, J.J., Gabbiani, G., and Chaponnier, C. (2001) Alpha-smooth muscle actin expression upregulates fibroblast contractile activity. *Mol Biol Cell* 12, 2730-2741

[51]   Almaca, J., Weitz, J., Rodriguez-Diaz, R., Pereira, E., and Caicedo, A. (2018) The Pericyte of the Pancreatic Islet Regulates Capillary Diameter and Local Blood Flow. *Cell Metab* 27, 630-644 e634

[52]   Stallcup, W.B. (2018) The NG2 Proteoglycan in Pericyte Biology. *Adv Exp Med Biol* 1109, 5-19

[53]   Lindahl, P., Johansson, B.R., Leveen, P., and Betsholtz, C. (1997) Pericyte loss and microaneurysm formation in PDGF-B-deficient mice. *Science* 277, 242-245

[54]   Benjamin, L.E., Hemo, I., and Keshet, E. (1998) A plasticity window for blood vessel remodelling is defined by pericyte coverage of the preformed endothelial network and is regulated by PDGF-B and VEGF. *Development* 125, 1591-1598

[55]   Zhang, Z., Warner, K.A., Mantesso, A., and Nor, J.E. (2022) PDGF-BB signaling via PDGFR-beta regulates the maturation of blood vessels generated upon vasculogenic differentiation of dental pulp stem cells. *Front Cell Dev Biol* 10, 977725

[56]   Lin, D.S.Y., Guo, F., and Zhang, B. (2019) Modeling organ-specific vasculature with organ-on-a-chip devices. *Nanotechnology* 30, 024002

[57]   Ivanov, K.P. (2017) Supply of the Alveoli with Blood and Circulation in the Alveoli. *Journal of Respiratory Research* 3, 125-128

[58]   Tracy, L.E., Minasian, R.A., and Caterson, E.J. (2016) Extracellular Matrix and Dermal Fibroblast Function in the Healing Wound. *Adv Wound Care (New Rochelle)* 5, 119-136

Chapter 4 – Engineering Hierarchical Vascular Chimeras by Combining Human Microvessels with Explanted Murine Macrovessels

*This chapter is in preparation for submission as a peer reviewed journal article.

4.1 Introduction

Cardiovascular disease, the leading cause of death worldwide [1], causes damage to both large-scale arteries and small-scale capillaries, but most clinical interventions (e.g., stents, grafts) focus only on the macroscale vessels. In the field of tissue engineering, strategies to engineer arterial grafts [2-6] and microvasculature [7-10] separately have emerged, but efforts to bridge these two length scales to create a multiscale vascular network capable of supporting an engineered tissue or restoring perfusion to an ischemic tissue have been limited [11, 12]. Such a construct could be applicable in peripheral artery disease in particular, where the arteries blocked with atherosclerotic plaque lead to further adverse effects in the downstream capillaries supplying blood and nutrients to the surrounding muscle tissue [13]. Pro-atherosclerotic stimuli drive a decrease in pericyte coverage of the downstream capillaries, a buildup of reactive oxygen species, and increased leukocyte recruitment. These stimuli overall lead to endothelial dysfunction, capillary rarefication, and decreased blood flow to the surrounding tissues. Despite interventions to reopen the atherosclerotic artery, the decreased capillary density remains leading to continued decreased blood flow and limiting the recovery of the ischemic tissue [13].

Over the last half century, a significant number of studies have used aortic ring assays to study angiogenic sprouting from large, quiescent arteries [14-26]. These assays have primarily

96

been used to study angiogenesis in a more complex, physiologic model in contrast to simplistic *in vitro* models that may not replicate the complexity of various cell types, growth factors, and matrix present *in vivo*. One study investigated sprouting from vessels isolated from different regions throughout the body and compared sprouting from arteries and veins [27]. Though these models do result in a multiscale construct consisting of an artery segment and sprouted capillaries, sprouting from the lumenal end of the artery diminishes their capability to be sutured into circulation, limiting their therapeutic application. A study employing a similar technique investigated capillary sprouting from isolated large-scale vessels to bridge artery and vein segments together with the sprouted capillaries [28]. In that study, an artery and vein were positioned on either side of a micropatterned hydrogel and angiogenic factors were employed to induce sprouting between the two segments and ultimately connect them. While this study is more translatable in that there is a free, suturable end on both sides of the construct, if implanted, this would bridge arterial circulation with the small-scale capillaries connecting the two large vessels and does not vascularize the surrounding tissue.

The work presented here aimed to create hierarchical tissue constructs spanning multiple length scales by evaluating the ability of macroscopic vessels isolated from mice to sprout and form functional connections to engineered human capillary networks *ex vivo*. To our knowledge, this is the first exhibition of sprouting from the abluminal edge of a quiescent macroscopic vessel. The experimental model developed here also provides a platform to better understand the mechanisms of inosculation that lead to the spontaneous formation of host-graft anastomoses, which remain poorly understood.

4.2 Materials and Methods

4.2.1 Cell culture

Normal human lung fibroblasts (LF; Lonza, Walkersville, MD) were cultured in Dulbecco's modified eagle medium (DMEM; Gibco, Waltham, MA) supplemented with 10% fetal bovine serum (FBS; Gibco) with medium changes every other day. LF were used between passage 10 and 15. Human umbilical vein endothelial cells (EC) were isolated from fresh umbilical cords obtained from Mott's Children's Hospital via an IRB exempt protocol. EC between passage 4 and 7 were cultured in EGM-2 (Lonza) with medium changes every other day. All cells were maintained in 5% CO_2 at 37°C.

4.2.2 Murine vessel harvest

All animal procedures were compliant with the NIH Guide for Care and Use of Laboratory Animals and approved by the University of Michigan's Institutional Animal Care and Use Committee. Male BALB/c mice (Taconic Farms, Rensselaer, NY) between 5 and 7 weeks of age were used for this study. Animals were acclimated to their surroundings for 3 days following delivery. Animals were anesthetized using 2% inhaled isoflurane. Fur was removed from the lower legs and abdomen on the ventral side of the animal via shaving followed by the application of depilatory cream to remove residual fur. First the femoral bundles from each leg were removed. An incision was made over the vessels and the fascia was separated from the vessel-nerve bundle. Gentle dissection was used to separate the bundle from the surrounding muscle and subsequently the artery-vein (AV) bundle from the nerve (Fig. 4.1D). The same procedure was repeated on the second limb. The animal was then euthanized by 5% overdose of isoflurane. Subsequently, the

abdominal and thoracic cavities were opened to induce a pneumothorax and to expose the inferior vena cava (IVC) and aorta (Fig. 4.1C). Adventitia was removed from the IVC and aorta prior to isolation. Vessels were rinsed thrice in sterile saline to remove residual blood and tissue. The aorta was cannulated and flushed with saline through the lumen; other vessels were too small in diameter to do the same.

4.2.3 Hydrogel fabrication and culture

Individual vessels or vessel bundles were embedded in fibrin hydrogels (cellular or acellular) (Fig. 4.1A). The final composition of resultant hydrogels was 5 mg/mL bovine fibrinogen (Sigma), 1 U/mL bovine thrombin (Sigma), and 10% FBS. Cellular hydrogels contained a 1:1 ratio of EC and LF at a final density of 500K cells/mL. Hydrogels were cultured to day 1, 7, or 14 in standard EGM-2 or EGM-2 containing 2.2 µM aprotinin (Sigma, St. Louis, MO) with media exchanged on the first day and every other day thereafter.

4.2.4 Rheological characterization

Hydrogel stiffness was measured using parallel plate shear rheology on an AR-G2 rheometer (TA Instruments; New Castle, DE) with an 8 mm diameter measurement head. Hydrogels containing explants and controls (no explant) were measured with 6% strain amplitude and a 1 rad/sec frequency on days 1 and 7 to obtain shear modulus values (G'). Hydrogels were maintained in the culture plates on a stage heated to 37°C to ensure measurement conditions matched culture conditions. Three independent replicates (N = 3) were measured for each

condition and time point. Only cellular hydrogels and acellular hydrogels with aprotinin were analyzed.

4.2.5 Immunofluorescent staining and imaging

Gels were fixed on the last day of culture with Zinc Formalin Fixative (Z-fix; Anatech; Battle Creek, MI) for 15 minutes at room temperature and washed 3 times for 5 minutes each with tris buffered saline (TBS). Fixed gels were stained with 4', 6-diamidino-2-phenylindol (DAPI; 1 ug/L; Fisher Scientific), AlexaFluor 488 Phalloidin (1:200 dilution; Fisher Scientific), DyLight 649-conjugated Griffonia Simplicifolia Lectin I Isolectin B4 (1:50 dilution; Vector Labs, Burlingame, CA), and rhodamine-conjugated Ulex europaeus Agglutinin I (cellular only; UEA; 1:200 dilution; Vector Labs). Staining dilutions were made in TBS and samples were incubated with staining solution overnight at 4°C. Following staining, samples were washed with TBS for at least 24 hours.

Samples were imaged on an Olympus IX81 outfitted with a confocal disc spinning unit (DSU; Olympus America, Center Valley, PA) and Metamorph software (Molecular Devices, Sunnyvale, CA). Confocal z-stacks (300 um, 7 slices) were obtained at 4x magnification and compressed into maximum intensity projections preceding sprout distance analysis. Additionally, phase contrast, whole-well, single z-plane scans were obtained for analysis of degradation and sprout percentage.

4.2.6 Analysis of degradation

Acellular samples were imaged in phase using the scan slide application in Metamorph to obtain an entire well image of each construct consisting of an explanted vessel in fibrin. Degradation was measured as the absence of fibrin surrounding the vessel (Fig. 4.1E). The entire explant perimeter and the degraded perimeter were measured. To obtain a percent degraded metric, the perimeter of the explant that exhibited degradation was divided by the total explant perimeter. Degradation analysis was performed on 3 independent replicates at day 7 only.

4.2.7 Analysis of sprouting

Multiple metrics were used to assess sprouting from vessel explants into the surrounding fibrin hydrogel. The first metric was a percentage of the explant that exhibited sprouting (Fig. 4.1F). The perimeter of the explant that exhibited sprouting was divided by the total explant perimeter to obtain a percent sprouted metric. Second, sprout distance was measured as the average distance sprouts reach from the explant edge and was measured only in sprouted regions (Fig. 4.1G). For this metric, 15+ measurements were taken per explant across multiple images. For all measurements, $N = 3$ independent replicates were analyzed per condition per timepoint. Lumenal sprouting refers to sprouts originating from the transverse section of the vessel at the lumen opening. Abluminal sprouting refers to sprouts originating from the vessel wall along the longitudinal edge of the vessel.

4.2.8 Fabricating three-scale vascular hierarchies

To fabricate three-scale hierarchies with embedded mesovessels, we fabricated a polydimethylsiloxane (PDMS; Sylgard 184, Ellsworth Adhesives, Germantown, WI) mold with

reservoirs to seed arteriole-scale channels with EC (Fig. 4.1H), as described previously [29]. Briefly, 290 μm acupuncture needles were coated in 2% gelatin (Sigma) and inserted into the PDMS chamber. Cellular or acellular hydrogels were fabricated as described above and cast around the needles with an aorta placed in between the two needles. Needles were removed leaving behind empty cavities that were seeded with EC to form mesovessels.
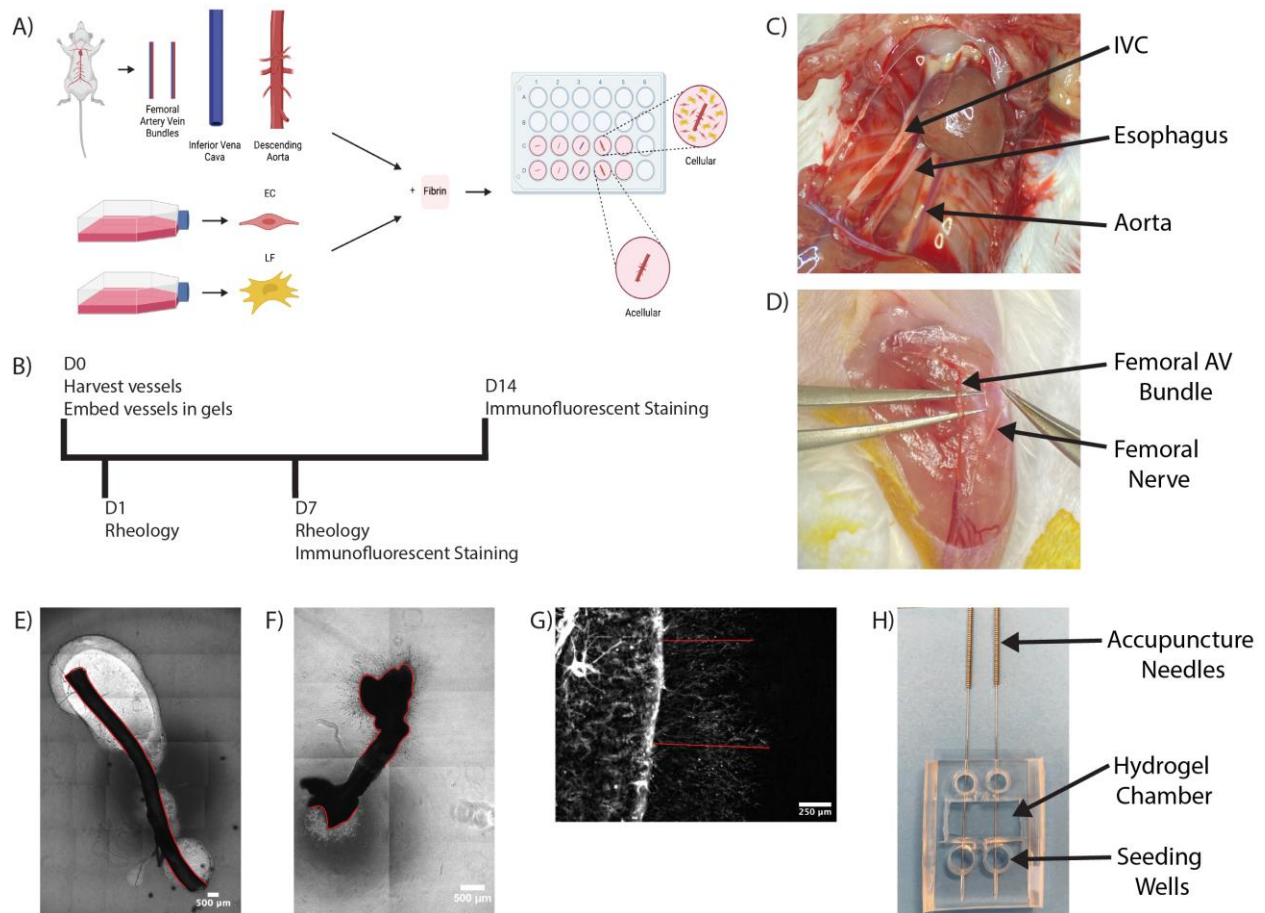
Figure 4.1: Methodology for the fabrication and analysis of hierarchical vascular networks containing explanted murine macrovessels. *(A) Schematic diagram of cell and vessel harvest procedures and hydrogel fabrication approach. (B) Experimental timeline. (C) Surgical view of thoracic cavity showing the two explanted vessels and the esophagus which was avoided. (D) Surgical view of the left femoral muscle showing the AV bundle and the femoral nerve which was avoided. (E-G) Methods for analysis of explants. (E) Degradation analysis – red lines indicate degraded perimeter. (F) Percent sprouted analysis – red lines indicate sprouted perimeter (G) Sprout distance analysis – red lines indicate sample traces of cell sprouting. (H) Color image of the PDMS mold for fabricating 3-scale vascular hierarchies bonded to glass with needles inserted.*

4.2.9 Statistics

Data were analyzed using Prism 9 (GraphPad, San Diego, CA). All data are represented as mean ± standard deviation. All data points represent a vessel from an individual animal, where, for some types of analyses, multiple measurements were averaged to obtain the data point from each animal. Analysis was conducted on N = 3 animals per measurement type. Data were analyzed using a one-way ANOVA with Sidak's multiple comparisons *post hoc* test for pre-specified comparisons or a nonparametric test with Dunn's *post hoc* test for pre-specified comparisons. Comparisons were made between vessel types at the same timepoint or between timepoints for the same vessel type. $p < 0.05$ was considered statistically significant.

4.3 Results

4.3.1 Quiescent large vessels sprout into acellular fibrin hydrogels

We examined sprouting from murine aortae, vena cavae, and femoral AV bundles embedded in fibrin hydrogels (Fig. 4.1). We observed significant sprouting from vessels in acellular fibrin hydrogels. Both stromal cell (SC) and EC sprouting occurred from all three vessel types (Fig. 4.2C, D). Explants embedded in acellular hydrogels sprouted in a collective, multicellular morphology (Fig. 4.2C, D), but significantly degraded the fibrin surrounding the vessel (Fig. 4.2A). There was significantly less fibrinolysis around aortae compared to vena cavae and AV bundles (Fig. 4.2B). Sprouting primarily occurred in the degraded regions of the hydrogel, resulting in cord-like endothelial structures that appeared to stretch across areas devoid of matrix. The nuclear staining showed clusters of cells rather than a vessel-like arrangement with a hollow lumen between nuclei (Fig. 4.2D, Nuclei). These constructs were not further analyzed for sprouting

metrics as the large degree of fibrinolysis would limit their utility as transplantable engineered vascularized tissue constructs.

To mitigate the significant fibrinolysis, aprotinin, a protease inhibitor, was added to the culture medium. In the presence of aprotinin, explants did not degrade the surrounding fibrin (Fig. 4.3A), and sprouts were morphologically different in the surrounding hydrogel. In contrast to the multicellular clusters observed without aprotinin, these explants sprouted as single cells (Fig. 4.3D, E). All vessels sprouted from the cut, lumenal edge (Fig. 4.3D) in addition to the abluminal edge (Fig. 4.3E). Though all vessels sprouted, aortae sprouted from a greater percentage of the vessel perimeter (Fig. 4.3B) and had a trend of increased sprout distance from the vessel edge compared to vena cavae and femoral AV bundles (Fig. 4.3C).
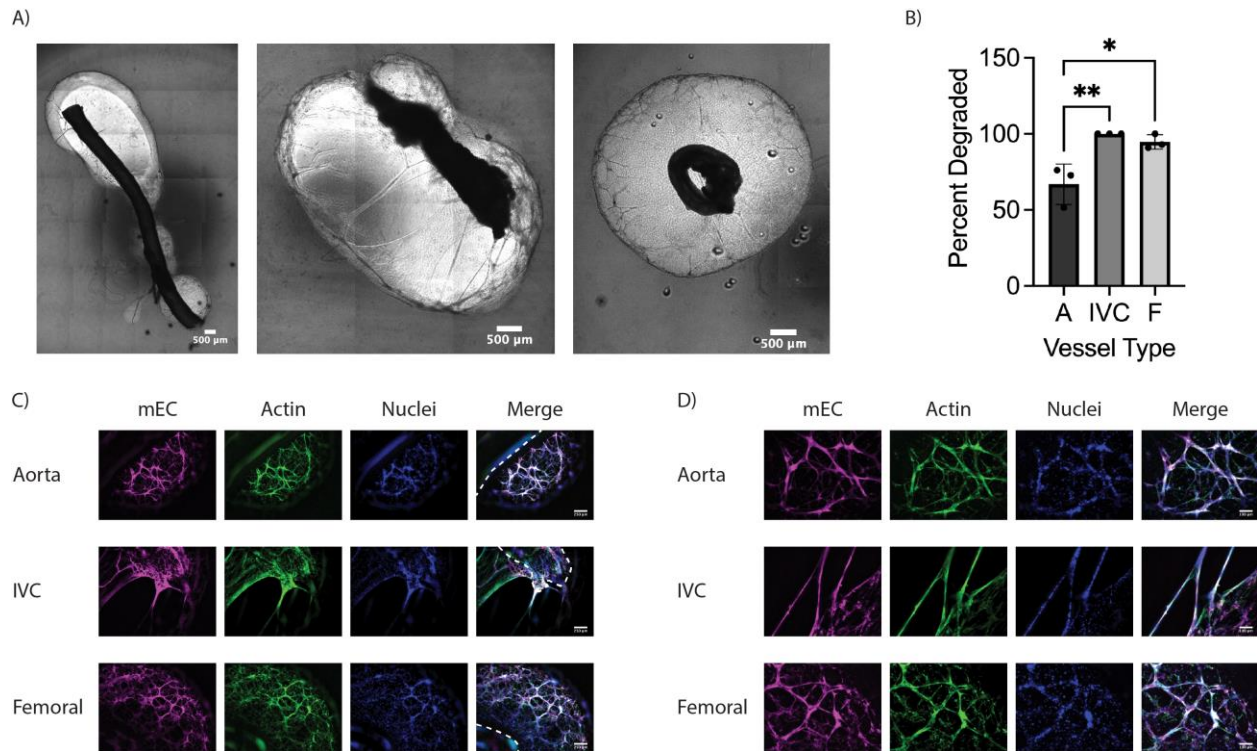
*Figure 4.2: Explanted macrovessels embedded in acellular fibrin hydrogels cause significant fibrinolysis. (A) Macroscopic phase contrast images of the entire explant and surrounding degraded fibrin hydrogel. (B) Quantification of explant perimeter with degraded fibrin. (C) Representative fluorescent images of sprouting from the explant edge into degraded fibrin regions. (D) Magnified view of vessel-like structures. * p < 0.05, ** p < 0.01 Magenta – mEC, Green – Actin, Blue – Nuclei. Dashed lines demarcate explant edge.*

When cultured for an additional week, explants continued to sprout further into the hydrogel, with a significant increase in sprout distance from aortae (Fig. 4.3C). Femoral bundles and vena cavae displayed increased sprout distance, though not statistically significant. Additionally, the trend in increased sprout distance from aortae compared to other vessel types at day 7 became significant at day 14. The dominant sprouting morphology at day 14 remained single cells (Fig. 4.3F), but in some instances, there was evidence of multicellular cluster sprouting predominantly from the cut edge (Fig. 4.3G). This morphology was observed more from vena cavae and femoral AV bundles than aortae and was only observed in two thirds of the vessels of each type analyzed. When this morphology was observed from aortae, it typically occurred from the ends of intercostal branches (Fig. 4.3G, Aorta), not the main aorta. Additionally, the multicellular sprouts from vena cavae and aortae tended to be thinner than those from femoral bundles.

4.3.2 Sprouting persists in cellular fibrin hydrogels with evidence of chimeric microvasculature

We next examined how these EC sprouts from explants would interact with human EC and SC capable of vasculogenic self-assembly in the surrounding fibrin matrix. Mouse EC continued to sprout into cellular fibrin hydrogels. The presence of human cells in the bulk hydrogel attenuated explant-induced fibrinolysis at day 7 (Fig. 4.4A), but this effect did not persist to day 14 (Fig. 4.4B). Further, the degradation was not consistent across explant types, with femoral and vena cavae explants exhibiting the most degradation, consistent with the degradation observed in acellular hydrogels (Fig. 4.2). Human EC in the bulk hydrogel self-assembled into capillaries (Fig. 4.4 D, E, hEC) over the course of culture as mouse EC sprouted out into the hydrogel (Fig. 4.4 D, E, mEC). In regions that did not degrade, the EC sprouting morphology was comparable to that of

105
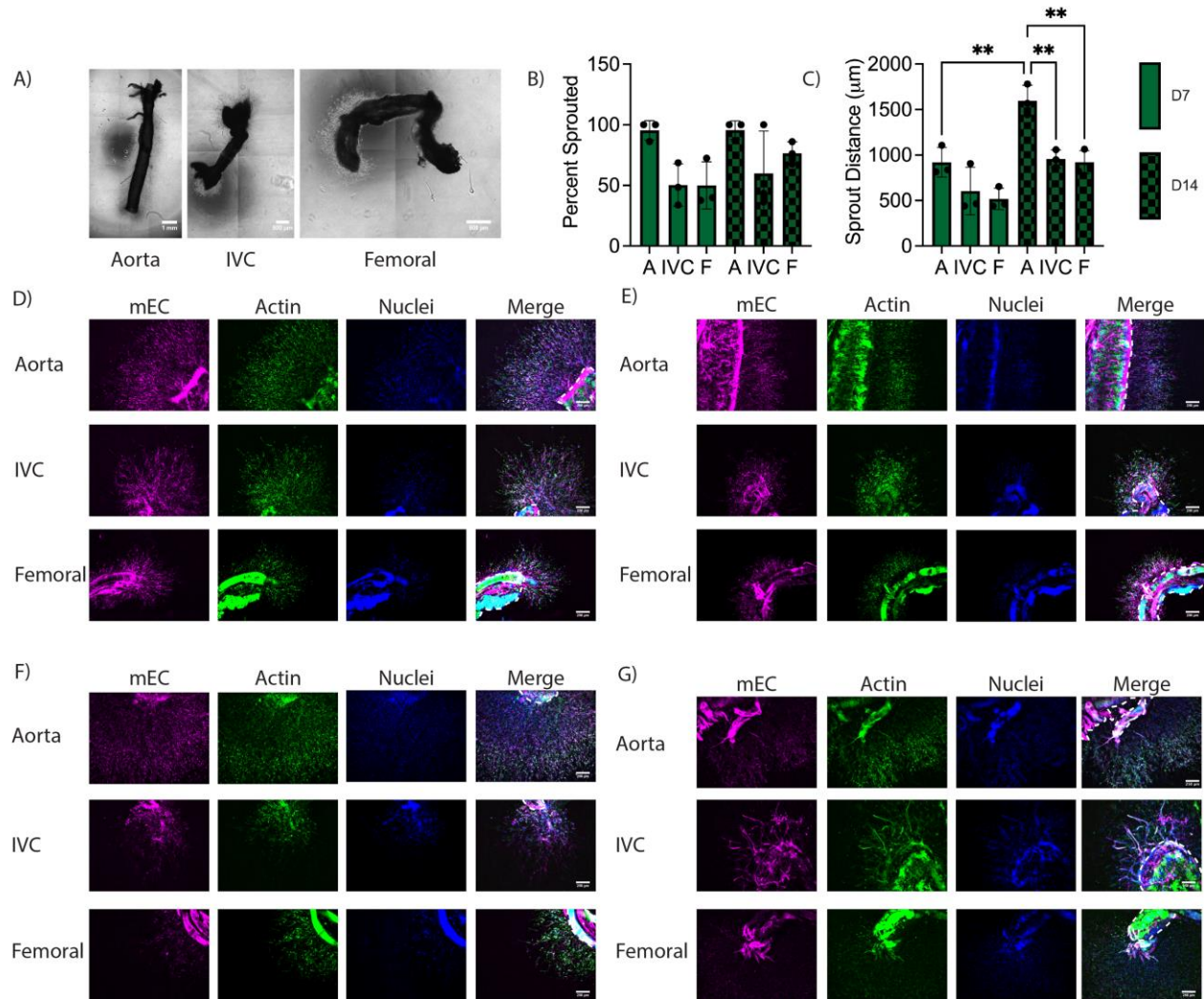
Figure 4.3: Explanted macrovessels embedded in acellular fibrin hydrogels with protease inhibitors yield significant sprouting from the abluminal and lumenal edges. (A) Macroscopic phase contrast images of the entire explant and surrounding fibrin hydrogel. (B) Quantification of explant perimeter with sprouted cells. (C) Quantification of mEC sprout distance from explant edge. (D) Representative fluorescent images of sprouting from the lumenal explant edge at D7. (E) Representative fluorescent images of sprouting from the longitudinal explant edge at D7. (F) Representative fluorescent images of sprouting from the explant edge at D14 with the same morphology as at D7. (G) Representative fluorescent images of sprouting from the explant edge at D14 with a new multicellular morphology. ** p < 0.01 Magenta –mEC, Green – Actin, Blue – Nuclei. Dashed lines demarcate explant edge.

the explants in acellular hydrogels cultured in the presence of aprotinin (Fig. 4.4D compared to Fig. 4.3D, E). In regions that did degrade, the sprouting morphology was comparable to the acellular sprout morphology (Fig. 4.4E femoral compared to Fig. 4.2C, D). Sprouting occurred

from both lumenal and abluminal edges, though the number of sprouted regions was attenuated in comparison to acellular samples with aprotinin supplement. This may be a result of the presence of human cells consuming nutrients from the medium or the proximity of human cells undergoing vasculogenesis to the explant causing local changes in fibrin stiffness.
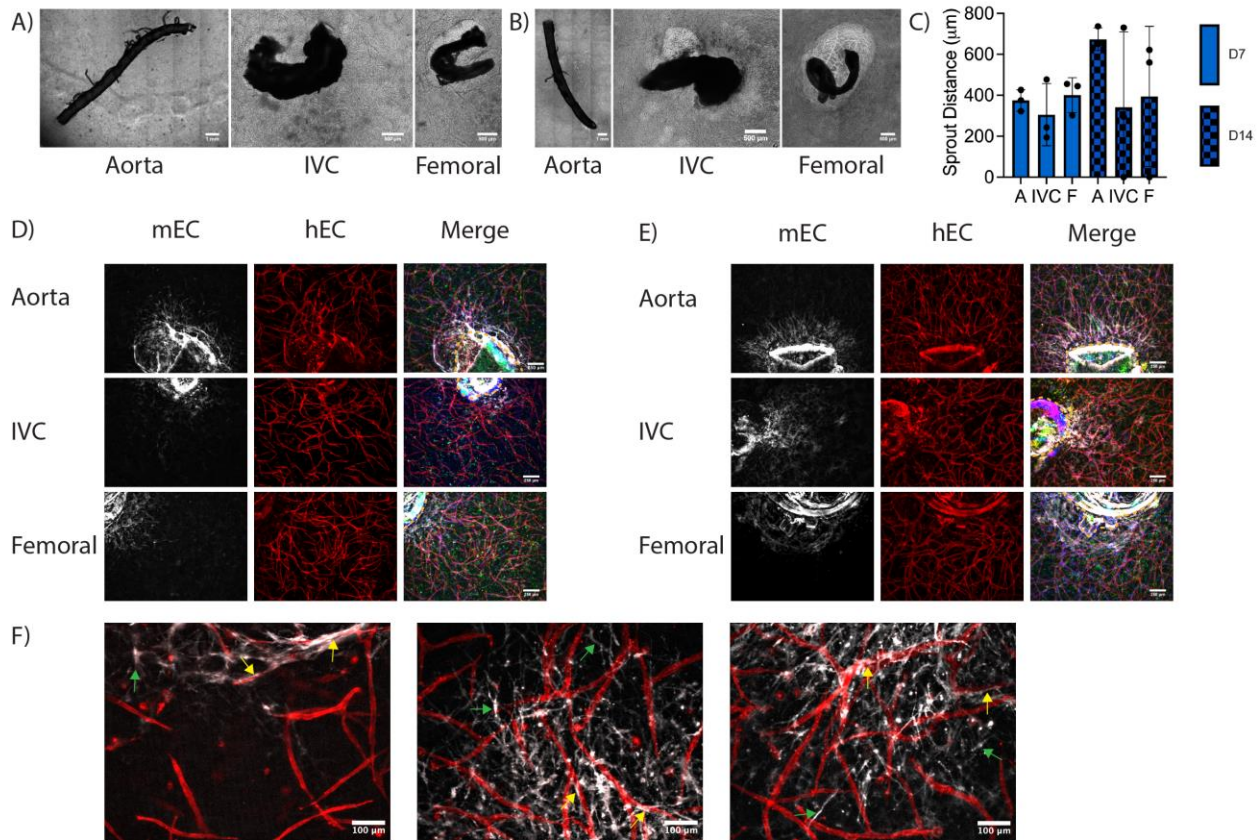
Figure 4.4: Formation of chimeric vascular structures. (A, B) Macroscopic phase contrast images of the entire explant and surrounding fibrin at (A) D7 and (B) D14. (C) Quantification of mEC sprout distance from the explant edge into the hydrogel. (D, E) Representative fluorescent images of mEC sprouting from explants at (D) D7 and (E) D14. (F) Representative magnified fluorescent images of mEC-hEC interactions and morphologies. Red – hEC, White – mEC, Green – Actin, Blue – Nuclei. Yellow arrows – mEC interacting with hEC. Green arrows – mEC sprouted into the hydrogel not interacting with hEC. Dashed lines demarcate explant edge.

At higher magnification, two different migration morphologies were observed. In some cases, mouse EC sprouted into the gel without interacting with human EC (Fig. 4.4F, green arrows). In other cases, mouse EC sprouted towards and began wrapping around human EC vessels

(Fig. 4.4F, yellow arrows). Further, the morphology of the mEC interacting with hEC was different than mEC sprouting solely into the gel. mEC in the hydrogel exhibited a spindle-like morphology somewhat akin to that of fibroblasts, while mEC interacting with hEC did not appear spindly, but rather elongated along the hEC vessel.

In addition to hEC altering the morphology of mEC, the presence of explants within the hydrogels also induced morphological changes to the bulk human vasculature. At regions close to the explant, all three explant types had some evidence of human vasculature directly next to the explant (Fig. 4.5A, bottom), while some regions showed single cells that did not self-assemble into vasculature directly next to the explant (Fig. 4.5A, top). In the bulk of the hydrogel, at distances >1 mm from the explant edge, the density of human vasculature was comparable to gels without explants (Fig. 4.5B, C). However, explants did induce some morphological differences in vascular assembly throughout the bulk hydrogel. Most regions contained a normal vascular density (Fig. 4.5D, middle) comparable to gels without an explant (Fig. 4.5C), though some regions exhibited dense (Fig. 4.5D, left) or sparse (Fig. 4.5D, right) vascular density.

Comparable to the effect in acellular gels, aprotinin eliminated explant induced fibrinolysis in cellular hydrogels (Fig. 4.6A, B). When aprotinin was incorporated into the media for cellular hydrogels, the sprout morphology remained unchanged compared to those without aprotinin; mEC still sprouted as single cells (Fig. 4.6C, D) to similar distances (Fig. 4.6E). Chimeric vasculature was observed again with some EC sprouting towards and wrapping around human microvessels (Fig. 4.6F, yellow arrows).
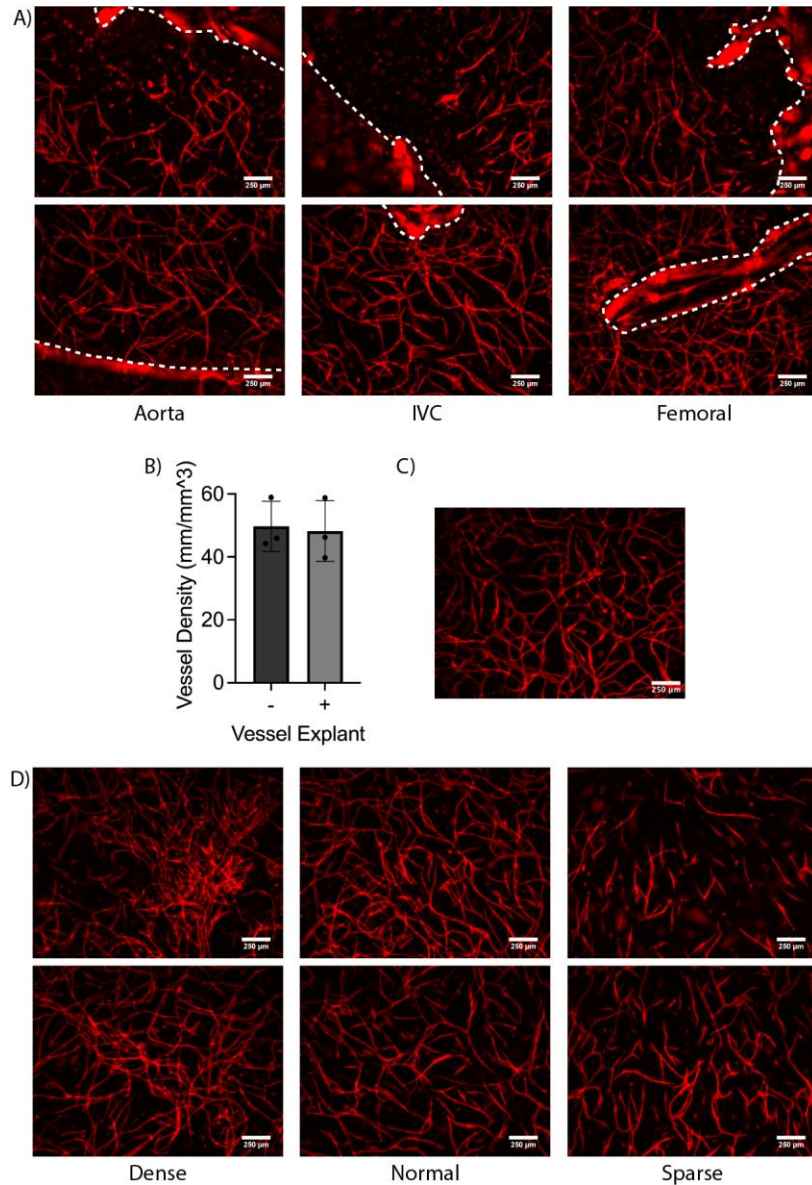
Figure 4.5: Macrovessel explants induce changes to capillary morphology but not capillary density*. (A) representative images of human self-assembled capillaries formed around explants. (B) Quantification of vessel density in hydrogels with or without explants. (C) Representative image of capillaries in a hydrogel without an explant. (D) Representative images of three different capillary morphologies. Red – hEC. N = 3 vessels from 3 separate mice per vessel type. N = 3 independent replicates examined. Vessel explant types merged for each replicate. Dashed lines demarcate explant edge.*

4.3.3 Human cells attenuate sprouting from murine explants

When sprout distance data for all three conditions (Acellular + Aprotinin, Cellular, and Cellular + Aprotinin) were examined, clear trends arose. The presence of human cells in the bulk

109

hydrogel attenuated sprouting over time compared to acellular hydrogels with the aprotinin supplement (Fig. 4.7). At day 7, aortae sprouted significantly less in both cellular conditions compared to acellular hydrogels with the aprotinin supplement. At day 14, all three vessel types and both thoracic vessels displayed significantly attenuated sprouting in cellular hydrogels and cellular hydrogels with the aprotinin supplement, respectively, compared to acellular hydrogels with the aprotinin supplement. Further, the presence of aprotinin did not affect sprout distance in cellular hydrogels with no significant differences observed between these conditions.
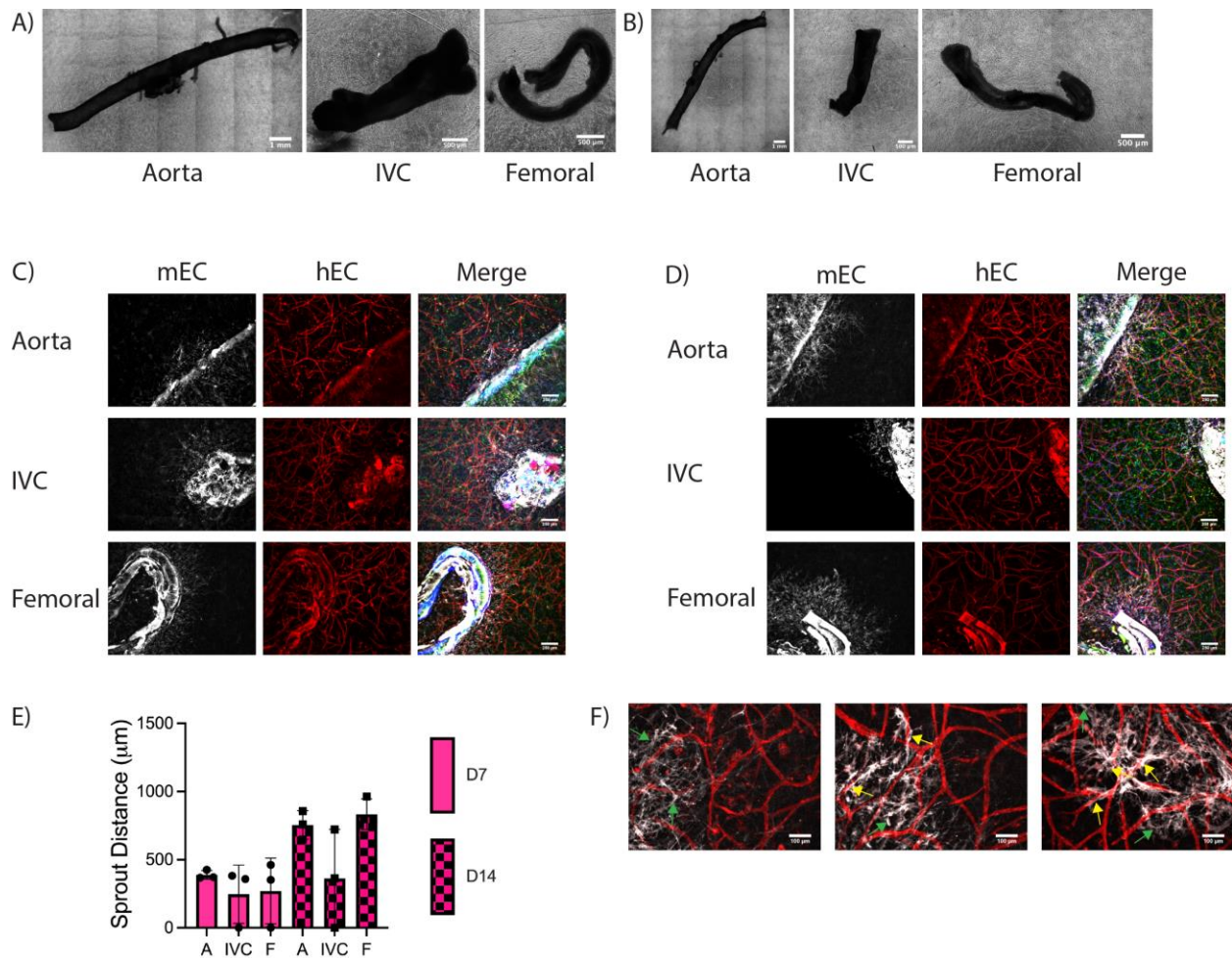
Figure 4.6: Formation of chimeric vascular structures. *(A, B) Macroscopic phase contrast images of the entire explant and surrounding fibrin at (A) D7 and (B) D14. (C, D) Representative fluorescent images of mEC sprouting from explants at (C) D7 and (D) D14. (E) Quantification of mEC sprout distance into the hydrogel. (F) Representative magnified fluorescent images of mEC-hEC interactions and morphologies. Red – hEC, White – mEC, Green – Actin, Blue – Nuclei. Yellow arrows – mEC interacting with hEC. Green arrows – mEC sprouted into the hydrogel not interacting with hEC.*

4.3.4 Sprout distance is correlated with hydrogel stiffness

We examined hydrogel stiffness via bulk parallel plate rheology to determine if explant sprouting yielded increases in hydrogel stiffness as we have observed in other hydrogel systems [30]. The presence of an explant within the hydrogel did not cause significant differences in hydrogel stiffness (Fig. 4.8A). Sprouting into the hydrogels did not significantly increase hydrogel stiffness in either acellular hydrogels with the aprotinin supplement or cellular hydrogels (Fig. 4.8A). We then examined the correlation between hydrogel stiffness and sprout distance after 7 days in culture. When sprout distance significantly increased between some vessel types (i.e., Acellular + Aprotinin Aorta as shown Fig. 4.3C), there was a correlation between sprout distance and hydrogel stiffness. In the acellular + aprotinin conditions, stiffness and sprout distance were well correlated with an R^2 value of 0.9377 (Fig. 4.8B). When sprout distance was equal among the different vessel types (i.e., Cellular as shown in Fig. 4.4C), the two parameters were not well correlated as evidenced by an R^2 value of 0.6686 in the cellular condition (Fig. 4.8B).
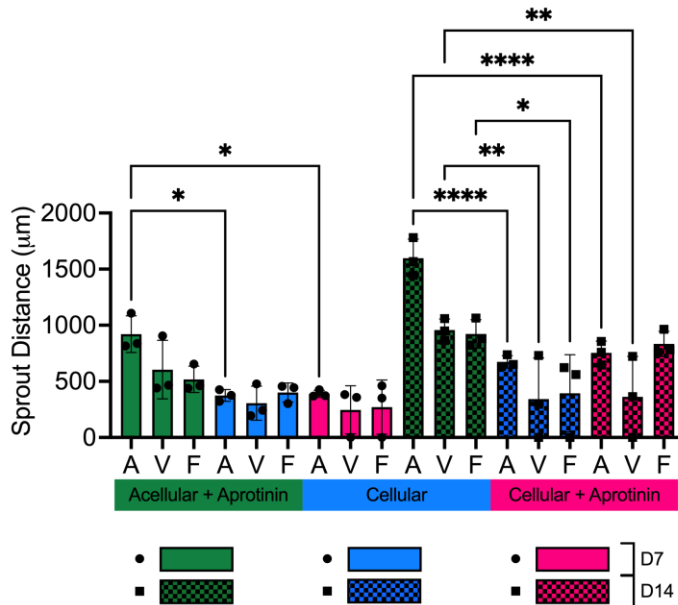
Figure 4.7: The presence of cells in the bulk hydrogels diminishes mEC sprout distance*. Quantification of mEC sprout distance into fibrin hydrogels of different compositions. Data reproduced from figures 4.3C, 4.4C, and 4.6E. * p < 0.05, ** p < 0.01, **** p < 0.0001.*
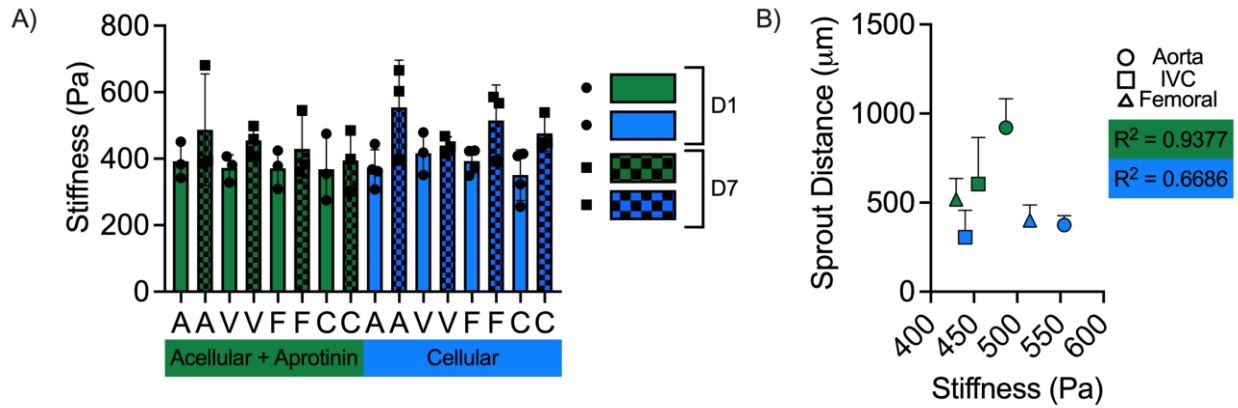
Figure 4.8: Sprout distance and hydrogel stiffness are interdependent in some hydrogel conditions. *(A) Quantification of hydrogel stiffness via macro rheology. (B) Correlation between sprout distance and hydrogel stiffness at day 7. Green – acellular + aprotinin samples, Blue – cellular samples.*

4.3.5 Creating three-scale vascular hierarchies

One major drawback of current vascular tissue constructs is the lack of a multiscale vascular hierarchy within the tissue construct. Therefore, we sought to incorporate mesovessels within our constructs to fabricate a more complete hierarchy containing all three vascular length scales (Fig. 4.9). We incorporated the suturable aorta into a hydrogel with self-assembled capillaries and two mesovessels thereby creating a complete vascular hierarchy containing a microvascular network, mesovssels, and a macrovessel.

We fabricated both cellular hydrogels (Fig. 4.9A) and acellular hydrogels with the aprotinin supplement (Fig. 4.9B). We primarily observed the same sprout morphology as previously shown in day 7 cellular constructs in Figure 4.4. Additionally, we also observed a more vessel-like phenotype not previously observed in day 7 cellular constructs (Fig. 4.9A, middle). The mesovessels were perfusable (Fig. 4.9A, right) though inosculation between the meso- and microvasculature, as previously shown in Chapter 3, was not observed here. The acellular + aprotinin sample was cultured for 21 days to allow sprouted cells to reach the mesovessel and

integrate (Fig. 4.9B, left and middle). We observed the same multicellular phenotype shown previously at day 14 from an intercostal branch (Fig. 4.9B, right)
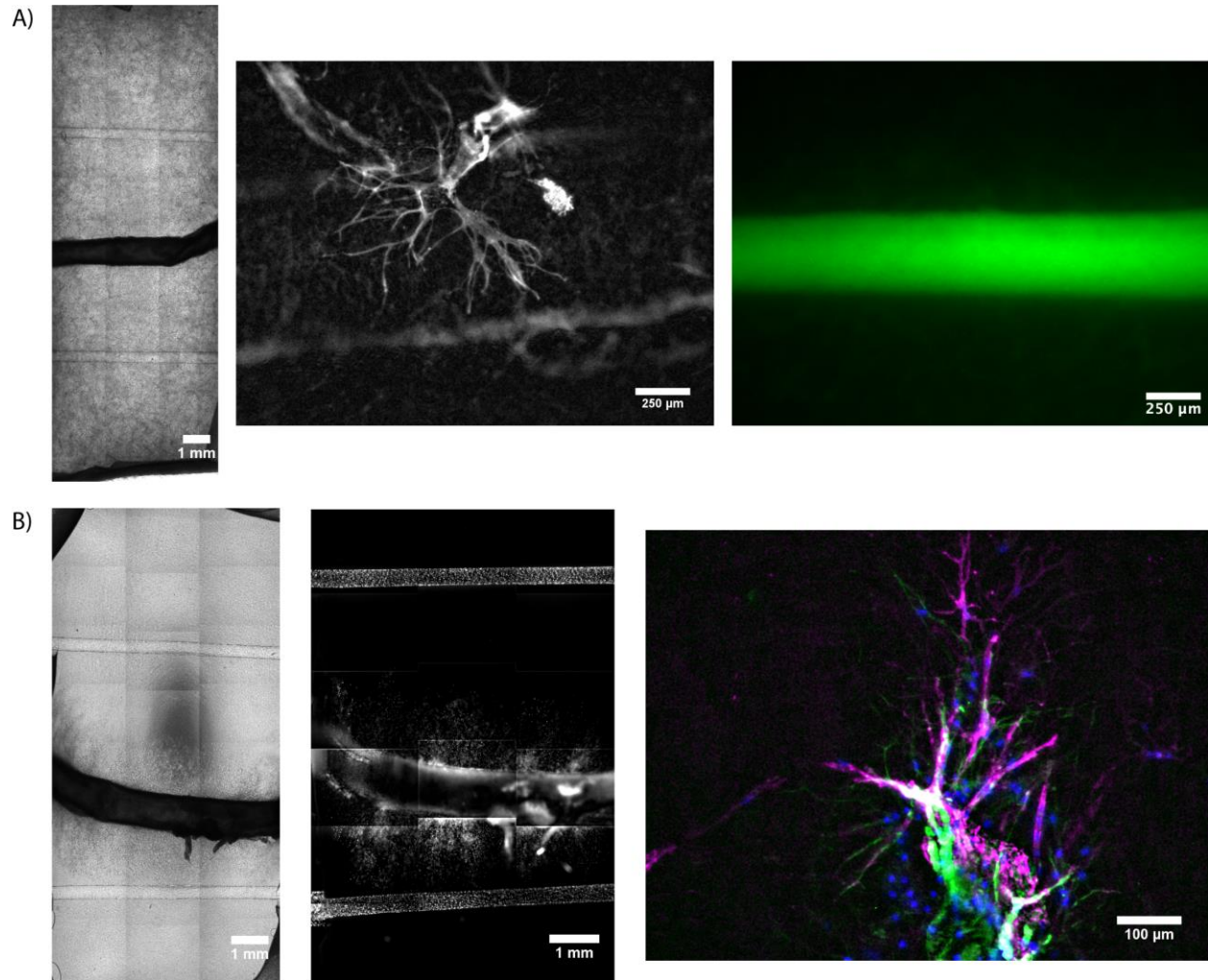
Figure 4.9: Engineered three-scale vascular hierarchies with murine aortas as a macrovessel. *(A) Aorta embedded in cellular fibrin hydrogels. Whole sample phase contrast scan (left), mEC vessel-like sprout morphology (middle), dextran perfusion through mesovesel (right). (B) Aorta embedded in acellular fibrin hydrogel with the aprotinin supplement. Whole sample phase contrast scan (left) and nuclei scan (middle). High magnification view of vessel-like sprouts (right). A middle: white – mouse EC, A right: green – dextran. B middle: white – nuclei. B right: magenta – mEC, green – actin, blue – nuclei.*

4.4 Discussion

The engineering of hierarchical vasculature is a critical next step for the field of tissue engineering and regenerative medicine to advance engineered tissues and organs one step closer to clinical translation. While microvascular sprouting from macroscopic murine vessels has been previously studied using aortic ring assays, to the best of our knowledge, this is one of the first reports using a full-length vessel with observation of sprouting from the abluminal edge of a macrovessel in addition to the lumenal cut edge, and of sprouting from a macrovessel for inosculation with engineered capillaries to yield a hierarchical vascular tissue construct. One other study reported the use of longer vessel segments, but with sprouting still solely from the cut end. Chiu, et al. report the interconnection of two longer vessel segments, an artery and a vein, by sprouted capillaries using topographical and biological cues to guide nascent sprouts [28]. Their study induced sprouting from the cut edge, thereby connecting two macrovessels with sprouted capillaries.

In our initial acellular hydrogels, we observed significant explant-induced fibrinolysis of the surrounding fibrin hydrogels. Similar results have been observed in foundational studies using the aortic ring assay [31]. Several studies using these ring assays implicate MMPs, specifically MMP-2, for their role in the initiation of microvessel formation and in microvessel regression at later timepoints in the vascular morphogenesis cascade in aortic ring cultures [32, 33]. MMPs 3, 9, 10, 11 and MT1-MMP have also been implicated in the outgrowth of microvascular structures in aortic ring cultures [26]. Zhu et al. observed a reduction in vascular sprouting from aortic rings concurrent with a marked reduction in collagen lysis when aortic rings were cultured with MMP inhibitors batimastat and marimastat [33]. These results are consistent with our results shown in Figure 4.2 where there is significant fibrinolysis and vessel formation in acellular hydrogels and

in Figure 4.3 when fibrinolysis is eliminated as is vessel formation in the presence of the protease inhibitor aprotinin. These results suggest that regardless of hydrogel composition, degradation of the hydrogel is critical for vessel sprouting to occur. In support of this, Chun et al. cultured aortic rings in collagen hydrogels and fluorescent staining for collagen degradation products revealed that both proteolyzed and denatured collagen were present in the perivascular region surrounding nascent vessels [34]. They also found that sprouting from rings from plasminogen null mice was indistinguishable from control mice, suggesting that angiogenic sprouting persists in the absence of plasminogen, a known regulator of fibrin degradation. Their study was conducted in collagen hydrogels but is consistent with our results in fibrin as we showed that when fibrinolysis was inhibited, EC still sprouted from the vascular explants. Another study of angiogenesis from aortic rings in fibrin gels found that neither plasminogen nor plasminogen activator were required for neovessel formation, rather MMPs were a critical regulator of vessel sprout formation in fibrin hydrogels [35]. Together, these results suggest a future experiment where acellular hydrogels are cultured at early timepoints without aprotinin to initiate angiogenic sprouting and then at later timepoints with aprotinin to prevent subsequent microvessel regression and fibrinolysis.

Despite the dogmatic view that large quiescent vessels do not sprout, or only do so from cut or damaged ends as observed in aortic ring assays, we observed sprouting in both acellular and cellular hydrogels. In this study, we examined sprouting from arteries and veins from both thoracic and femoral origins. We observed differences in sprout percentage and sprout distance from aortae and vena cavae in acellular hydrogels with the aprotinin supplement. These results could be due to several reasons. First, arteries have a thicker vessel wall with greater numbers of cells and the presence of a vasa vasorum compared to thinner vein walls that are less densely populated with cells. Sprouting from arteries into the surrounding fibrin hydrogels may have originated from the

vasa vasorum. Second, arteries and veins are exposed to very different blood pressures. Due to its proximity to the heart, the aorta is exposed to high blood pressure as blood is pumped from the heart to the rest of the circulatory system, while the vena cava is exposed to much lower blood pressure as blood in returned to the heart. Though the vessels were not cultured under flow in this study, their predisposition to various flow rates and blood pressures may impact their angiogenic potential when examined in this assay. Finally, the sprout potential may be affected by the presence of tissue around the vessels. Removal of the connective tissue and/or muscle tissue around the vessels required significant mechanical manipulation of the vessels. The aorta is a strong muscular artery, and therefore could withstand this force without sustaining damage to the vessel. In contrast, the vena cava has a thin, non-muscular wall that easily ripped when pressure was applied by forceps to remove connective tissue. Therefore, these vessels were not cleaned as thoroughly as aortae, leaving extra tissue behind that could have hindered sprouting. Similar results were reported by Vaghela, et al. comparing the aortic ring assay from various vessel origins [27].

Another factor potentially affecting sprout distance is the presence of nutrient (and/or pro-angiogenic growth factor) gradients. In acellular hydrogels, cells are inclined to directionally sprout into the hydrogel towards higher concentrations of these cues as evidenced by increased EC sprouting between day 7 and day 14. The relatively small numbers of cells in the bulk of the gel consume lower amounts of nutrients, whereas in the proximity of the explant there are many cells consuming nutrients. The bulk hydrogel acts as a source and the explant acts as a sink, thereby establishing a gradient that likely induces cells to sprout out of the explant into the hydrogel toward regions of higher concentration. This type of angiogenic sprouting model has been described previously wherein cells migrate from one vessel to another via a source of nutrients and growth factors [36, 37]. In contrast, in cellular hydrogels, human cells in the bulk consume these nutrients

and growth factors, so any gradients that exist would presumably be much shallower and less capable of driving murine EC sprouting into the cell-laden hydrogels. Cells may initially sprout further into the hydrogel and then regress by the day 7 or day 14 timepoints. This could explain the attenuation of sprout distance observed in cellular hydrogels compared to acellular hydrogels as shown in Figure 4.8. These findings are consistent with Barkefors et al. who observed that cells in proximity to the peak concentration of nutrients migrated negligibly compared to cells experiencing a sharper gradient of nutrients [38].

While sprout distance was the predominant quantitative metric used in this study, in cellular hydrogels with or without the aprotinin supplement, inosculation between human engineered microvessels and sprouted mouse EC is arguably equally, if not more, important for the successful creation of a hierarchical vasculature. We observed anastomoses between human and mouse EC in hydrogels containing all three vessel types. Further, our analysis only examined median and end points of culture and thus may have missed any vessel regression. A number of prior studies report regression of vessel sprouts over time [15, 27]. In contrast, we reported an increase in sprout distance in acellular hydrogels with the aprotinin supplement and a maintenance of sprout distance over time in cellular hydrogels with or without the aprotinin supplement. Although human cells may be inhibitory to significant sprouting of mouse EC from the large vessels in this system, these results suggest their presence may support the viability and maintenance of sprouted cells over long-term culture periods. This result, together with the observed sprouting from the abluminal edge of vessel explants, supports the potential use of these chimeric constructs as transplantable vascularized tissue constructs. Minimal manipulation of these hydrogels to expose the lumenal end could be achieved while maintaining the interaction between mEC and hEC within the hydrogel prior to implantation in an animal model.

Despite differences in EC sprout distance from vessels of different origins, the identity of sprouted cells remained consistent between vessel types. Figures 4.2 and 4.3 show similar populations of EC and SC from aortae, vena cavae, and femoral bundles. Similarly, EC sprouted from all vessel types in cellular hydrogels (Figs. 4.4, 4.6). Mouse SC also likely sprouted from these vessels as well but cannot be distinguished from human SC with the fluorescent stains used.

In an effort to better understand how hydrogel mechanics may impact sprouting in this chimeric system, we examined bulk rheology of hydrogels with and without explants. Our analysis identified no significant differences in hydrogel stiffness between day 1 (pre-sprouting) and day 7 hydrogels in both acellular samples with the aprotinin supplement and cellular samples. In acellular hydrogels with the aprotinin supplement, where there was not only significant sprouting from all vessels but significant differences between sprouting from different vessel types, our analysis yielded a correlation between hydrogel stiffness and EC sprout distance into the hydrogel after 7 days in culture. Our lab has shown that vascular morphogenesis induces hydrogel stiffening in PEG [7, 30, 39] and fibrin [40] hydrogels. Unpublished work suggests that fibroblast-mediated vessel morphogenesis in fibrin gels only yields significant stiffening after 14 days in culture, rather than earlier 7-day timepoints observed in PEG hydrogels. This suggests that in our current study, the correlation observed between EC sprouting and hydrogel stiffening that is not significant at day 7 may become significant at later timepoints. This correlation between EC sprout distance and hydrogel stiffness in acellular hydrogels, may also be due to local changes in hydrogel stiffness around sprouted EC, that does not yield significant bulk hydrogel stiffening. Microrheological measurements in our prior fibrin study revealed local changes in hydrogel stiffness near EC undergoing sprouting angiogenesis [40]. Therefore, in this system, sprouted EC may have a significant role in mechanical properties of the hierarchical vascular tissue constructs. Local

118

changes in matrix stiffness around the explant or other explant-induced changes to matrix stiffness may also play a role in the vascular morphological differences observed in Figure 4.5.

The incorporation of a third vascular length scale did not significantly alter sprouting morphology in acellular hydrogels but yielded more multicellular sprouting in cellular hydrogels. These results suggest that our model is amenable to fabrication of an integrated hierarchical vasculature. However, some modifications will be required to achieve full perfusion across all three length scales. Our prior work with mesovessels revealed that LF-EC integrated meso-microvascular constructs inosculated and perfused 55-75% of the time [29]. In the present study, we did not observe inosculation of the two length scales, potentially due to the increase in fibrin density from 2.5 to 5 mg/mL that was required for successful removal of tissues from the PDMS mold (data not shown) for translational applications. Though we did not observe perfusion across the entire hierarchy, perfusion may occur more rapidly when surgically anastomosed *in vivo* and immediately connected to the blood circulation.

Very little is known about the mechanisms by which transplanted microvascular networks inosculate with host vessels upon implantation. One prior study coined the term "wrapping and tapping anastomosis" to describe this phenomenon [41]. Using intraviral microscopy in cranial and dorsal window chamber rodent models, Cheng, et al. showed implanted EC wrapped around nearby host vessels causing displacement of the original host endothelium. The implanted EC replace segments of the original host vessels and tap into the blood supply connecting vessels from the host and the implant. The morphologies observed in Figures 4.4F and 4.6F are remarkably similar to the wrapping and tapping morphology previously observed. Our model could be useful to further study host-implant inosculation mechanisms and potentially investigate using explants from mice of different ages, sexes, and cardiovascular health backgrounds. Similar experiments

119

have been conducted using the aortic ring model using rings from genetically modified mice where the chemokine receptor CXCR2 was disrupted. These results showed a 50-70% decrease in sprouting compared to control mice [42]. Mice of different ages and from different backgrounds also respond differently to angiogenic factors [16]. One study evaluated sprouting angiogenesis from four strains of mice at five different ages in response to two different angiogenic factors to assess how age and genetic background affect the angiogenic response from murine aortae [16]. BALB/c mice had the highest angiogenic response to basic fibroblast growth factor (bFGF) and the second highest angiogenic response to vascular endothelial growth factor (VEGF) at early 6-day timepoints of the four strains analyzed. When they examined C57BL/6 mice of various ages, 2-month-old mice had the highest angiogenic response to bFGF and 1-month-old mice had the highest response to VEGF. Overall, 1–3-month-old mice had the highest angiogenic responses to both growth factors, while 6-month-old and 10.5-month-old mice consistently had the lowest angiogenic response. These results motivated our use of 6-week-old BALB/c mice in the present study explored here, in order to yield the most significant sprouting and the best potential for the formation of hierarchical vasculature. This also suggests that results from mice with age and health conditions matching the aging population could be potentially transformative in advancing engineered vascular tissues to the clinic.

Our findings suggest that quiescent large vessels are capable of sprouting as clusters of EC or single EC into the surrounding acellular and cellular hydrogels, respectively. This finding is critical to the development of hierarchical vascular tissue constructs. While this type of sprouting has been documented in aortic ring assays over the past several decades, to our knowledge, this is the first report of sprouting from the abluminal edge of large arteries and veins combined within a single construct with mesovessels yielding a hierarchical vascular tissue construct. Sprouting from

the abluminal edge is critical for the use of large vessels in microsurgical anastomosis, as not to disrupt sprouting from the lumenal edge during the anastomosis procedure and keep the sprouted vessels intact. When we cultured aorta in the hierarchical mold with the lumenal edges exposed (i.e., not encased within the hydrogel), we still observed sprouting from the abluminal edge consistent with prior results. We observed significant sprouting from aortae, counter to the dogmatic view that large vessels to not sprout, which are the most feasible of the vessels examined to be amenable to surgical anastomosis as they are the only vessels we successfully cannulated prior to embedding within the fibrin hydrogels. Though the sprouting from large vessels, specifically arteries, does not represent a physiologic vascular hierarchy, it is likely that this primitive hierarchy would be remodeled upon implantation and exposure to physiologic fluid flow. This proof-of-concept study lays the groundwork for more rigorous analysis of host-implant inosculation and the engineering of more complex perfusable hierarchical vascular tissue constructs.

4.5 Supplementary Data

Prior to engineering chimeric hierarchical vasculature, we investigated two candidate possibilities for fabricating single species vascular hierarchies. We first examined the use of human umbilical vessels as a source of macrovessel for more translatable human cell-based constructs employing the extensive research our lab has conducted using human cells for vascular morphogenesis. We also investigated murine EC and SC for the potential to form vascular networks in vitro to combine with the explanted murine vessels for a complete murine cell-based construct. The benefit of a murine hierarchical vascular tissue construct is the ability to test the

construct in an immunocompetent model to assess the influence of the immune system on vascular inosculation between host and engrafted cells.

4.5.1 Investigating human umbilical cords as a source of macrovessels

Prior to using murine macrossels, we explored using human umbilical cords as a source of macrovessels suitable for surgical anastomosis. Umbilical arteries have been studied previously for the development of small diameter vascular grafts [43]. We began developing protocols for isolating the two umbilical arteries and one umbilical vein from the umbilical cord. We successfully isolated the arteries (Fig. S4.1) and made great strides in the venous isolation (data not shown) prior to the onset of the COVID-19 pandemic. The pandemic halted our ability to obtain human tissue for this project. By the time we were able to resume obtaining human tissue from the hospital, the research had advanced significantly beyond the point of initial testing and vessel sourcing.
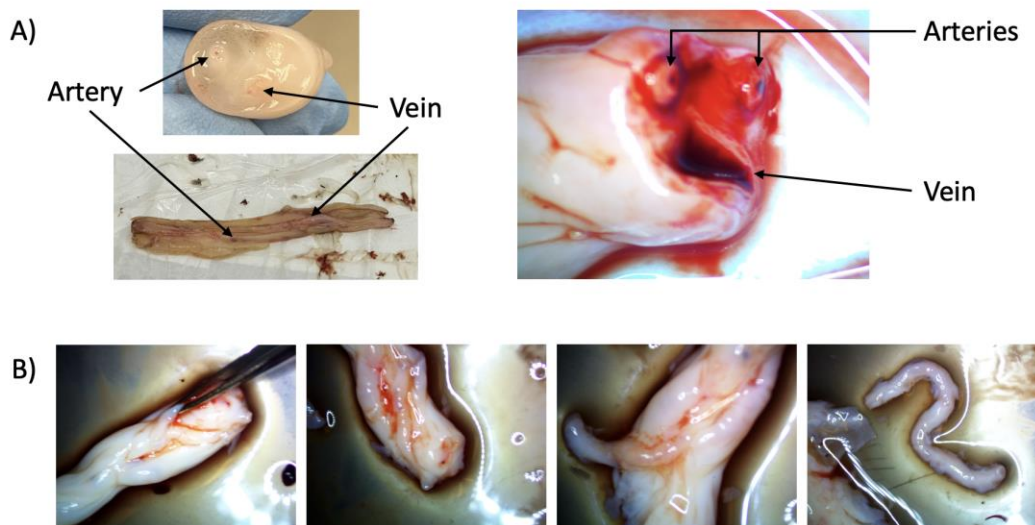
Supplementary Figure 4.1: Umbilical artery isolation. *(A) Identification of the umbilical arteries and vein within cross sections of cords and longitudinal cut open umbilical cords. (B) Successive isolation of an umbilical artery from the Wharton's Jelly, and eventual removal of an arterial segment.*

4.5.2 Investigating the vasculogenic and angiogenic potential of murine EC and SC for the development of murine hierarchical vasculature

We purchased murine dermal fibroblasts (mDF) and murine dermal endothelial cells (mDEC) from Celprogen for use in these experiments. We investigated the vasculogenic potential of these cells co-cultured in 3D fibrin hydrogels, in 2D on top of fibrin hydrogels (data not shown), and in 3D collagen hydrogels. Additionally, we investigated the angiogenic potential of these cells in 3D fibrin hydrogels using the Cytodex bead assay as described in Chapter 3.

In 3D fibrin hydrogels, murine cells failed to undergo vascular morphogenesis (Fig. S4.2A) and instead primarily proliferated (Fig. S4.2B). The significant proliferative activity of these cells also led to substantial degradation of the fibrin hydrogel (Fig. S4.2C). We examined the standard cell density used in our lab in bulk 3D fibrin hydrogels (500 K/mL 1:1 ratio of EC to SC), and a 5x lower density with consistent results between the two. In the lower density condition, we did observe more cell spreading, but ultimately no vessel formation. To minimize degradation, we cultured the cells in 3D fibrin hydrogels with the protease inhibitor aprotinin. The presence of aprotinin in the media qualitatively changed the phenotype of cells within the hydrogel (Fig. S4.2D), though cells still proliferated extensively (Fig. S4.2E) and did not undergo vascular morphogenesis. We hypothesized that culturing cells in collagen may limit the proliferative capacity of the cells and potentially focus cellular metabolic energy on vascularization processes. While we did observe substantially less proliferation, cell morphology remained consistent with the morphology observed in fibrin hydrogels and we did not observe any vascular morphogenesis.

We next investigated the angiogenic potential of these cells using a bead-based sprouting assay. Consistent with the vasculogenic assay in 3D fibrin hydrogels, we observed significant degradation of the fibrin hydrogel and no mDEC sprouting from the beads (Fig. S4.2H). The

mDEC remained adhered to the beads, not even sprouting as single cells into the surrounding hydrogel. Interestingly, compared to the vasculogenesis assay, we did not observe cell proliferation in this angiogenic assay. Over time in culture, the degraded area of the hydrogel significantly increased beyond just the region around the individual beads. Ultimately, murine cells failed to undergo vascular morphogenesis in a variety of culture conditions and using two different means of vascular morphogenesis – angiogenesis and vasculogenesis. Therefore, these cells were not suitable for the fabrication of murine hierarchical vascular tissue constructs.
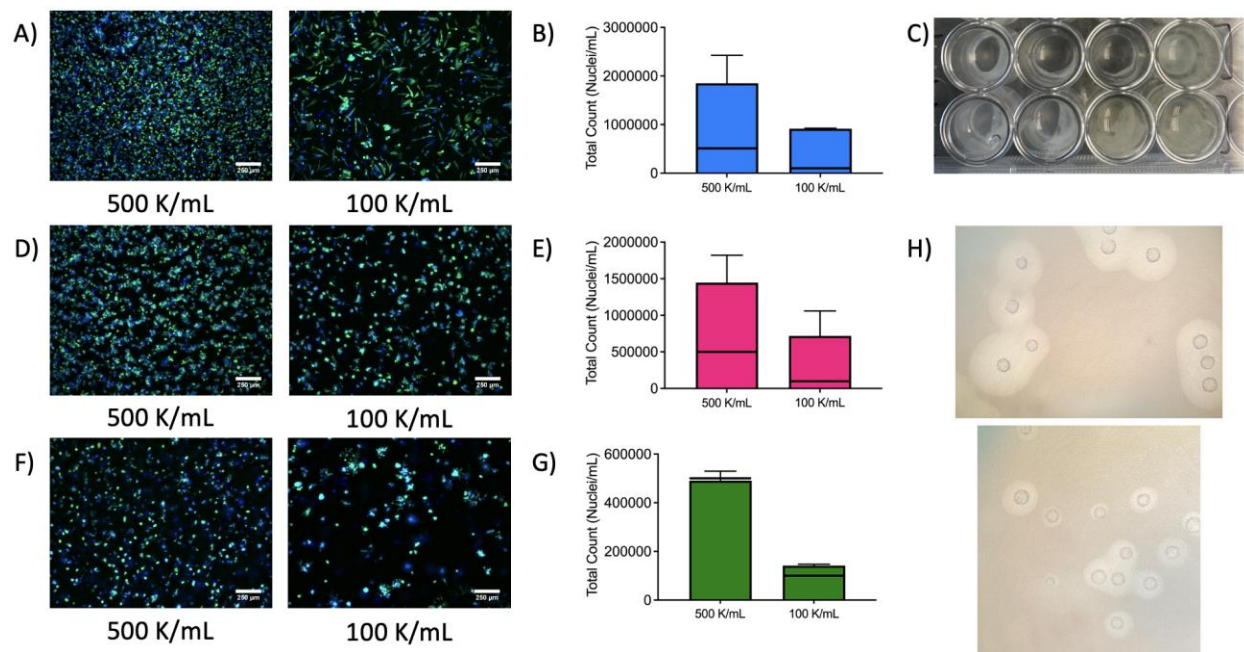
Supplementary Figure 4.2: Murine cells fail to undergo vascular morphogenesis in 3D fibrin and collagen hydrogels. *Co-cultures of mDF and mDEC in (A-C) 5 mg/mL fibrin hydrogels cultured in EGM2, (D, E) 5 mg/mL fibrin hydrogels cultured in EGM2 + aprotinin, (F, G) 3.2 mg/mL collagen hydrogels cultured in EGM2. (A, D, F) Fluorescent images of co-cultures. Green – actin, blue – nuclei. (B, E, G) Quantification of nuclei density after 7 days in culture compared to the original theoretical density (horizontal line over each bar). (C) Macroscopic image of hydrogel degradation. (H) Brightfield images of mDEC coated Cytodex beads in 5 mg/mL fibrin hydrogels.*

4.6 References

[1]   Tsao, C.W., Aday, A.W., Almarzooq, Z.I., Alonso, A., Beaton, A.Z., Bittencourt, M.S., Boehme, A.K., Buxton, A.E., Carson, A.P., Commodore-Mensah, Y., Elkind, M.S.V., Evenson, K.R., Eze-Nliam, C., Ferguson, J.F., Generoso, G., Ho, J.E., Kalani, R., Khan, S.S., Kissela, B.M., Knutson, K.L., Levine, D.A., Lewis, T.T., Liu, J., Loop, M.S., Ma, J., Mussolino, M.E., Navaneethan, S.D., Perak, A.M., Poudel, R., Rezk-Hanna, M., Roth, G.A., Schroeder, E.B., Shah, S.H., Thacker, E.L., VanWagner, L.B., Virani, S.S., Voecks, J.H., Wang, N.Y., Yaffe, K., and Martin, S.S. (2022) Heart Disease and Stroke Statistics-2022 Update: A Report From the American Heart Association. *Circulation* 145, e153-e639

[2]   Elliott, M.B., Ginn, B., Fukunishi, T., Bedja, D., Suresh, A., Chen, T., Inoue, T., Dietz, H.C., Santhanam, L., Mao, H.Q., Hibino, N., and Gerecht, S. (2019) Regenerative and durable small-diameter graft as an arterial conduit. *Proc Natl Acad Sci U S A* 116, 12710-12719

[3]   Strobel, H.A., Hookway, T.A., Piola, M., Fiore, G.B., Soncini, M., Alsberg, E., and Rolle, M.W. (2018) Assembly of Tissue-Engineered Blood Vessels with Spatially Controlled Heterogeneities. *Tissue Eng Part A* 24, 1492-1503

[4]   Syedain, Z.H., Graham, M.L., Dunn, T.B., O'Brien, T., Johnson, S.L., Schumacher, R.J., and Tranquillo, R.T. (2017) A completely biological "off-the-shelf" arteriovenous graft that recellularizes in baboons. *Sci Transl Med* 9

[5]   Li, X., Xu, J., Bartolak-Suki, E., Jiang, J., and Tien, J. (2020) Evaluation of 1-mm-diameter endothelialized dense collagen tubes in vascular microsurgery. *J Biomed Mater Res B Appl Biomater* 108, 2441-2449

[6]   Kirkton, R.D., Santiago-Maysonet, M., Lawson, J.H., Tente, W.E., Dahl, S.L.M., Niklason, L.E., and Prichard, H.L. (2019) Bioengineered human acellular vessels recellularize and evolve into living blood vessels after human implantation. *Sci Transl Med* 11

[7]   Beamish, J.A., Juliar, B.A., Cleveland, D.S., Busch, M.E., Nimmagadda, L., and Putnam, A.J. (2019) Deciphering the relative roles of matrix metalloproteinase- and plasmin-mediated matrix degradation during capillary morphogenesis using engineered hydrogels. *J Biomed Mater Res B Appl Biomater* 107, 2507-2516

[8]   Friend, N.E., Rioja, A.Y., Kong, Y.P., Beamish, J.A., Hong, X., Habif, J.C., Bezenah, J.R., Deng, C.X., Stegemann, J.P., and Putnam, A.J. (2020) Injectable pre-cultured tissue modules catalyze the formation of extensive functional microvasculature in vivo. *Sci Rep* 10, 15562

[9]   Lin, R.Z., Lee, C.N., Moreno-Luna, R., Neumeyer, J., Piekarski, B., Zhou, P., Moses, M.A., Sachdev, M., Pu, W.T., Emani, S., and Melero-Martin, J.M. (2017) Host non-inflammatory neutrophils mediate the engraftment of bioengineered vascular networks. *Nat Biomed Eng* 1

[10]   Wei, Z., Schnellmann, R., Pruitt, H.C., and Gerecht, S. (2020) Hydrogel Network Dynamics Regulate Vascular Morphogenesis. *Cell Stem Cell* 27, 798-812 e796

[11]   Szklanny, A.A., Machour, M., Redenski, I., Chochola, V., Goldfracht, I., Kaplan, B., Epshtein, M., Simaan Yameen, H., Merdler, U., Feinberg, A., Seliktar, D., Korin, N., Jaros, J., and Levenberg, S. (2021) 3D Bioprinting of Engineered Tissue Flaps with Hierarchical Vessel Networks (VesselNet) for Direct Host-To-Implant Perfusion. *Adv Mater* 33, e2102661

[12]   Grigoryan, B., Paulsen, S.J., Corbett, D.C., Sazer, D.W., Fortin, C.L., Zaita, A.J., Greenfield, P.T., Calafat, N.J., Gounley, J.P., Ta, A.H., Johansson, F., Randles, A., Rosenkrantz, J.E., Louis-Rosenberg, J.D., Galie, P.A., Stevens, K.R., and Miller, J.S. (2019) Multivascular networks and functional intravascular topologies within biocompatible hydrogels. *Science* 364, 458-464

[13]   Ziegler, T., Abdel Rahman, F., Jurisch, V., and Kupatt, C. (2019) Atherosclerosis and the Capillary Network; Pathophysiology and Potential Therapeutic Strategies. *Cells* 9

[14]   Kapoor, A., Chen, C.G., and Iozzo, R.V. (2020) A simplified aortic ring assay: A useful ex vivo method to assess biochemical and functional parameters of angiogenesis. *Matrix Biol Plus* 6-7, 100025

[15]   Nicosia, R.F. (2009) The aortic ring model of angiogenesis: a quarter century of search and discovery. *J Cell Mol Med* 13, 4113-4136

[16]   Zhu, W.H., Iurlaro, M., MacIntyre, A., Fogel, E., and Nicosia, R.F. (2003) The mouse aorta model: influence of genetic background and aging on bFGF- and VEGF-induced angiogenic sprouting. *Angiogenesis* 6, 193-199

[17]   Devy, L., Blacher, S., Grignet-Debrus, C., Bajou, K., Masson, V., Gerard, R.D., Gils, A., Carmeliet, G., Carmeliet, P., Declerck, P.J., Noel, A., and Foidart, J.M. (2002) The pro- or antiangiogenic effect of plasminogen activator inhibitor 1 is dose dependent. *FASEB J* 16, 147-154

[18]   Iqbal, F., Szaraz, P., Librach, M., Gauthier-Fisher, A., and Librach, C.L. (2017) Angiogenic potency evaluation of cell therapy candidates by a novel application of the in vitro aortic ring assay. *Stem Cell Res Ther* 8, 184

[19]   Moulton, K.S., Vakili, K., Zurakowski, D., Soliman, M., Butterfield, C., Sylvin, E., Lo, K.M., Gillies, S., Javaherian, K., and Folkman, J. (2003) Inhibition of plaque neovascularization reduces macrophage accumulation and progression of advanced atherosclerosis. *Proc Natl Acad Sci U S A* 100, 4736-4741

[20]   Aplin, A.C. and Nicosia, R.F. (2019) The plaque-aortic ring assay: a new method to study human atherosclerosis-induced angiogenesis. *Angiogenesis* 22, 421-431

[21]   Aplin, A.C., Gelati, M., Fogel, E., Carnevale, E., and Nicosia, R.F. (2006) Angiopoietin-1 and vascular endothelial growth factor induce expression of inflammatory cytokines before angiogenesis. *Physiol Genomics* 27, 20-28

[22]   Aplin, A.C., Fogel, E., Zorzi, P., and Nicosia, R.F. (2008) The aortic ring model of angiogenesis. *Methods Enzymol* 443, 119-136

[23]   Aplin, A.C., Zhu, W.H., Fogel, E., and Nicosia, R.F. (2009) Vascular regression and survival are differentially regulated by MT1-MMP and TIMPs in the aortic ring model of angiogenesis. *Am J Physiol Cell Physiol* 297, C471-480

[24]   Bonanno, E., Iurlaro, M., Madri, J.A., and Nicosia, R.F. (2000) Type IV collagen modulates angiogenesis and neovessel survival in the rat aorta model. *In Vitro Cell Dev Biol Anim* 36, 336-340

[25]   Brill, A., Dashevsky, O., Rivo, J., Gozal, Y., and Varon, D. (2005) Platelet-derived microparticles induce angiogenesis and stimulate post-ischemic revascularization. *Cardiovasc Res* 67, 30-38

[26]   Burbridge, M.F., Coge, F., Galizzi, J.P., Boutin, J.A., West, D.C., and Tucker, G.C. (2002) The role of the matrix metalloproteinases during in vitro vessel formation. *Angiogenesis* 5, 215-226

[27]   Vaghela, R., Arkudas, A., Steiner, D., Heltmann-Meyer, S., Horch, R.E., and Hessenauer, M. (2022) Vessel grafts for tissue engineering revisited-Vessel segments show location-specific vascularization patterns in ex vivo ring assay. *Microcirculation* 29, e12742

[28]   Chiu, L.L., Montgomery, M., Liang, Y., Liu, H., and Radisic, M. (2012) Perfusable branching microvessel bed for vascularization of engineered tissues. *Proc Natl Acad Sci U S A* 109, E3414-3423

[29]   Margolis, E.A., Cleveland, D.S., Kong, Y.P., Beamish, J.A., Wang, W.Y., Baker, B.M., and Putnam, A.J. (2021) Stromal cell identity modulates vascular morphogenesis in a microvasculature-on-a-chip platform. *Lab Chip* 21, 1150-1163

[30]   Juliar, B.A., Beamish, J.A., Busch, M.E., Cleveland, D.S., Nimmagadda, L., and Putnam, A.J. (2020) Cell-mediated matrix stiffening accompanies capillary morphogenesis in ultra-soft amorphous hydrogels. *Biomaterials* 230, 119634

[31]   Nicosia, R.F. and Ottinetti, A. (1990) Growth of microvessels in serum-free matrix culture of rat aorta. A quantitative assay of angiogenesis in vitro. *Lab Invest* 63, 115-122

[32]   Hata-Sugi, N., Kawase-Kageyama, R., and Wakabayashi, T. (2002) Characterization of rat aortic fragment within collagen gel as an angiogenesis model; capillary morphology may reflect the action mechanisms of angiogenesis inhibitors. *Biol Pharm Bull* 25, 446-451

[33]   Zhu, W.H., Guo, X., Villaschi, S., and Francesco Nicosia, R. (2000) Regulation of vascular growth and regression by matrix metalloproteinases in the rat aorta model of angiogenesis. *Lab Invest* 80, 545-555

[34]   Chun, T.H., Sabeh, F., Ota, I., Murphy, H., McDonagh, K.T., Holmbeck, K., Birkedal-Hansen, H., Allen, E.D., and Weiss, S.J. (2004) MT1-MMP-dependent neovessel formation within the confines of the three-dimensional extracellular matrix. *J Cell Biol* 167, 757-767

[35]   Hiraoka, N., Allen, E., Apel, I.J., Gyetko, M.R., and Weiss, S.J. (1998) Matrix metalloproteinases regulate neovascularization by acting as pericellular fibrinolysins. *Cell* 95, 365-377

[36]   Nguyen, D.H., Stapleton, S.C., Yang, M.T., Cha, S.S., Choi, C.K., Galie, P.A., and Chen, C.S. (2013) Biomimetic model to reconstitute angiogenic sprouting morphogenesis in vitro. *Proc Natl Acad Sci U S A* 110, 6712-6717

[37]   van Duinen, V., Zhu, D., Ramakers, C., van Zonneveld, A.J., Vulto, P., and Hankemeier, T. (2019) Perfused 3D angiogenic sprouting in a high-throughput in vitro platform. *Angiogenesis* 22, 157-165

[38]   Barkefors, I., Le Jan, S., Jakobsson, L., Hejll, E., Carlson, G., Johansson, H., Jarvius, J., Park, J.W., Li Jeon, N., and Kreuger, J. (2008) Endothelial cell migration in stable gradients of vascular endothelial growth factor A and fibroblast growth factor 2: effects on chemotaxis and chemokinesis. *J Biol Chem* 283, 13905-13912

[39]   Friend, N.E., McCoy, A.J., Stegemann, J.P., and Putnam, A.J. (2023) A combination of matrix stiffness and degradability dictate microvascular network assembly and remodeling in cell-laden poly(ethylene glycol) hydrogels. *Biomaterials* 295, 122050

[40]   Juliar, B.A., Keating, M.T., Kong, Y.P., Botvinick, E.L., and Putnam, A.J. (2018) Sprouting angiogenesis induces significant mechanical heterogeneities and ECM stiffening across length scales in fibrin hydrogels. *Biomaterials* 162, 99-108

[41]   Cheng, G., Liao, S., Kit Wong, H., Lacorre, D.A., di Tomaso, E., Au, P., Fukumura, D., Jain, R.K., and Munn, L.L. (2011) Engineered blood vessel networks connect to host vasculature via wrapping-and-tapping anastomosis. *Blood* 118, 4740-4749

[42]   Gelati, M., Aplin, A.C., Fogel, E., Smith, K.D., and Nicosia, R.F. (2008) The angiogenic response of the aorta to injury and inflammatory cytokines requires macrophages. *J Immunol* 181, 5711-5719

[43]   Gui, L., Muto, A., Chan, S.A., Breuer, C.K., and Niklason, L.E. (2009) Development of decellularized human umbilical arteries as small-diameter vascular grafts. *Tissue Eng Part A* 15, 2665-2676

Chapter 5 – Fabrication of Tissue Engineered Vascular Grafts (TEVG) to Enable the Formation of Hierarchically Vascularized Tissue Constructs Suitable for Microsurgical Anastomosis

*This chapter is in preparation for submission as a peer reviewed journal article.

5.1 Introduction

There is a significant unmet clinical need for small diameter tissue engineered vascular grafts (TEVG) for the treatment of various cardiovascular diseases (CVD) including coronary artery bypass grafting (CABG), treatment of peripheral artery disease (PAD), and pediatric or congenital vascular defects. The current clinical standard of care in CABG procedures is the use of an autologous vessel as a graft, most commonly the radial artery, saphenous vein, or internal mammary artery [1-3]. The use of autologous vessels requires a second surgery to obtain the vessel yielding an additional surgical site and is limited by the quality of vessels obtained from the patient. Further, the quality of vessels in patients with CVD is less than that of a young, healthy patient. When autologous vessels are unavailable, synthetic grafts made of Dacron and expanded polytetrafluoroethylene (ePTFE) have been used, however, these grafts have a high rate of thrombosis in small diameter applications (< 6 mm). Further these grafts are highly susceptible to bacterial infection due to the highly porous nature of the material which promotes bacterial adherence, often resulting in graft rejection [4]. These grafts are particularly difficult to use in juvenile patients due to the nonliving nature of the synthetic materials used. An advantage of

TEVG is the ability of grafts to grow with the patient, which is critical for juvenile patients [5]. One group has examined TEVG in a juvenile lamb model and showed evidence of growth and vascular development 6 months post implantation [6].

The tissue engineering community has stepped in to create alternative vascular graft solutions that overcome many limitations of current vascular grafts. There are many TE strategies using synthetic and natural hydrogel materials [7-13], employing cell sheets [14, 15], and decellularizing human and animal tissues to use as arterial conduits [16]. One approach involves culturing vascular stromal cells (either SMC [17] or fibroblasts [18]) on a scaffold material and subjecting to pulsatile flow in a perfusion bioreactor over an extended culture period to enable the deposition of new cell-secreted matrix. Following this culture period, grafts are decellularized, implanted, and subsequently remodeled by host cells, as described in further detail in Chapter 2. The major drawback of this methodology is the lengthy culture period, typically 8 – 9 weeks, required to fabricate these grafts.

In addition to vascular grafting procedures, TEVG are critical for the transplantation of large, engineered tissues and organs. The TE community has focused on engineering capillaries [19-22], mesovessels [23-25], and vascular conduits separately [26, 27], rather than as an integrated vascular hierarchy [28]. A hierarchical vascular blood supply is a critical limitation in the translation of engineered tissues and organs. The development of a hierarchical vascular network containing a graft suitable for surgical anastomosis is a critical next step for the field of tissue engineering. Additionally, scaling meso- and microvascular tissue constructs from *in vitro* and small animal model sizes to human-scale constructs is critical. A hierarchical vascular tissue construct meeting these goals would be transformative for translating engineered tissues and organs to the clinic.

Herein, we describe the fabrication of a three-layer vascular graft mimicking the architecture of native arteries that takes 13 days to fabricate and culture, greatly reducing the culture time required in other strategies. We then incorporated this TEVG with integrated mesovessels and capillaries to fabricate a complete hierarchical vascular tissue construct. The engineered mesovessels were 3.67-fold longer than those developed in Chapter 3, and the overall construct volume was ~20-fold greater than in Chapter 3 and 1.5-fold greater than in Chapter 4. To our knowledge, only one similar fibrin-based hierarchical construct has been previously engineered [29]. Our work builds upon this prior report by engineering a higher density of interconnected capillaries within the surrounding bulk hydrogel, seeding of arteriole-scale channels to fabricate cellularized mesovessels, and a three-layer macrovessel design fabricated from lower density fibrin suitable for engineering a vasa vasorum while maintaining the mechanical properties required for surgical anastomosis.

5.2 Materials and Methods

5.2.1 Cell culture

Human umbilical vein endothelial cells (EC) were isolated from fresh cords obtained from Mott's Children's Hospital via an IRB-exempt protocol. EC were cultured in fully supplemented endothelial growth medium-2 (EGM-2; Lonza, Walkersville, MD) supplemented with 1x antibiotic-antimycotic (Anti-Anti; Gibco) and used between passage 5 and 7. Lung fibroblasts (LF; Lonza), were cultured in Dulbecco's modified eagle medium (DMEM; Gibco, Waltham, MA) supplemented with 10 % fetal bovine serum (FBS; Gibco) and 1x Anti-Anti and used between passage 8 and 15. Human aortic smooth muscle cells (SMC; ThermoFisher, Waltham, MA) were cultured in human vascular smooth muscle cell basal medium (ThermoFisher) supplemented with

smooth muscle growth supplement (ThermoFisher) and used between passage 3 and 9. All cells were cultured at 37 °C and 5% CO_2 with medium exchanges every other day.

5.2.2 Tissue engineered vascular graft (TEVG) fabrication

TEVG were fabricated by embedding various cell types in fibrin hydrogels and integrating them in discrete layers. Single-layer grafts composed of a tunica adventitia mimicking layer contained co-cultured LF and EC. Two-layer grafts composed of a tunica media mimicking layer and a tunica adventitia mimicking layer were fabricated in a two-step process, where the media layer contained SMC and the adventitia layer contained both LF and EC. Each layer was fabricated via an annular molding process (Fig. 5.1). The final hydrogel contained 5 or 10 mg/mL fibrin, 1 U/mL thrombin, 10% FBS, and a cell density of 1 M/mL, where co-cultured cells were incorporated in a 1:1 ratio. Multiple configurations of TEVG were explored in this study (Fig. 5.2).

To fabricate single layer grafts, a hydrogel-cell mixture was injected into the annular mold and polymerized for 35 minutes. After gelation, the outer glass housing and polydimethylsiloxane (PDMS) base were removed, and the hydrogel was cultured in a bioreaction tube (ThermoFisher) with appropriate medium (Fig. 5.1A, B). In cases of off mandrel culture, the mandrel was also removed. Prior to gelation, the annular mold components were pretreated with 0.5% Pluronic F-68 (Gibco) in 1x phosphate buffered saline (PBS; Gibco) for 1 hour immediately pre-fabrication. The annular mold components were custom made from McMaster Carr.

To fabricate two-layer grafts, the same process was followed, and the inner layer was cultured for 3 days prior to fabricating the second layer to allow for radial compaction of the graft. To fabricate the second layer, the mandrel with a tunica media mimicking layer around it was inserted back into the PDMS base and outer glass housing before a second hydrogel-cell mixture

was added around it (Fig. 5.1C, D). The two-layer graft was removed from the annular mold following the same steps. The inner lumen of vascular grafts (either one- or two-layer) were seeded with a 2 M/mL suspension of EC to fabricate a tunica intima layer (Fig. 5.1E). This protocol was adapted from another study seeding the lumens of natural hydrogel material-based TEVG, specifically collagen-based TEVG [9]. Briefly, 24 well plates were coated with Pluronic F-68 for 1 hour prior to seeding. Using a stereoscope to visualize the lumen, the EC suspension was inserted into the lumen. This process was repeated from the other end of the vessel. The vessel was suspended in the EC suspension for 1 hour in a shaking incubator. The vessel was transferred to another Pluronic F-68 coated well in a 12 well plate with fresh media and cultured free floating for 3 days to allow cells to adhere to and spread within the lumen.

5.2.3 Fabricating PDMS molds

Molds for engineering three scale vascular hierarchies were fabricated from PDMS. PDMS base and crosslinker were mixed at a 10:1 ratio and poured into 40 x 22 x 20 mm Epredia Peel-a-Way disposable molds (ThermoFisher) with 22 G or 23 G needles inserted through the 22 mm edge. The molds were incubated in a 70 °C oven for at least 4 hours (up to overnight) to cure the PDMS. After curing, the needles were pulled out and the PDMS was detached from the Peel-a-Way mold. A hydrogel chamber, meso-channel seeding wells, and macrovessel holding wells were cut out with disposable biopsy punches and a scalpel. The hydrogel chamber was formed from 2 overlapping 12 mm punches and 4 seeding wells were fabricated from 6 mm punches. The final mold was rinsed with 100% isopropyl alcohol (IPA), 100% ethanol, and air dried before bonding to glass slides with a plasma etcher.

133
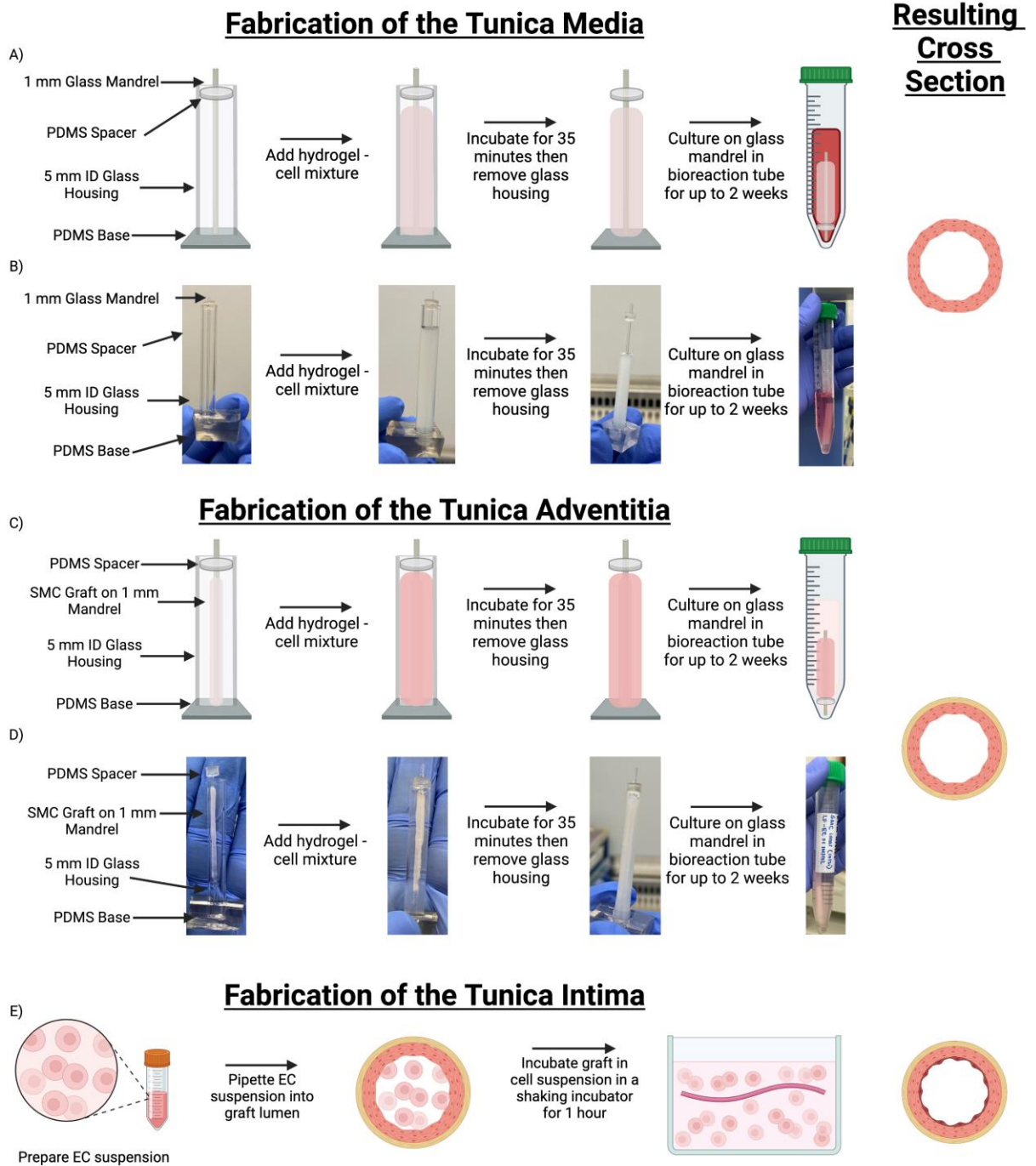
Figure 5.1: Fabrication process for 3-layer TEVG. *(A-B) Fabrication of the tunica media layer composed of fibrin and SMC. (A) Schematic. (B) Physical Images. (C-D) Fabrication of the tunica adventitia layer composed of fibrin, LF, and EC. (C) Schematic. (D) Physical Images. (E) Schematic of the seeding process for fabrication of the tunica intima composed of EC.*
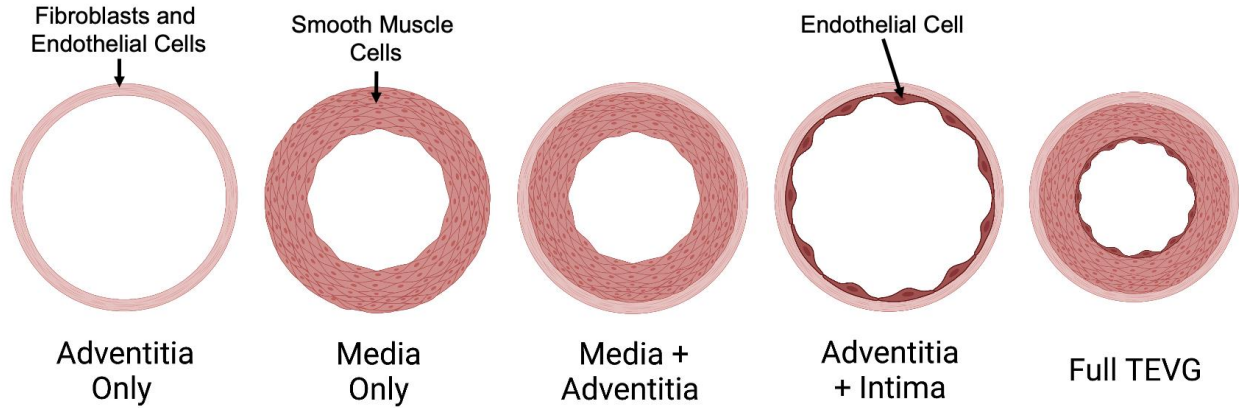
Figure 5.2: TEVG configurations used throughout the study mimicking the tunica intima, tunica media, and tunica adventitia layers of native arteries*. Single layer adventitia (Figs. 5.4 and 5.5) and media only (Fig. 5.6) grafts, dual layer media + adventitia (Figs. 5.6 and 5.7) and adventitia + intima (Fig. 5.8), and complete three-layer graft composed of intima, media, and adventitia layers (Fig. 5.9).*

5.2.4 Engineering multiscale vascular hierarchies

TEVG were embedded in 5 mg/mL fibrin hydrogels (as described above), either cellular or acellular, to assess sprouting from the vasa vasorum within the TEVG and interconnection to capillaries within the surrounding bulk hydrogel. The vessel ends were exposed to allow perfusion of the constructs at culture endpoints and to facilitate surgical anastomosis.

To fabricate three-scale vascular hierarchies, 2% gelatin coated 290 μm acupuncture needles were inserted into the PDMS mold, a TEVG was placed within the mold between two acupuncture needles, and a cellular hydrogel was cast around the needles and graft and allowed to polymerize for 35 minutes (Fig. 5.3). After gelation and swelling, needles were removed leaving behind two empty cavities subsequently seeded with EC to form mesovessels. The entire multiscale, hierarchical vascular construct was cultured with media exchanges every other day for up to two weeks.
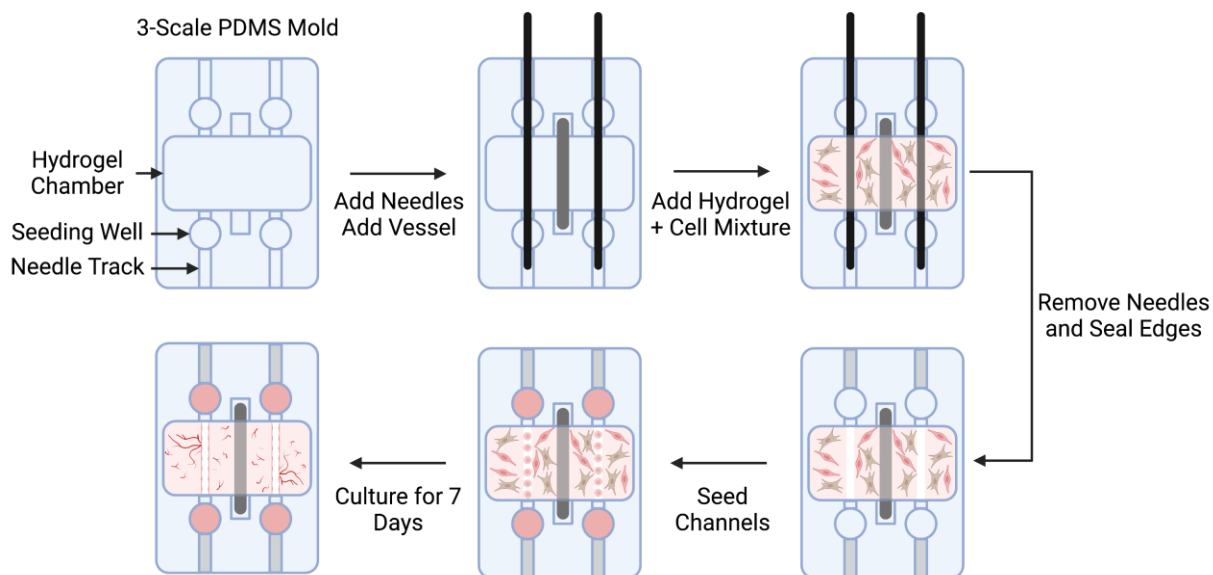
Figure 5.3: Fabrication of three-scale vascular hierarchies using custom PDMS molds. *Schematic detailing the fabrication process for three-scale vascular hierarchies composed of a microvascular network, two mesovessels, and a three-layer TEVG.*

5.2.5 Immunofluorescence staining and imaging

TEVG and multiscale gels were fixed on the last day of culture with Zinc Formalin Fixative (Z-fix; Anatech; Battle Creek, MI) for 15 minutes at room temperature and washed 3 times for 5 minutes each with tris-buffered saline (TBS). Fixed gels were stained with 4', 6-diamidino-2-phenylindol (DAPI; 1 ug/mL; Fisher Scientific), AlexaFluor 488 Phalloidin (1:200 dilution; Fisher Scientific), and rhodamine-conjugated Ulex europaeus Agglutinin I (UEA; 1:200 dilution; Vector Labs). Staining dilutions were made in TBS and samples were incubated with staining solution overnight at 4°C. Following staining, samples were washed 3x with TBS for at least 24 hours.

Select samples were further stained for pericyte markers alpha smooth muscle actin (αSMA; Sigma, A2547, mouse IgG$_{2a}$ isotype, 1:200 dilution), neuron-glial antigen 2 (NG2; abcam, ab255811, rabbit IgG isotype,1:200 dilution), and platelet derived growth factor receptor

beta (PDGFRβ; Sigma, HPA028499, 1:100 dilution). Samples were permeabilized with 0.5% Triton X-100 (Fisher Scientific, Waltham, MA) in TBS for 1 hour at 4°C and blocked in 2% bovine serum albumin (BSA; Sigma) in 0.1% Triton X-100 in TBS (TBS-T) overnight at 4°C. After blocking, samples were stained with primary antibodies for each pericyte marker overnight at 4°C. Samples were washed overnight in TBS-T at 4°C prior to secondary antibody staining. Samples were stained with the corresponding secondary antibody, either Alexa Fluor 488 conjugated secondary antibody (Invitrogen, A11001, goat-*anti*-mouse IgG$_{H+L}$, 1:200 dilution) or Alexa Fluor 488 conjugated secondary antibody (Invitrogen, A11008, goat-*anti*-rabbit IgG$_{H+L}$, 1:500 dilution) overnight at 4°C. Samples were washed overnight 4°C prior to imaging. All antibody dilutions were made in 1% BSA in TBS-T.

Samples were imaged on an Olympus IX81 outfitted with a confocal disc spinning unit (DSU; Olympus America, Center Valley, PA) and Metamorph software (Molecular Devices, Sunnyvale, CA). Low magnification confocal z-stacks (300 μm, 7 slices) were obtained at 4x magnification. Higher magnification confocal z-stacks (150 μm, 7 slices or 90 μm, 7 slices) were obtained at 10x magnification.

5.3 Results

5.3.1 Culture conditions influence the formation of a vasa vasorum in tissue engineered tunica adventitia

Single layer vascular grafts containing LF and EC in fibrin hydrogels mimicking the tunica adventitia fabricated via an annular molding process were cultured in suspension in bioreaction tubes. Suspension culture yielded significant compaction of the vascular grafts both axially and

137

radially. We investigated two densities of fibrin hydrogels to support the formation of an adventitial layer. Lower density 5 mg/mL hydrogels compacted significantly in the first day of culture to around half of their original size, while higher density 10 mg/mL grafts exhibited very minimal compaction (Fig. 5.4A). Compaction continued throughout the culture period (Fig. 5.4A). The substantially compacted 5 mg/mL gels supported very little vessel formation after 14 days of culture (Fig. 5.4B, C, left), likely due to the remodeling of the fibrin yielding a hydrogel with matrix biophysical properties not conducive to vessel formation (i.e., too dense and/or too stiff). In higher density fibrin hydrogels that compacted more slowly, vessel formation within the graft was observed (Fig. 5.4B, C, right). In addition to vasa vasorum-like vessel formation, we also
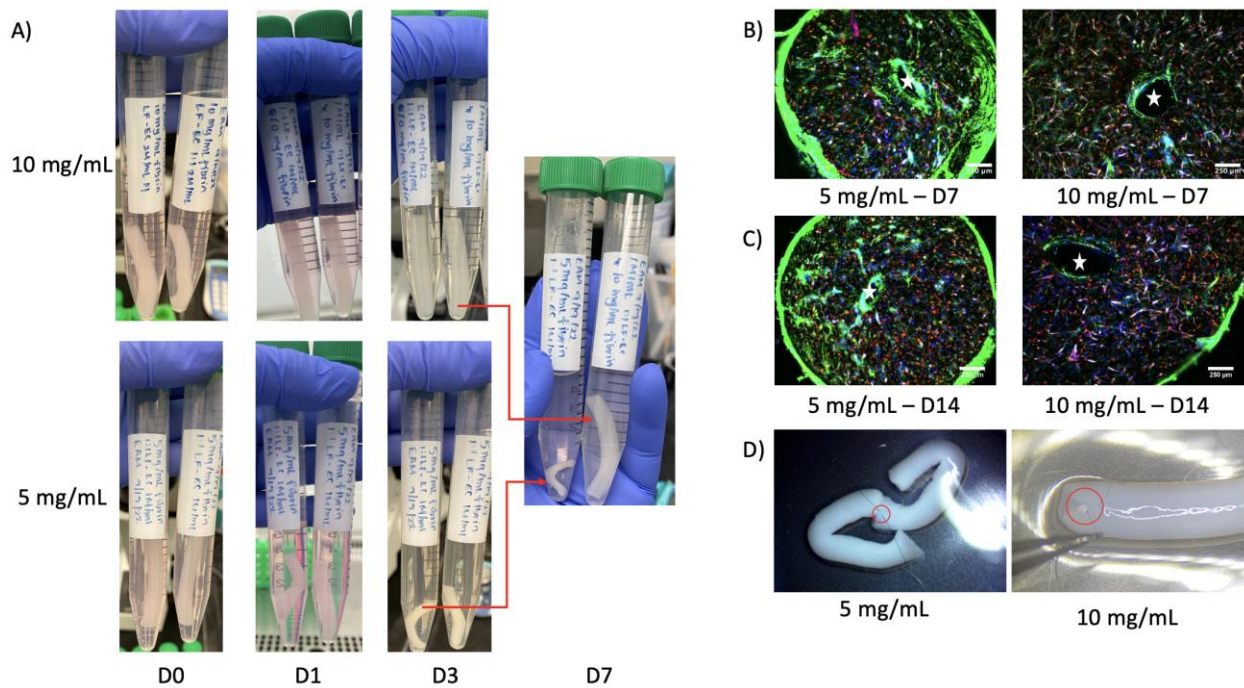
Figure 5.4: Free-floating suspension culture of single-layer adventitia grafts is not suitable for translatable TEVG. *(A) Macroscopic images of 10 mg/mL (top) and 5 mg/mL (bottom) grafts in culture over a 7-day period showing compaction of the graft structure. (B, C) Immunofluorescent images of graft after (B) 7 days and (C) 14 days fabricated with 5 mg/mL (left) and 10 mg/mL (right) fibrin. (D) Representative images of suture placement in graft wall for 5 mg/mL (left) and 10 mg/mL (right) grafts. Red circles show the suture locations. Red – EC, Green – actin, Blue – nuclei.*

observed fibroblasts formed a sheath around the abluminal side of the graft in both fibrin densities (Fig. 5.4B, C, green). We next attempted to suture these grafts as our goal was to fabricate a vascular hierarchy suitable for surgical transplantation. The suturability of these grafts correlated with the compaction: grafts fabricated from lower density fibrin with higher compaction yielded grafts strong enough to withstand the placement of a single suture (Fig. 5.4D, 5 mg/mL). In contrast, higher density grafts that did not compact and remodel did not withstand the placement of a suture and ripped as the suture was pulled through (Fig. 5.4D, 10 mg/mL).

To minimize radial compaction of the lumen, second generation grafts were cultured on-mandrel rather than in suspension. On-mandrel culture yielded a more organized radial compaction of graft thickness (Fig. 5.5A) but the presence of the mandrel prevented complete lumen closure. We observed minimal, if any, axial compaction despite mandrels being pre-treated with Pluronic F-68. For grafts fabricated using the lower density 5 mg/mL fibrin hydrogels and cultured on-madnrel, this decreased compaction yielded vessel formation within the graft resembling a vasa vasorum typically found within the adventitia of large arteries. Cross sectional images of tissue rings showed evidence of small vascular segments and the presence of a fibroblast sheath around the outside of the graft (Fig. 5.5B). Longitudinal images showed long capillaries oriented parallel to the lumen (Fig. 5.5C, Fig. S5.2). The aligned vasculature persisted to day 14 (Fig. S5.2). The LF displayed a pericyte-like phenotype with positive expression of αSMA, NG2, and PDGFR-β (Fig. 5.5E). This expression was present within the sheath of fibroblasts and in some cases localized around vessels within the graft.

To assess if capillaries within the adventitia could sprout into a surrounding hydrogel, we embedded vascular grafts within acellular fibrin hydrogels. We observed the invasion of EC

(UEA-positive cells) as multicellular vessel-like structures and LF (UEA-negative nuclei) as single

cells that reached further distances into the hydrogel (Fig. 5.5D).
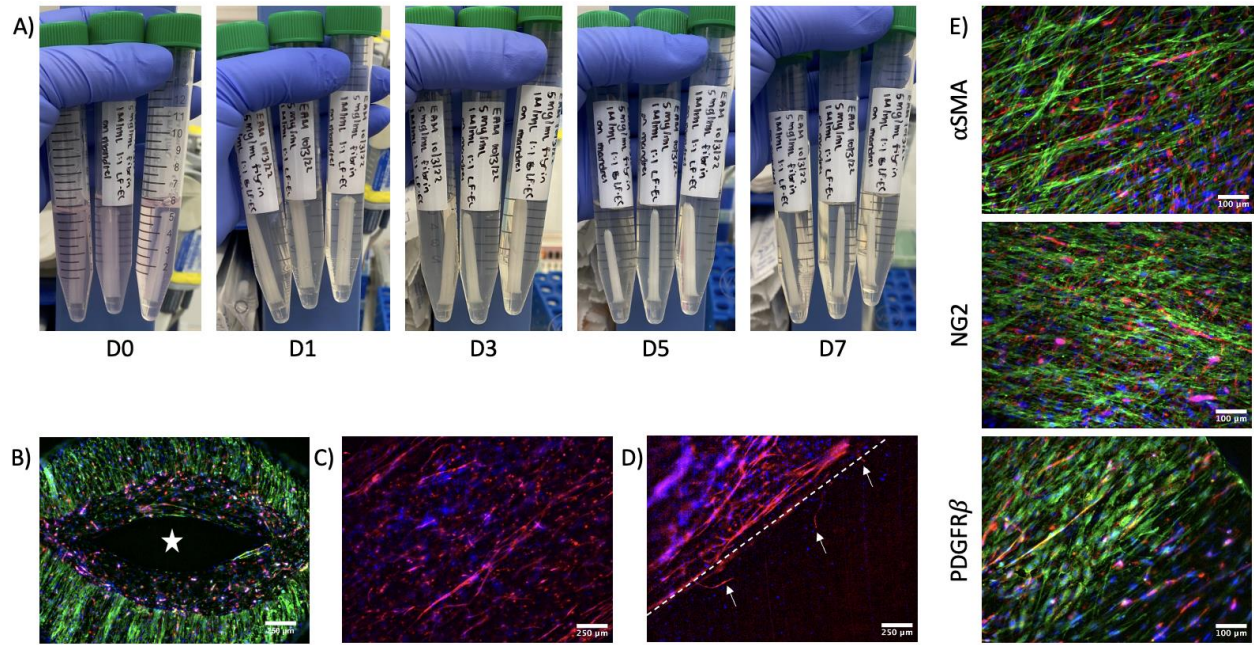
Figure 5.5: On-mandrel TEVG culture limits compaction, yields vasa vasorum formation, and induces a pericyte phenotype of supporting fibroblasts. (A) Macroscopic images of grafts in culture over a 7-day culture period showing limited axial compaction and some radial compaction of wall thickness. (B) Fluorescent image of a tissue ring showing small vessel segments and a distinct fibroblast sheath around the outside of the graft. (C-D) Fluorescent images of grafts embedded in acellular fibrin imaged longitudinally showing (C) capillaries aligned in the direction of the lumen and (D) sprouting into the surrounding hydrogel (white arrows). White dashed line denotes the boundary between the graft (upper left) and the hydrogel (lower right). White arrows indicate sprouted vessels. (E) fluorescent images showing that fibroblasts in the graft take on a pericyte like phenotype as shown by expression of αSMA (top), NG2 (middle) and PDGFRβ (bottom). Red – EC, Green – actin (B) or pericyte markers (E), Blue – nuclei.

5.3.2 Two-layer vascular grafts maintained discrete layers, displayed increased mechanical strength, and sprouted into cellular hydrogels

The tunica media was fabricated from 5 mg/mL fibrin containing SMC to mimic the thick

muscular layer of arteries via an annular molding process as described above. The SMC induced

heterogeneous radial compaction of the vessel wall with some regions of the graft reaching a

140

thinner final thickness than others (Fig. 5.6A, dashed lines). Despite this, SMC were well spread within the entire graft and exhibited two distinct orientations within the layer (Fig. 5.6B). Adjacent to the lumen, the SMC oriented circumferentially around the mandrel, characteristic of native tunica media morphology, while the SMC toward the abluminal edge, closer to the media source during culture, oriented perpendicular to the lumen (Fig. 5.6B). A longitudinal view shows these SMC at the abluminal edge form a sheath of cells around the outside of the graft oriented in the direction of the lumen as observed with adventitia only grafts previously (Fig. 5.6C). Further, these SMC were characterized by αSMA, a known marker of vascular smooth muscle cells that plays an important role in mechanical force generation (Fig. 5.6D) [30].

When integrated with a tunica adventitia fabricated around the tunica media, the two layers maintained their discrete locations as shown by the absence of UEA-positive cells in the inner layer (i.e., the tunica media) (Fig. 5.6E, F). The SMC appeared to lose the alignment observed in media only grafts and began to spread in a less distinct morphology (Fig. 5.6F, left). In some cases, the SMC appeared to cluster into dense regions of cells within the inner media layer (Fig. 5.6F, right, dashed line). These two-layer grafts showed increased mechanical strength and permitted the placement of two sutures to connect the graft to an explanted rat femoral artery. The grafts withstood the significant manipulation required for the partial surgical anastomosis, only sustaining minimal damage to the outer layer (Fig. 5.6G). The lumen of the graft could be stretched to permit suturing without damaging the vessel (Fig. 5.6G, top). Following the placement of two sutures, the lumen of the graft and the artery remained patent (Fig. 5.6G, middle) and the sutures could be pulled to show mechanical integrity and stability of the anastomosis points without ripping through the graft or the vessel (Fig. 5.6G, bottom). Despite the difference in overall size, the lumens of the graft and rat artery are of comparable inner diameter (~1 mm). Compared to

adventitia only grafts, two-layer grafts were significantly easier to handle during microsurgical

anastomosis and showed notably less damage to the graft.
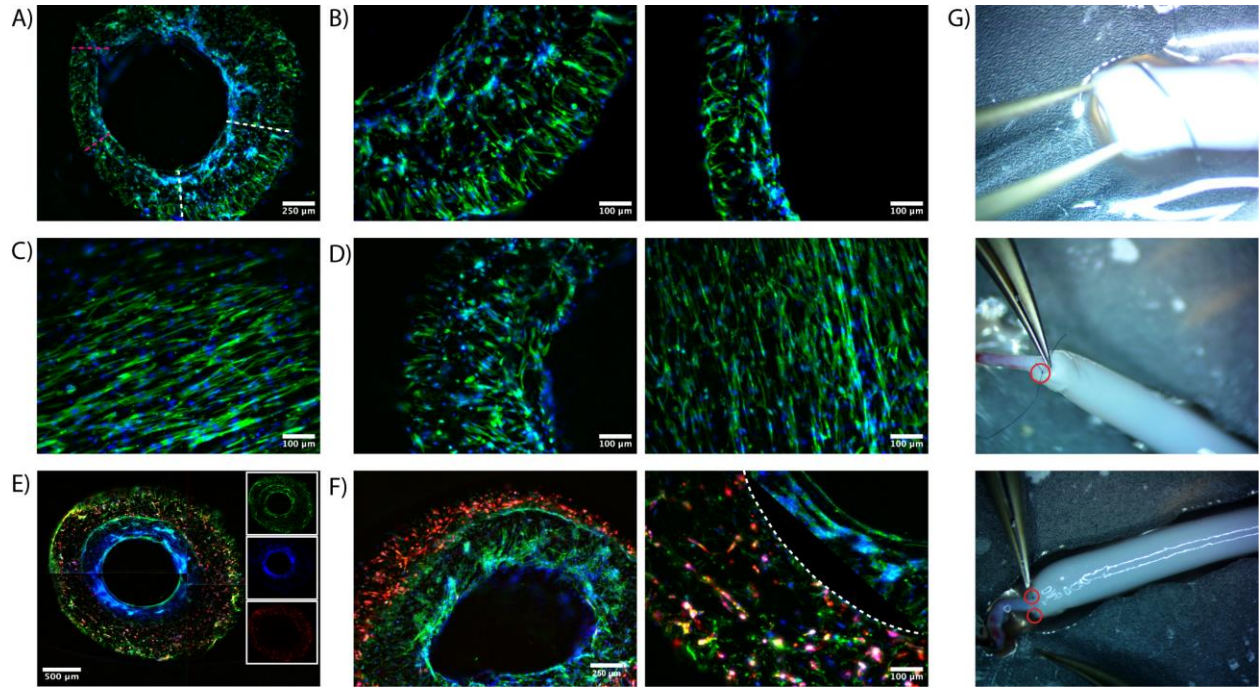
Figure 5.6: SMC display spread morphology in various TEVG configurations and improve mechanical properties of TEVG. (A-D) Immunofluorescent images of SMC only TEVG. (A, B) Cross sectional images show distinct morphologies of SMC within fibrin grafts. Regions between dashed lines in (A) shown in (B), white (left), magenta (right). (C) Abluminal view of graft shows SMC oriented in the direction of the lumen in a highly organized manner. (D) Immunofluorescent αSMA staining of SMC only TEVG in cross section (left) and longitudinal section (right). (E-F) Immunofluorescent images of dual layer TEVG. (E) Whole graft scan of multi-layer graft showing distinct layers. (F) Magnified views showing new SMC morphology in the media and EC present only in the adventitia. Dashed line demarcates the interface between the two layers. (G) Surgical anastomosis of multi-layer TEVG to explanted rat femoral artery. Red circles indicate sutures. Red – EC, Green – actin (A-C, E-F) or αSMA (D), Blue – nuclei.

Two-layer vascular grafts were embedded within cellular fibrin hydrogels to fabricate two-

scale vascular hierarchies composed of a vascular graft and a surrounding capillary network (Fig.

5.7). LF and EC within the bulk hydrogel self-assembled into capillaries over a 7-day culture

period (Fig. 5.7A, middle top, blue inset) as capillaries within the adventitia layer (Fig. 5.7A right,

yellow inset) of the vascular graft sprouted out into the surrounding hydrogel (Fig. 5.7A, middle

142

bottom, green inset). We observed that the duration of culture of the adventitia layer, prior to embedding, impacted the sprouting potential of vascular grafts into the bulk hydrogel. Adventitia cultured for three days showed primitive vessel formation within the graft and only minimal, if any, points of sprouting into the hydrogel (Fig. 5.7B). By contrast, adventitia cultured for seven days showed both more substantial vessel formation within the graft and sprouting into the surrounding hydrogel (Fig. 5.7C). The presence or lack of sprouting from the adventitia layer into the hydrogel was consistent along the entire length of the TEVG.

5.3.3 Fabrication of a tunica intima

We next fabricated a tunica intima by seeding the inner lumen of single layer adventitia only vascular grafts. Three days after seeding the lumen, EC had spread and formed a confluent monolayer on the inner lumenal surface of the graft (Fig. 5.8A). The seeding process caused some compaction of the grafts, consistent with suspension culture as described previously. The compaction was minimal, and grafts maintained an open lumen. Nuclei were present along the entire curved inner surface of the graft lumen (Fig. 5.8B, C). Further, the grafts were cultured in an EC suspension during the seeding process which may have led to adherence of EC to the outside of the graft. Though the intention was to seed the inner lumen and allow flow of EC into the lumen of the graft, EC adherence to the abluminal side was not a concern as EC were present within the adventitial layer of the graft already. Further, these additional EC may aid in sprouting from the graft into the surrounding hydrogel when embedded to fabricate three-scale hierarchies.
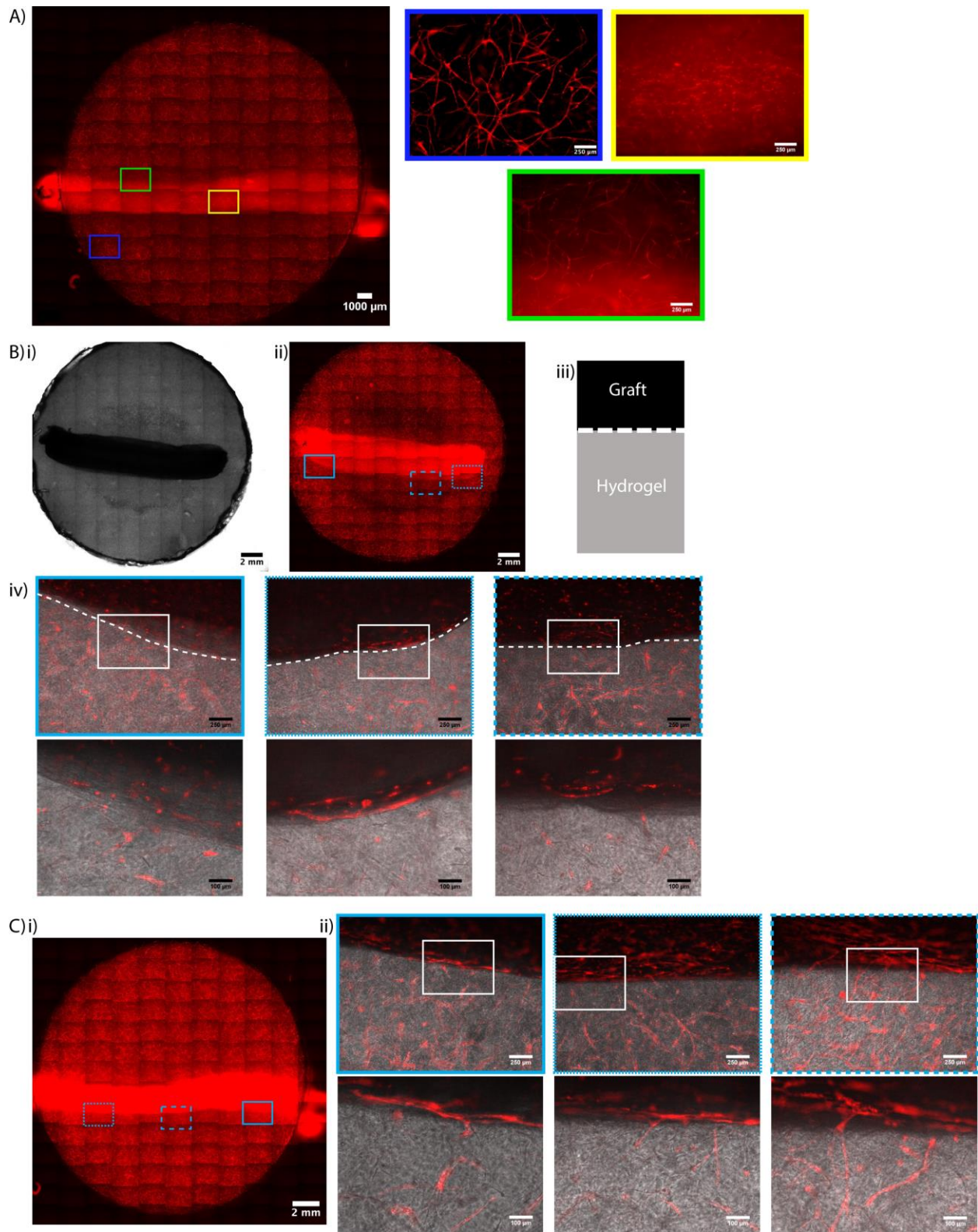
Figure 5.7: Two-layer TEVG sprout into surrounding hydrogels containing microvascular networks. (A) Whole construct scan of two-scale hierarchical vascular construct. TEVG is embedded within the center of the construct. Blue box: surrounding capillary network. Green box: interface between graft and

144

surrounding network. Yellow box: vessels within the graft comprising a vasa vasorum. Phase contrast and fluorescent images of vascular grafts sprouting into the surrounding matrix after (B) 3 days of adventitia culture or (C) 7 days of adventitia culture. (Bi) Phase contrast whole construct scan. (Bii) Fluorescent whole construct scan. (Biii) schematic of phase images showing graft as dark black regions and surrounding bulk hydrogel as light grey regions. (Biv) Zoomed in regions from blue boxes in (Bii), white boxes are further zoomed in images. (Ci) Fluorescent whole construct scan. (Cii) Zoomed in regions from blue boxes in (Ci), white boxes are further zoomed in images.

5.3.4 Engineering complete, 3-scale vascular hierarchies

Finally, we embedded vascular grafts within PDMS molds to support the fabrication of a complete, 3-scale vascular hierarchy (Fig. 5.9). TEVG were embedded in cellular fibrin hydrogels between two acupuncture needles used to template the mesoscale channels as in Chapters 3 and 4. Following removal of the needles after gelation, the resulting tubular voids were seeded with EC to fabricate mesovessels, while the EC and LF within the bulk hydrogel self-assembled into capillary networks. EC within the mesovessels sprouted out and inosculated with capillaries in the bulk yielding perfusion of the mesovessels and interconnected capillaries (Fig. 5.9C). Capillaries within the adventitia layer sprouted into the surrounding hydrogel as previously observed in Figure 5.7

5.4 Discussion

The focus of this study was two-fold: to first create a TEVG suitable for surgical anastomosis and then engineer a three-scale vascular hierarchy composed of the TEVG, two mesovessels, and a self-assembled network of capillaries. Significant progress has been made in the advancement of TEVG to the clinic [17, 31-34], but considerably less progress has been made on advancing integrated hierarchical networks. Here we report the fabrication of a three-layer vascular graft closely mimicking the three layers of native arteries (tunica intima, tunica media,

and tunica adventitia), a new technique for generating aligned microvasculature within fibrin-based tissue constructs, and the engineering of a complete vascular hierarchy composed of all three vascular length scales.
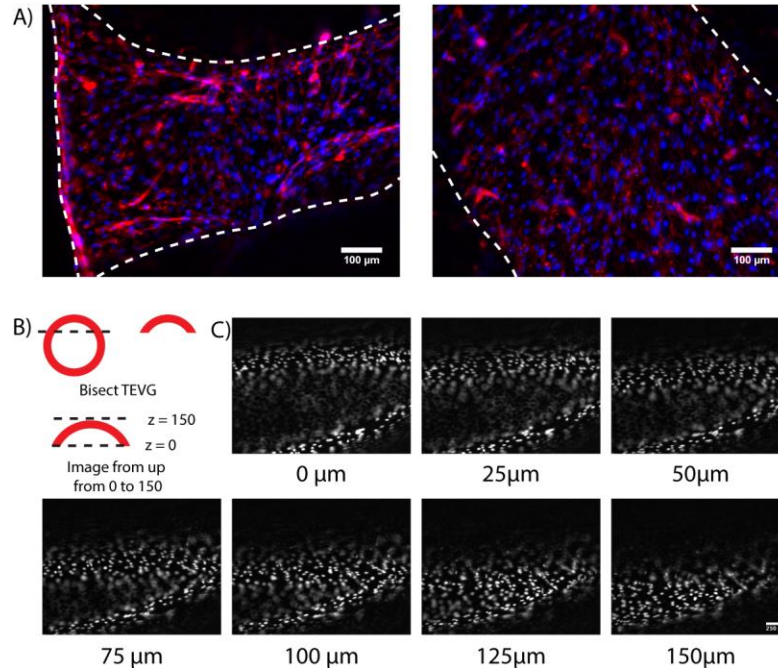
Figure 5.8: Lumenal seeding procedure results in confluent EC monolayer yielding an intact tunica intima. *(A) fluorescent images of tunica intima showing coverage of the graft with EC monolayers and some vessels in the adventitia behind the monolayer. Dashed lines indicate the boundary of the graft. Red – hEC, blue – nuclei. (B) Schematic of imaging process. (C) Progression of nuclei (white) along the curved lumen of a TEVG seeded with EC. Nuclear staining shows confluent endothelium across the entire curved surface.*

Initial efforts in the field to create TEVG focusing on recreating the medial and intimal layers of small-diameter arteries using cell + scaffold approaches. Remarkably, recent commercialization efforts focused on acellular, single-layer grafts have shown promising results in both preclinical and clinical models by demonstrating that decellularized TEVG can be remodeled and populated with host cells following transplantation *in vivo* to eventually develop functional adventitial and intimal layers [17, 18]. These decellularized grafts are making significant strides in the advancement of vascular therapies to the clinic and are already providing significant benefit to small numbers of patients. However, we envision an additional potential

146
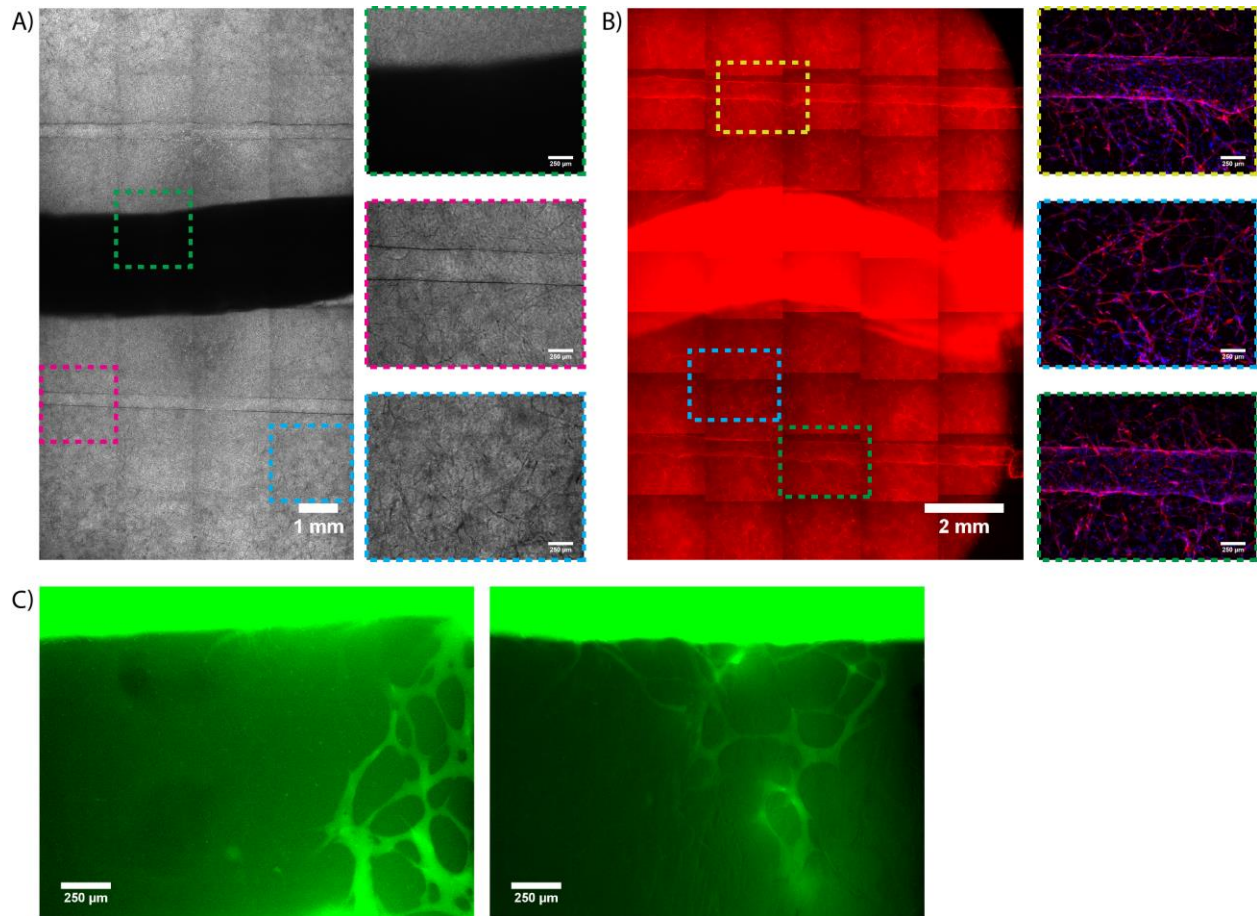
Figure 5.9: TEVG support the formation of three-scale vascular hierarchies that are perfusable across two length scales. *(A) Phase contrast scan slide image of a three-scale vascular hierarchy containing a TEVG (green box), two mesovessels (pink box), and a capillary network (blue box). (B) Fluorescent scan slide. Image of a three-scale vascular hierarchy containing a TEVG (middle, bright red), two mesovessels (green and yellow boxes) and a capillary network (blue box). (C) Fluorescent dextran perfusion from mesovessels (top) into interconnected capillary networks within the three-scale hierarchy.*

application of TEVG will be as a component of a multiscale hierarchical vascular construct, one in which the TEVG can serve as the macroscale vessel. In this study, we report the development of a TEVG embedded within a fibrin hydrogel capable of undergoing angiogenic sprouting from the adventitial layer and thereby initiating inosculation with a capillary network within the surrounding tissue mimic (Figs. 5.7 and 5.9). Although flow through the lumen of a native artery would not be expected to go through the vascular wall and into the vasa vasorum in the adventitial

layers, it is possible that such a non-physiologic connection may be perfusable within our engineered network. We hypothesize a subset of the capillaries would undergo flow-mediated adaptation and arteriogenesis, especially once the primitive hierarchy is implanted *in vivo* and further remodeled both cellularly and biomechanically. Future work will build upon the prototypes developed here to evaluate this remodeling hypothesis by surgically anastomosing the construct in the femoral circulation of rodents and evaluating their functionality.

We first focused on engineering single-layer adventitial grafts to assess microvessel formation within the graft wall to yield a vasa vasorum towards engineering integrated vascular hierarchies. We then sought to transition this graft towards translational application in an animal model. This endeavor was twofold: increase suturability of the graft and decrease the risk of thrombus formation upon implantation. To improve mechanical stability of the graft to better facilitate surgical anastomosis we incorporated a SMC-based medial layer composed of SMC in fibrin. The addition of the SMC-based medial layer successfully improved the ability to suture the grafts (Fig. 5.6G vs. Fig. 5.4D). Finally, to prevent thrombosis upon initial implantation into an animal model we fabricated an intimal layer composed of an EC lining on the interior surface of the vessel. Another method to prime TEVG prior to implantation and improve the mechanical properties of the graft is pulsatile perfusion culture in a bioreactor. Though some groups have had success implanting grafts cultured in static conditions [8, 9], perfusion and/or cyclic stretch bioreactor culture has shown great promise [35-37]. Perfusion culture was outside the scope of this study but could be a future direction to prime grafts for exposure to the hemodynamic forces of the arterial circulation.

The three-layer TEVG developed here further improves upon a similar prior study embedding SMC, EC, and SC within fibrin hydrogels for vascular graft fabrication. Helms, et al.

148

previously reported a mechanically stable three-layer TEVG capable of withstanding extended perfusion culture [7]. However, cells within the graft, particularly the medial layer, did not spread and remodel the tissue. In their study, SMC within the medial layer stained positively for αSMA, but the cell morphology was rounded rather than spread and cells were individually isolated within the tissue rather than clustered. Herein, we show two distinct spreading morphologies of SMC arranged circumferentially around the lumen or aligned perpendicular to the lumen. This distinction is likely due to the composition of the matrix. We used a hydrogel with $1/5^{th}$ the density of fibrin compared to Helms, et al. allowing for significantly more remodeling of the matrix by embedded cells and cell-cell communication. Fibrin degradation has been linked to increased SMC proliferation and matrix deposition in fibrin-based vascular grafts [38], suggesting that for optimal fabrication of tunica media equivalents, lower density fibrin may be more appropriate.

Further, Helms, et al. reported that pulsatile perfusion culture was required for EC in the adventitia layer to form aligned microvasculature. Their group published a follow-up study investigating how longitudinal tension, pulsatile perfusion with cyclic stretch, and tension + pulsatile perfusion influence the alignment of microvasculature in the adventitial layer of a TEVG [39]. They found that tension and tension + pulsatile perfusion yielded significantly more alignment than pulsatile perfusion alone or static controls. Further the combined regime yielded the greatest alignment of microvessels. Another group investigated the alignment of microvessels in fibrin gels and found that hydrogel compaction and interstitial flow were both critical for vessel alignment [40]. Other groups have reported the critical need for fluid shear stress in endothelial monolayer alignment [41-43] and the need for flow-induced alignment in reorganization of the vascular plexus [44]. Here we report a new phenomenon that microvessels are capable of aligning in the absence of fluid flow-induced shear stress. Microvessels in the adventitial layer of our grafts

aligned as early as 3 days and continued to form an aligned capillary network by 14 days (Fig. S5.2), even in the absence of flow. The cells' ability to spread within the matrix and form capillaries aligned in the lumenal direction was critical for sprouting into surrounding hydrogels and integrating with capillary networks, as shown by the lack of sprouting in grafts with shorter adventitia culture periods (Fig. 5.8 B vs. C). Our method yields aligned microvasculature through the use of a simple static culture system that relies only on hydrogel compaction against the fixed surface of the mandrel. These vascular grafts could be cut off the mandrel and unrolled into millimeter-scale aligned microvascular tissue constructs. Such a construct could be instrumental in engineering functional tissues such as myocardium or skeletal muscle that require aligned vasculature for proper functioning and maintenance of parenchymal muscle cells [45].

Another technique to fabricate hierarchical vasculature that is gaining traction in the field is 3D printing [46-48]. One recent study quite similar to ours integrated macrovessels and self-assembled capillaries within a 3D printed collagen gel. The macrovessel was fabricated from a PLLA-PLGA polymer containing holes regularly spaced along the length to allow integration between the lumen of the macrovessel and the capillaries within the surrounding hydrogel [47]. Overall, this yielded a macro- and microvascular hierarchy suitable for surgical anastomosis with the aid of polymer cuffs. Our work presented herein yields a similar result, but with a living TEVG as the macrovessel rather than a polymer-based acellular graft with limited compliance. Other techniques have fabricated meso- and microvascular hierarchical networks in cell-dense tissues more replicative of native tissue cell density [49, 50]. Through the use of cell-dense organoids [49] or dense cell sheets [50], hierarchical vascular networks have been embedded within millimeter-scale tissues containing 100-200 million cells. Though this is beyond the scope of the present

study, combining hierarchical vascular networks with cell-dense tissues will be critical for the development of engineered tissues and organs for transplant.

The use of TEVG in this study as opposed to explanted murine vessels used in Chapter 4, represents a step toward clinical translation by creating vascular hierarchies without the need to harvest an autologous vessel. Further, the incorporation of mesovessels yields a vascular hierarchy spanning from arteries all the way down to the capillary scale, with perfusion of the hierarchy across two out of three length scales. Prior work has shown integration of the capillaries and mesovessels (Chapter 3) and current work showed integration of the capillaries and TEVG and capillaries and mesovessels. Overall, this research yielded a complete hierarchical vascular tissue construct that brings the field one step closer to translating hierarchical vasculature to the clinic.

5.5 Supplementary Figures
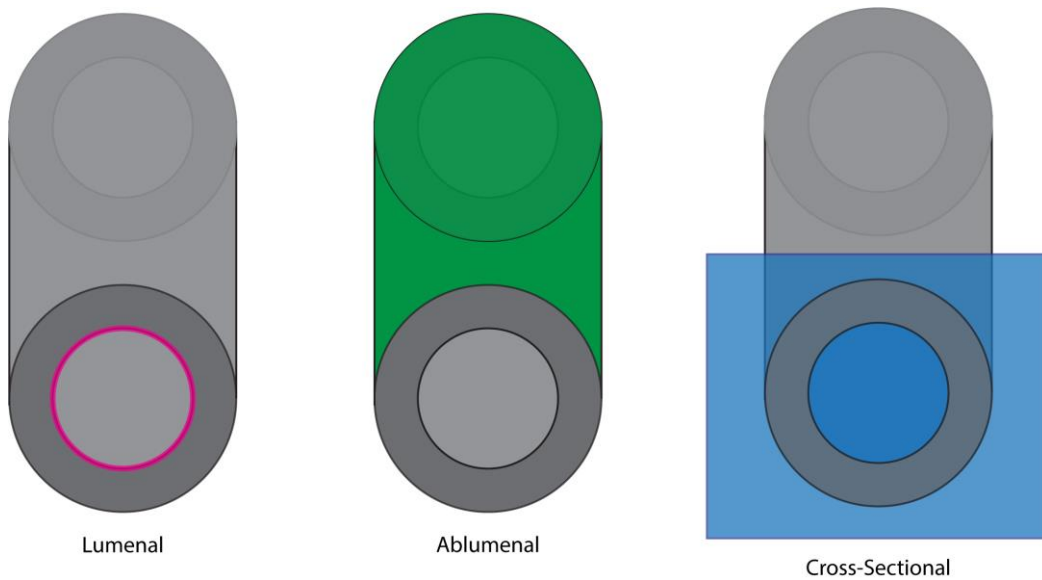
Supplementary Figure 5.1: Imaging plane schematics. *Schematics of the three different imaging planes used throughout the study.*
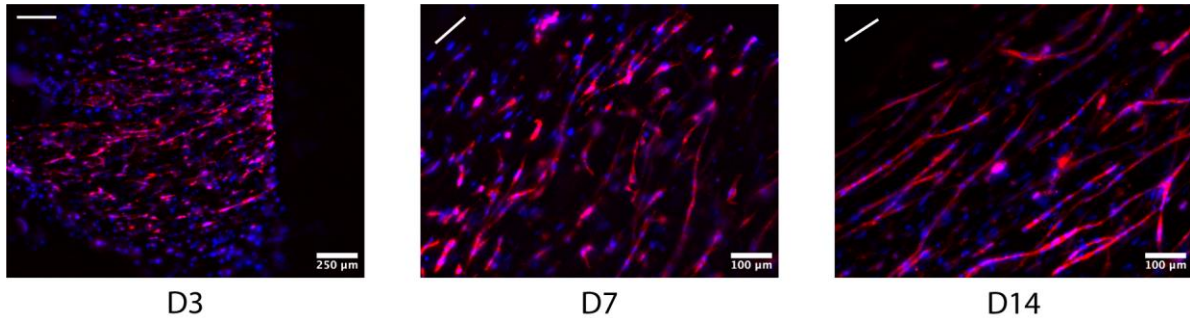
Supplementary Figure 5.2: Static culture yields increasingly more aligned vasculature over time. *Fluorescent images of longitudinal sections of grafts at day 3 (left), day 7 (middle), and day 14 (right) showing vasculature aligned in the direction of the lumen (white line in top left corners). Red – EC, blue – nuclei.*

5.6 References

[1]   Lawton, J.S., Tamis-Holland, J.E., Bangalore, S., Bates, E.R., Beckie, T.M., Bischoff, J.M., Bittl, J.A., Cohen, M.G., DiMaio, J.M., Don, C.W., Fremes, S.E., Gaudino, M.F., Goldberger, Z.D., Grant, M.C., Jaswal, J.B., Kurlansky, P.A., Mehran, R., Metkus, T.S., Nnacheta, L.C., Rao, S.V., Sellke, F.W., Sharma, G., Yong, C.M., and Zwischenberger, B.A. (2022) 2021 ACC/AHA/SCAI Guideline for Coronary Artery Revascularization. *Journal of the American College of Cardiology* 79, e21-e129

[2]   Tsao, C.W., Aday, A.W., Almarzooq, Z.I., Anderson, C.A.M., Arora, P., Avery, C.L., Baker-Smith, C.M., Beaton, A.Z., Boehme, A.K., Buxton, A.E., Commodore-Mensah, Y., Elkind, M.S.V., Evenson, K.R., Eze-Nliam, C., Fugar, S., Generoso, G., Heard, D.G., Hiremath, S., Ho, J.E., Kalani, R., Kazi, D.S., Ko, D., Levine, D.A., Liu, J., Ma, J., Magnani, J.W., Michos, E.D., Mussolino, M.E., Navaneethan, S.D., Parikh, N.I., Poudel, R., Rezk-Hanna, M., Roth, G.A., Shah, N.S., St-Onge, M.-P., Thacker, E.L., Virani, S.S., Voeks, J.H., Wang, N.-Y., Wong, N.D., Wong, S.S., Yaffe, K., and Martin, S.S. (2023) Heart Disease and Stroke Statistics—2023 Update: A Report From the American Heart Association. *Circulation* 147, e93-e621

[3]   Desai, N.D., Cohen, E.A., Naylor, C.D., Fremes, S.E., and Radial Artery Patency Study, I. (2004) A randomized comparison of radial-artery and saphenous-vein coronary bypass grafts. *N Engl J Med* 351, 2302-2309

[4]   Gharamti, A. and Kanafani, Z.A. (2018) Vascular Graft Infections: An update. *Infect Dis Clin North Am* 32, 789-809

[5] Patterson, J.T., Gilliland, T., Maxfield, M.W., Church, S., Naito, Y., Shinoka, T., and Breuer, C.K. (2012) Tissue-engineered vascular grafts for use in the treatment of congenital heart disease: from the bench to the clinic and back again. *Regen Med* 7, 409-419

[6] Brennan, M.P., Dardik, A., Hibino, N., Roh, J.D., Nelson, G.N., Papademitris, X., Shinoka, T., and Breuer, C.K. (2008) Tissue-engineered vascular grafts demonstrate evidence of growth and development when implanted in a juvenile animal model. *Ann Surg* 248, 370-377

[7] Helms, F., Lau, S., Aper, T., Zippusch, S., Klingenberg, M., Haverich, A., Wilhelmi, M., and Boer, U. (2021) A 3-Layered Bioartificial Blood Vessel with Physiological Wall Architecture Generated by Mechanical Stimulation. *Ann Biomed Eng* 49, 2066-2079

[8] Kimicata, M., Allbritton-King, J.D., Navarro, J., Santoro, M., Inoue, T., Hibino, N., and Fisher, J.P. (2020) Assessment of decellularized pericardial extracellular matrix and poly(propylene fumarate) biohybrid for small-diameter vascular graft applications. *Acta Biomater* 110, 68-81

[9] Li, X., Xu, J., Bartolak-Suki, E., Jiang, J., and Tien, J. (2020) Evaluation of 1-mm-diameter endothelialized dense collagen tubes in vascular microsurgery. *J Biomed Mater Res B Appl Biomater* 108, 2441-2449

[10] Smith, R.J., Jr., Yi, T., Nasiri, B., Breuer, C.K., and Andreadis, S.T. (2019) Implantation of VEGF-functionalized cell-free vascular grafts: regenerative and immunological response. *FASEB J* 33, 5089-5100

[11] Wang, D., Maharjan, S., Kuang, X., Wang, Z., Mille, L.S., Tao, M., Yu, P., Cao, X., Lian, L., Lv, L., He, J.J., Tang, G., Yuk, H., Ozaki, C.K., Zhao, X., and Zhang, Y.S. (2022) Microfluidic bioprinting of tough hydrogel-based vascular conduits for functional blood vessels. *Sci Adv* 8, eabq6900

[12] Sundaram, S., Echter, A., Sivarapatna, A., Qiu, C., and Niklason, L. (2014) Small-diameter vascular graft engineered using human embryonic stem cell-derived mesenchymal cells. *Tissue Eng Part A* 20, 740-750

[13] Lee, Y.U., Yi, T., Tara, S., Lee, A.Y., Hibino, N., Shinoka, T., and Breuer, C.K. (2014) Implantation of inferior vena cava interposition graft in mouse model. *J Vis Exp*

[14] Ahn, H., Ju, Y.M., Takahashi, H., Williams, D.F., Yoo, J.J., Lee, S.J., Okano, T., and Atala, A. (2015) Engineered small diameter vascular grafts by combining cell sheet engineering and electrospinning technology. *Acta Biomater* 16, 14-22

[15] L'Heureux, N., Paquet, S., Labbe, R., Germain, L., and Auger, F.A. (1998) A completely biological tissue-engineered human blood vessel. *FASEB J* 12, 47-56

[16] Gui, L., Muto, A., Chan, S.A., Breuer, C.K., and Niklason, L.E. (2009) Development of decellularized human umbilical arteries as small-diameter vascular grafts. *Tissue Eng Part A* 15, 2665-2676

[17]   Kirkton, R.D., Santiago-Maysonet, M., Lawson, J.H., Tente, W.E., Dahl, S.L.M., Niklason, L.E., and Prichard, H.L. (2019) Bioengineered human acellular vessels recellularize and evolve into living blood vessels after human implantation. *Sci Transl Med* 11

[18]   Syedain, Z.H., Graham, M.L., Dunn, T.B., O'Brien, T., Johnson, S.L., Schumacher, R.J., and Tranquillo, R.T. (2017) A completely biological "off-the-shelf" arteriovenous graft that recellularizes in baboons. *Sci Transl Med* 9

[19]   Brown, A., He, H., Trumper, E., Valdez, J., Hammond, P., and Griffith, L.G. (2020) Engineering PEG-based hydrogels to foster efficient endothelial network formation in free-swelling and confined microenvironments. *Biomaterials* 243, 119921

[20]   Friend, N.E., McCoy, A.J., Stegemann, J.P., and Putnam, A.J. (2023) A combination of matrix stiffness and degradability dictate microvascular network assembly and remodeling in cell-laden poly(ethylene glycol) hydrogels. *Biomaterials* 295, 122050

[21]   Beamish, J.A., Juliar, B.A., Cleveland, D.S., Busch, M.E., Nimmagadda, L., and Putnam, A.J. (2019) Deciphering the relative roles of matrix metalloproteinase- and plasmin-mediated matrix degradation during capillary morphogenesis using engineered hydrogels. *J Biomed Mater Res B Appl Biomater* 107, 2507-2516

[22]   Chen, Y.C., Lin, R.Z., Qi, H., Yang, Y., Bae, H., Melero-Martin, J.M., and Khademhosseini, A. (2012) Functional Human Vascular Network Generated in Photocrosslinkable Gelatin Methacrylate Hydrogels. *Adv Funct Mater* 22, 2027-2039

[23]   Mirabella, T., MacArthur, J.W., Cheng, D., Ozaki, C.K., Woo, Y.J., Yang, M., and Chen, C.S. (2017) 3D-printed vascular networks direct therapeutic angiogenesis in ischaemia. *Nat Biomed Eng* 1

[24]   Alimperti, S., Mirabella, T., Bajaj, V., Polacheck, W., Pirone, D.M., Duffield, J., Eyckmans, J., Assoian, R.K., and Chen, C.S. (2017) Three-dimensional biomimetic vascular model reveals a RhoA, Rac1, and N-cadherin balance in mural cell-endothelial cell-regulated barrier function. *Proc Natl Acad Sci U S A* 114, 8758-8763

[25]   Mandrycky, C., Hadland, B., and Zheng, Y. (2020) 3D curvature-instructed endothelial flow response and tissue vascularization. *Sci Adv* 6

[26]   Shi, X., He, L., Zhang, S.M., and Luo, J. (2021) Human iPS Cell-derived Tissue Engineered Vascular Graft: Recent Advances and Future Directions. *Stem Cell Rev Rep* 17, 862-877

[27]   Ong, C.S., Zhou, X., Huang, C.Y., Fukunishi, T., Zhang, H., and Hibino, N. (2017) Tissue engineered vascular grafts: current state of the field. *Expert Rev Med Devices* 14, 383-392

[28]   Sekine, H., Shimizu, T., Sakaguchi, K., Dobashi, I., Wada, M., Yamato, M., Kobayashi, E., Umezu, M., and Okano, T. (2013) In vitro fabrication of functional three-dimensional tissues with perfusable blood vessels. *Nat Commun* 4, 1399

[29]   Helms, F., Zippusch, S., Theilen, J., Haverich, A., Wilhelmi, M., and Boer, U. (2022) An encapsulated fibrin-based bioartificial tissue construct with integrated macrovessels, microchannels, and capillary tubes. *Biotechnol Bioeng* 119, 2239-2249

[30]   Wang, J., Zohar, R., and McCulloch, C.A. (2006) Multiple roles of alpha-smooth muscle actin in mechanotransduction. *Exp Cell Res* 312, 205-214

[31]   Gutowski, P., Gage, S.M., Guziewicz, M., Ilzecki, M., Kazimierczak, A., Kirkton, R.D., Niklason, L.E., Pilgrim, A., Prichard, H.L., Przywara, S., Samad, R., Tente, B., Turek, J., Witkiewicz, W., Zapotoczny, N., Zubilewicz, T., and Lawson, J.H. (2020) Arterial reconstruction with human bioengineered acellular blood vessels in patients with peripheral arterial disease. *J Vasc Surg* 72, 1247-1258

[32]   Benrashid, E., McCoy, C.C., Youngwirth, L.M., Kim, J., Manson, R.J., Otto, J.C., and Lawson, J.H. (2016) Tissue engineered vascular grafts: Origins, development, and current strategies for clinical application. *Methods* 99, 13-19

[33]   Hibino, N., McGillicuddy, E., Matsumura, G., Ichihara, Y., Naito, Y., Breuer, C., and Shinoka, T. (2010) Late-term results of tissue-engineered vascular grafts in humans. *J Thorac Cardiovasc Surg* 139, 431-436, 436 e431-432

[34]   Kurobe, H., Maxfield, M.W., Breuer, C.K., and Shinoka, T. (2012) Concise review: tissue-engineered vascular grafts for cardiac surgery: past, present, and future. *Stem Cells Transl Med* 1, 566-571

[35]   Schmidt, J.B. and Tranquillo, R.T. (2016) Cyclic Stretch and Perfusion Bioreactor for Conditioning Large Diameter Engineered Tissue Tubes. *Ann Biomed Eng* 44, 1785-1797

[36]   Syedain, Z., Reimer, J., Lahti, M., Berry, J., Johnson, S., and Tranquillo, R.T. (2016) Tissue engineering of acellular vascular grafts capable of somatic growth in young lambs. *Nat Commun* 7, 12951

[37]   Dahl, S.L., Kypson, A.P., Lawson, J.H., Blum, J.L., Strader, J.T., Li, Y., Manson, R.J., Tente, W.E., DiBernardo, L., Hensley, M.T., Carter, R., Williams, T.P., Prichard, H.L., Dey, M.S., Begelman, K.G., and Niklason, L.E. (2011) Readily available tissue-engineered vascular grafts. *Sci Transl Med* 3, 68ra69

[38]   Ahmann, K.A., Weinbaum, J.S., Johnson, S.L., and Tranquillo, R.T. (2010) Fibrin degradation enhances vascular smooth muscle cell proliferation and matrix deposition in fibrin-based tissue constructs fabricated in vitro. *Tissue Eng Part A* 16, 3261-3270

[39]   Helms, F., Zippusch, S., Aper, T., Kalies, S., Heisterkamp, A., Haverich, A., Boer, U., and Wilhelmi, M. (2022) Mechanical Stimulation Induces Vasa Vasorum Capillary Alignment in a Fibrin-Based Tunica Adventitia. *Tissue Eng Part A* 28, 818-832

[40]   Morin, K.T., Dries-Devlin, J.L., and Tranquillo, R.T. (2014) Engineered microvessels with strong alignment and high lumen density via cell-induced fibrin gel compaction and interstitial flow. *Tissue Eng Part A* 20, 553-565

[41]   Levesque, M.J. and Nerem, R.M. (1985) The elongation and orientation of cultured endothelial cells in response to shear stress. *J Biomech Eng* 107, 341-347

[42]   Steward, R., Jr., Tambe, D., Hardin, C.C., Krishnan, R., and Fredberg, J.J. (2015) Fluid shear, intercellular stress, and endothelial cell alignment. *Am J Physiol Cell Physiol* 308, C657-664

[43]   Ostrowski, M.A., Huang, N.F., Walker, T.W., Verwijlen, T., Poplawski, C., Khoo, A.S., Cooke, J.P., Fuller, G.G., and Dunn, A.R. (2014) Microvascular endothelial cells migrate upstream and align against the shear stress field created by impinging flow. *Biophys J* 106, 366-374

[44]   Franco, C.A., Jones, M.L., Bernabeu, M.O., Geudens, I., Mathivet, T., Rosa, A., Lopes, F.M., Lima, A.P., Ragab, A., Collins, R.T., Phng, L.-K., Coveney, P.V., and Gerhardt, H. (2015) Dynamic Endothelial Cell Rearrangements Drive Developmental Vessel Regression. *PLOS Biology* 13, e1002125

[45]   Schaefer, J.A., Guzman, P.A., Riemenschneider, S.B., Kamp, T.J., and Tranquillo, R.T. (2018) A cardiac patch from aligned microvessel and cardiomyocyte patches. *J Tissue Eng Regen Med* 12, 546-556

[46]   Lee, A., Hudson, A.R., Shiwarski, D.J., Tashman, J.W., Hinton, T.J., Yerneni, S., Bliley, J.M., Campbell, P.G., and Feinberg, A.W. (2019) 3D bioprinting of collagen to rebuild components of the human heart. *Science* 365, 482-487

[47]   Szklanny, A.A., Machour, M., Redenski, I., Chochola, V., Goldfracht, I., Kaplan, B., Epshtein, M., Simaan Yameen, H., Merdler, U., Feinberg, A., Seliktar, D., Korin, N., Jaros, J., and Levenberg, S. (2021) 3D Bioprinting of Engineered Tissue Flaps with Hierarchical Vessel Networks (VesselNet) for Direct Host-To-Implant Perfusion. *Adv Mater* 33, e2102661

[48]   Miller, J.S., Stevens, K.R., Yang, M.T., Baker, B.M., Nguyen, D.H., Cohen, D.M., Toro, E., Chen, A.A., Galie, P.A., Yu, X., Chaturvedi, R., Bhatia, S.N., and Chen, C.S. (2012) Rapid casting of patterned vascular networks for perfusable engineered three-dimensional tissues. *Nat Mater* 11, 768-774

[49]   Skylar-Scott, M.A., Uzel, S.G.M., Nam, L.L., Ahrens, J.H., Truby, R.L., Damaraju, S., and Lewis, J.A. (2019) Biomanufacturing of organ-specific tissues with high cellular density and embedded vascular channels. *Sci Adv* 5, eaaw2459

[50]   Wu, P., Asada, H., Hakamada, M., and Mabuchi, M. (2022) Bioengineering of High Cell Density Tissues with Hierarchical Vascular Networks for Ex Vivo Whole Organs. *Adv Mater*, e2209149

Chapter 6 – Conclusions and Future Directions

6.1 Introduction

In this chapter, I outline current limitations of existing vascular tissue constructs, summarize my contributions to the field detailed within this dissertation, and discuss future work that may bring the field closer to clinical realization of hierarchical vascular constructs and other vascular therapies.

6.2 Limitations within the Field of Vascular Tissue Engineering

The understanding of native vascular development and progress in engineering biomimetic vascular tissues have been greatly advanced within the last several decades [1-7]. However, the challenge of engineering a hierarchical vascular tissue construct suitable for surgical transplantation has yet to be overcome [8]. Three key hurdles exist within the field including a consensus on cell types used for vascular applications, the application of fluid flow within engineered tissues, and progress towards engineering a hierarchical vasculature within a single tissue.

As discussed in Chapter 2, research on engineered vascular tissues typically uses cell types that are not clinically translatable and represent a proof-of-concept for understanding vascular tissue development. Therefore, despite the plethora of research on engineered vascular tissues at

all length scales, very few cellular therapies for vascularization have advanced to the clinic. The therapies that have advanced to the clinic primarily use cells easily obtainable through biopsies.

Another limitation within the field is the development of vascular tissue constructs in the absence of fluid flow. After the formation of the vascular plexus, fluid flow plays an important role in remodeling the vasculature into a hierarchical structure composed of arteries, veins, and capillaries. This fluid flow is a driver of vascular phenotype, for example, the presence of a significant muscular layer in arteries compared to a relatively thin muscular layer in veins which experience lower blood velocities and pressures. The presence of flow within engineered vasculature may prime vascular tissues for implantation and facilitate more rapid inosculation with host vasculature and integration with surrounding host tissues. Many studies have tried to incorporate fluid flow within engineered tissues by subjecting constructs to a back-and-forth motion using a rocker plate [9-12]. However, this represents situational or a pathologic oscillatory flow profile. Blood typically flows in a unidirectional pattern, except at bifurcations [13-15] or near thrombi [16] where secondary flows are generated, so the presence of this flow pattern may not appropriately prime tissues for implantation. Unidirectional flow has been applied with the use of pumps/bioreactors [17-22] or hydrostatic pressure gradients [23-26], though these are not always applied at the appropriate pressure, speed, or shear stress values as observed within different regions of the native human vascular system.

Finally, as thoroughly outlined in Chapter 2, very little research has focused on bridging vascular length scales to create an integrated, perfusable vascular hierarchy for clinical applications of engineered tissues and organs.

6.3 Summary of Findings, Conclusions, and Contributions of this Dissertation Work to the Fields of Tissue Engineering and Regenerative Medicine

The primary goal of this dissertation was to engineer a complete, perfusable, vascular hierarchy suitable for surgical anastomosis and immediate perfusion of the construct *in vivo*. More specifically, this dissertation focused on inosculation between vessels of two different length scales, and then integrated all three length scales for a complete hierarchical vascular tissue. A secondary aim of this work was to develop systems that can be used to better understand vascular morphogenesis and inosculation. Each aim of this dissertation yielded an advancement in hierarchical engineered tissue constructs and the development of a model system that can be used to further investigate vascular morphogenesis and improve engineered tissues toward clinical translation. In Chapter 3, I detailed the development of two-scale capillary-mesovascular hierarchies and the development of a model system that may be used for the study of tissue-specific vasculature. I employed this system to investigate the role of tissue-specific SC on the morphogenesis, inosculation, and perfusion of engineered hierarchical vasculature. This model system could be further developed toward using tissue-specific EC in conjunction with tissue specific SC toward biological mimicry of organ-specific vasculature. In Chapter 4, I developed a two-scale capillary-artery vascular hierarchy and investigated properties of hydrogel composition resulting in various sprouting morphologies. This model system could be used to investigate inosculation mechanisms at different scales of the vascular system and mechanisms of host-implant inosculation. Finally, in Chapter 5, I developed a novel technique to fabricate three-layer TEVG mimicking native artery physiology composed of a tunica intima, media, and adventitia, amenable to cellular remodeling, and suitable for surgical anastomosis. These grafts were used to

investigate the integration of vasculature across three length scales toward the fabrication of a complete, three-scale hierarchical vascular tissue construct.

6.3.1 Aim 1 – Engineered two-scale vascular micro-mesovascular hierarchies and the development of a platform enabling the study of tissue-specific vascular morphogenesis

To form two-scale vascular hierarchies containing capillaries and mesoscale vessels, I adapted an established microfluidic lab-on-a-chip system previously used to study GF-mediated angiogenic sprouting in the absence of vascular supportive SC [10]. My modifications to the system enabled the formation and perfusion of microvascular capillary beds with connections to arteriole-scale endothelialized channels resulting in a perfusable hierarchical vasculature. This system permitted the investigation into how SC identity influences EC morphogenesis. I investigated LF, DF, and MSC for their ability to support EC morphogenesis, inosculation, and subsequent perfusion of hierarchical vascular networks in fibrin hydrogels. These studies pave the way for future use of this system with tissue-specific SC and EC to investigate tissue-specific vascular morphogenesis and the development of drugs and/or biologics that interact with tissue-specific vasculature.

Conclusions: This work showed that all three SC types supported vascular morphogenesis, with LF in particular yielding microvascular morphologies with the highest vascular density, vessel diameter, and vessel interconnectivity. Further, LF were the only SC type to support functional perfusion of hierarchical vascular networks. While significant work in the literature has focused on the tissue-specific nature of EC, this work identified that SC may also take on lineage-specific roles in vascular morphogenesis, depending on the organ of origin. Though not typically

considered a pericyte, LF displayed three pericyte-like markers, αSMA, NG2, and PDGFRβ, in perivascular locations and directly associated with the microvasculature.

6.3.2 Aim 2 – Two-scale micro-macrovascular hierarchies and a potential platform to study host-implant inosculation mechanisms and vascular development from aged and diseased populations

To enable surgical anastomosis of engineered vascular hierarchies, I incorporated explanted murine arteries and veins yielding two-scale capillary-macrovascular hierarchies (Chapter 4). The system developed in Chapter 4 could be further used to explore host-implant inosculation mechanisms and vascular sprouting using diseased and/or aged donor tissue to provide insights into vascular development critical for clinical translation.

Conclusions: Aortae were the easiest vessels to isolate, the only explanted vessel type successfully cannulated, and yielded the greatest EC sprouting compared to the other vessels examined. Therefore, these vessels represent the greatest translatable potential to further test in a murine ischemia model where the explanted aorta and surrounding microvasculature would be transplanted via surgical anastomosis. The presence of human cells within the bulk hydrogels diminished murine EC sprouting from the macrovessels, but the murine and human EC still interacted and appeared to inosculate. Murine EC migrated along or wrapped around existing capillaries forming interconnections between the macro- and microvasculature. In acellular hydrogels, endothelial sprout distance and hydrogel stiffness were linearly correlated indicating that hydrogel stiffening underlies vascular morphogenesis, in line with previous work.

6.3.3 Aim 3 – Fabrication of TEVG and a multiscale, integrated, hierarchical vascular tissue construct

Though murine macrovessels could be suitable for surgical anastomosis in an animal model, TEVG were fabricated as a means to scale these vascular hierarchies toward human clinical use. The current standard of practice for bypass surgeries is to take a vessel from another location within the body, thus yielding two surgical sites. TEVG hold great promise for clinical applications as they would eliminate the need for a donor vessel. In Chapter 5, I developed a new method to fabricate multi-layer vascular grafts mimicking the three native layers of arteries: tunica intima, tunica media, and tunica adventitia. I then integrated these grafts with the meso-microvascular hierarchies developed in Chapter 3, yielding a complete vascular hierarchy composed of capillaries, mesovessels, and macrovessels perfusable across two length scales and suitable for surgical anastomosis. This prototype hierarchical vasculature has the potential to address a critical unmet need in the field of tissue engineering and regenerative medicine.

Conclusions: Soft fibrin hydrogels were critical for cell spreading and cell-mediated graft compaction. In initially stiffer 10 mg/mL fibrin hydrogels, grafts did not undergo cell-mediated compaction yielding a graft not permissible to surgical anastomosis. In contrast, initially softer 5 mg/mL hydrogels permitted substantial cell-mediated remodeling and compaction of the matrix ultimately yielding a tough graft that could be sutured, extensively stretched, and handled. On-mandrel culture was critical for maintaining lumen diameter and supporting alignment of capillaries within the adventitia layer. Incorporating SMC in a media layer was critical for increasing mechanical strength of the grafts for successful suture placement. Finally, the duration of adventitia layer culture was critical for the successful creation of a hierarchical vascular tissue constructs. When only cultured for 3 days, capillaries in the vasa vasorum did not sprout out and

162

interconnect with surrounding capillaries, whereas when cultured for 7 days, capillaries in the vasa vasorum did sprout out towards capillaries in the surrounding bulk hydrogel.

6.3.4 Impact

In summary, this dissertation has yielded a model system enabling the study of tissue-specific vascular morphogenesis, a model system enabling the study of host-implant inosculation mechanisms, and a complete, integrated vascular hierarchy suitable for surgical anastomosis. These model systems build on prior work and pave the way for future research to enable the development of tissue-specific vasculature for engineered tissues and organs.

This work builds upon prior research integrating capillaries and macroscale vessels. Significant progress has been made prior to this dissertation work by numerous research groups. Chiu et al. integrated rodent arteries and veins by inducing capillary sprouting from the cut lumenal ends of the vessel thereby bridging arterial circulation with microscale capillaries [27]. Chapter 4 builds upon this work by inducing sprouting from the longitudinal edge of the vessel yielding a construct that contains capillaries and arteries without breaking the arterial circulation to transplant the construct. Szklanny et al. fabricated a vascular graft from a synthetic polymeric material and integrated this graft with a surrounding bulk hydrogel containing a capillary network [28]. Micro holes along the graft wall allowed integration of endothelial cells in the graft and capillaries in the bulk hydrogel. In Chapter 5, we built upon this work by fabricating a hydrogel-based vascular graft containing capillaries replicative of a vasa vasorum that could integrate with capillaries in the bulk hydrogel by sprouting out of the graft wall into the surrounding hydrogel. The use of a hydrogel-based graft allows for more cell-mediated remodeling of the graft and potentially more integration with the host following transplantation.

The hierarchical vascular tissue construct developed within this dissertation paves the way to vascularize tissues for the transplantation of any parenchymal cell type including skeletal myoblasts, cardiomyocytes, islets, hepatocytes, osteoblasts, neurons, and others. This construct when cultured with parenchymal cells could be applied clinically as a free tissue flap surgically anastomosed by the TEVG. To my knowledge, only one prior study has investigated the use of hierarchical vasculature as a free tissue flap to support parenchymal cell function. Sekine et al. investigated hierarchical vascular tissue constructs containing cardiomyocyte- and capillary-laden cell sheets layered on top of the macro- and mesovascular scale vessels [29]. The model developed in this dissertation supports the integration of parenchymal cells within the bulk hydrogel surrounding the meso- and macro-vessels thereby yielding increased integration of the hierarchical vasculature and parenchymal cells. This model further advances upon the prior study by eliminating the use of native host vessels that requires an additional surgical site. This hierarchical vascular tissue construct could have potentially transformative results for the clinical translation of 3D tissues and organs.

6.4 Limitations of this Work

As mentioned in Chapter 2, there is a significant unmet clinical need for engineered hierarchical vascular tissue constructs. Though the work presented within this dissertation makes significant strides towards this goal, there are some limitations of the studies described in this dissertation.

First, the endothelial source used throughout this dissertation is a proof-of-concept cell source. The clinical translatability of HUVEC has been questioned in part because these EC are derived from venous origins and would likely be unsuitable as an autologous cell source for

therapeutic applications. Additionally, these EC and all of the SC used in the scope of this dissertation were derived from young, healthy donors, not necessarily representative of a more aged patient population. These cell types facilitate the robust and reliable formation of vasculature *in vitro* and *in vivo*, but to aid clinical translation these strategies should also be evaluated using more clinically relevant cell sources [30, 31]. However, further complicating this, a field-wide consensus on clinically relevant cell sources has not been determined (as discussed in Chapter 2).

Perfusion of engineered vasculature is critical as native vasculature is continually perfused. In this dissertation, perfusion was only assessed at the endpoints of culture following a static culture period. Exposure to physiologically-relevant shear stresses and blood pressures may alter the results found here and may better facilitate inosculation across length-scales prior to implantation *in vivo*. In Chapter 3, perfusion may have prevented the collapse of mesovessels in DF- and MSC-containing samples, perhaps yielding hierarchies with all three organ-specific SC types and may have facilitated a greater percentage of perfused hierarchies in LF-containing samples. In Chapter 4, perfusion may have yielded increased sprouting from explanted macrovessels and more inosculation points between sprouted and engineered vasculature from murine and human origins, respectively.

Finally, the complete hierarchy presented in Chapter 5 represents a structure that does not truly replicate native anatomy. While macro-, meso-, and microvasculature are all present within the engineered tissue construct, arteries do not directly connect to capillaries in the native vascular hierarchy. Rather vasculature tapers, gradually reducing diameter and wall thickness as vessels progress from arteries to capillaries. It is likely that when anastomosed to the host arterial circulation, the network will undergo flow-induced remodeling, potentially connecting the TEVG and capillary bed through remodeling of existing capillaries into larger vessels via a process called

arteriogenesis. Fluid shear stress (FSS) is a critical driver of arteriogenesis [32], in contrast to hypoxia-induced angiogenesis; therefore since the implanted network is a non-physiologic arrangement of vessels, it is likely that FSS will induce significant arteriogenesis and remodeling of the network. This work did not reach the point of testing *in vivo*.

6.5 Future Directions

The results from these studies provide a new methodology for engineering hierarchical vasculature and new platforms that could be used to gain a better understanding of various aspects of vascular development relevant for clinical translation.

6.5.1 Aim 1 – Increasing the replication of organ-specific vascular phenotypes, perfusion culture, and increased replication of arteriole anatomy

The hierarchical vascular model developed here could be further improved to gain a better understanding of organ-specific vascular morphogenesis and aid research efforts towards engineering functional organs. We tested various organ-specific SC (lung, skin, and bone marrow), though the arguably more critical cell type in organ-specific vasculature is the EC which play a role in regulating vascular permeability. The permeability of continuous, fenestrated and sinusoidal capillaries should not be equal, and to my knowledge this comparison in engineered tissues has not yet been made within the field. Sinusoidal capillaries are found in the bone marrow while continuous capillaries are found in the lung and skin, therefore using EC specific to these organs could help to better understand and control the development of organ-specific vasculature with relevant permeability and functionality. Most permeability studies in the literature focus on

achieving tight barrier replicative of continuous capillaries or venules [24, 33-40]. The system developed within this thesis, modified by the use of organ-specific EC, could elucidate the means to develop vasculature with organ-specific functions and a mechanistic understanding of vascular permeability to facilitate the translation of engineered organs.

As mentioned above, a limitation of both the field and this study is the lack of fluid flow applied in a physiologic manner at physiologic shear stress levels. Future studies could explore how EC morphogenesis and vessel perfusion are impacted by flow in this system. It is likely that exposure to constant fluid flow will reduce mesovessel collapse and potentially support greater inosculation between capillaries and mesovessels in LF-supported samples and enable this inosculation in DF- and MSC-supported samples.

Finally, this model could be adapted to engineer multilayered arteriole-scale vessels. Currently, the mesochannels are seeded in a single step process seeding only EC. This process could be modified to a two-step process in which organ-specific SC are first seeded and allowed to adhere, followed by a second seeding of EC to fabricate a two-layer mesovessel. A similar procedure was employed by Alimperti et al. in a model of single mesovessels [9]. This process would facilitate the fabrication of physiologically-relevant mesovessels to more fully replicate arteriole biology in the layers of perivascular cells within their tunica media, and potentially facilitate regulation of arteriole diameter, a physiologic function not yet achieved in engineered tissues.

6.5.2 Aim 2 – Improved fabrication of vascular hierarchies and developing an improved understanding of host-implant inosculation

The hierarchical vascular construct developed here could be further improved and further tested as a means to restore perfusion to ischemic tissues. Our results showed significant sprouting from explants embedded in acellular hydrogels, which was attenuated when cells were incorporated into the bulk hydrogel. Further, we showed evidence of anastomosis between sprouted mouse EC (mEC) and human EC (hEC) that formed vessels in the bulk. Together, these results motivate a potential direction to combine this work with our established microbead platform [41]. Cellular microbeads containing the same cells as our bulk hydrogel are capable of sprouting into and vascularizing acellular fibrin hydrogels [41]. Microbeads could be dispersed throughout the hydrogel and yield capillary sprouting into the surrounding acellular bulk hydrogel concurrent with mEC sprouting from the explant ultimately yielding integration between sprouted capillaries from the beads and sprouted mEC from the explants. Additionally, future studies could explore these constructs in animal models of hindlimb ischemia as a means to restore blood flow to surrounding tissues. Our lab has primarily assessed microvascular therapies in hindlimb ischemia models (unpublished), though this construct could be tested as a therapeutic to address the multiscale damage to ischemic tissues [42].

The focus of Aim 2 (Chapter 4) was to develop a hierarchical vasculature containing a macrovessel suitable for surgical anastomosis. However, the model system developed could also be used to study host-implant inosculation mechanisms *ex vivo*. To my knowledge, there is only one group that has extensively studied host-implant inosculation through the use of complex animal models and intravital imaging techniques [43]. The morphology of sprouting observed in our model is remarkably similar to the morphology observed by their group (Fig. 6.1). Our model allows the investigation into how host and implant EC interact in a simple 3D hydrogel culture model using confocal microcopy imaging techniques and without the need for costly animal

husbandry for extended periods. While our model employed explanted vessels from young, healthy mice from a BALB/c background, this model could be further modified by obtaining vessels from aged, diseased, or genetically-modified mice to match the aging population and provide better insights for clinical translation of implanted vasculature.

This model paves the way to answer numerous scientific questions regarding host-implant inosculation. How does a sprouted cell determine where to sprout to and whether to sprout towards an empty region within the hydrogel or another vessel? Is this dependent on the density of vasculature in the surrounding region? Does sprouting speed play a role in inosculation dynamics? How does a sprouted cell transition from direct cell-cell contact to replacement of the cell in the position of the vessel? Answers to these questions could potentially be obtained using this model and will greatly impact the future of engineered vascular therapies.
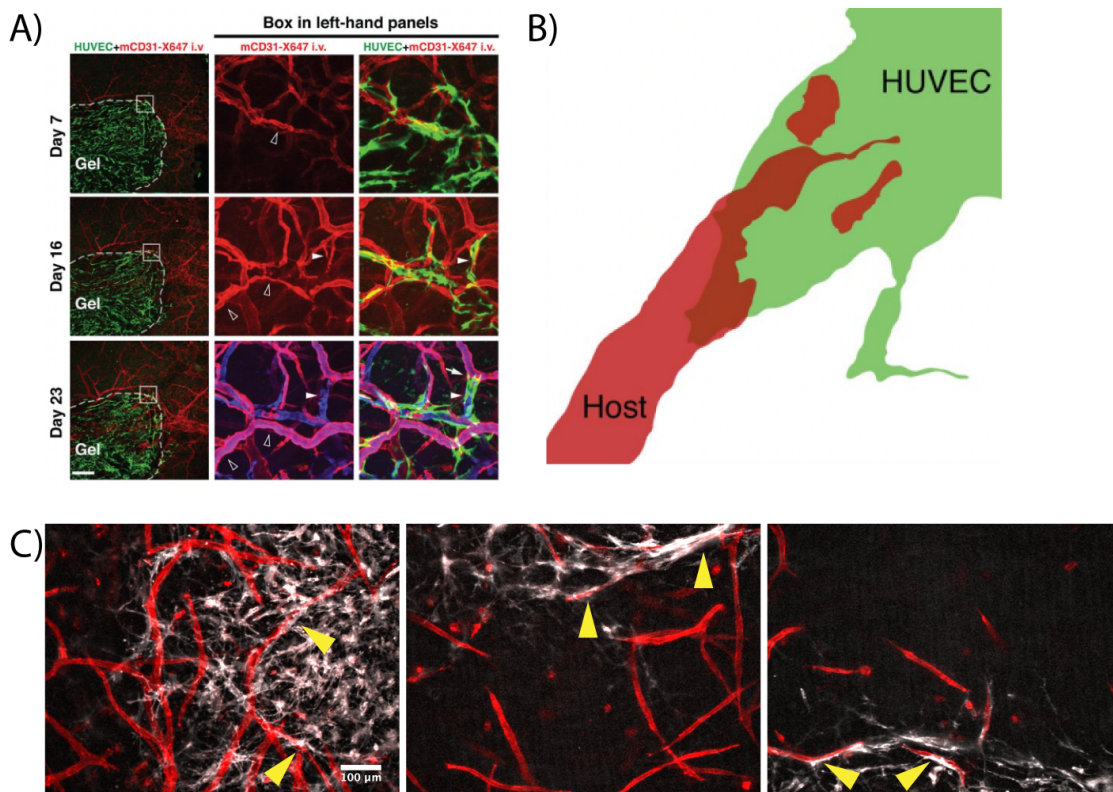
Figure 6.1: Mechanisms for investigating host-implant anastomosis. *(A) Sample data from Cheng at al. showing how implanted HUVEC sprout towards and wrap around host vessels to tap into the host blood supply. (B) Cheng et al. proposed mechanism for how this process occurs. (A, B) Reproduced with permission from Elsevier from reference [43]. Copyright 2011, The American Society of Hematology. (C)*

Sample images from Chapter 4 studies showing a similar "wrapping and tapping" morphology (yellow arrowheads).

6.5.3 Aim 3 – Improving the TEVG, developing preclinical models of transplanted cells and tissue, and developing better organ-specific hierarchical vasculature

The TEVG developed within this dissertation is in the early stages of development. Further research to improve the mechanical properties of the graft to enable it to withstand the hemodynamic forces present within the arterial circulation would facilitate translation of the hierarchical tissue. This will require increased mechanical characterization of the tunica media layer, as well as the SMC morphology and arrangement within the hydrogel. Additionally, adding flow preconditioning to the graft may improve sprouting potential *in vitro* and *in vivo* and prime the graft to better withstand physiologic hemodynamic forces.

Flow conditioning will be critical not only though the vascular graft, but also through the mesovessels and capillary structures. Future studies could examine integration of all three length scales by connecting the construct to a perfusion culture system to better understand the influence of flow-mediated remodeling on vessel development and inosculation in this system. Culturing this hierarchical construct under flow through the TEVG and the mesovessels may improve inosculation of each vascular length scale to the surrounding capillaries, and thereby support increased perfusion within the entire tissue construct. Static conditioning of TEVG has been successful in prior studies [44, 45], though perfusion culture would likely improve the mechanical characteristics of the grafts developed herein and aid in the interconnection of vasculature across length scales. To enable perfusion culture, a better bioreactor mold is required. The current PDMS mold developed in this dissertation allowed the preliminary fabrication of complete vascular hierarchies. However, it does not easily support perfusion of multiple length scales. Bioreactors

with specific inlets for the vascular graft and mesovessels will facilitate increased perfusion of the entire vasculature. There are several existing bioreactors that could be adapted to fit the needs of the current vascular hierarchy developed in this dissertation. Commercially available bioreactors designed for vascular grafts could be employed after seeding the arteriole-channels with EC to fabricate the mesovessels. Such bioreactors have been previously used to culture TEVG [21]. A recent Nature Protocols paper describes detailed methodologies for fabricating a similar bioreactor and used it to seed mesoscale vessels (Fig. 6.2) [46]. This protocol may enable the fabrication of a custom bioreactor with multiple inlets and outlets for seeding mesovessels and providing flow to mesovessels and macrovessels within the bioreactor.

Increased perfusion may also be achieved by incorporating microvascular patterning techniques to better control the location of micro- and mesovascular structures within the construct [47]. Though our model represents a significant advancement in the development of a hierarchical vascular tissue construct, no organ contains vasculature arranged in this way. Our hierarchical construct could be modified via patterning to replicate organ-specific vascular hierarchical morphologies. The liver lobule for example contains a hepatic artery that branches into arterioles in the liver lobule which supply blood to the sinusoidal capillaries within the lobule. This vasculature is patterned in a distinct morphology which could be incorporated into the hierarchical vascular construct developed here.

Patterned vascular structures within the hierarchy may also be achievable through a 3D printing technology currently being developed within our lab. 3D printing will enable the fabrication of mesovasculature with specific patterns and orientations into a bead slurry which could contain organ-specific parenchymal cells and microvasculature to engineer organ-specific

171

hierarchically vascularized tissues. A vascular graft, like the TEVG developed in this thesis, could be embedded within this construct to complete the hierarchy.
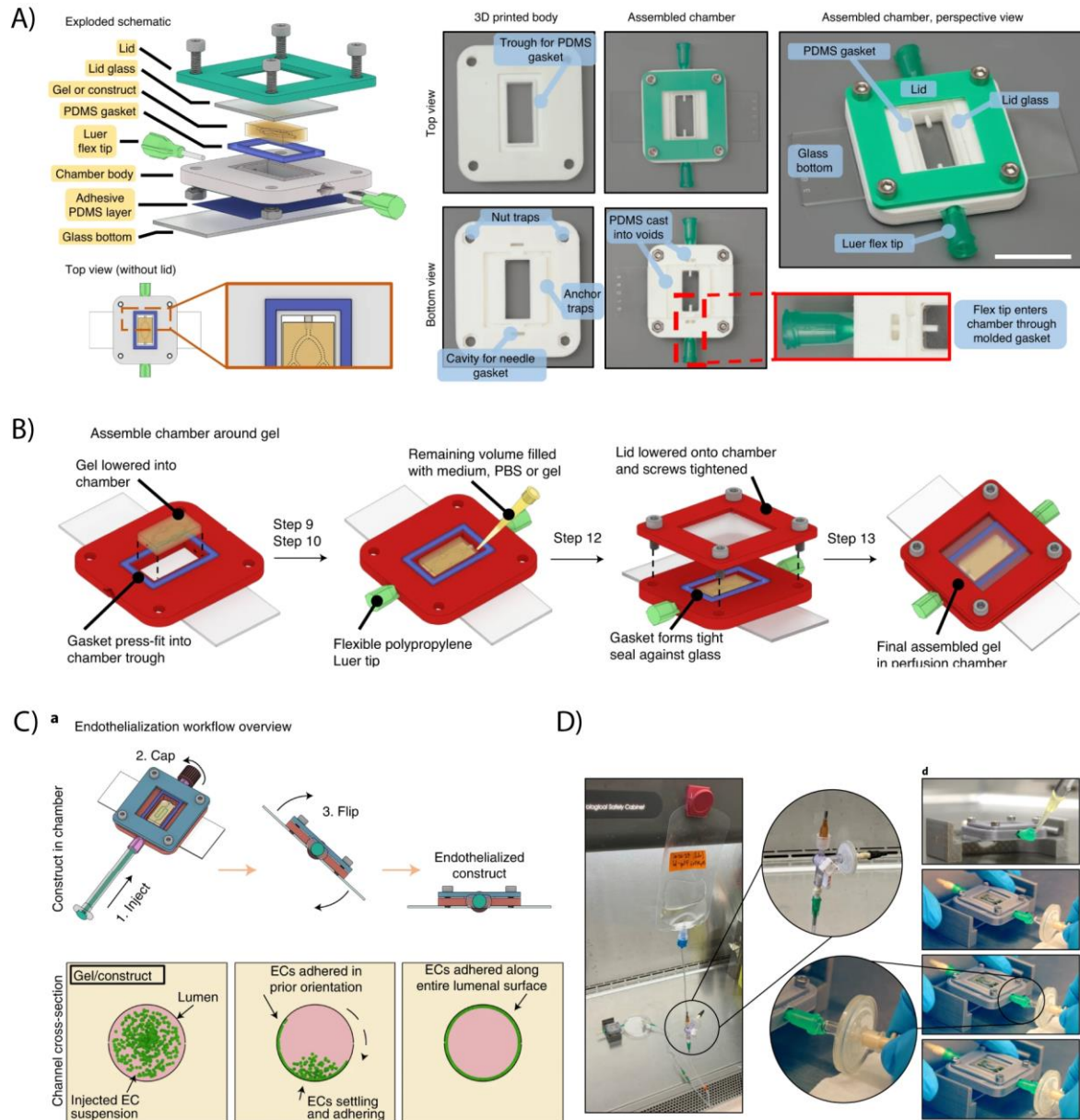
Figure 6.2: New closed loop bioreactor mold for sterile culture and perfusion that could be applied to hierarchical vascular tissue constructs developed by Kinstlinger et al. *(A) Customizable perfusion chamber. (B) Assembly of hydrogel into the perfusion chamber. (C) Schematic of closed loop seeding process for mesovessels. (D) Methods for setting up sterile closed loop fluidic circuit. Figures reproduced from reference [46] with permission from Springer Nature. Copyright 2021, Kinstlinger, I.S., et al.*

Finally, this model could be implanted into the arterial circulation in an animal model as a means to restore perfusion to ischemic tissues or support the transplant of parenchymal cells. I developed the necessary microsurgical skillset to anastomose 1 mm diameter vessels at the Columbia University Department of Orthopedics basic microsurgery course (Fig. 6.3). The course taught arterial and venous anastomosis, and interpositional grafting, which are all applicable to future work for anastomosing grafts into the circulation. Our lab has worked extensively with hindlimb ischemia models by implanting microvascular hydrogel constructs to restore macroscopic perfusion to ischemic limbs and increase vascularization of the surrounding muscle tissue. The model developed here could be surgically anastomosed into the femoral circulation to enable immediate perfusion of the macroscopic vessels and increased blood flow to the surrounding muscle tissue via perfusion of the capillaries and mesovessels within the hierarchical construct. This hierarchical vascular tissue construct could also be cultured with muscle cells and anastomosed to the femoral circulation as a therapy for volumetric muscle loss. Finally, this hierarchical vasculature could theoretically support the survival of a wide range of parenchymal cells as a free flap. One example would be to anastomose the hierarchical vasculature into the mesenteric circulation along with co-transplanted islets, providing immediate perfusion to the grafted cells to support their abilities to produce insulin in response to glucose stimulation as a therapy for the treatment of diabetes.

Critical next steps for this work are to demonstrate fully interconnected hierarchies with dextran perfusion *in vitro* and blood perfusion *in vivo*. We believe the primitive hierarchy presented herein provides a clear path forward for future work toward engineering hierarchical vascular tissue constructs at clinical scale.

A) End-to-end: Arterial

End-to-end: Venous

End-to-side: A to V

Release Clamp → Start Blood Flow

End-to-side: V to A

Interpositional: CA into FA

B)
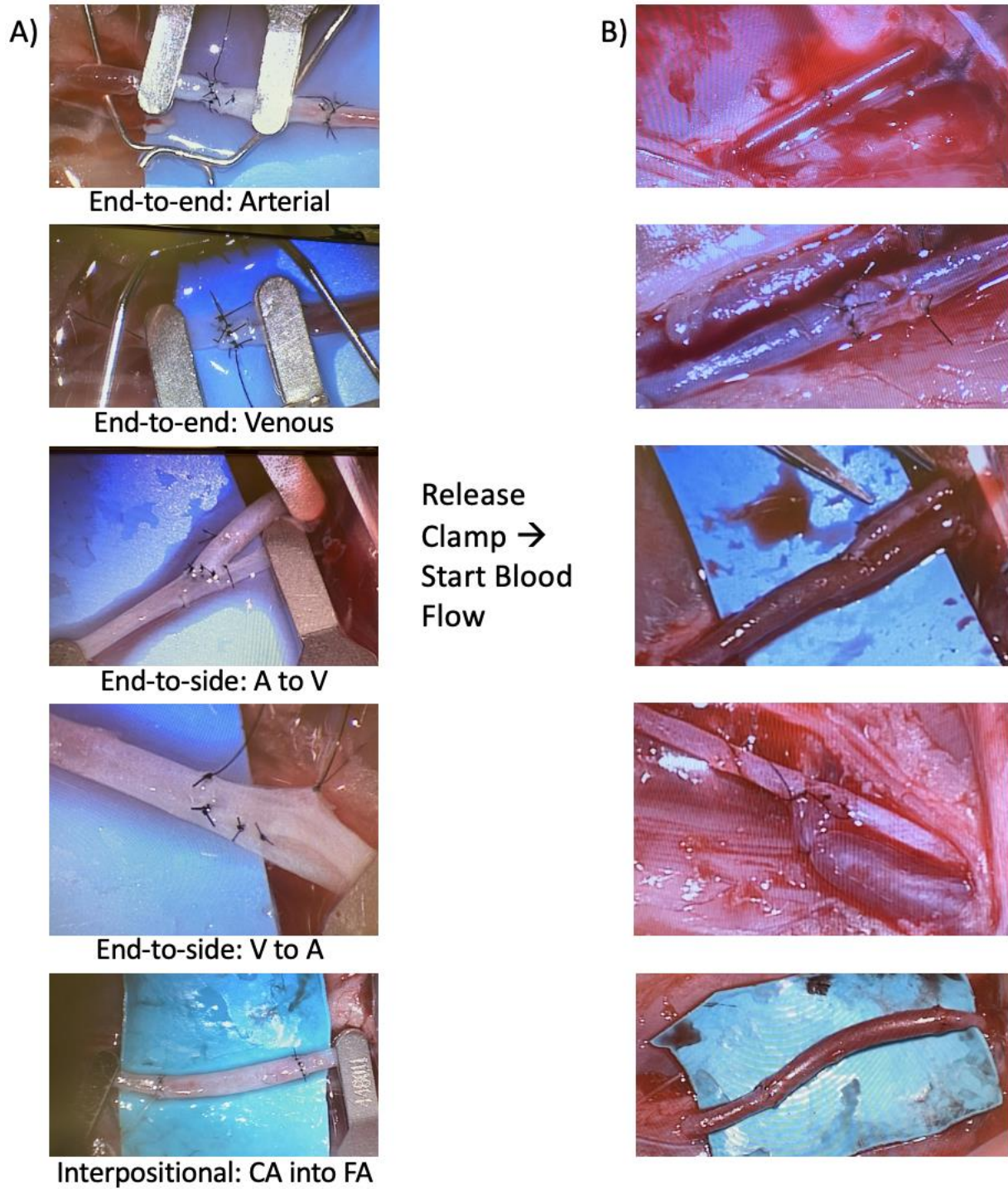
Figure 6.3: Microsurgical anastomosis of rat femoral vessels. *(A) Images of clamped vessels showing the sutures and complete surgical anastomoses for various types of anastomoses. (B) Images following release of the clamp and start of blood flow. A – artery, V – vein, CA – carotid artery, FA – femoral artery. Images obtained during the basic microsurgery course at Columbia University Department of Orthopedics.*

6.6 Concluding Remarks

The result of this body of work is three new model systems to study vascular morphogenesis, and one of the first models of hierarchical vasculature spanning all length scales of the vascular tree from capillaries to arteries. Importantly, this dissertation lays the groundwork for significant future work in both mechanistic understandings of vascular development and translational work to progress hierarchical vasculature into the clinic. The continued advancement of hierarchical vascular tissue constructs and further understanding of vascular inosculation mechanisms will greatly enhance the ability of TE to deliver on the promise of implantable tissues and whole organs.

6.7 References

[1]   Rouwkema, J. and Khademhosseini, A. (2016) Vascularization and Angiogenesis in Tissue Engineering: Beyond Creating Static Networks. *Trends Biotechnol* 34, 733-745

[2]   Rouwkema, J., Rivron, N.C., and van Blitterswijk, C.A. (2008) Vascularization in tissue engineering. *Trends Biotechnol* 26, 434-441

[3]   Khan, O.F. and Sefton, M.V. (2011) Endothelialized biomaterials for tissue engineering applications in vivo. *Trends Biotechnol* 29, 379-387

[4]   Abbott, R.D. and Kaplan, D.L. (2015) Strategies for improving the physiological relevance of human engineered tissues. *Trends Biotechnol* 33, 401-407

[5]   Browne, S., Gill, E.L., Schultheiss, P., Goswami, I., and Healy, K.E. (2021) Stem cell-based vascularization of microphysiological systems. *Stem Cell Reports* 16, 2058-2075

[6]   Williams, M.A.C., Mair, D.B., Lee, W., Lee, E., and Kim, D.H. (2022) Engineering Three-Dimensional Vascularized Cardiac Tissues. *Tissue Eng Part B Rev* 28, 336-350

[7]   Song, H.G., Rumma, R.T., Ozaki, C.K., Edelman, E.R., and Chen, C.S. (2018) Vascular Tissue Engineering: Progress, Challenges, and Clinical Promise. *Cell Stem Cell* 22, 340-354

[8]   Fleischer, S., Tavakol, D.N., and Vunjak-Novakovic, G. (2020) From arteries to capillaries: approaches to engineering human vasculature. *Adv Funct Mater* 30

[9]   Alimperti, S., Mirabella, T., Bajaj, V., Polacheck, W., Pirone, D.M., Duffield, J., Eyckmans, J., Assoian, R.K., and Chen, C.S. (2017) Three-dimensional biomimetic vascular model reveals a RhoA, Rac1, and N-cadherin balance in mural cell-endothelial cell-regulated barrier function. *Proc Natl Acad Sci U S A* 114, 8758-8763

[10]   Wang, W.Y., Lin, D., Jarman, E.H., Polacheck, W.J., and Baker, B.M. (2020) Functional angiogenesis requires microenvironmental cues balancing endothelial cell migration and proliferation. *Lab Chip* 20, 1153-1166

[11]   van Duinen, V., Zhu, D., Ramakers, C., van Zonneveld, A.J., Vulto, P., and Hankemeier, T. (2019) Perfused 3D angiogenic sprouting in a high-throughput in vitro platform. *Angiogenesis* 22, 157-165

[12]   Song, H.G., Lammers, A., Sundaram, S., Rubio, L., Chen, A.X., Li, L., Eyckmans, J., Bhatia, S.N., and Chen, C.S. (2020) Transient Support from Fibroblasts is Sufficient to Drive Functional Vascularization in Engineered Tissues. *Adv Funct Mater* 30

[13]   Giddens, D.P., Tang, T.D., and Loth, F. (1995) Fluid Mechanics of Arterial Bifurcations. In *Biological Flows* (Jaffrin, M.Y. and Caro, C.G., eds), pp. 51-68, Springer US

[14]   Guha, A. and Pradhan, K. (2017) Secondary motion in three-dimensional branching networks. *Phys Fluids (1994)* 29, 063602

[15]   Motomiya, M. and Karino, T. (1984) Flow patterns in the human carotid artery bifurcation. *Stroke* 15, 50-56

[16]   Wootton, D.M. and Ku, D.N. (1999) Fluid mechanics of vascular systems, diseases, and thrombosis. *Annu Rev Biomed Eng* 1, 299-329

[17]   Baba, K., Mikhailov, A., and Sankai, Y. (2021) Dynamic flow priming programs allow tuning up the cell layers properties for engineered vascular graft. *Sci Rep* 11, 14666

[18]   Gao, G., Park, J.Y., Kim, B.S., Jang, J., and Cho, D.W. (2018) Coaxial Cell Printing of Freestanding, Perfusable, and Functional In Vitro Vascular Models for Recapitulation of Native Vascular Endothelium Pathophysiology. *Adv Healthc Mater* 7, e1801102

[19]   Hoyle, H.W., Stenger, C.M.L., and Przyborski, S.A. (2022) Design considerations of benchtop fluid flow bioreactors for bio-engineered tissue equivalents in vitro. *Biomaterials and Biosystems* 8, 100063

[20]   Song, J.W. and Munn, L.L. (2011) Fluid forces control endothelial sprouting. *Proc Natl Acad Sci U S A* 108, 15342-15347

[21]   Elliott, M.B., Ginn, B., Fukunishi, T., Bedja, D., Suresh, A., Chen, T., Inoue, T., Dietz, H.C., Santhanam, L., Mao, H.Q., Hibino, N., and Gerecht, S. (2019) Regenerative and durable small-diameter graft as an arterial conduit. *Proc Natl Acad Sci U S A* 116, 12710-12719

[22] Strobel, H.A., Hookway, T.A., Piola, M., Fiore, G.B., Soncini, M., Alsberg, E., and Rolle, M.W. (2018) Assembly of Tissue-Engineered Blood Vessels with Spatially Controlled Heterogeneities. *Tissue Eng Part A* 24, 1492-1503

[23] Linville, R.M., Boland, N.F., Covarrubias, G., Price, G.M., and Tien, J. (2016) Physical and Chemical Signals That Promote Vascularization of Capillary-Scale Channels. *Cell Mol Bioeng* 9, 73-84

[24] Price, G.M., Wong, K.H., Truslow, J.G., Leung, A.D., Acharya, C., and Tien, J. (2010) Effect of mechanical factors on the function of engineered human blood microvessels in microfluidic collagen gels. *Biomaterials* 31, 6182-6189

[25] Zhang, S., Wan, Z., Pavlou, G., Zhong, A.X., Xu, L., and Kamm, R.D. (2022) Interstitial flow promotes the formation of functional microvascular networks in vitro through upregulation of matrix metalloproteinase-2. *Adv Funct Mater* 32

[26] Lee, G.H., Huang, S.A., Aw, W.Y., Rathod, M.L., Cho, C., Ligler, F.S., and Polacheck, W.J. (2022) Multilayer microfluidic platform for the study of luminal, transmural, and interstitial flow. *Biofabrication* 14

[27] Chiu, L.L., Montgomery, M., Liang, Y., Liu, H., and Radisic, M. (2012) Perfusable branching microvessel bed for vascularization of engineered tissues. *Proc Natl Acad Sci U S A* 109, E3414-3423

[28] Szklanny, A.A., Machour, M., Redenski, I., Chochola, V., Goldfracht, I., Kaplan, B., Epshtein, M., Simaan Yameen, H., Merdler, U., Feinberg, A., Seliktar, D., Korin, N., Jaros, J., and Levenberg, S. (2021) 3D Bioprinting of Engineered Tissue Flaps with Hierarchical Vessel Networks (VesselNet) for Direct Host-To-Implant Perfusion. *Adv Mater* 33, e2102661

[29] Sekine, H., Shimizu, T., Sakaguchi, K., Dobashi, I., Wada, M., Yamato, M., Kobayashi, E., Umezu, M., and Okano, T. (2013) In vitro fabrication of functional three-dimensional tissues with perfusable blood vessels. *Nat Commun* 4, 1399

[30] Perry, L., Flugelman, M.Y., and Levenberg, S. (2017) Elderly Patient-Derived Endothelial Cells for Vascularization of Engineered Muscle. *Mol Ther* 25, 935-948

[31] Freiman, A., Shandalov, Y., Rozenfeld, D., Shor, E., Segal, S., Ben-David, D., Meretzki, S., Egozi, D., and Levenberg, S. (2016) Adipose-derived endothelial and mesenchymal stem cells enhance vascular network formation on three-dimensional constructs in vitro. *Stem Cell Res Ther* 7, 5

[32] van Oostrom, M.C., van Oostrom, O., Quax, P.H., Verhaar, M.C., and Hoefer, I.E. (2008) Insights into mechanisms behind arteriogenesis: what does the future hold? *J Leukoc Biol* 84, 1379-1391

[33] Jeon, J.S., Bersini, S., Whisler, J.A., Chen, M.B., Dubini, G., Charest, J.L., Moretti, M., and Kamm, R.D. (2014) Generation of 3D functional microvascular networks with human mesenchymal stem cells in microfluidic systems. *Integr Biol (Camb)* 6, 555-563

[34] Vickerman, V. and Kamm, R.D. (2012) Mechanism of a flow-gated angiogenesis switch: early signaling events at cell-matrix and cell-cell junctions. *Integr Biol (Camb)* 4, 863-874

[35] Chrobak, K.M., Potter, D.R., and Tien, J. (2006) Formation of perfused, functional microvascular tubes in vitro. *Microvasc Res* 71, 185-196

[36] Zheng, Y., Chen, J., Craven, M., Choi, N.W., Totorica, S., Diaz-Santana, A., Kermani, P., Hempstead, B., Fischbach-Teschl, C., Lopez, J.A., and Stroock, A.D. (2012) In vitro microvessels for the study of angiogenesis and thrombosis. *Proc Natl Acad Sci U S A* 109, 9342-9347

[37] Kim, S., Lee, H., Chung, M., and Jeon, N.L. (2013) Engineering of functional, perfusable 3D microvascular networks on a chip. *Lab Chip* 13, 1489-1500

[38] Bang, S., Lee, S.R., Ko, J., Son, K., Tahk, D., Ahn, J., Im, C., and Jeon, N.L. (2017) A Low Permeability Microfluidic Blood-Brain Barrier Platform with Direct Contact between Perfusable Vascular Network and Astrocytes. *Sci Rep* 7, 8083

[39] Bichsel, C.A., Hall, S.R., Schmid, R.A., Guenat, O.T., and Geiser, T. (2015) Primary Human Lung Pericytes Support and Stabilize In Vitro Perfusable Microvessels. *Tissue Eng Part A* 21, 2166-2176

[40] Wang, X., Phan, D.T., Sobrino, A., George, S.C., Hughes, C.C., and Lee, A.P. (2016) Engineering anastomosis between living capillary networks and endothelial cell-lined microfluidic channels. *Lab Chip* 16, 282-290

[41] Friend, N.E., Rioja, A.Y., Kong, Y.P., Beamish, J.A., Hong, X., Habif, J.C., Bezenah, J.R., Deng, C.X., Stegemann, J.P., and Putnam, A.J. (2020) Injectable pre-cultured tissue modules catalyze the formation of extensive functional microvasculature in vivo. *Sci Rep* 10, 15562

[42] Ziegler, T., Abdel Rahman, F., Jurisch, V., and Kupatt, C. (2019) Atherosclerosis and the Capillary Network; Pathophysiology and Potential Therapeutic Strategies. *Cells* 9

[43] Cheng, G., Liao, S., Kit Wong, H., Lacorre, D.A., di Tomaso, E., Au, P., Fukumura, D., Jain, R.K., and Munn, L.L. (2011) Engineered blood vessel networks connect to host vasculature via wrapping-and-tapping anastomosis. *Blood* 118, 4740-4749

[44] Li, X., Xu, J., Bartolak-Suki, E., Jiang, J., and Tien, J. (2020) Evaluation of 1-mm-diameter endothelialized dense collagen tubes in vascular microsurgery. *J Biomed Mater Res B Appl Biomater* 108, 2441-2449

[45]   Li, X., Xu, J., Nicolescu, C.T., Marinelli, J.T., and Tien, J. (2017) Generation, Endothelialization, and Microsurgical Suture Anastomosis of Strong 1-mm-Diameter Collagen Tubes. *Tissue Eng Part A* 23, 335-344

[46]   Kinstlinger, I.S., Calderon, G.A., Royse, M.K., Means, A.K., Grigoryan, B., and Miller, J.S. (2021) Perfusion and endothelialization of engineered tissues with patterned vascular networks. *Nat Protoc* 16, 3089-3113

[47]   Redd, M.A., Zeinstra, N., Qin, W., Wei, W., Martinson, A., Wang, Y., Wang, R.K., Murry, C.E., and Zheng, Y. (2019) Patterned human microvascular grafts enable rapid vascularization and increase perfusion in infarcted rat hearts. *Nat Commun* 10, 584

Appendices

The following appendices contain protocols that were critical for carrying out the research presented in this dissertation.

Appendix A – Thawing, Culturing, Passaging, and Freezing Cells

All cell culture reagents should be kept sterile, and all cell culture work should be conducted in the Biological Safety Cabinet (BSC).
Any items brought into the BSC should be sprayed with 70% ethanol to sterilize. Exceptions: cell culture flasks, well plates, and bioreaction tubes.

Materials
- Conical tubes (50 and 15 mL)
- Sterile DMSO
- Cryovials
- Cell culture media (DMEM, EGM2, RoosterNourish, SMGM, etc. as needed for specific cell types)
- Trypsin (0.05%)
- PBS (1x, no calcium or magnesium)
- Mr. Freezy
- Cell culture flasks with filter caps (T75, T150, T182, T225 depending on experiment)
- Serological pipettes
- FBS

Thawing Cells
1. Aliquot one tube of D10 per vial of cells to thaw and warm up in the 37°C water bath.
   a. Each tube should be 9 mL such that when 1 mL of frozen cells are added the total volume is 10 mL.
   b. If thawing a vial of a different volume, adjust the volume of D10 accordingly.
2. Warm up media for plating cells.
   a. Media should be cell type specific (Table 1), and the volume should correspond to the flask size that the cells will be cultured in (Table 2).
3. Retrieve cell vials from the liquid nitrogen dewar and thaw in the water bath.
   a. Do not leave cells in the water bath for an extended amount of time because liquid DMSO is toxic to cells.
   b. Twirl the cell vial(s) in the water bath until a small chunk of ice is remaining.
4. Bring thawed cell vials and D10 tubes back to the hood.
5. Transfer the contents of each cell vial to the corresponding tube of D10.
6. Centrifuge cells at 200G for 5 minutes.
7. Bring flasks and media to the hood.
8. Aspirate the supernatant from the cell pellet and resuspend in 1 mL of media.
9. Transfer cell suspension to the flask.

10. Transfer remaining media volume to the flask.
11. In a figure eight motion, swirl the cell suspension around for even distribution of the cells upon settling out of suspension.
12. Repeat steps 8-11 for each vial of cells being thawed.
13. Place cell flasks in the 37°C incubator for standard cell culture maintenance.
14. Remove cell vials thawed from the cell culture log in the lab Google Drive.

Culturing Cells
1. Warm up media in the 37°C water bath.
   a. Media should be cell type specific (Table 1), and the volume should correspond to the flask size that the cells will be cultured in (Table 2).
2. Examine cells under the light microscope.
   a. Use 4x objective to assess confluency and 10x objective (or higher if needed) to assess morphology.
   b. Ensure cells have the appropriate morphology (e.g., long spindle shape for LFs or cobblestone for ECs).
3. If cells are not yet confluent, transfer flask to the BSC and aspirate the media. If cells are confluent, follow the passaging protocol below.
4. Replace media with fresh warmed media.
5. Notes:
   a. Media should be changed every other day after thawing or passaging. Exceptions: if there is a substantial number of dead cells after thawing, media could be changed the day after plating and then every other day thereafter.
   b. Cells should reach ~80-90% confluency to achieve maximum cell yield without affecting future passages. Allowing cells to reach a higher confluency or complete confluency can alter the morphology and therefore yield inconsistent results when used in cellular assays. This can also decrease the maximum number of passages.
   c. Each cell type has a maximum passage number based on the point at which cell morphology changes (anecdotal evidence) or manufacturer recommendation.
      i. HUVECs: P7
      ii. NHLFs and NHDFs: P15
      iii. MSCs: P7
      iv. HASMCs: P20

Passaging Cells
1. Examine cells under the microscope to check for confluency. If cells are confluent, proceed with passaging protocol. If cells are not confluent, follow the culturing cells protocol above.
2. Thaw trypsin for each flask.
   a. The volume should correspond to the flask size (Table 2).
3. Aliquot one tube of D10 per flask of cells to passage and warm up in the 37°C water bath.
   a. The volume should correspond to the volume of trypsin used to detach cells from the plate (Table 2).
4. Warm up media for replating cells.

a. Media should be cell type specific (Table 1), and the volume should correspond to the flask size that the cells will be cultured in (Table 2).
5. When trypsin is thawed, bring it to the BSC along with PBS, sterile pipettes and the cell culture flask.
6. Aspirate cell culture media from each flask.
    a. Be sure to change the yellow tip on the aspirator between each flask. This is especially important when the flasks are different cell types.
    b. If multiple flasks are being combined into one aliquot, then yellow tip does not need to be changed.
7. Add PBS to each flask (enough to coat the flask). Tilt the flask back and forth to wash the surface the saline and remove media proteins.
8. Aspirate PBS from each flask, changing tips as necessary.
9. Add trypsin to each flask and incubate in the incubator for 5 minutes.
10. During this wait step, bring the hemocytometer and the warmed D10 to the BSC.
    a. The hemocytometer should be cleaned with 70% ethanol prior to bringing it into the BSC to remove any cellular remnants from the prior user.
11. When the time is up, check the flasks under the microscope. Most cells should be rounded up and beginning to detach or already detached and floating. Tap the flask against the back of the microscope a few times to dislodge any remaining cells.
    a. Move quickly here as trypsin is toxic to cells if left on too long before neutralization.
12. Add D10 to each flask (volumes should be equal).
13. Using a pipette, wash the surface of the flask with the media several times and then pipette up and down to break up any clumps of cells.
    a. Skipping this step can yield cell clumps on the hemocytometer resulting in an inaccurate cell count.
14. Transfer cell, trypsin, media mixture to a conical tube.
15. Invert the tube several times or mix with a pipette. Then take a 10 μL suspension and place it on the hemocytometer.
16. Centrifuge cells for at 200G for 5 minutes.
17. Count cells according to cell counting protocol (Appendix ?).
18. Aspirate the supernatant and resuspend in cell specific media to reach desired concentration based on cell count.
19. Take desired number of cells and add it to a new flask. Then add the corresponding media.
20. In a figure eight motion, swirl the cells around to distribute evenly.
21. If there are remaining cells to be frozen down, follow the freezing protocol below.

Freezing Cells
1. Follow passaging steps 2-3 and 5-17.
2. Prepare freeze media.
    a. Recipe: 20% FBS, 10% DMSO, 70% cell specific media.
    b. The volume should correspond to how cells are frozen down. Typically cells are frozen down at 1 M/mL.
        i. Ex: If you have 4.6 M cells, you will need 4.6 mL of freeze media. In order to not run out, make a little extra (5 mL total).

3. When cells are done centrifuging, keep cells and freeze media on ice until ready to use.
    a. DMSO is toxic to cells when in liquid form, so it is best to prepare as much as possible before mixing it with cells.
4. Label the appropriate number of cryovials based on the cell count. (This should be done in the BSC).
    a. Label should include:
        i. Cell type (Ex: HUVECs)
        ii. The current passage and the passage the vial will be when it is thawed (Ex: P5→P6)
        iii. The number of cells
        iv. Your initials
        v. The date frozen
5. Retrieve a Mr. Freezy from the fridge and mark it with your initials and the date.
6. Bring the cells and freeze media to the hood.
7. Aspirate the supernatant from the cells and resuspend the pellet in freeze media.
8. Pipette 1 mL into each cryovial and secure the cap.
9. Put each vial into a slot in the Mr. Freezy and place it in the -80.
    a. The cells should be stored in the -80 for at least 24 hours. This can be longer if needed but not too long so that other lab members can use the Mr. Freezy.
10. Transfer vials from the -80 to the liquid nitrogen dewar and record the additions on the cell log on the lab google drive.

Appendix B – Isolating HUVEC From Fresh Umbilical Cords

*Protocol amended from Davis J., Crampton S.P., Hughes C.C.W. (2007). Isolation of Human Umbilical Vein Endothelial Cells (HUVEC). JoVE. 3. doi: 10.3791/183

Notes:
- Cords should be used within 1 week or less from birth (hospital collection). *The sooner the cord is used the more viable the isolated cells will be.*
- You can do two cords at one time

Materials Needed for One Cord:
- 2 Haemostats
- 1 pair of scissors
- 2 L beaker
- Foil and autoclave tape
- 2, 5 mL syringe
- 1, 33 mm, 0.22 um Millex filter
- 2, 20 mL syringes
- Butterfly needle
- 1, 18-gauge needle (or 16-gauge needle)
- 40 mL of sterile PBS
- 5 mL of 0.1% collagenase (sterile-filter) → 5ml PBS + 5 mg collagenase
- 5 mL of EGM-2
- 1 T-25 flask
- Umbilical Cord

Protocol:
Day before doing this protocol:
- Place 2 haemostats, and 1 pair of scissors in a 2 L beaker.
- Cover the beaker with aluminum foil and then tape one side of the aluminum foil to the beaker using autoclave tape.
- Autoclave beaker using the textiles setting.
    - a. Sterilization time: 45 minutes
    - b. Drying time: 10 minutes
- Check to make sure water level of pipe in the autoclave is at the specific set level. Then start the process.
    ----
1. Place the umbilical cord and the sterile PBS in the water bath. *Make sure that the cord is in the biohazard delivery bag to avoid contaminating the water bath.*

2. Make 5 mL of 0.1% of collagenase in PBS. *Make sure to make this solution every time this*
   protocol is repeated, DO NOT store solution after experiment is completed.
   [Concentration = 5 mg/mL]
3. Sterile filter the 0.1% collagenase solution using a 5 mL syringe with a 33 mm, 0.22 μm Millex filter.
4. Connect an 18-gauge needle to a 5 mL syringe and suction 5 mL of the sterile-filter collagenase. Place the syringe back in its wrapper for storage.
5. Remove the needle from the syringe carefully and throw it in the sharps needle biohazard container. *Make sure you don't recap the needle.*
6. Suction 20 mL of PBS in each 20 mL syringe. Put the syringes back in their wrappers for storage.
7. Sterilize the hood and all the materials needed in this protocol prior to putting them in the hood.
8. Place paper towels inside the hood *(use sufficient amount to cover your working area properly).*
9. Soak the towels with bleach *(make sure surface is completely wet with bleach)* starting at the edges.
10. Put on a second pair of gloves prior to placing the umbilical cord in the container and especially prior to opening the umbilical cord container. *Always use a second pair of gloves when handling human tissue.*
11. Take out the umbilical cord and PBS from the water bath and place them inside the hood after wiping them down with ethanol.
12. Take out the umbilical cord from its container and wipe off the clotted blood in the paper towels. Role the cord around on the bleach-soaked towels.
13. Locate the lines where they clamped the haemostats on both ends of the cord. Cut the cord
    below the clamp marks. *Use cord container as a waste container for the pieces cut from the*
    cord. The cleaner the cut is the easier it is to locate the veins and arteries.
14. Gently slide half of the butterfly needle into the vein and clamp the cord with the needle using the haemostat. There will be two arteries and one vein, locate the artery wall for both arteries then the vein will be the vessel with the larger diameter. *You must spiral the needle around because vein spirals around the outside. NOTE – Leave the plastic casing of the butterfly needle covering the needle when inserting it into the vein. The vein looks like a stretch mark. You shouldn't have to put a lot of force when inserting the needle to the vein, there should be no resistance.*
15. Remove the extra part of the butterfly needle so that you only have the tube connected to the butterfly needle. Attach the first 20mL syringe of PBS and inject all of it slowly into the vein making sure there are no clots. If there are still clots, repeat the process with more PBS. *Make sure the cord is on top of the waste container.*
16. Attach the collagenase syringe and begin injecting the solution until the liquid coming down changes its color to gold. (It takes approximately 1 mL of collagenase of color change to occur). *Make sure to put the cord on top of the white towel to make it easier to notice the liquid color change.*

17. Clamp the other end of the cord and very carefully re-inflate the vein with the 4 mL of collagenase remaining in the syringe.
18. Carefully place everything in the autoclaved beaker which initially contained the haemostats and scissors. Cover the top with the aluminum foil taped at one side of the beaker. Be careful not to puncture the cord at any point. *Cord puncture will lead to loss of endothelial cells.*
19. Remove your outer pair of gloves and take the 2 L beaker to the incubator.
20. Leave the cord in the incubator for **20 min**.
21. Put on a second pair of gloves and take out the cord from the incubator. Remove the haemostat that is *not* holding the needle and then attach the last 20 mL syringe of PBS.
22. Place the cord on **top** of a 50 mL centrifuge tube and begin injecting the PBS in the vein very slowly to wash off the cells but avoid bursting the vein. Collect the entire solution in the 50mL tube and then discard the cord in the waste container after removing the needle and the
    haemostat holding it in place.
23. Centrifuge the tube on Setting 1 (200g for 5 min).
24. Make sure all waste goes in the biohazard bag. Clean up the hood with bleach and ethanol.
25. Take out a T-25 flask and place it in the clean hood. Label it: "HUVEC P.0, Date, Your initials, Date of Cord Harvest".
26. Remove the 50 mL tube from the centrifuge and aspirate off the supernatant. *Make sure to do*
    it carefully to avoid aspirating off the HUVECs.
27. Add 5 mL of EGM-2 into centrifuge tube and mix well. Put the cell-media solution into the flask.
28. Place the flask in the incubator overnight.
29. Place flask in the hood and aspirate off the medium. Add 5 mL of PBS and rock the flask.
30. Aspirate off the PBS and add 5 mL of PBS (2X).
31. Remove PBS and add 5 mL of EGM-2.
32. Make sure to check on HUVECs under microscope every day. Cells should be confluent (~80%) in less than 1 week. If not, throw the cells away.
33. Once the cells are confluent, trypsinize and passage them into two T-75 flasks (P0 → P1).
34. Grow to confluency and freeze them down. Label them P1 → P2. This means they will be P2 when plated.
35. Before using HUVECs for experiments, test them in vasculogenesis assay to ensure robust vessel formation consistent with prior data within the lab.

Appendix C – Preparing Microfluidic Chips for Cell Culture

*Protocol adapted from David Cleveland.

Notes:
This protocol requires the use of equipment in the Baker lab. Please email Dr. Baker for permission to use and the necessary training required.

Materials:
- PDMS (base and curing agent)
- Transfer pipette
- Microfluidic chip molds (3D printed from Protolabs)
- Vice grip (threaded rods, wingnuts, metal sheets, rubber)
- Glass coverslips (45x50 mm)
- Ethanol (100%)
- Isopropyl alcohol (IPA, 100%)
- Spatula
- Forceps
- L-Glutaraldehyde (Sigma: G6257-100mL) (0.5% - must dilute)
- Poly-L-Lysine (PLL, Sigma P8920-100mL) (0.1% - comes this way from manufacturer)
- MilliQ water
- Acupuncture needles
- Micro spatula

Equipment:
- Oven (37°C)
- Oven (60°C)
- Plasma etcher
- UV ozone

Protocol:

Day 1: Prepare PDMS molds
1. Mix PDMS base and curing agent at a ratio of 10:1 in a plastic cup and mix thoroughly with a plastic stirrer.
2. Degas PDMS under vacuum until all bubbles have been removed (time depends on volume of PDMS made but typically 30 minutes).

3. While PDMS is degassing, prepare the vice grip with plastic microfluidic mold.
   a. Each mold contains a piece of plastic bonded to rubber.
   b. One metal sheet in the vice grip has a piece of attached rubber and one does not.
   c. Stack plastic molds against the vice grip such that the front of each plastic mold is pressed against a piece of rubber.
   d. Tighten the wingnuts so the molds are securely held between the two metal sheets.
4. Cut off the tip of a transfer pipette to increase the area and use this to transfer PDMS from the cup to the molds.
5. Transfer PDMS into the molds by drizzling small amounts onto the right half of the molds.
   a. *Do this step slowly to reduce bubbles.*
   b. *Only fill the right half of the molds and allow PDMS to naturally move and fill up the left half (this reduces bubbles).*
6. When the molds are completely filled with PDMS, degas them for 10 minutes to remove bubbles.
7. Bubbles will rise out of the molds reducing the volume of PDMS within the molds, so repeat steps 5 and 6 twice more until the molds are completely full.
8. Degas the molds for 3 hours.
9. Move molds into a 37°C oven to cure for 2 days.

Day 3: Remove molds from vice grip, bond to glass coverslips, and treat for cell culture
   1. Remove molds from the oven.
   2. Unscrew wingnuts.
   3. Use a spatula to separate one metal sheet from the mold, separate the first mold from the second, and separate the second mold from the other metal sheet.
   4. Gently insert forceps into the top of the mold to separate the cured PDMS chip from the mold.
   5. Inject 100% ethanol to help release the PDMS from the mold.
   6. Use the forceps to gently remove the entire PDMS chip from the mold.
      a. *Be very careful not to break the thin plastic features on the mold.*
      b. *If the PDMS chip is stuck to the mold, add more ethanol to help release it.*
   7. Use a razor blade to cut the extra sliver of PDMS at the edge so the chip will fit on a glass coverslip.
   8. Clean the glass coverslips and PDMS chips with IPA and ethanol rinses.
      a. Rinse a coverslip with IPA on both sides.
      b. Rinse the coverslip with ethanol on both sides.
      c. Use the air gas line with tubing attached to dry the coverslip.
      d. Place the cleaned coverslip rested against the lid of a petri dish.
   9. Repeat step 8 for all coverslips and PDMS chips.
   10. Take the cleaned chips and coverslips down to the Baker lab to use the plasma etcher to bond the two pieces together.
   11. Place an equal number of coverslips and PDMS chips in the plasma treating cage (two of each fit).
      a. *The chips should be feature side up (i.e., upside down).*
   12. Run the plasma cycle for 1 minute.

      a. If the plasma etcher is not set to 1 minute you must change the time (commands → plasma time → change to 1 minute).

      b. If the plasma etcher is set to 1 minute you are ready to run it (commands → plasma → start)

      c. If the plasma etcher has not run for the day, it can take a few minutes to reach the vacuum set point.

13. Once the cycle is over, release the hinge to open the door. Once the vacuum is released, the door will open.

14. Remove one coverslip and one PDMS chip from the cage and place them together.

      a. Adhere the two surfaces that were upward facing during the plasma cycle.

      b. The feature side of the chip should be facing down and adhered to the glass.

      c. Use your fingers to ***gently*** press the two together.

      d. Place the bonded chip down on the bench and use your finger as a rolling pin going over the PDMS side of the chip (not the glass side) multiple times to ensure it is well adhered.

      e. Use your finger to place extra pressure on the surfaces you want to be extra sure are adhered (the gel chamber and each piece between two media wells).

15. Transfer the chips to a 60°C oven for at least 1 minute.

16. Remove the chips from the oven and place them on the bench.

17. Use your finger as a rolling pin again to flatten out the chip (the glass can bend while in the oven).

18. Place a kimwipe over the chip.

19. Place a weight on top of each chip for 5 minutes.

      a. The Baker lab has two petri dishes filled with metal beads to use, but it could be anything heavy if these are in use.

20. Attempt to lift each corner of the PDMS from the glass. If the corner does not lift, then it is well sealed. If the corner does lift, the chip is not well adhered to the glass and may not be suitable for culture.

21. Repeat steps 11-20 for all remaining chips.

22. Bring bonded chips back to our lab.

23. Take a P2 pipette tip and insert it into all of the insertion ports to make sure there is not a thin film of PDMS covering the port.

      a. Any PDMS film over these ports will cause fluids to not be inserted uniformly into the gel chamber.

24. Inject PLL into the insertion ports for each device and leave at room temperature for 1 hour.

      a. Soak a paper towel with water and ring it out. Place this next to the chips and cover with an ice bucket. This will prevent evaporation of the PLL.

25. Aspirate the PLL from each device.

26. Inject MilliQ water into each device to rinse out the PLL.

27. Aspirate the MilliQ water.

28. Repeat steps 26 and 27 once more.

29. Inject 0.5% glutaraldehyde into each device and leave at room temperature for 15 minutes.

      a. Soak a paper towel with water and ring it out. Place this next to the chips and cover with an ice bucket. This will prevent evaporation of the PLL.

30. Aspirate the glutaraldehyde from each device.
31. Inject MilliQ water into each device to rinse out the glutaraldehyde.
32. Aspirate the MilliQ water.
33. Repeat steps 31 and 32 twice more.
34. Place chips in an oven overnight to dry (temperature is not critical).

Day 4: Insert needles and UV ozone treat the chips
1. Ensure needles are cleaned.
2. Place a single needle in each needle track (8 per chip).
3. Use a micro spatula to push on the needle within each media well and on either side of the chip to ensure they are all at the same level.
4. Bring the devices and a sterile P150 petri dish to the Baker lab.
5. Place the chips in the UV ozone and sterilize for 5 minutes.
6. After the cycle has completed, place the sterilized chips in the sterile petri dish.
7. Bring the sterilized chips back to our lab. They are now ready for cell culture.

Appendix D – Encapsulating Cells in a 3D Microfluidic Chips

Materials:
- Bovine Thrombin
- Bovine Fibrinogen
- FBS
- Media (SF-EGM2, EGM2, DMEM + 10% FBS)
- PDMS coated plates
- Trypsin (0.05%)
- PBS (1x, no calcium or magnesium)
- Microfluidic chips prepared according to Appendix C
- Vacuum Grease
- Forceps
- 18 G needle
- 5 mL syringe
- 33 mm 0.22 μm filter
- Microcentrifuge tubes
- 150 mm petri dish
- 100 mm petri dishes (coated with cured PDMS)

Protocol:
1. Get fibrinogen alliquot from -20ºC freezer and place it on the counter to warm to room temperature (15-20 min).
2. Put trypsin and all media needed (SF EGM2, DMEM +10% FBS, EGM2) in the 37ºC water bath.
3. Prepare an ice bucket for cells and reagents.
4. Get FBS from sterile fridge and place on ice.
5. Get thrombin from -20ºC freezer. Thaw by on ice or by holding in palm for a minute or so.
6. Spray off PDMS plates (1 per chip) with ethanol and place in the hood to dry.
7. Measure the fibrinogen needed to get to final concentration of 2.5 mg/mL for all gels (for 2 chips plus 2 bulk gels need 1.2 mL plus some extra for filter loss --> make at least 1.5 mL). Need 5.55 mg/mL for chips, can use any concentration for bulk gels that will satisfy the clottable and pure protein percentages.
8. Add appropriate amount of SF EGM2 to reach 5.55 mg/mL. Allow solution to dissolve in 37ºC water bath.
9. Trypsinize cells as in other protocols
    1. Aspirate media

2. Wash with 1xPBS and aspirate
3. Add appropriate amount of trypsin for flask size (3 mL for T75, 10 mL for T225)
4. Incubate for 5 min
5. Check under microscope to ensure all cells have been trypsizined and are lifted off of the plate. If not fully lifted, tap the edges of the flask to dislodge the adhered cells.
6. Quench trypsin with appropriate amount of serum containing DMEM (regardless of cell type i.e., this is fine for HUVECs too)
10. Clean off hemocytometer (spray with ethanol) and coverslip and bring both into the hood.
11. Spray with ethanol a tube for each cell type and bring into the hood (tube size will depend on flask size)
12. After quenching trypsin, remove a 10 μL sample of each cell suspension for the hemocytometer.
13. Centrifuge cells on program 1 (200g for 5 min).
14. Count cells on the hemocytometer.
15. Suspend cells in SF EGM2 at desired concentration for each cell type (typically 20M/mL stromal cells, 10M/mL endothelial cells).
16. Place cells in ice bucket until ready to use.
17. Swirl fibrinogen solution if not fully dissolved.
18. Sterile filter the fibrinogen solution. Attach an 18G needle to a syringe and pull up the solution. Remove needle and attach 0.22 μm filter. Filter into a clean tube.
19. Prepare 1.5 mL centrifuge tubes for fibrin solutions. New tube for each set of 4 devices.
20. Mix the ingredients in this order:
    1. 20 μL HUVEC suspension
    2. 20 μL stromal cell suspension
    3. 20 μL FBS
    4. 4 μL thrombin
    5. 136 μL fibrinogen
21. Add the fibrin solution to each device (start with right side and fill until it reaches the left gasket).
22. Allow devices to gel for 5 min in the hood (pipette aid off).
23. Move the devices to the incubator for 30 min.
    i. 7 minutes rightside up
    ii. 8 minutes upside down
    iii. 15 minutes rightside up
24. Place remaining HUVECs on ice (they will be used later to seed the channels).
25. After 30 min of gelation, add EGM2 to all of the wells so gels can swell.
26. After swelling, remove half the media in each well and remove needles with sterile forceps/tweezers.
27. Transfer device to PDMS plate.
28. Add vacuum grease to all holes (middle and edges).
29. If not already diluted, dilute remaining HUVECs to 2.5 M/mL solution in EGM2.
30. Add 20 μL of 2.5 M/mL HUVEC suspension to both channels of each device and incubate for 30 minutes upside down.

       i.   Check each channel for flow of cells through the channels. If cells are not flowing, remove air bubbles or adjust hydrostatic pressure by adding media to opposite well.

31. Add 20 µL of 2.5 M/mL HUVEC suspension to both channels of each device and incubate for 30 minutes right side up.
       i.   Check each channel for flow of cells through the channels. If cells are not flowing, remove air bubbles or adjust hydrostatic pressure by adding media to opposite well.

32. Aspirate all media and add EGM2 to all wells.
33. If media does not flow through, check all the channels for air bubbles.
34. Change media every day until permeability measurements/fixing/staining.

Appendix E – Traction Force Microscopy Protocols

*Protocol adapted from Yen Kong

Functionalizing Coverglass with Glutaraldehyde (per Aratyn et al. from the Gardel Lab) (~3-4 hours) (Day 1)

PPE: lab coat, gloves, safety glasses. During piranha part also wear face shield and black apron. (can wear special silver gloves as well – if you do not, be very careful not to get piranha on your gloves). Change gloves after using piranha.

1. Load coverglass into silver metal slide holders.
2. Clean coverglass with piranha (3:1) for 30 minutes in a clean 2000 mL beaker.
   a. To make piranha, add 100 mL H_2O_2 to 300 mL H_2SO_4 in the beaker (contained within a water bath). *The water bath prevents the piranha solution from heating up too high and etching the metal coverglass holders.*
      i. Place H_2SO_4 in the piranha beaker and place beaker in the water bath (DI water).
      ii. Slowly add H_2O_2 and wait for steam to settle.
      iii. Place the metal coverglass holders in the piranha solution using the spring-loaded handle/holder.
      iv. Gently swish around the fluid a few times during the 30 minutes.
   b. Hydrogen peroxide (H_2O_2) is kept in the deli fridge and sulfuric acid (H_2SO_4) is kept below the fume hood.
3. During step 1 wait time, start warming the glutaraldehyde (GA) in a water bath. Fill a beaker with DI water and place on the hot plate in the fume hood. Turn to 60 °C. Put a stir bar in the bath and turn on stirring function. Add the conical tube of GA from the -20 freezer (pre aliquoted) and make sure the cap is sealed tightly.
4. Rinse coverglass in DI water for 5 minutes under a constant flow of water.
   a. Remove the piranha beaker from the water bath and dump the piranha into a waste container. *Do not cap this waste container too tightly because it could explode. Waste bottle should be a special coated bottle. NO OTHER WASTE CAN GO IN THIS BOTTLE—PIRANHA ONLY.*
   b. Dump the water out of the water bath glass container and wipe it down with paper towels.
   c. Place the slides in the glass container and bring to the DI water spout in the Stegemann lab. Fill the container so the slides are fully covered (careful not to

point the flow the water directly at the slides so they do not move out of the holders).

5. Final rinse in IPA while preparing the next step (time not specific, as long as it takes to prepare the next step).
   a. Transfer the coverglass holders to the IPA wash bucket and cover the slides with IPA.
   b. Partially dry the coverglass.
6. Prepare 2% 3-aminopropyltrimethoxysilane in the gray plastic tub and soak coverglass for 10 minutes.
   a. There is a marked glass Pasteur pipette (black marking is one mL). Use this marked pipette to make a new one to use today (the solution dissolves the marker). Only use glass, not plastic (will dissolve it).
      i. Rinse the new glass Pasteur pipette with IPA (draw up and eject).
   b. Bring a new stir plate and stir bar into the fume hood → use small stir bar because gray tubs are small and you do not want to hit the glass slides.
   c. Add 7 mL of 3-aminopropyltrimethoxysilane to 350 mL of IPA in the gray tub.
   d. Place coverglass holders in the solution for 10 minutes (stirring).
7. Rinse 3x 5 minutes with ddH$_2$O. Rinse 1x 10 minutes with ddH$_2$O.
   a. Dump the IPA into a new waste bottle.
   b. Wash the 3-aminopropyltrimethoxysilane gray tub with IPA and dump into waste container.
   c. Wash the slides in a new glass rinse beaker.
   d. Dump the first two rinses into the waste containers. Third and fourth rinse can go down the sink.
8. When GA is thawed, add 14 mL of 25% GA to 336 mL ddH$_2$O (final concentration 1% GA) in the gray tub. Soak coverglass in GA for 30 minutes (stirring).
9. Rinse 3x 10 minutes with ddH$_2$O.
   a. Pour GA into waste bucket then rinse the gray tub.
   b. Rinse in the same glass rinse beaker.
   c. First rinse goes into waste, the remaining two rinses can go down the drain.
10. Dry the glass slides at room temperature under the laminar flow hood and cover with aluminum foil.
    a. Functionalized coverglass can be kept in aluminum foil at RT for two months maximum.

Preparing Polyacrylamide (PA) Gels with Fluorescent Beads (~3 hours) (Day 2)

1. Make sure each molds have a small piece of double sided tape on the center
2. Clean coverglass mold 24x60 mm with 100% ethanol under biosafety hood and leave to dry. Dry near the back of the hood because that's where there is the most air flow.
3. Place treated coverglass in the hood and expose to UV for 10 minutes.
4. Mix 40% acrylamide, 2% bisacrylamide, 10x DPBS, and ddH$_2$O to form the prepolymer solution in a microcentrifuge tube. *See table for amounts of each.*

E (KPA)	ACRYLAMIDE	BIS-ACRYLAMIDE	VOLUME OF ACRYLAMIDE (UL)	BIS-ARYL. VOLUME (UL)	10X DPBS (UL)	H2O (UL)
0.2	3%	0.03%	75	15	100	**810**
2.0	4%	0.1%	100	50	100	**750**
20.0	8%	0.264%	200	132	100	**568**
50.0	12%	0.145%	300	72.5	100	**527.5**
90.0	12%	0.28%	300	140	100	**460**
127.0	12%	0.55%	300	275	100	**325**
200.0	**15%**	**0.9%**	**375**	**450**	**100**	75

Table E.1: *Volumes of reagents needed to fabricate acrylamide gels with varying Young's Modulus (E).*

5. Vortex mixture and then pulse for 5 seconds on the centrifuge to remove everything from the cap.
6. Degas the mixture for 15 minutes. Periodically tap the vacuum jar to dislodge gas bubbles from the microcentrifuge tubes.
7. Prepare fluorescent beads by mixing 3 μL of fluorescent beads (from commercial stock solution or alliquot) with 27 μL of ddH$_2$O in the sterile hood.
8. Sonicate bead mixture for a few seconds to prevent beads from clumping together (very important because clumps make it hard to do analysis/post processing).
9. Prepare 10% APS solution mixed in ddH$_2$O in a microcentrifuge tube. *APS is in chemical cabinet (brown bottle with yellow label).*
10. Prepare the centrifuge (el sayed centrifuge not ours) with counterbalance: 500 rpm for 10 minutes.
11. When prepolymer solution has degassed, add 0.5 μL of TEMED (in flammable cabinet-small bottle with red top) catalyst and add 5 μL of APS to the prepolymer solution. Vortex for 2 seconds.
12. Filter the prepolymer solution (100 μL total) with 0.22 μm syringe filter.
13. Add 20 μL of fluorescent beads to prepolymer solution.
14. Place 24 μL drop of prepolymer solution onto each coverglass mold.
15. Place treated coverslip on each drop of gel. Be careful not to get any bubbles. If bubbles are formed, attempt to move the coverslip around to get rid of them (if not removed the substrate cannot be used).
16. Centrifuge the substrates for 10 minutes.

17. Let the substrates stand for an additional 20 minutes.
    a. Or you can modify steps 16 and 17 (ex: centrifuge for 20 min and let stand for an additional 10 min), but the total time should be 30 min.
    b. Could do 30 min centrifuge and no additional time as well.
18. Prepare buffer solution
    a. X = number of substrates made
    b. X+1 x 2 mL of DPBS + 1/1000th gentamicin in 50 mL tube
    c. Add 2 mL of buffer solution to each well of a 6-well plate (one substrate per well)
19. After the gel has polymerized, spread 500 μL of ethanol around the edges of the coverglass (drop with a pipette).
20. Carefully wedge a razor blade between the gel and mold to remove coverglass.
21. Grab coverglass/substrate with forceps and place it in the buffer with the gel side facing up.
22. Wrap well plates in parafilm then aluminum foil.
23. Store in 4 °C fridge for up to one week.

Conjugating ECM (collagen) onto PA hydrogels with Sulfo-Sanpah (Day 3)

1. Bring UV lamp (with plastic boxes for support), MES buffer, sulfo-sanpah, 6-well plates, and PA substrates to the sterile hood.
    a. Sulfo-sanpah is 100 mg/mL stock solution in DMSO.
    b. 0.1 M MES, 0.5 M NaCl pH=6.0 buffer (MES buffer)
2. Rinse PA gels with MES Buffer (careful not to get too close to the gel with the aspirator).
3. Dilute sulfo-sanpah (30 μL sulfo-sanpah with 12 mL of MES buffer) in a 50 mL tube. Cover sulfo-sanpah with aluminum foil. *Total volume will depend on how many substrates you are making.*
    a. Calculation: 2*number of substrates*(30/12) = μL of sulfo-sanpah needed (add an extra 0.5 mL – 1mL to the number of substrates number to account for pipetting loss. EX: making 5 substrates, instead of 2*5 = 10 use 10.5 or 11
4. Aspirate buffer from PA gels Add 1mL of sulfo-sanpah solution to each well. Remove the cover and place the plate under the UV lamp for 8 minutes. Shake the plate around. Leave under UV for another 8 minutes.
5. Aspirate sulfo-sanpah and rinse with 2 mL of buffer per wash for 3 washes. Between each wash, lift the substrates off the plastic well (just one side to get fluid under the substrate). *This is very difficult to lift the substrates so take time to do it carefully.*
6. Dilute collagen with DPBS (without Ca^{2+} and Mg^{2+}) to 50 μg/mL.
    a. Need 1 mL per substrate.
    b. Add collagen to the conical tube first then add PBS to the collagen dropwise while gently shaking the tube to mix.
    c. μg need/stock concentration (μg/mL)
        i. EX: 8 substrates → need 400 μg of collagen to get 50 ug/mL
            1. Stock collagen is 5.9 mg/mL
            2. 400 μg / 5900 μg/mL = 67.8 μL of collagen needed
7. Add 2 mL of DPBS to each well. Aspirate DPBS. Add 1 mL of collagen solution to each well. Set plates on the rocker at speed 3 for 2.5 hours (covered in aluminum foil).

8. Aspirate collagen solution. Rinse with 2 mL of DPBS in each well. Remove DPBS.
9. Add PBS with 1/1000th gentamicin.

Plating Cells onto the Substrates (~45 minutes) (Day 4)

1. Trypsinize and count cells.
2. Suspend cells to be seeded at 1000 cells/cm^2
   a. 22 mm^2 (0.22 cm^2) coverglass → need a total of 220 cells per coverslip
   b. 1 mL of cell suspension added to each well → 220 cells/mL suspension needed
3. Aspirate PBS.
4. Add 1 mL of cell suspension to each well.

Imaging (Day 5)

*add calcein AM before imaging if using that instead of phase (follow instructions in the kit in -

20C freezer)

1. Warm up environmental chamber to 37 °C, 5% CO$_2$. *This is important to prevent thermal drift which can alter saved positions.*
2. Clean 24x50 mm coverglass in 100% ethanol.
3. Place substrate on top of big coverglass (cell side in contact with the glass).
4. Use magnets to place 24x50 mm coverglass in place in the environmental chamber.
5. Pin the substrate to one side of the larger coverglass (move the substrate so the edge is lined up to one edge of the larger glass).
6. Set up brightfield - Adjust for Koehler illumination
   a. Move phase ring to 3.
   b. Close iris on the top of the microscope.
   c. Lower condenser until you see the iris through the eyepiece (move closer to center with the knobs).
   d. Open iris back up.
   e. Move phase ring to 1 or 2 if you can't see the cells.
7. Move the stage and set the origin at the upper left corner (or any corner you choose). This is critical so you can find cells again if the stage skips.
8. Find focus. Make sure you see two different bead planes so you are imaging in the well (if you do not see two bead planes, move locations).
9. Image at the upper bead plane (that's where the cells are). Image away from the pinned side so the cells lyse easier.
10. Find focus on cell plane in 20x.
    a. First find focus in 4x. then find focus in 10x and then find focus in 20x. This will help ensure you know where you are imaging.
11. For BF: in the acquire window, increase the exposure time so the histogram of pixel intensity (green) is centered (~100 ms).

12. Find cells and focus. Center the cell in the image. Make sure there is only one cell in the image → no parts of other cells can be in the field of view.
13. Hit memorize in the move stage to absolute position window.
14. Label the position as the cell number you are on (1,2,3,4…
15. Skip any weird looking cells as this could alter the data. Don't use cells with really long fillapodia that go to the corners because you won't get the full force/displacement field in the image.
16. Every once in a while, switch to red channel to make sure you still see two bead planes (can usually see the edge of the well in BF).
17. After you have found all the cells, go through the list and check that each cell is still there (in case the stage skipped or anything else happened). It is okay if z focus is off because you will refocus before imaging.
18. Image each cell in phase, red (beads), green (calcein AM).
    a. 100 ms for phase, 400 ms for fluorescent channels.
    b. Change neutral density (ND) filters on the left side of metamorph screen if the intensity is too high.
    c. Refocus for each image. For beads, usually need to zoom in to see if it is in focus.
    d. On the green channel, let any photobleaching occur until the green is only within the cell's location not outside the cell.
    e. To move from cell to cell, hit move to next in memory list.
    f. If the stage skips, go back to the corner you set the origin at and set the origin again (but do not change the relative positions saved in the memory list).
        i. Go back and check the previous cell and then image the next one.
19. After all images are acquired, add lysis buffer to the three unpinned sides, being VERY careful not to touch the slide and move it. Let lysis buffer sit for 10 min.
    a. Lysis buffer is 10% SDS in water. *Takes a long time to dissolve when making it.*
        i. 1% = 10mg/mL, 10% = 100 mg/mL
20. While lysis buffer is on the slide, save all acquired images.
21. After lysis, switch to red channel at 400 ms.
22. Close all images, except red (bead planes).
23. Make sure the live window is the same size as the acquired bead plane images.
24. Start at cell 1 to image the bead planes after lysis. Align the live view with the acquired image at the top edge and the side edge. Acquire new image.
25. Check overlay of the cells (only need to do this for one or two because this will all be done in photoshop for post processing). Display → overlay images. Pick red for one image and green for the second image. If fully aligned, the color will be yellow. Align the corners (should align well), center won't be aligned because of cell traction.
    a. In some cases there is rotation, which is accounted for in post processing.

Post Processing (Any day)

1. **Photoshop → align the bead planes**
    a. Open both bead images and cell image (either calcein AM image or phase image) in imageJ and convert to 8-bit images
        i. Do this for every image all together

1. Process → batch → convert
   a. Input: choose folder where images are saved
   b. Output: make a new folder
   c. Interpolation: bilinear
   d. Output format: 8-bit TIFF
b. Open images in photoshop (one cell at a time → both bead planes and cell image)
c. Convert beads 2 image into RGB color (image → mode → RGB color)
d. In the layers tab: right click background and label it beads 2
e. In channels tab: choose red color, delete blue and green (control a, delete)
f. Shift F5 to make the background black on green and blue channels → need to get red beads on black background to show
g. Beads 1 → copy image (control a, control c)
h. In beads 2 image, layers tab: add new player and paste beads 1 image in.
   i. Control shift n to get a new layer.
   ii. Control v to paste beads 1 .
   iii. Label this image beads 1.
   iv. Close beads 1 image.
i. On the beads 1 layer, delete red and blue → get green beads on black background
j. Copy cell image: control a, control c
k. Make a new layer in the beads 2 image: control shift n
   i. Paste cell image in the new layer: control v
   ii. Label as cell.
   iii. Close cell image.
l. Beads 1 layer should be on top of beads 2 layer. Cell layer in the middle.
m. Link cell image and beads 1 so they move together
   i. Click on both layers, right click, link layers
n. Make beads 1 layer 50% opacity.
o. Zoom in to a corner and align the two bead layers (yellow is a complete overlay). Check all four corners and ensure they have fully yellow beads.
   i. Use move tool in toolbar and the arrow keys to control it.
   ii. If it is yellow in one corner and not in another that means there is rotation which needs to be accounted for.
      1. To account for rotation, select the rotation tool and change the angle of the image (usually less than 1 degree). *Will need to move the crosshair tool around on the image.*
p. Crop the image to avoid any edges where the images are not aligned. Save the image as a cell#_crop.psd.
q. Make beads 1 100% opacity.
r. On beads 1 layer, copy the green channel into the red and blue channels and clock RGB (should see white beads on black background). Do this for beads 2 as well.
s. Create a new window (control n). Copy beads 1 and paste it in the new window. Flatten the image (layer → flatten image). Save this as cell#_beads1_aligned.TIFF
t. Repeat step s for beads 2 and the cell images.

2. **ImageJ → make a stack, PIV, FTTC**
   a. Make a stack in imageJ of both bead images.
      i. Open both images. Image → stacks → images to stack

201

      ii. Make sure beads 2 is the first image in the stack and beads 1 is the second image in the stack (system reads no traction first then traction). If it is backwards: image → stacks → tools → reverse

b. PIV analysis (creates a map of displacement vectors created by the traction of the cells)
      i. Plugins → PIV → PIV basic
      ii. Save the output file.

c. FTTC Analysis (quantifies the displacement vectors created by the cells)
      i. Plugins → FTTC → zeroth order
           1. Parameters
               a. Pixel size for 20x images: 0.32786
               b. Poisson ratio: 0.5
               c. Young's modulus: 2000 Pa
               d. Keep everything else the same (0s)
           2. Choose the PIV file you saved in step B. the output from FTTC will automatically save in the same folder.

d. MATLAB (Yen's custom script uses the FTTC displacement vector quantifications to determine total traction, mean traction, etc.)
      i. Run Yen's code using the FTTC file.
      ii. Copy total traction, mean traction, and median traction into excel or graphpad.

Appendix F – Fluorescent and Immunofluorescent Staining and Imaging

Staining
*These protocols assume samples have already been fixed and washed. Once samples are fixed and washed, staining can be done immediately or delayed to a different day.

Solutions Needed:

1x TBS:
1. Start by preparing 10x TBS
   a. Measure out 44 g of sodium chloride and add to a 500 mL glass bottle.
   b. Measure out 15.75 g of tris base and add to the same bottle.
   c. Add 500 mL of DI H_2O.
   d. Balance the pH to 7.4 with hydrochloric acid.
   e. Fill remaining volume to 500 mL with DI H_2O.
2. Dilute 10x TBS to 1x TBS.
   a. Add 100 mL of 10x TBS and 900 mL of DI H_2O to a 1 L glass bottle.

TBS-T (0.1% Triton X-100 in 1x TBS)
1. Calculate the amount of Triton needed for desired volume of TBS-T.
2. Add this volume to the TBS and vortex to mix into solution.

2% BSA in TBS-T
1. Weigh out BSA powder at 20 mg/mL (i.e., 2%) and place in a conical tube.
2. Add appropriate volume of TBS-T based on final mass of BSA weighed out.
3. Place conical tube in the rotisserie to dissolve BSA into solution.

1% BSA in TBS-T
1. Weigh out BSA powder at 10 mg/mL (i.e., 1%) and place in a conical tube.
2. Add appropriate volume of TBS-T based on final mass of BSA weighed out.
3. Place conical tube in the rotisserie to dissolve BSA into solution.
4. Alternative is to dilute 2% BSA solution 1:1 with fresh TBS-T.

*Note: BSA solutions are only stable for 1 week at 4°C.

Fluorescent Staining using Pre-conjugated Stains

UEA (red, identifies endothelial cells, human only), DAPI (blue, identifies all cell nuclei, not species specific), Phalloidin (green, identifies F-actin, not species specific), GSL (far red, identifies endothelial cells, for rodent cells). These stains do not require permeabilization or blocking.

1. Prepare staining solution in 1x TBS.
   a. 1:200 UEA (vector laboratories)
   b. 1 ug/mL DAPI (1:100 from our stock)
   c. 1:200 Phalloidin (Invitrogen)
      i. This dilution is for when the stock vial is reconstituted in methanol. If DMSO is used, the dilution is different because the stock is then a different concentration.
2. Add staining solution to gels (usually half the volume used to feed gels – ex: gels in 48 well plate use 500 µL of media for feeding but 250 µL of stain solution) overnight at 4C covered in foil.
   a. One exception is microfluidic chips in which the media reservoirs need to be filled with stain solution.
3. Remove staining solution and wash 2x 5 minutes and then overnight in 1x TBS.
4. Wash 1x 5 minutes in 1x TBS.
5. Remove 1x PBS and replace with fresh 1x TBS.
6. Parafilm samples and maintain covered in foil in a 4°C fridge until ready to image.
   a. If performing quantitative analysis on samples, be sure to image within similar timeframes for all sample sets. If just qualitative, images can be taken when convenient.

Immunofluorescent Staining with Primary and Secondary Antibodies

1. Permeabilize samples in 0.5% Triton X-100 in 1x TBS for 1 hour at 4°C.
2. Remove permeabilization solution and wash 3x 5 minutes each with 1x TBS.
3. Prepare blocking solution: 2% BSA in TBS-T.
4. Block samples in blocking solution overnight at 4°C.
5. Remove blocking solution and wash 3x 5 minutes each.
6. Prepare primary antibody stain in 1% BSA in TBS-T and stain overnight at 4°C.
7. Remove antibody stain solution and wash 2x 5-minute washes and then overnight with TBS-T.
8. Wash 1x 5 minutes in TBS-T.
9. Prepare secondary antibody stain in 1% BSA in TBS-T and stain overnight at 4°C covered in foil.
   a. *If staining for any pre-conjugated stains (i.e., UEA, DAPI), include them in the secondary antibody solution.*
   b. *Multiple secondary antibodies can be used in one solution as long as the primary and secondary antibodies were raised in different hosts.*
10. Remove antibody stain solution and wash 2x 5-minute washes and then overnight with TBS-T.
11. Wash 1x 5 minutes in TBS-T.
12. Remove TBS-T and replace with fresh TBS-T.
13. Image samples within 1 week after antibody staining.

*Note: Once samples are fixed and washed, they do not need to be stained right away. If there is a delay between fixing/washing and staining/washing, parafilm samples and keep in a 4°C

fridge. There can be a break after any washing step (i.e., after fixing and washing before any staining and/or after primary antibody staining and washing before secondary antibody staining).

*Note: All wash steps use the same volume as the volume of media during culture, volume is only reduced for stains to prevent excessive use of antibodies.

*Note: Samples can be maintained long term in TBS or TBS-T at 4°C covered in foil.

*Note: For quantitative analysis, imaging should be done on the same day using the same imaging parameters.

*Note: Triton X-100 is very viscous and takes a long time to fill up and eject from a pipette. Ensure you wait about 30 seconds – 1 min for fluid to fully fill the pipette before use. When ejecting these fluids, eject slowly. Pipette up and down in the solution to wash the remaining triton from the inside of the pipette to ensure the right amount is used in your solution. Vortex the solution until the triton goes fully into solution (this creates a lot of bubbles, but they will eventually settle out).

Imaging on the Olympus IX81 with Hamamatsu Camera

Microscope Basics
1. Take the cover off of the microscope.
2. Turn on the microscope.
   a. Turn on the UCB (main microscope).
   b. Turn on the Hamamatsu camera.
   c. Turn on the Prior automated stage.
   d. Turn on the mercury bulb if doing fluorescent staining.
      i. Mark the date, bulb hours, time, and initials on the sheet.
3. Open Metamorph Premiere software.
4. To take images and use the automated stage, two key windows are needed – acquire window and move stage to absolute position.
   a. Open acquire window: in the tool bar select acquire and then in the drop-down menu select acquire.
   b. Open stage window: in the tool bar select devices then in the drop down select stage → move stage to absolute position.
5. Acquire window basics
   a. Acquire: captures the current field of view.
   b. Auto scaling: automatically determines the minimum and maximum exposure limits for the field of view.
   c. Show live: this opens a window showing the live view of the sample. To close this window you must click stop live (the show live buttons turns to stop live when live is on), it will not close by clicking the x in the right corner.
6. Move stage to absolute position basics
   a. Set origin: this creates a new 0, 0, 0 origin at the current location

b. X, Y, Z location boxes: this shows the current x, y, z location relative to the arbitrarily set origin.

c. Move to origin: moves the field of view from current location to origin.

7. View options

a. The microscope has three view option: binoculars, camera, and DSU.

b. Binoculars: view through the microscope eye pieces. If you click "show live" the window that pops up will show static in the color channel you are on and only have a clear view through the binoculars.

c. Camera: view through the Hamamatsu camera

d. DSU: uses the DSU to enter confocal mode and view a single z plane.

8. Filters

a. The microscope has four fluorescent filter cubes and brightfield/phase options. *Red, green, blue, and brightfield are in the left-hand panel, far red must be accessed through the camera/filter drop down menu.

b. Red: mCherry filter (binoculars, camera, and DSU)

c. Green: GFP filter (binoculars, camera, and DSU)

d. Blue: DAPI filter (binoculars, camera, and DSU)

e. Far red: Cy5 filter (camera and DSU only)

f. Gray: brightfield and phase

    i. Brightfield and phase are both within the gray color selection that uses the standard lamp not the mercury lamp

    ii. To change between brightfield and phase, the ring must be switched.

Imaging Modes

- Brightfield (BF) imaging using the standard halogen lamp on the microscope illuminating the same from above and imaging from below the sample. Features within the sample will diffract light causing optical disparity and contrast within the image.

- Phase contrast imaging also uses the halogen lamp illuminating the same from above and imaging from below the sample. However, phase contrast imaging provides better contrast to view the sample through the use of annular phase rings. On our microscope, the phase rings must be changed for 4x and 10x imaging or BF imaging.

- Widefield (WF) imaging uses the epifluorescent mode of the microscope. In this mode, the sample is illuminated with light exposing the entire field of view with unfocused light. The sample is illuminated and imaged from below the sample. WF imaging is good for a single plane image, but not for z-stacks.

- Confocal microscopy increases the optical resolution of images by focusing light through a pinhole to eliminate out of focus light and thus yields a better signal-to-noise ratio than WF imaging. Laser scanning confocal microscopes use a single pinhole, while disc spinning units (DSU) employ a disc that is covered with pinholes. The pinholes block out of focus light and therefore requires longer exposure times than WF imaging. Confocal imaging should be used for all z-stacks. All vessel quantifications should be done using Z-stacks obtained using the DSU.

<u>Journals</u>
*Journals are automated imaging settings that allow you to set the image location and depth and then the journal will instruct the microscope through the rest of the process. These are ideal for imaging confocal Z-stacks using the DSU.

*It is far easier to save someone's existing journal and modify it as needed for your imaging needs.

1. Open the journal editor.
    a. Select journal in the tool bar and then select edit journal from the dropdown menu to bring up an existing journal.
    b. In the journal editor window, select file, then save as and rename the journal with your initials for your own needs (typically the colors used and size of Z-stack/slice depth).
    c. Required journal elements to capture Z-stacks:
        i. Select magnification: this allows you to select the magnification to run the journal on. *If the microscope is not set to this magnification when you run the journal, the journal will prompt the microscope to switch it.*
        ii. Run journal, acquire – Load Setting, acquire Z series
            1. These three elements are required for each color channel you want a stack of.
            2. Run journal loads journals that have already been established on the computer for loading the appropriate view and color options.
                a. i.e., "GFP_DSU" journal sets the microscope up to image using the GFP filter cube using the DSU and "mCherry_camera" journal sets the microscope up to image using the mCherry filter using the camera without DSU in the widefield settings.
            3. Acquire – load setting will load the settings in the acquire window (i.e., exposure time, auto scaling, etc.).
            4. Acquire Z series instructs the microscope to image a Z-stack with specified total depth, slice depth, and number of slices.
                a. This information is input by the user and must be identical for all color channels used.
                b. In this window, you will also select where you want the stack to start at. I use origin so I can set the origin at the plane I am interested in imaging. If it is set to something else, be sure it is consistent for all stacks and use the stage window accordingly.
        iii. Run journal, acquire – Load Setting, acquire – start live
            1. These three are for showing the live window after all Z-stacks have been acquired.
            2. Typically, this is set to the mCherry widefield setting to view UEA stained vessels and find a new imaging position.
    d. After editing the journal, save it. The microscope will not run an unsaved journal.
2. Image using your journal.

a. There are two options to use the journal.
b. If you are only taking one set of Z-stacks, choose the run journal option.
  i. From the toolbar select journal, then in the drop-down menu select run journal.
  ii. *This command runs the journal once without opening the journal window.*
c. If you are taking multiple sets of Z-stacks, choose the edit journal option.
  i. From the toolbar select journal, then in the drop-down menu select run journal.
  ii. *This command opens the journal editor window. From here you can select the run journal button. After running, the editor window will remain open, and you can easily press the button again once you have moved to a new imaging position.*
d. If you want to image only some stains within your journal, choose the edit journal option.
  i. From the toolbar select journal, then in the drop-down menu select run journal.
  ii. *In the journal editor window, you can disable commands. So, if your journal is for red, green, and blue but you only want to image red and blue, use the same journal and just disable the green commands and save the journal. You can reenable them at any time.*
e. When used in this way, the journal will image through the entire Z-stack for one color channel, then change filters and image the next color, and so on. You will then have separate Z-stacks for each color at the same position.

Scan Slide
- Scan slide is used when a sample is larger than the field of view. The app will stitch multiple images together to capture the entire sample.
- To run the scan slide, you need to set the save location and image name, set the location by setting the top left and bottom right corners, select the view and filter options, and set the number of wavelengths.
  o Once you set the corners, the program will determine the number of images to take and stitch together.
  o If using multiple wavelengths, the program runs differently than journals. It will image each wavelength at one position before moving to the next. The end result is still a single stitched image for each wavelength.
    ▪ The program saves every individual image and the stitched image in the folder set by the user.
- Scan slide can only be single plane images, not Z-stacks.
- If the objects in a stitched image are not properly aligned, then the calibration needs to be redone. Use the calibrate from live mode option.

*Scripts modified from Ben Juliar

Generating Maximum Intensity Projections from Z-stacks for Vessel Quantification
*Used on 4x and 10x stacks

//This macro creates maximum intensity projections of all z stacks in the user-specified folder.
//Each maximum intensity projection is processed and saved to a folder created within the user-specified folder.

```
dir = getDirectory("Choose a Directory");
newdir = dir + "/Recon/"
File.makeDirectory(newdir);
list = getFileList(dir);

for(i=0; i<list.length; i++) {
        if (endsWith(list[i], ".tif")){
                open(dir+list[i]);
                imgName=getTitle();
                run("Z Project...", "Max Intensity");
                run("Enhance Contrast", "saturated=0.1 normalize process_all use");
                run("Subtract Background...","rolling=50");
                run("Despeckle");
                run("Smooth");
                saveAs("Tiff", newdir + "Recon " + imgName);
                while (nImages>0) {
                        selectImage(nImages);
                        close();
                }
        }
}
```

Generating Maximum Intensity Projections from Z-stacks for DAPI Counting
//This macro creates maximum intensity projections of all z stacks in the user-specified folder.

//Each maximum intensity projection is processed and saved to a folder created within the user-specified folder.

```
dir = getDirectory("Choose a Directory");
newdir = dir + "/Modified/"
File.makeDirectory(newdir);
list = getFileList(dir);

for(i=0; i<list.length; i++) {
        if (endsWith(list[i], ".tif")){
                open(dir+list[i]);
                imgName=getTitle();
                run("Z Project...", "Max Intensity");
                run("Enhance Contrast", "saturated=0.1 normalize process_all use");
                run("Subtract Background...","rolling=10");
                //run("Despeckle");
                //run("Smooth");
                saveAs("Tiff", newdir + "Modifed " + imgName);
                while (nImages>0) {
                        selectImage(nImages);
                        close();
                }
        }
}
```

Counting DAPI-labeled nuclei from Maximum Intensity Projections
*Best results from 10x stacks

```
dir = getDirectory("Choose a Directory");
newdir = dir + "/DAPI Counted2/"
File.makeDirectory(newdir);
list = getFileList(dir);

for(i=0; i<list.length; i++) {
        if (endsWith(list[i], ".tif")){
                open(dir+list[i]);
                imgName=getTitle();
                run("8-bit");
                setAutoThreshold("Moments dark");
                run("Convert to Mask");
                run("Watershed");
                run("Analyze Particles...", "size=20-100 circularity=0.00-1.00 show=Outlines
display include summarize");
                saveAs("jpeg", newdir + imgName);
                while (nImages>0) {
```

```
                                selectImage(nImages);
                                close();
                        }
                }
        }

        selectWindow("Summary");
        saveAs("Measurements", newdir+"Summary.xls");
        run("Close");
```

Appendix H – Surgery Preparation and Procedure for PRO00010188: Isolating Rodent Cells and Tissues for Creation of a Hierarchical Vascular Construct

*Sections of this protocol that are consistent for all animal procedures were modified from Nicole Friend's protocol for hindlimb ischemia surgeries.

Surgery Room Preparations

- Turn on bead bath – set to 279C (press and hold button)
- Clean the bench space with ethanol
- Prep 15 mL of PBS per mouse (sterile)
- Weigh charcoal canister and record the weight/date → get a new canister (on top shelf above LDPI machine) if the canister is spent
- Pour isoflurane into the chamber → unscrew the knob and fill until the liquid level is between the two white arrows but closer to the top)

Retrieve Animals from the Vivarium

- Animals are housed in 1411C
- Find animal cage on the racks within the room. Pull the cage out and bring it to the hood.
- Spray down the hood with cleaner. Bring a fresh cage into the hood.
- Dip hands in the spore cleanse bucket and grab one mouse to transfer to the new cage.
- Bring the remaining animals in the original cage back to the housing room (check the lixit before putting the cage back in). If there is only one animal remaining, add another form of enrichment to the cage.
- Use a gown or tshirt to cover the cage to carry the animal upstairs to the surgery room.

Final Preparations

- Turn heating pad on to setting 3 (if using, it is in the third drawer on the right)
- Turn on the oxygen tank (key is to the right of the tank)
- Turn on the snorkel (to a 12 pm clock position – originally in 3 pm)

- Turn on isoflurane pump with the switch on the back (machine should make a humming noise (much louder when flow is to the nose cone) - if there is no hum, unplug and re-plug in machine)
  - Make sure the induction chamber is pushed fully in towards the machine before turning on
- Turn the hose knobs to the proper position for flow into the induction chamber (orange in the tube, green and red off)
- Turn the green knob at the back so the ball in the chamber goes to setting 1
- Put a paper towel open into the induction chamber
- Turn iso to level 5 (push down the white lever and then turn the silver knob)
- Pick up the mouse and transfer to the induction chamber
- Pinch the foot to check for reaction (if the mouse flinches, then they are still awake and need longer in the chamber)
- Pick up the mouse and weigh them on the scale (in the plastic bucket) and record the weight on the surgical record
- Place the mouse back in the induction chamber
- Turn the red and green knobs into the tubing and then turn the orange knob off (always turn on then off – don't want there to be no flow)
- Lay out a sterile drape
- Place Q-tips and eye lube on a fresh sterile drape
- Move the mouse to the sterile drape, put on the eye lube over the eyes (enough to cover), and put the mouse's face into the nose cone
  - With the mouse on its back, the bar in the nose cone should be in the upper position
- Turn iso to level 2
- Continue to monitor that breathing stays slow

Preparation of the Mouse

- Shave the mouse (razor and nair in second drawer on the right) – entire region of interest (hind limbs for femoral vessels, body/chest cavity for aorta)
- Nair the mouse (squirt a small amount on your fingers and rub over the shaved area)
- Wipe the mouse with an ethanol pad to remove the nair (may need 2)
- Get out a new sterile drape and place the mouse on this drape – throw out the drape that is covered in fur
- Dispose of gloves and don a pair of sterile gloves

Femoral Vessel Surgical Procedure

- Use forceps to lift the skin (make a tent for incision) and scissors to create a small cut in the skin over the leg
- Separate the skin from the fascia to expose the femoral vein (should be visible by eye)
- Fully expose the vein from the inguinal ligament to the proximal/caudal bifurcation

- o Ligament will be visible by eye
- o Use the stereoscope to visualize the femoral nerve and artery (nerve is white in color, artery is translucent, vein is red)
- o The nerve and artery will be to the outside edge of the leg (i.e., on the right side for the mouse's left leg (mouse on its back so this will be human's right side) and on the left side for the mouse's right leg (mouse on its back so this will be human's left side))
- Carefully separate the fascia from the muscle – only clip on the side that does not have the artery and nerve to avoid cutting the vessel (forceps and scissors are best for this)
- Use a Q-tip in a rolling motion over the vessel to further remove the fascia layer (will start to appear less shiny)

Thoracic Surgical Procedure

- Turn iso up to 5 to euthanize the animal
- Once breathing has slowed to one breath per minute or less, use scissors to puncture the lungs (pneumothorax)
- Use forceps to lift the skin (make a tent for incision) and scissors to create a small cut in the skin over the abdominal cavity
- Cut upwards towards the chest cavity to expose the rib cage
- Cut through the rib cage (and other surrounding tissue) to expose the heart and lungs
- Move other organs out of the way as much as possible

Vessel Isolation Procedures

Femoral

- Separate the vessels from the underlying muscle using scissors (insert closed and then open them to separate the muscle from the vessel)
- Once separated, cut the distal end and then the proximal end to completely isolate the vessel

Thoracic

- First identify the inferior vena cava (connected to heart and liver)
  - o Using forceps, remove as much surrounding tissue and adventitia as possible from the vessel.
  - o Cut the vessel from the liver side first and then the heart side.
- Identify the aorta
  - o Segment towards the spine (dorsal side of the animal) is the descending aorta
    - ▪ Use the same technique as with the femoral vessels to separate the vessel from the spine and other tissue (insert closed scissors below the vessel and then open them to separate vessel and tissue)

- - Remove as much surrounding tissue and adventitia as possible from the vessel.
    - Cut at the distal end and then proximal end to completely isolate the vessel
- Be sure to avoid the esophagus. It can be clearly tracked into the stomach to differentiate from the other vessels.

General

- Place all isolated vessels in PBS and keep in the fridge until ready to embed in gels

Procedural Wrap up

- Place the carcass inside of a large glove, then another glove and tie it off
- Label the glove "Putnam" and the date
- Reset the iso knobs into the induction chamber (orange open, red and green closed)
- Turn off iso machine
- Turn off oxygen
- Dispose of all drapes, tubes, gauze, etc. in the trash outside of the surgery room
- Clean tools
  - Soak in enzol solution for 5 min (swirl it around in the solution if extra bloody)
  - Spray with water
  - Spray with ethanol
  - Air dry
  - Package in autoclave bags
- Fill out remaining information on surgical record sheet
- Complete remaining surgeries (if doing multiple).
- Bring carcass, cage, and surgical sheet down to vivarium
  - Place cage in the dirty cage rack
  - Place surgical sheet in the blue Putnam lab binder
  - Place carcass in the fridge
- Turn off bead bath
- Clean surgery room with ethanol and UV the hood (set timer for 1 hour to come back and turn it off)

Appendix I – Embedding Murine Explants in Fibrin Hydrogels

Materials:
- Bovine Thrombin
- Bovine Fibrinogen
- FBS
- Media (SF-EGM2, EGM2, DMEM + 10% FBS)
- Trypsin (0.05%)
- PBS (1x, no calcium or magnesium)
- Forceps
- 18 G needle
- 5 mL syringe
- 33 mm 0.22 μm filter
- Murine vessel explants (as prepared in Appendix H)
- Microcentrifuge tubes

Protocol:
1. Prepare cells according to cell passaging protocol if making cellular gels.
2. Prepare one aliquot per gel in a microcentrifuge tube- 250K/mL each cell type (500K/mL total). (If making acellular gels – prep the aliquot of just FBS for each gel).
3. Centrifuge combined cell suspension and leave the pellets with supernatant on ice during surgery. Cover the ice bucket with lid to prevent melting.
4. Remove thrombin from freezer and place it in the ice bucket.
5. Isolate femoral bundles, IVC, and descending aorta according to surgical protocol and place in PBS.
6. Flush the lumen of the aorta with PBS via cannulation
7. 2x PBS washes in a 24 well plate (1 mL per well) during gel preparation (at least 5 minutes per wash)
8. Prepare fibrinogen solution.
   a. Weigh out desired amount of fibrinogen for 5 mg/mL fibrin hydrogels
      i. $X*(0.71)*(0.89)*(0.88) = 5$ mg/mL $\rightarrow$ X = 8.99 mg/mL
         1. Current lot of fibrinogen (SLCG6303) is 71% protein and 89% clottable
         2. 88% of hydrogel recipe is fibrinogen solution (see recipe below)
         3. Determine the mass to weigh out based on the desired volume and concentration of 8.99 mg/mL to achieve a 5 mg/mL gel
      ii. With Lot SLCG6306 it is harder to dissolve – make only ~3-4 mL aliquots and combine multiple at the filtering step.
   b. Determine volume needed based on amount of powder weighed out.

c. Aliquot appropriate media volume (warmed SF-EGM2) in the cell culture hood and bring back to the scale.
d. Place the powder into the tube on top of the media and tap on the counter several times to suspend.
e. Twirl fibrinogen in the water bath and tap on the sides to dislodge and help with dissolving. Do this every break during prep (every 5-15 min).
9. Prepare gel aliquots
   a. For cellular gels – aspirate the supernatant, suspend the pellet in FBS, add thrombin
   b. For acellular gels – add thrombin to FBS already in the tube
10. Filter fibrinogen solution
    a. Use a 5 or 10 mL syringe depending on volume and a 33 mm 0.33 um filter
    b. Remove plunger from syringe and attach filter
    c. Balance the syringe + filter on an open 15 mL conical tube
    d. Pipet fibrinogen solution into the syringe and then push plunger to filter the solution into the conical tube.
    e. Keep filtered fibrinogen on ice until ready to use
11. Label well plates for each fixing day (D1, D7, D14, etc.)
    a. Femoral bundles and IVC can be cultured in 24 well plate
    b. Aorta should be cultured in 12 well plate due to larger size of the vessel
    c. Aorta for rheology should be cut in half and cultured in 24 well plate
12. Place one vessel per well as centered as possible using sterile forceps
13. Add fibrinogen to (cell)/FBS/thrombin mixture, mix well (5-7 times), and pipette into the well. Use forceps to make sure the vessel is not adhered to the bottom of the plate and remains centered within the gel.
14. Allow gels to solidify for 10 minutes in the hood (this is double the normal time for 2.5 mg/mL gels). Transfer the plates to the incubator to complete gelation for 30 minutes.
15. Add media to each gel: 1 mL for 24 well plates, 2 mL for 12 well plates.
    a. If adding aprotinin to the culture media, add it to the whole aliquot before adding media to each gel to avoid using too small of a volume.

Component	500 μL	1 mL
Thrombin	10 μL	20 μL
FBS	50 μL	100 μL
Fibrinogen	440 μL	880 μL

Table I.1: *Fibrin gel recipe for fabricating constructs with murine explants.*

Appendix J – Rheology of Fibrin Hydrogels

*Protocol adapted from Nicole Friend.

Materials:
- AR-G2 shear rheometer with Peltier stage attached for standard measurements
- 8 mm measurement head with adapter and longer spindle rod for in plate hydrogel characterization
- Glass plate to balance well plates (if measuring directly in well)
- Double sided scotch tape
- Course grit wet sandpaper (800 grit or lower is best)
- 8mm biopsy punch and/or scalpel

Notes:

- Experiments tracking cell-mediated changes to matrix mechanics are done with the 8mm measurement head.
- Getting a transducer initialization error has become more common over the last couple years. This error is most likely caused by a problem with the rotary optical encoder that keeps track of the displacement and velocity of the bearing spindle. If you receive this error quickly turn off the instrument because rotation of the spindle starts to accelerate out of control. Usually restarting the instrument and software a couple times will fix the problem. The error only occurs at start up. When simply restarting doesn't work, I have had some success with starting the instrument with the measurement lowered to be in contact with the measurement plate to hold it in place, which seems to allow the encoder to register the spindle more easily. You will get a magnetic bearing instability warning however, at which point, raise the measurement head and restart the software, but not the instrument.
    - TA instruments suggestions for dealing with transducer initialization failure: Transducer initialization is reporting a problem with the rotary optical encoder that keeps track of the displacement and velocity of the bearing spindle. The rotary encoder is positioned at the top of the air bearing motor/transducer assembly. When it fails to report a position change the error will be posted. There could be some dust in and around the encoder, try blowing compressed air thru the opening where the draw rod sits. If you are comfortable taking things apart

you could remove the cowl cover and top encoder cover to better inspect and blow out any dust. If the error is persistent, I would recommend a service call.

- To avoid initialization failure, it is ok to **leave the instrument running for long periods of time**, however, it is important to **turn off the cooling pump when not in use** because the pump will overheat if left running over night, this is bad for the pump, and also heats the water bath, such that the Peltier stage can't cool down to an appropriate temperature to perform experiments. Only leave the rheometer and air on.

- Measurement parameters for fibrin are typically performed in a 24-well plate or larger, with the 8mm measurement head indented into the hydrogel ~300 um, 0 N normal force, 6% strain, 1 rad/sec.

Procedure:

1. Log in to the "Rheometer" profile on the rheometer computer in the Putnam lab space
2. Plug in the water pump to the power strip.
   a. Check water bath level for Peltier stage cooling pump and top off if necessary, exchange with fresh water if cleaning is needed.
3. Open on the Rheological Advantages software to control the AR-G2 rheometer.
4. Load or create new test procedure. Procedure -> open, or Procedure -> new.
   a. Procedures are typically "oscillation" procedures. When you click new procedure, it will open the default tab to input procedure steps and test parameters. New oscillation procedures will default to have 3 steps: 1) conditioning 2) frequency sweep 3) post-experiment. You can right click on a step to add another step to the procedure. You can uncheck the box to turn off a particular step. In addition to oscillation frequency sweep, we commonly perform an oscillation strain sweep for initial characterization of a hydrogel, then oscillation time sweeps as the primary measure for comparison between conditions for a particular type of hydrogel/material.
   b. To input parameters for each step; click on the step in the procedure, then fill in the desired parameters for the step in the tabs that appear to the right.
   c. To save a procedure go to File-> Save As
5. Prepare the stage for hydrogel measurement
   a. Find the glass plate that is kept under the rheometer (~ 0.1 x 14 x 18 cm) and place on the Peltier stage. This keeps the plate level.
   b. If you are going to use a specific temperature for your measurement, you can set the stage to this temperature now to save time at the start of you your first measurement run. Always run cellular gels at 37°C.
6. Zero the geometry gap ⬚. If you are doing in-well measurements, make sure to zero into an empty well. Say "NO" to move head to back off distance, this moves the head all the way up and wastes time. Move head up manually using arrow buttons on rheometer or in the software.

7. Zero the normal force . You may need to press the zero button several times for it to give a negligible value (< 0.01 N, usually in the E-10 range)
8. Load sample onto the stage. Make sure the well of the plate is well centered under the measurement head. If the head is off to the side, it will give larger than expected measurement because of the extra contact area.
9. Sample measurement. Before lowering the measurement head or pipetting in sample for in situ gelation STOP ROTATION of measurement head to prevent shearing
    a. Bring the measurement head into contact with the hydrogel, then input a gap height 300um lower to start indenting into the hydrogel.
        i. Do this step slowly. Incrementally lower the measurement head until a meniscus forms when the head and hydrogel come in contact.
10. When you press the start measurement button in the top left corner you will be prompted to put in run information. Include all important information in the file name, and make sure it is saving to the appropriate Directory to find the file.
    a. Repeat for all samples, zeroing the normal force between samples if it does not return to < 0.01 after removing samples from stage.
11. Data can be loaded from the TA data analysis program, then exported to excel for analysis.
    a. I have not done this as I usually record values (mainly stiffness, G') in my lab notebook/personal excel file.
    b. When you open a file, nothing will immediately happen, and you will need to select view as table.
12. System shut down.
    a. We are currently leaving the instrument on between uses, but require **the pump be turned off**. To do so, set the required stage temperature to room temp (20-25C), wait for the stage to reach this value and remain there for a few minutes, then instrument → set temperature system idle. After, unplug the pump for the pump.
    b. Shut down the software and log off of the Rheometer profile.

Appendix K – Fabricating PDMS Molds for Engineering Hierarchical Vascular Tissue Constructs

Note:
This protocol requires the use of equipment in the Baker lab. Please email Dr. Baker for permission to use and the necessary training required.

Materials:
- PDMS (base and curing agent)
- Transfer pipette
- Epredia Peel-A-Way Mold
- 22 G Needles
- Glass coverslips (22x40 mm)
- Ethanol (100%)
- Isopropyl alcohol (IPA, 100%)
- MilliQ water
- Acupuncture needles
- Gelatin (2% solution)

Equipment:
- Oven
- Plasma etcher
- UV ozone

Protocol:

Day 1: Prepare PDMS molds
10. Mix PDMS base and curing agent at a ratio of 10:1 in a plastic cup and mix thoroughly with a plastic stirrer.
11. Degas PDMS under vacuum until all bubbles have been removed (time depends on volume of PDMS made but typically 30 minutes).
12. While PDMS is degassing, prepare peel-a-way molds
    a. Insert two 22G needles into the 22 mm edge of the plastic mold close to the bottom.
13. Cut off the tip of a transfer pipette to increase the area and use this to transfer PDMS from the cup to the molds.
14. Transfer PDMS into the molds on the scale to get 5 g in each mold.
    a. *Pop any bubbles by pocking them with a pipette tip.*

15. Move molds into a 70°C oven to cure for a minimum of 4 hours and up to overnight.
16. Place extra PDMS in the deli fridge to use for day 2.
    a. *PDMS can remain liquid at cool temperatures (typically only for an additional day) but will solidify if left overnight at RT.*

Day 2: Bond to glass coverslips
1. Remove molds from the oven.
2. Remove needles from the PDMS.
3. Peel the plastic mold apart from the PDMS mold.
4. Cut the 22 mm edges off the PDMS to remove the curved edge features.
5. Over the needle tracks, use a 5 mm biopsy punch to create seeding reservoirs.
6. Use a 12 mm biopsy punch and punch two overlapping circles to create the hydrogel chamber.
7. Clean the glass coverslips and PDMS molds with IPA and ethanol rinses.
    a. Rinse a coverslip with IPA on both sides.
    b. Rinse the coverslip with ethanol on both sides.
    c. Use the air gas line with tubing attached to dry the coverslip.
    d. Place the cleaned coverslip rested against the lid of a petri dish.
8. Repeat step 8 for all coverslips and PDMS chips.
9. Take the cleaned chips and coverslips down to the Baker lab to use the plasma etcher to bond the two pieces together.
10. Place an equal number of coverslips and PDMS chips in the plasma treating cage (three of each fit).
11. Run the plasma cycle for 1 minute.
    a. If the plasma etcher is not set to 1 minute you must change the time (commands → plasma time → change to 1 minute).
    b. If the plasma etcher is set to 1 minute you are ready to run it (commands → plasma → start)
    c. *If the plasma etcher has not run for the day, it can take a few minutes to reach the vacuum set point.*
12. Once the cycle is over, release the hinge to open the door. Once the vacuum is released, the door will open.
13. Remove one coverslip and one PDMS mold from the cage and place them together.
    a. Adhere the two surfaces that were upward facing during the plasma cycle.
    b. Use your fingers to ***gently*** press the two together.
    c. Place the bonded mold down on the bench and use your palm to press into the PDMS side of the mold (not the glass side) multiple times to ensure it is well adhered.
14. Transfer the molds to a 60°C oven for at least 1 minute.
15. Remove the molds from the oven and place them on the bench.
16. Use your palm again to ensure the bond it tight.
17. Place a kimwipe over the chip.
18. Place a weight on top of each chip for 5 minutes.
    a. The Baker lab has two petri dishes filled with metal beads to use, but it could be anything heavy if these are in use.

19. Repeat steps 10-18 for all remaining molds.
20. Bring bonded molds back to our lab.
21. Retrieve PDMS from the deli fridge.
    a. The glass is a near exact fit in width for the molds so they must be further sealed with PDMS to ensure the edges are well sealed.
22. Use a pipette tip to seal the long edges of the mold with PDMS.
23. Cure PDMS in the oven for at least 2 hours and up to overnight.

Day 3: Insert needles and UV ozone treat the chips
1. Ensure needles are cleaned.
2. Warm 2% gelatin solution in the water bath.
3. Dip each needle in the gelatin solution and then place in a petri dish.
4. Allow gelatin to solidify for 5 minutes at 4°C.
5. Place a single needle in each needle track (2 per mold).
6. Bring the molds and a sterile P150 petri dish to the Baker lab.
7. Place the molds in the UV ozone and sterilize for 5 minutes.
8. After the cycle has completed, place the sterilized molds in the sterile petri dish.
9. Bring the sterilized molds back to our lab. They are now ready for cell culture.

Appendix L – Engineering Three Layer Biomimetic Tissue Engineered Vascular Grafts

Materials:
- Bovine Thrombin
- Bovine Fibrinogen
- FBS
- Media (SF-EGM2, EGM2, DMEM + 10% FBS, SMGM)
- Trypsin (0.05%)
- PBS (1x, no calcium or magnesium)
- Forceps
- 5- or 10-mL syringe
- 33 mm 0.22 μm filter
- Microcentrifuge tubes
- 1 mm glass mandrels (custom ordered from McMaster Carr)
- 5 mm ID glass cylinders (custom ordered from McMaster Carr)
- PDMS support pieces for annular molds
- 15 mL bioreaction tubes (CellTreat)
- Pluronic F-68 (0.5% and 0.01%)
- Glass jar

Protocol:

Day 0: Fabricate Tunica Media Layer
1. Bring assembled annular molds (autoclaved for sterile use) into the hood.
2. Place annular molds onto the inner surface of the lid of the glass jar.
3. Add 0.5% Pluronic F-68 to each mold and allow to sit for 1 hour at RT.
4. Prepare cells according to appendix A. SMC are needed for the media layer.
5. Prepare fibrinogen solution.
   a. Weigh out desired amount of fibrinogen for 5 mg/mL fibrin hydrogels
      i. $X*(0.75)*(0.93)*(0.76) = 5$ mg/mL $\rightarrow$ X = 9.432 mg/mL
         1. Current lot of fibrinogen (SLCL8080) is 75% protein and 93% clottable
         2. 76% of hydrogel recipe is fibrinogen solution (see recipe below)
         3. Determine the mass to weigh out based on the desired volume and concentration of 9.432 mg/mL to achieve a 5 mg/mL gel.
   b. Determine volume needed based on amount of powder weighed out.
   c. Place powder into a conical tube and add the appropriate amount of. PBS.

      d. Twirl fibrinogen in the water bath and tap on the sides to dislodge and help with dissolving. Do this every 5-15 min.
6. Prepare one aliquot per vascular graft.
      a. The final cell concentration of SMC for each graft should be 1M/mL. Add the appropriate volume of stock cell suspension to achieve this volume in the final graft to a microcentrifuge tube.
            i. i.e., if cells are suspended at 1M/mL, add 850 μL to the microcentrifuge tube.
      b. Centrifuge cells in the microcentrifuge at 200g for 5 minutes.
      c. Aspirate supernatant and suspend pellet in SF-EGM2 according to recipe.
      d. Add FBS to mixture.
      e. Add thrombin to mixture.
            i. Wait to add thrombin until ready to cast the gels. If there are 20 minutes left on the timer, keep aliquots on ice and add thrombin later.
      f. Place tubes on ice.
7. Filter fibrinogen solution
      a. Use a 5- or 10-mL syringe depending on volume and a 33 mm 0.33 um filter
      b. Remove plunger from syringe and attach filter
      c. Balance the syringe + filter on an open 15 mL conical tube
      d. Pipet fibrinogen solution into the syringe and then push plunger to filter the solution into the conical tube.
      e. Keep filtered fibrinogen on ice until ready to use
8. Aspirate the Pluronic from the annular molds.
9. One gel at a time, add fibrinogen to the gel aliquot and mix thoroughly (5-7 times).
10. Inject gel solution into the annular mold.
11. Push the PDMS space into the glass cylinder to ensure the mandrel stays centered within the mold.
      a. Place your finger under the PDMS base to prevent the mandrel from sliding through.
12. Incubate grafts for 35 minutes at 37°C.
13. While grafts are gelling, warm SMGM (5 mL per graft).
14. Add 5 mL of warm media to each bioreaction tube (1 per graft).
15. Remove grafts from mandrel.
      a. First remove glass cylinder by gently dislodging from the PDMS base.
      b. Remove PDMS base.
      c. Place graft (still on the mandrel) in the bioreaction tube with the PDMS spacer at the bottom so the graft does not slip off.
16. Culture for 3 days at 37°C with media exchange on day 1.

Day 3: Fabricate Tunica Adventitia Layer
1. Bring assembled annular molds (autoclaved for sterile use) into the hood.
      a. In this case, instead of the full mandrel, use a broken mandrel. The mandrel is just needed to plug the hole at the bottom of the PDMS base during Pluronic coating and will be removed and replaced with the mandrel containing the SMC graft during gelation.

2. Place annular molds onto the inner surface of the lid of the glass jar.
3. Add 0.5% Pluronic F-68 to each mold and allow to sit for 1 hour at RT.
4. Prepare cells according to appendix A. EC and LF are needed for the adventitia layer.
5. Prepare fibrinogen solution.
    a. Weigh out desired amount of fibrinogen for 5 mg/mL fibrin hydrogels
        i. $X*(0.75)*(0.93)*(0.76) = 5$ mg/mL $\rightarrow$ X = 9.432 mg/mL
            1. Current lot of fibrinogen (SLCL8080) is 75% protein and 93% clottable
            2. 76% of hydrogel recipe is fibrinogen solution (see recipe below)
            3. Determine the mass to weigh out based on the desired volume and concentration of 9.432 mg/mL to achieve a 5 mg/mL gel.
    b. Determine volume needed based on amount of powder weighed out.
    c. Place powder into a conical tube and add the appropriate amount of. PBS.
    d. Twirl fibrinogen in the water bath and tap on the sides to dislodge and help with dissolving. Do this every 5-15 min.
6. Prepare one aliquot per vascular graft.
    a. The final cell concentration of cells for each graft should be 1M/mL in a 1:1 ratio of LF and EC. Add the appropriate volume of stock cell suspension to achieve this volume in the final graft to a microcentrifuge tube.
        i. i.e., if cells are suspended at 1M/mL, add 425 μL of each cell type to the microcentrifuge tube.
    b. Centrifuge cells in the microcentrifuge at 200g for 5 minutes.
    c. Aspirate supernatant and suspend pellet in SF-EGM2 according to recipe.
    d. Add FBS to mixture.
    e. Add thrombin to mixture.
        i. Wait to add thrombin until ready to cast the gels. If there are 20 minutes left on the timer, keep aliquots on ice and add thrombin later.
    f. Place tubes on ice.
7. Filter fibrinogen solution
    a. Use a 5- or 10-mL syringe depending on volume and a 33 mm 0.33 um filter
    b. Remove plunger from syringe and attach filter
    c. Balance the syringe + filter on an open 15 mL conical tube
    d. Pipet fibrinogen solution into the syringe and then push plunger to filter the solution into the conical tube.
    e. Keep filtered fibrinogen on ice until ready to use
8. Aspirate the Pluronic from the annular molds.
9. Prepare the SMC grafts.
    a. Remove the graft from the media and use forceps to gently slide the graft down away from the spacer so the spacer can be pushed back into the cylinder during gelation.
    b. Insert mandrel with graft into the glass cylinder.
10. One gel at a time, add fibrinogen to the gel aliquot and mix thoroughly (5-7 times).
11. Inject gel solution into the annular mold.
12. Push the PDMS space into the glass cylinder to ensure the mandrel stays centered within the mold.

a. Place your finger under the PDMS base to prevent the mandrel from sliding through.
13. Incubate grafts for 35 minutes at 37°C.
14. While grafts are gelling, warm EGM2 media (5.4 mL per graft).
15. Aspirate SMGM from bioreaction tubes.
16. Add 5 mL of warm EGM2 to each bioreaction tube (1 per graft).
17. Remove grafts from mandrel.
   a. First remove glass cylinder by gently dislodging from the PDMS base.
   b. Remove PDMS base.
   c. Place graft (still on the mandrel) in the bioreaction tube with the PDMS spacer at the bottom so the graft does not slip off.
18. Culture for 7 days at 37°C with media exchange on days 4, 6, 8.

Day 10: Fabricate Tunica Intima Layer

Note:
This protocol requires the use of equipment in the Stegemann lab. Please email Dr. Stegemann for permission to use and the necessary training required.

1. Bring a 24 well plate and a 12 well plate into the hood.
2. Coat 2 wells per graft with 0.01% Pluronic F-68 (1 well per plate).
3. Prepare EC according to Appendix A.
4. Suspend EC at 2M/mL in EGM2.
5. Add 1 mL of cell suspension to each well of the 24 well plate.
6. Bring the plate to the surgery room.
7. Inject cell suspension into the graft lumen.
   a. Use the stereoscope to view the lumen.
   b. Use sterile forceps to hold the graft
   c. Using a P200 pipette, inject 200 μL of cell suspension into the lumen.
   d. Repeat from the other side.
8. Incubate for 1 hour at 37°C in the rotating incubator in the Stegemann lab.
9. Warm EGM2 in the water bath (6 mL per graft).
10. Add 6 mL of media to each coated well of the 12 well plate.
11. Transfer grafts to the 12 well plate (1 graft per well).
12. Culture for 3 days at 37°C with media exchanges on day 11.
13. Grafts are now ready for endpoint analyses or future use in 3-scale hierarchical vascular tissue constructs.

Component	850 μL
Thrombin	17 μL
FBS	85 μL
SF-EGM2	100 μL
Fibrinogen	648 μL

Table L.1: *Fibrin gel recipe for fabricating vascular grafts.*

Appendix M – Fabricating 3-Scale Hierarchical Vascular Tissue Constructs

Materials:
- Bovine Thrombin
- Bovine Fibrinogen
- FBS
- Media (SF-EGM2, EGM2, DMEM + 10% FBS)
- Trypsin (0.05%)
- PBS (1x, no calcium or magnesium)
- Forceps
- 5- or 10-mL syringe
- 33 mm 0.22 μm filter
- Microcentrifuge tubes
- PDMS molds prepared according to Appendix L
- Vacuum grease
- 35 mm petri dish
- 150 mm petri dish

Protocol:

1. Bring PDMS molds into the hood.
2. Prepare LF and EC according to appendix A.
3. Prepare fibrinogen solution.
   a. Weigh out desired amount of fibrinogen for 5 mg/mL fibrin hydrogels
      i. $X*(0.75)*(0.93)*(0.76) = 5$ mg/mL $\rightarrow$ $X = 9.432$ mg/mL
         1. Current lot of fibrinogen (SLCL8080) is 75% protein and 93% clottable
         2. 76% of hydrogel recipe is fibrinogen solution (see recipe below)
         3. Determine the mass to weigh out based on the desired volume and concentration of 9.432 mg/mL to achieve a 5 mg/mL gel.
   b. Determine volume needed based on amount of powder weighed out.
   c. Place powder into a conical tube and add the appropriate amount of. PBS.
   d. Twirl fibrinogen in the water bath and tap on the sides to dislodge and help with dissolving. Do this every 5-15 min.
4. Prepare one aliquot per mold.
   a. The final cell concentration should be 250K/mL in a 1:1 ratio of LF to EC. Add the appropriate volume of stock cell suspension to achieve this volume in the final graft to a microcentrifuge tube.

i. i.e., if cells are suspended at 1M/mL, add 250 µL to the microcentrifuge tube.
b. Centrifuge cells in the microcentrifuge at 200g for 5 minutes.
c. Aspirate supernatant and suspend pellet in SF-EGM2 according to recipe.
d. Add FBS to mixture.
e. Add thrombin to mixture.
i. Wait to add thrombin until ready to cast the gels. If there are 20 minutes left on the timer, keep aliquots on ice and add thrombin later.
f. Place tubes on ice.

5. Filter fibrinogen solution
a. Use a 5- or 10-mL syringe depending on volume and a 33 mm 0.33 um filter
b. Remove plunger from syringe and attach filter
c. Balance the syringe + filter on an open 15 mL conical tube
d. Pipet fibrinogen solution into the syringe and then push plunger to filter the solution into the conical tube.
e. Keep filtered fibrinogen on ice until ready to use

6. Remove TEVG from well plate and place in the PDMS mold, laying the ends in the cut section of the mold.
a. Do this step graft/mold at a time.

7. One gel at a time, add fibrinogen to the gel aliquot and mix thoroughly (5-7 times).
8. Inject gel solution into the PDMS mold.
9. Allow fibrin to solidify for 5 minutes at RT in the hood.
10. Incubate grafts for 35 minutes at 37°C.
11. While grafts are gelling, warm EGM2 (11 mL per mold).
12. Also prepare the EC for cell seeding. Suspend the remaining EC at 2M/mL in EGM2.
13. After gelation, add 1 mL of EGM2 to each mold (fill the wells and gently place the remaining volume over the gel being careful not to overflow the PDMS) to allow the gel to swell.
14. Incubate for 30 minutes at 37°C.
15. Using forceps, remove the acupuncture needles from each mold.
16. Seal the needle tracks with vacuum grease.
17. Remove all media.
18. Inject a suspension of 2M/mL EC into the channels through the circular reservoirs.
a. Start with 20 µL per channel.
b. Visualize under microscope to ensure cells are flowing into the channel.
c. Add more cells if needed.
d. Balance the hydrostatic pressure gradient with EGM2 in the other well if cells are flowing too fast.

19. Culture molds for 30 minutes to allow cells to adhere.
20. Repeat steps 18 and 19 but flip the mold upside down to allow cells to adhere to the top surface of the channel.
21. Transfer each mold to its own 35 mm petri dish.
22. Remove cell suspension from molds.
23. Add EGM2 to all molds (10 mL per mold).
a. First fill the reservoirs.

      b.   Then using a serological pipette, dispense remaining media to fill the entire petri dish

24. Culture at 37°C with media exchanges every other day.

Component	850 μL
Thrombin	20 μL
FBS	100 μL
SF-EGM2	120 μL
Fibrinogen	760 μL

Table M.1: *Fibrin gel recipe for fabricating 3-scale vascular hierarchies.*